2006-03

Impact of GFO satellite and ocean nowcast/forecast systems on Naval antisubmarine warfare (ASW)

Amezaga, Guillermo R.

Monterey, California. Naval Postgraduate School

NAVAL POSTGRADUATE SCHOOL

MONTEREY, CALIFORNIA

THESIS

IMPACT OF GFO SATELLITE AND OCEAN NOWCAST/FORECAST SYSTEMS ON NAVAL ANTISUBMARINE WARFARE (ASW)

by

Guillermo R. Amezaga, Jr.

March 2006

Thesis Advisor: Peter C. Chu
Second Reader: Eric Gottshall

Approved for release; distribution is unlimited

THIS PAGE INTENTIONALLY LEFT BLANK

REPORT DOCUMENTATION PAGE			Form Approved OMB No. 0704-0188
Public reporting burden for this collection of information is estimated to average 1 hour per response, including the time for reviewing instruction, searching existing data sources, gathering and maintaining the data needed, and completing and reviewing the collection of information. Send comments regarding this burden estimate or any other aspect of this collection of information, including suggestions for reducing this burden, to Washington headquarters Services, Directorate for Information Operations and Reports, 1215 Jefferson Davis Highway, Suite 1204, Arlington, VA 22202-4302, and to the Office of Management and Budget, Paperwork Reduction Project (0704-0188) Washington DC 20503.			
1. AGENCY USE ONLY *(Leave blank)*	**2. REPORT DATE** March 2006	**3. REPORT TYPE AND DATES COVERED** Master's Thesis	
4. TITLE AND SUBTITLE: Impact of GFO Satellite and Ocean Nowcast/Forecast Systems on Naval Antisubmarine Warfare (ASW)			**5. FUNDING NUMBERS**
6. AUTHOR(S) Guillermo R. Amezaga, Jr.			
7. PERFORMING ORGANIZATION NAME(S) AND ADDRESS(ES) Naval Postgraduate School Monterey, CA 93943-5000			**8. PERFORMING ORGANIZATION REPORT NUMBER**
9. SPONSORING /MONITORING AGENCY NAME(S) AND ADDRESS(ES) N/A			**10. SPONSORING/MONITORING AGENCY REPORT NUMBER**
11. SUPPLEMENTARY NOTES The views expressed in this thesis are those of the author and do not reflect the official policy or position of the Department of Defense or the U.S. Government.			
12a. DISTRIBUTION / AVAILABILITY STATEMENT Approved for release; distribution is unlimited			**12b. DISTRIBUTION CODE**

13. ABSTRACT (maximum 200 words)

The purpose of this thesis is to investigate the value-added of the Navy's nowcast/forecast and GFO satellite to the naval antisubmarine warfare (ASW) and anti-surface warfare. For the former, the nowcast/forecast versus observational fields were used by the WAPP to determine the suggested presets for MK 48 variant torpedo. The metric used to compare the two sets of outputs is the relative difference in acoustic coverage area generated by WAPP. Output presets are created for five different scenarios, two anti-surface warfare scenarios and three ASW scenarios, in each of two regions: the East China Sea and South China Sea. Analysis of the output reveals that POM outperforms MODAS in all tactic scenarios. For the latter, the MODAS (T, S) profiles were used by the WAPP to determine suggested presets for Mk 48 variant torpedo. The only difference in the MODAS fields was the altimeter used to initialize the respective MODAS fields. The same metrics used in the nowcast/forecast case were used to generate and compare the acoustic coverages. Analysis of the output reveals that, in most situations, WAPP output is not very sensitive to the difference in altimeter orbit.

14. SUBJECT TERMS Satellite Altimetry, MODAS, Anti-Submarine Warfare, ASW, MK-48 Torpedo, WAPP, POM, GFO, Topex			**15. NUMBER OF PAGES** 154
			16. PRICE CODE
17. SECURITY CLASSIFICATION OF REPORT Unclassified	**18. SECURITY CLASSIFICATION OF THIS PAGE** Unclassified	**19. SECURITY CLASSIFICATION OF ABSTRACT** Unclassified	**20. LIMITATION OF ABSTRACT** UL

NSN 7540-01-280-5500 Standard Form 298 (Rev. 2-89)
Prescribed by ANSI Std. 239-18

THIS PAGE INTENTIONALLY LEFT BLANK

Approved for public release; distribution is unlimited

IMPACT OF GFO SATELLITE AND OCEAN NOWCAST/FORECAST SYSTEMS ON NAVAL ANTISUBMARINE WARFARE (ASW)

Guillermo R. Amezaga, Jr.
Lieutenant, United States Navy Reserve
B.A., University of Colorado – Boulder, 2001

Submitted in partial fulfillment of the
requirements for the degree of

MASTER OF SCIENCE IN METEOROLOGY AND PHYSICAL OCEANOGRAPHY

from the

NAVAL POSTGRADUATE SCHOOL
March 2006

Author: Guillermo R. Amezaga, Jr.

Approved by: Peter C. Chu
Thesis Advisor

Eric Gottshall
Second Reader

Mary Batteen
Chairman, Department of Oceanography

THIS PAGE INTENTIONALLY LEFT BLANK

ABSTRACT

The purpose of this thesis is to investigate the value-added of the Navy's nowcast/forecast and GFO(GEOSAT Follow On) satellite to the naval antisubmarine warfare (ASW) and anti-surface warfare. For the former, the nowcast/forecast versus observational fields were used by the WAPP to determine the suggested presets for Mk 48 variant torpedo. The metric used to compare the two sets of outputs is the relative difference in acoustic coverage area generated by WAPP(Weapon Acoustics Preset Program). Output presets are created for five different scenarios, two anti-surface warfare scenarios and three ASW scenarios, in each of two regions: the East China Sea and South China Sea. Analysis of the output reveals that POM(Princeton Ocean Model) outperforms MODAS(Modular Ocean Data Assimilation System)in all tactic scenarios. For the latter, the MODAS (T, S) profiles were used by the WAPP to determine suggested presets for MK 48 variant torpedo. The only difference in the MODAS fields was the altimeter used to initialize the respective MODAS fields. The same metrics used in the nowcast/forecast case were used to generate and compare the acoustic coverages. Analysis of the output reveals that, in most situations, WAPP output is not very sensitive to the difference in altimeter orbit.

THIS PAGE INTENTIONALLY LEFT BLANK

TABLE OF CONTENTS

THIS PAGE INTENTIONALLY LEFT BLANK

LIST OF FIGURES

LIST OF TABLES

THIS PAGE INTENTIONALLY LEFT BLANK

ACKNOWLEDGMENTS

First, I acknowledge that my personal relationship with God, Jesus Christ, sustained me through the entire process of research, data analysis and writing this thesis.

Second, I dedicated this thesis to the loving memory of the matriarch of the Amezaga family, Maria de Los Angeles Amezaga, *Abuelita*, who was the most influential person in my life during my formative years. She taught me to be considerate, a leader, a thinker, and a friend. I miss our conversations over games of Chinese Checkers.

Third, I thank my loving and beautiful wife and daughters for enduring all my moodiness and complaining while writing the thesis. Thanks for your patience, love, and support. I love you.

Finally, I thank Professor Peter Chu for his patience, guidance, encouragement, and insight through the entire process. Mr. Chenwu Fan thanks for the all the help with preparing the data and writing the MATLAB code. CDR Eric Gottshall thanks for your candor, wisdom, and dinner at the Army-Navy Club in DC.

Sola Scriptura

Solus Christus

Sola Gratia

Sola Fide

Sola Deo Gloria

THIS PAGE INTENTIONALLY LEFT BLANK

I. INTRODUCTION

A. BACKGROUND

The outcome of a battlefield engagement is often determined by the advantages and disadvantages held by each adversary. On the modern battlefield, the possessor of the best technology often has the upper hand, but only if that advanced technology is used properly and efficiently. In order to exploit this advantage and optimize the effectiveness of high technology sensor and weapon systems, it is essential to understand the impact on them by the environment (Mancini, 2004).

Understanding the ocean environment is imperative and directly coupled to the successful performance of ASW sensors and subsequent employment of an ASW weapon system. In order to optimize the performance of ASW sensors and weapons systems, it is crucial to gain an understanding of the acoustic wave propagation in the ocean. Having an accurate depiction of the ocean environment is therefore directly related to gaining a better understanding of the acoustic wave propagation.

How acoustic waves propagate from one location to another under water is determined by many factors, some of which are described by the sound speed profile (SSP). If the environmental properties of temperature and salinity are known over the entire depth range, the SSP can be compiled by using them in an empirical formula to calculate the expected sound speed in a vertical column of water. Two approaches are used to increase the accuracy of ocean environmental depiction: (1) ocean nowcast/forecast systems, and (2) satellite data assimilation.

The U.S. Navy has developed the ocean nowcast/forecast systems to determine or predict representative SSP. The nowcast system is called Modular Ocean Data Assimilation System (MODAS), which is built on the base of the optimal interpolation. The forecast system is called the Navy Coastal Ocean Model (NCOM), which is built on the base of the Princeton Ocean Model (POM). MODAS uses climatology as the initial guess and assimilates satellite and in-situ measurements such as altimetry, conductivity-temperature-depth (CTD), expendable bathythermographs (XBT), and ARGO casts. NCOM forecasts the ocean environment using observational data such as temperature,

salinity, and velocity. The capability of MODAS and POM to represent ocean environment (SSP through T, S profiles) was verified using the CTD data collected from the South China Sea Monsoon Experiment (SCSMEX) (Chu et al., 2001, 2004). However, the value-added of the nowcast/forecast system on the Naval ASW has not been investigated.

The satellites use radiometers to measure the thermal radiation emitted by the sea surface (from which sea surface temperature is derived) and radar altimeters to measure sea surface height (SSH). The satellite data assimilation of SSH into MODAS was previously studied by Perry (2003) and Mancini (2004). Perry compared the acoustic coverage of the Generalized Digital Environmental Model (GDEM) and MODAS, with SSH data assimilation, and Perry found that MODAS provided more realistic acoustic coverage than GDEM. Mancini compared the acoustic coverage of MODAS, without SSH data assimilation, and MODAS, with SSH data assimilation. Mancini found that MODAS, with SSH assimilation, provided more realistic acoustic coverage than MODAS, without SSH data assimilation. However, value-added of the Navy's Geo-Satellite Follow-up (GFO) on the Naval ASW has not been studied.

B. PURPOSE

MODAS, with SSH data assimilation, gives a better depiction of the ocean environment. Altimeters that have different exact overhead repeat period will have different temporal and spatial resolutions. An altimeter's capability to resolve mesoscale features in the ocean is directly relate to the altimeters exact overhead repeat period. MODAS fields derived from an altimeter with an exact overhead repeat pattern designed to detect mesocale features should be different from MODAS fields derived from an altimeter that is not designed to detect mesocale features, especially in regions of high mesoscale variability. Large differences in the MODAS fields are related to different depictions of the undersea environment. The differences in the depiction of undersea environment may then change the outcome of a tactical engagement.

This thesis tries to answer the following questions: (1) What is the impact of the nowcast/forecast ocean models on the Naval ASW? (2) What is the difference of the

impact between nowcast and forecast systems? What is the impact of the Navy's satellite (GFO) on the Naval ASW? To answer these questions, the Weapon Acoustic Preset Program (WAPP) for the Mk 48 torpedo is used as the yardstick.

These questions are answered through studying the sensitivity of an ASW weapon system of a naval ASW system, specifically the Mk 48 torpedo WAPP, to ocean nowcast/forecast systems and to satellite altimeter orbit. The sensitivity analysis is conducted by examining the relative difference (RD) in the output of WAPP when two different SSP input fields. The only difference is how to establish these SSP fields such as one from the nowcast system and other from the forecast system (nowcast/forecast effect), or one from MODAS using TOPEX/POSEIDON (TPX) altimetry data and the other from MODAS using GFO altimetry data. The parameters in WAPP are held constant; therefore, any differences in the output were attributed to differences in the input.

THIS PAGE INTENTIONALLY LEFT BLANK

II. AREA OF INTEREST

The two areas below (Figure 1) are selected for analysis because of the high mesocale variability (Figure 2), tactical significance, and the availability of hydrographic data in the South China Sea used to evaluate both MODAS and POM with South China Sea Monsoon Experiment (SCSMEX) data (Chu et al., 2001, 2004). The northern box is hereby referred to as the East China Sea (ECS) and is bound by 25° N, 30° N, 120° E, and 130° E. The southern box is hereby referred to as the South China Sea (SCS) and is bound by 19° N, 23° N, 118° E, and 123° E.

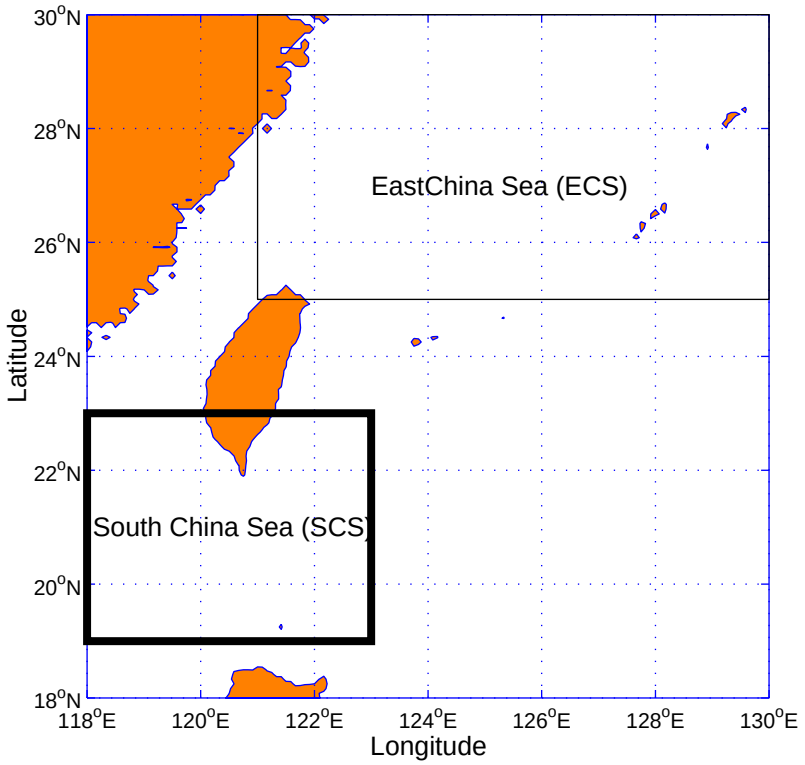

Figure 1. AOI for data analysis.

Data analysis was conducted in the ECS and SCS during the winter and summer of 2001. Six days (5, 10, 15, 20 25 and 30) and two months (JAN 2001 and JUL 2001) were selected for analysis in each box. A total of 24 cases (two areas of interest, two months, and six days in each month) were analyzed.

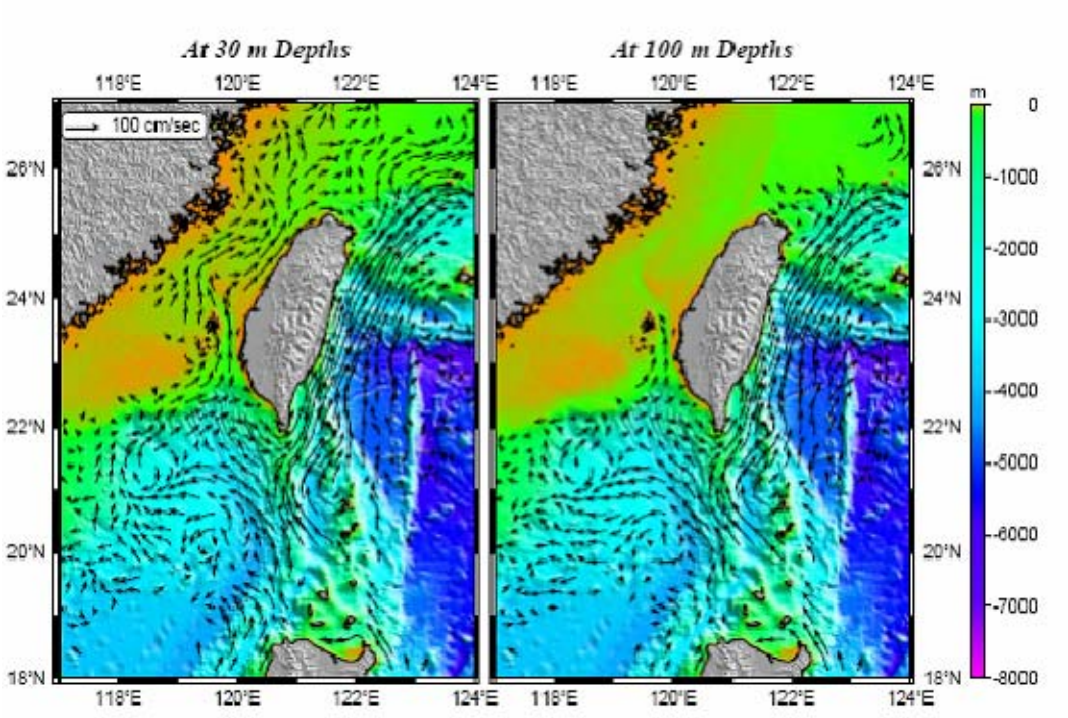

Figure 2. Composite of shipboard acoustic Doppler current profile (ADCP) during 1991-2001 in the vicinity of Taiwan. The left and right panel depict the complex subsurface structure at 30 and 100 meters, respectively (from Laing et al., 2002)

SCSMEX was a multi-national experiment in the SCS which studied the water and energy cycle of the Asian monsoon cycle (Chu et al., 2001). SCSMEX provided a unique opportunity to evaluate both the Princeton Ocean Model (POM) and MODAS. SCSMEX was conducted in the SCS from April through June 1998. During SCSMEX, the hydrographic data set included over 1700 CTD (Figure 3) and mooring stations (Chu et al., 2001).

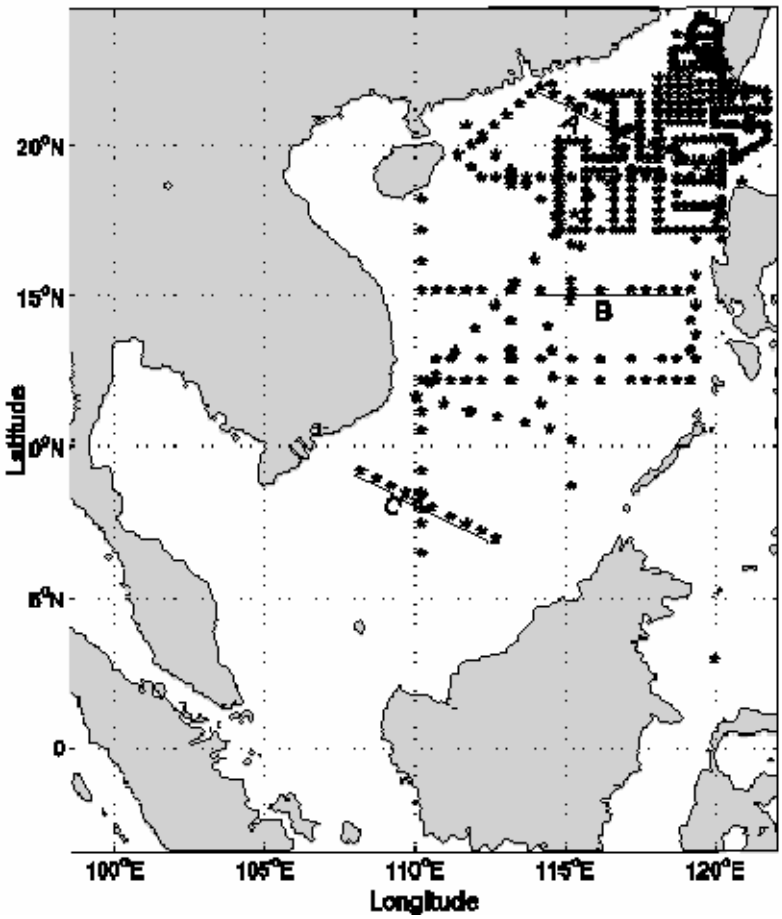

Figure 3. SCSMEX data has more than 1700 CTD observations. SCSMEX data was used to evaluate both POM and MODAS (from Chu et al., 2001).

THIS PAGE INTENTIONALLY LEFT BLANK

III. SATELLITE ORBIT ANALYSIS

GFO and TPX satellites have different exact overhead repeat patterns; therefore, GFO and TPX have different temporal and spatial resolutions. Orbit analysis was conducted in the ECS and SCS during the winter and summer of 2001 for both GFO and TPX satellites because of the high mesocale variability and the availability of hydrographic data in the ECS and SCS to evaluate both MODAS and POM performance.

Since GFO has smaller horizontal resolution, it is better at detecting mesocale features than TPX. The greatest difference in the MODAS fields generated by GFO and TPX will be in areas with the high mesoscale variability. Jiang et al. (1996) showed that spatially dense samples are preferred to temporal frequency samples in resolving mesoscale features in their simulated altimetry experiment for GEOSAT and TPX (Figure 4).

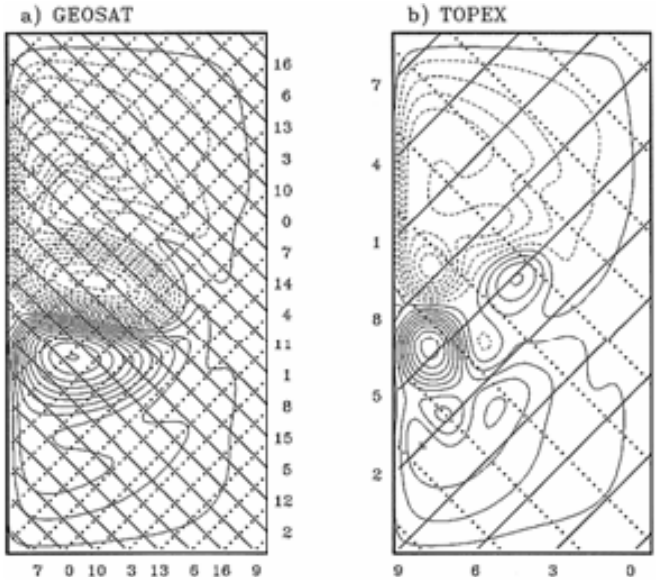

Figure 4. Resolution of mesoscale features such as the Western Boundary Currents and eddies identified from (a) GEOSAT , and (b) TPX. It is noted that GEOSAT has better resolution than TPX (from Jiang et. al., 1996).

A. GFO AND TPX ORBITS

The US Navy launched the GFO satellite in February 1998 from Vandenberg Air Force Base. GFO has an exact overhead repeat (+/- 1 kilometer) of 17 days with an orbit of 800 km, 108 degree inclination, 0.001 eccentricity, and 100-minute period.. The US

Navy launched GFO to resolve mesoscale features. GFO is capable of tracking the movement of El Nino and La Nina events across the Pacific and resolving eddies and western boundary currents.

NASA launched the TPX satellite on August 10, 1992 for a three-year mission from Kourou, French Guiana. TPX has an exact overhead repeat (+/- 1 kilometer) of 10 days with an orbit of 1336 km, circular, and 66-degree inclination. TPX was initially launched with 3-year mission that was extendable to six years. TPX ended up being in orbit for 12 years. JASON-1 was launched in 2001 to replace TPX. JASON-1 shadowed TPX and seamlessly replaced the TPX satellite altimeter.

GFO provides a better spatial resolution than TPX because GFO has a longer exact overhead repeat than TPX (Figure 5). Conversely, TPX provides a better temporal resolution than GFO because TPX has a shorter exact overhead repeat time than TPX. In fact, TPX completes three exact overhead repeat cycles during Julian dates 001-030 of 2001, and GFO completes approximately 1.76 exact overhead repeat cycles during Julian dates 001-030 of 2001.

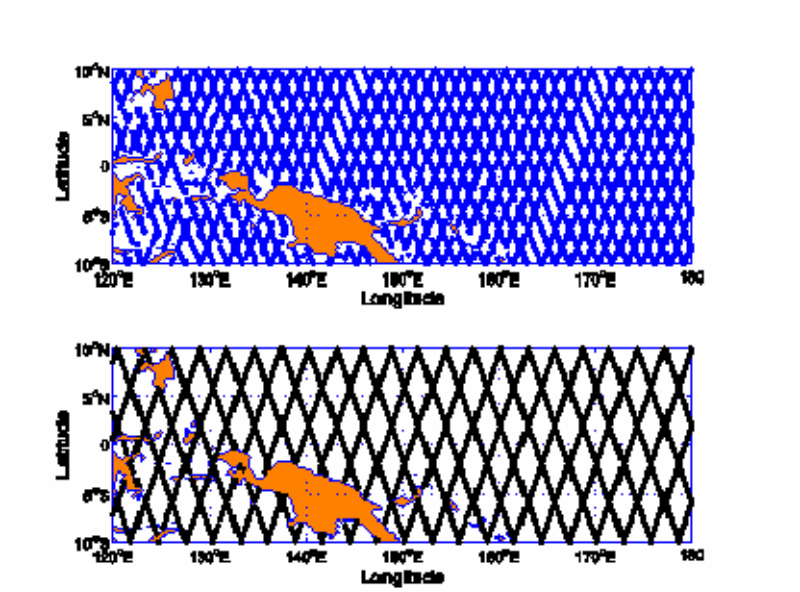

Figure 5. Equator Crossings GFO vs TPX. The blue orbital tracks on the top panel depict GFO orbit for Julian dates 001-030 in 2001, and The black orbital tracks on the bottom panel depict TPX orbit for Julian dates 001-030 in 2001. GFO has better spatial resolution, and TPX has better temporal resolution.

B. ORBIT ANALYSIS IN THE ECS AND SCS IN JANUARY 2001

Figures 6-8 depict the orbit tracks for GFO, TPX, and combined GFO and TPX coverage for ECS and SCS during Julian dates 001-030 in 2001. GFO clearly provides better spatial resolution than TPX because GFO has a spatially dense coverage than TPX for the same time period, as depicted in Figures 5 and 8.

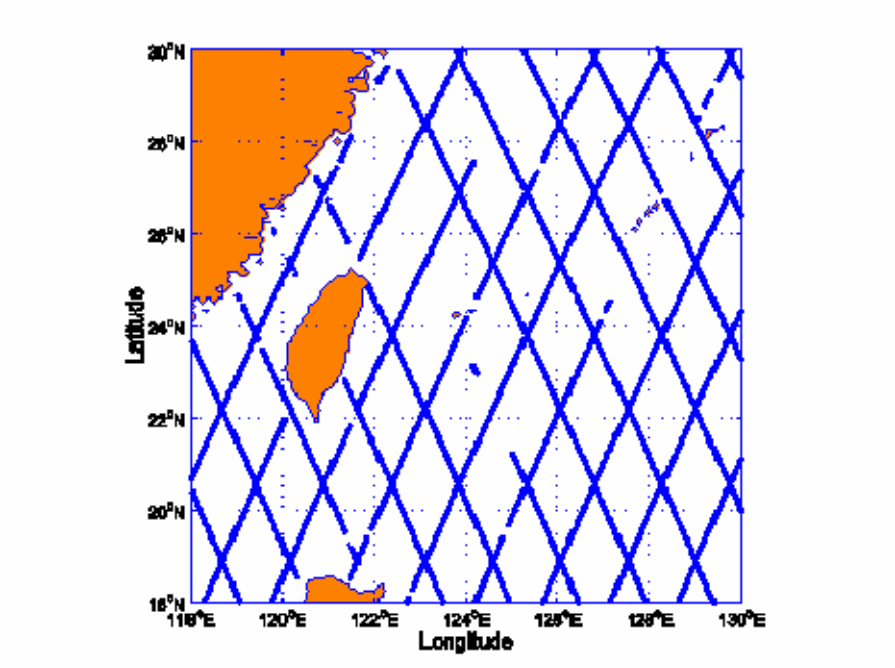

Figure 6. GFO orbital coverage of the ECS and SCS for Julian dates 001-030 in 2001.

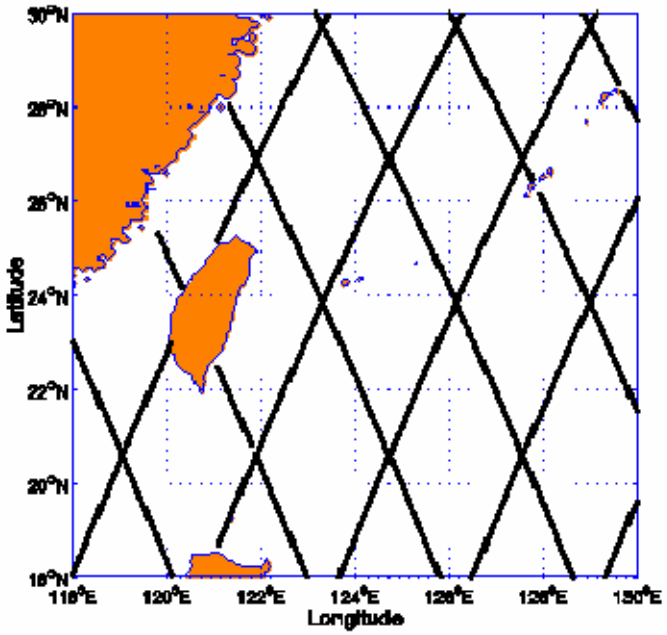

Figure 7. TPX orbital coverage of the ECS and SCS for Julian dates 001-030 in 2001.

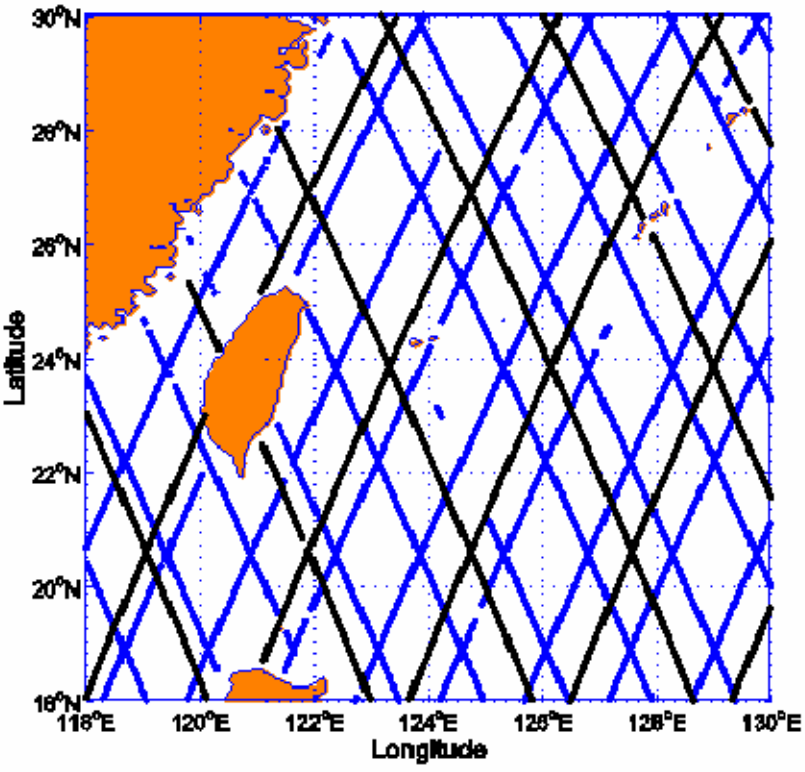

Figure 8. Combined GFO (Blue) and TPX (Black) orbital coverage of the ECS and SCS for Julian dates 001-030 in 2001.

IV. NAVY'S OCEAN NOWCAST/FORECAST SYSTEMS

A. MODAS

MODAS is the US Navy's premier dynamic climatology tool. MODAS operates in both a static and dynamic mode. In static mode, MODAS generates a bi-monthly, gridded climatology of temperature and salinity (Fox et al., 2002), which is similar to NOAA's World Ocean Atlas (WOA) climatology and the US Navy's Generalized Digital Environmental Model (GDEM). In the dynamic mode, MODAS provides the capability of modifying the historical climatology with remotely sensed SSH and SST, conductivity-temperature-depth (CTD), expendable bathythermograph (XBT), and air dropped expendable bathythermograph (AXBT) temperature and salinity profiles. MODAS can assimilate real-time observations and produce an "adjusted" climatology that more closely represents the actual ocean conditions. The dynamic climatology then provides the end user with nowcast depiction of the ocean's environment (Fox et al., 2002).

MODAS resolution ranges from ½ degree to 1/8 degree in gridded output. Since MODAS is comprised of temperature and salinity profiles in the above resolutions, the Sound Speed Profile for each temperature and salinity pair for each grid point can be calculated empirically, so MODAS provides a three dimensional output of temperature, salinity, and SSP (Fox et al., 2002).

Dynamic MODAS assimilates *in situ* measurements of the temperature and salinity by method known as Optimum Interpolation techniques (Fox et al. 2002). OI is a technique used for combining a first guess field and measured data by using a model of how nearby data are correlated. The first guess fields used by MODAS for the OI calculations are the previous day's field for SST and a large-scale weighted average of 35 days of altimetry for SSH. The static climatology is used for the SST first guess. Therefore, synthetic temperature profiles are generated by projecting these fields downward in the water column. The synthetic temperature profiles are projected to a depth of 1500 m utilizing an empirical relationships of the historical data which relates both SST and SSH to the subsurface temperature.

Similarly, OI is utilized in the salinity analysis, in situ salinity measurements can then be combined using OI to produce the final salinity analysis. The MODAS methodology is outlined in Figure 9. The final temperature and salinity analysis are what MODAS uses to produce the other derived fields, such as sound speed.

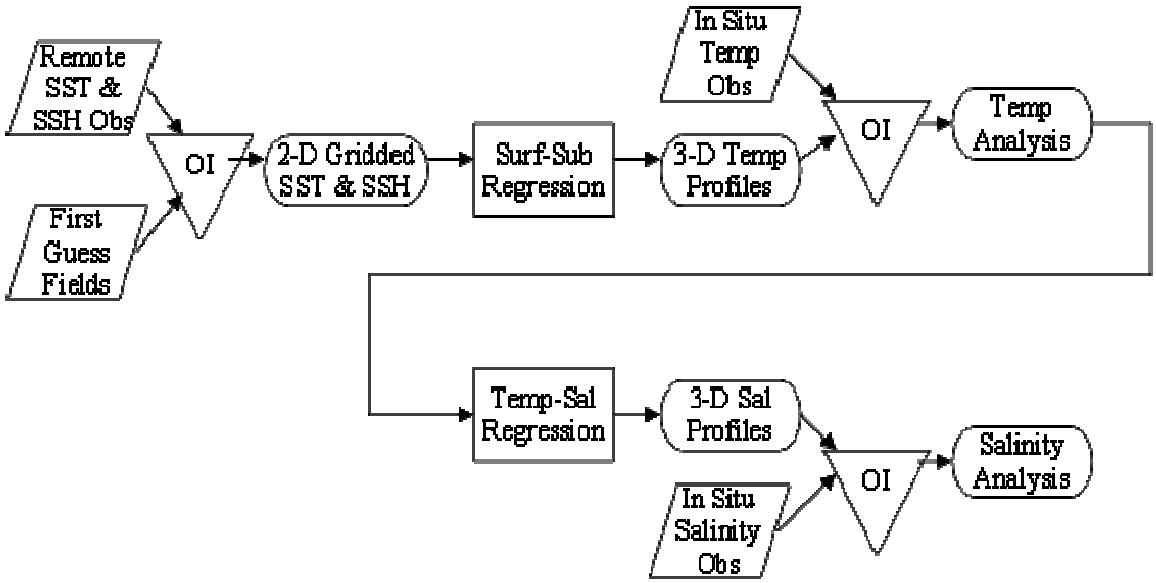

Figure 9. MODAS process flow. (from Mancini, 2004.)

B. EVALUATION OF MODAS USING SCSMEX DATA

Both observational and climatology where used in the verification of the value added of MODAS (Chu et al., 2004). The observational data were used as the benchmark to determine the error statistics for MODAS and climatology data. MODAS has added value if the difference between MODAS and observational data is smaller than the difference between climatological and observational data (Chu et al., 2004).

MODAS, climatological, and observational data are represented by ψ (temperature, salinity). The difference in ψ between MODAS and observational data is represented by

$$\Delta_m \psi(x_{i,} y_j, z, t) = \psi_m(x_{i,} y_j, z, t) - \psi_o(x_{i,} y_j, z, t) \tag{1}$$

The difference in ψ between climatology and observational data is

$$\Delta_c \psi(x_{i,} y_j, z, t) = \psi_c(x_{i,} y_j, z, t) - \psi_o(x_{i,} y_j, z, t) \tag{2}$$

The bias, mean-square–error (MSE), and root-mean-square-error (RMSE) between MODAS and observation are represented by

$$BIAS(m,o) = \frac{1}{N}\sum_i \sum_j \Delta_m \psi(x_{i,} y_j, z, t) \tag{3}$$

$$MSE(m,o) = \frac{1}{N}\sum_i \sum_j [\Delta_m \psi(x_{i,} y_j, z, t)]^2 \tag{4}$$

$$RMSE(m,o) = \sqrt{MSE(m,o)} \tag{5}$$

and between the climatology and observation are represented by

$$BIAS(c,o) = \frac{1}{N}\sum_i \sum_j \Delta_c \psi(x_{i,} y_j, z, t) \tag{6}$$

$$MSE(c,o) = \frac{1}{N}\sum_i \sum_j [\Delta_c \psi(x_{i,} y_j, z, t)]^2 \tag{7}$$

$$RMSE(c,o) = \sqrt{MSE(c,o)} \tag{8}$$

where N is the total number of horizontal points. To measure the model skill, we may compute the reduction of MSE over the climatological nowcast (Murphy 1988; Chu et al. 2001),

$$\mathrm{SS} = 1 - \frac{\mathrm{MSE}(m,o)}{\mathrm{MSE}(c,o)}, \tag{9}$$

which is called the skill score. SS is positive (negative) when the accuracy of the nowcast is greater (less) than the accuracy of the reference nowcast (climatology). Moreover, SS = 1 when MSE(*m*,*o*) = 0 (perfect nowcast) and SS = 0 when MSE(*m*,*o*)= MSE(*c*,*o*). To compute MSE(*c*, *o*), we interpolate the GDEM climatological monthly temperature and salinity data into the observational points (x_i, y_j, *z*, *t*).

Chu et al. (2004) show that MODAS has the capability to provide reasonably good temperature and salinity nowcast fields. The errors have a Gaussian-type distribution with mean temperature nearly zero and mean salinity of -0.2 ppt. The standard deviations of temperature and salinity errors are 0.98^{o}C and 0.22 ppt, respectively. The skill score of the temperature nowcast is positive, except at depth

between 1750 and 2250 m. The skill score of the salinity nowcast is less than that of the temperature nowcast, especially at depth between 300 and 400, where the skill score is negative (Figure 11).

Thermocline and halocline identified from the MODAS temperature and salinity fields are weaker than those based on SCSMEX data. The maximum discrepancy between the two is in the thermocline and halocline. The thermocline depth estimated from the MODAS temperature field is 10-40 m shallower than that from the SCSMEX data. The vertical temperature gradient across the thermocline computed from the MODAS field is around 0.14^{o}C/m, weaker than that calculated from the SCSMEX data (0.19^{o}-0.27^{o}C/m). The thermocline thickness computed from the MODAS field has less temporal variation than that calculated from the SCSMEX data (40-100 m). The halocline depth estimated from the MODAS salinity field is always deeper than that from the SCSMEX data. Its thickness computed from the MODAS field varies slowly around 30 m, which is generally thinner than that calculated from the SCSMEX data (28-46 m).

Using the SCSMEX observational data, the MODAS has better capability in 'nowcasting' temperature than 'nowcasting' salinity (Figure 10) evaluation of MODAS using SCSMEX demonstrates that MODAS provides reasonable 'nowcast' temperature and salinity field when compared to climatology (Chu et al., 2004). Chu et al. 2004, found that MODAS out performed climatology in temperature in depths less than 1750 meters (Figure 11) and that MODAS generally under predicted salinity fields in all depths.

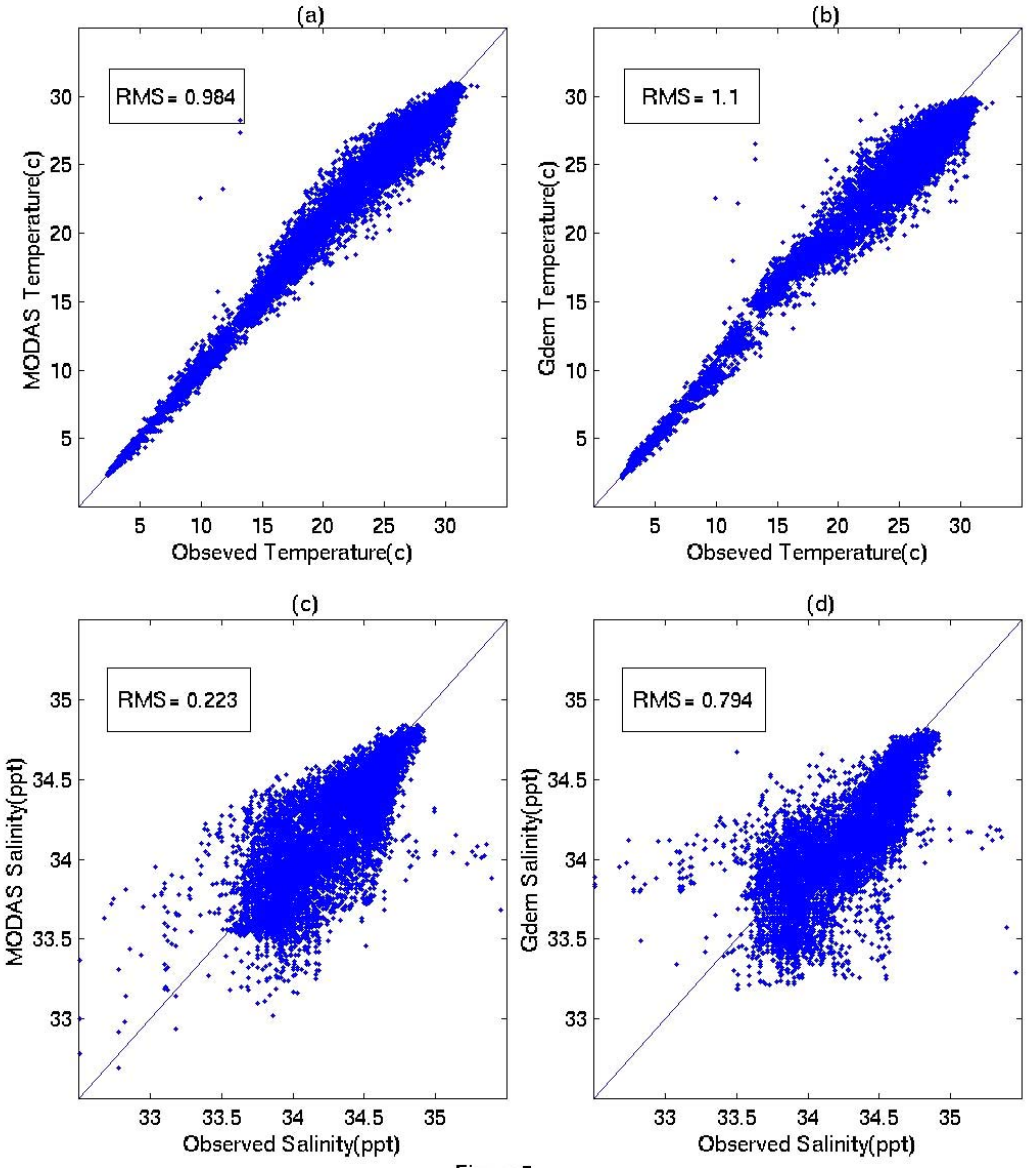

Figure 10. Scatter diagrams of (a) MODAS versus observational temperature, (b) MODAS versus observational salinity, (c) GDEM (climatology) versus observational temperature , (d) GDEM(climatology) versus observational salinity. (from Chu et al., 2004).

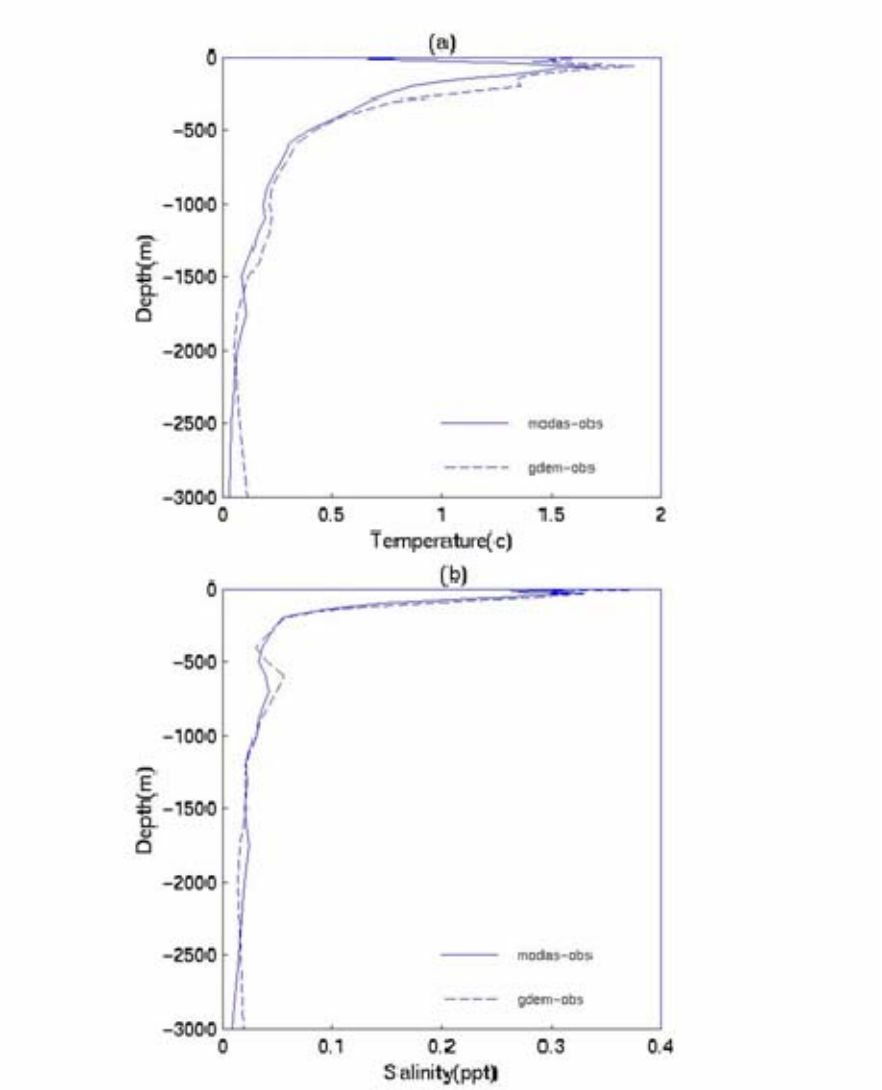

Figure 11. The RMSE between MODAS and observational data (solid) and between GDEM (climatology) and observational data (dashed): (a) temperature (deg C), and (b) salinity (ppt) (from Chu et al., 2004).

C. POM

POM is a general three dimensional gridded model that is time-dependent and utilizes primitive equations to model general circulation with realistic topography and a free surface (Chu et al., 2001, Mellor, 1998). POM was specifically developed to model nonlinear processes and mesocale eddy phenomena. POM has been proven to be an effective tool in investigating seasonal variability, multi-eddy dynamics, typhoon forcing, and synoptic forcing in the SCS.

D. EVALUATION OF POM USING SCSMEX DATA

Evaluation of the POM performance in the SCS was conducted by utilizing SCSMEX data. The evaluation of POM using SCSMEX data showed that POM has the capability to reasonably predict temperature fields and circulation patterns, but the POM was not skillful in predicting the salinity fields. However, when data was assimilated into the POM and allowed to run for one month, the hindcast capability of the POM increased for both the temperature and salinity fields. Data assimilation (Figure 12) into the POM therefore increased the POM's skill in hindcast capabilities (Chu et al., 2001).

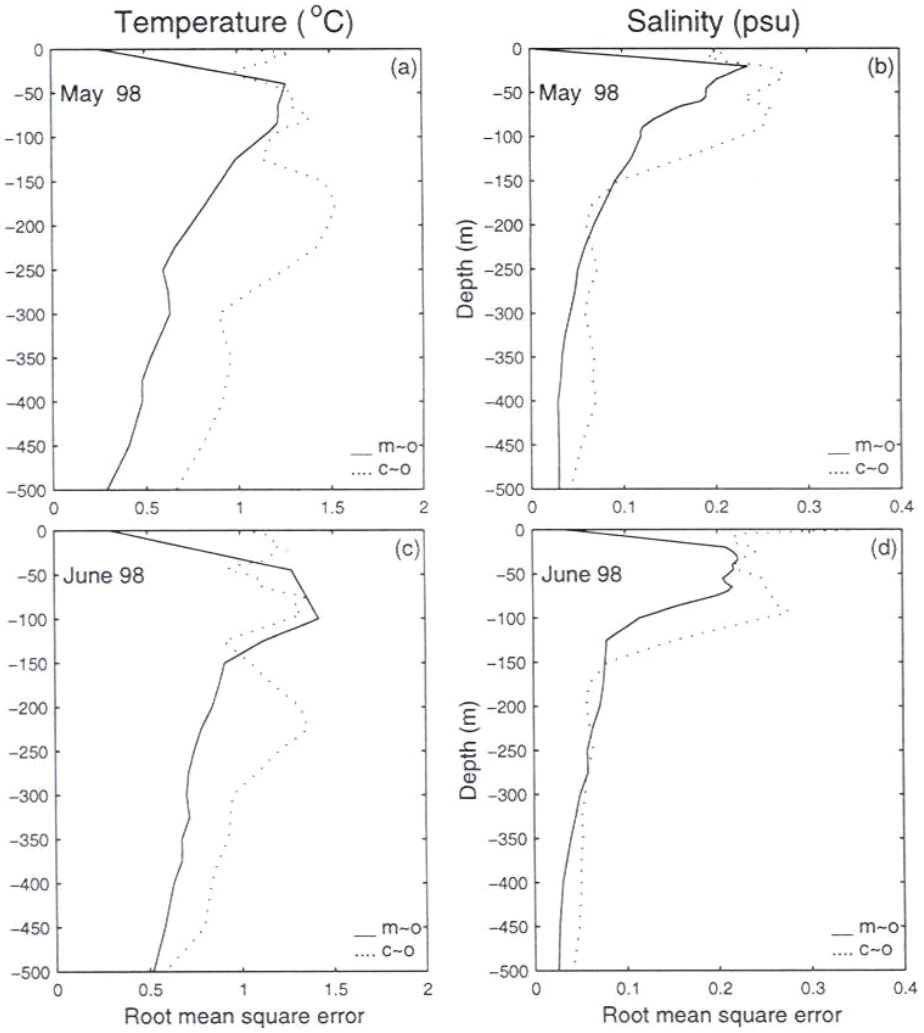

Figure 12. POM with data assimilation. The RMSE between POM (m) and SCSMEX observations (o) and between climo (c) and SCSMEX observations (o) for temperature and salinity during May and June 98. (from Chu et. al., 2001)

THIS PAGE INTENTIONALLY LEFT BLANK

V. WEAPON ACOUSTIC PRESET PROGRAM FOR ASW

A. WAPP

1. Background

WAPP provides the US Submarine Fleet with an on-board automated tool for generating the MK 48 and MK 48 ADCAP acoustic presets and visualizing the acoustic coverage for a given torpedo scenario. WAPP is based on Graphic User Interface (GUI) that allows the user to enter environmental, tactical, target, and weapon data. Once the user identifies the above presets for the weapon, WAPP generates a ranked list-set of search depth, search angle, pitch angle, laminar distance, ray trace, and an acoustic coverage map. The output from the WAPP enables the war-fighter to assess the tactical environment, acoustic environment, weapon presets, and current Target Motion Analysis (TMA).

The MK 48 and MK 48 ADCAP torpedoes utilize High-frequency sonar for search, detection, and homing on a given target. Accurate oceanographic environmental data is needed to correctly predict the acoustic coverage of the MK48 and MK 48 ADCAP torpedoes. The Applied Physics Laboratory and University Washington Technical Report 9407 (APL-UW TR 9407) High-Frequency Ocean Environmental Acoustic Models Handbook was used in programming the WAPP. APL-UW TR 9407 is the bible of High-Frequency modeling. High-Frequency SONAR models must incorporate volumetric sound scattering, sea state, shipping noise, biological ambient noise, and bottom loss to predict acoustic propagation accurately. The affect on acoustic propagation of above oceanographic parameters varies with frequency, so WAPP neglects the Low-Frequency and Medium-Frequency propagation effects and solely predicts the High-Frequency acoustic coverage for the MK 48 and MK 48 ADCAP torpedoes.

2. WAPP Ocean Environment Input

Ocean environment data is ingested by the WAPP from various operational oceanographic data sources, oceanographic models, and direct operator inputs. Base on the Date-Time-Group (DTG) and position of the submarine, WAPP extracts the projected

environment from the various data sources. Below Table 1 provides a summary of the data sources used by WAPP.

WAPP Environment Data Sources	
Data Source	Parameter
DBDB-V v4.2 (Level 2)	(Digital Bathymetric Data Base-Variable) Bottom Depth
GDEM-V v3.0	(Generalized Digital Environment Model) Sound Speed Profile
HIE (SN v5.3)	(Historical Ice Edge) Open Water/MIZ/Ice Cover (Under Ice warfare)
SMGC v2.0	(Surface Marine Gridded Climatology) Historic Wind Speed (Sea State)
BST v1.0	Bottom Sediment Type
VSS v6.3	Volume Scattering Strength Profile

Table 1. WAPP Environment Data Sources

The Environmental Data Entry Module (EDE), Figure 13, is the (GUI) that is used by the operator to enter environmental parameters. The EDE is the interface for entry and examination of the Sound Speed Profile (SSP) and entry of Sea State and Bottom Type.

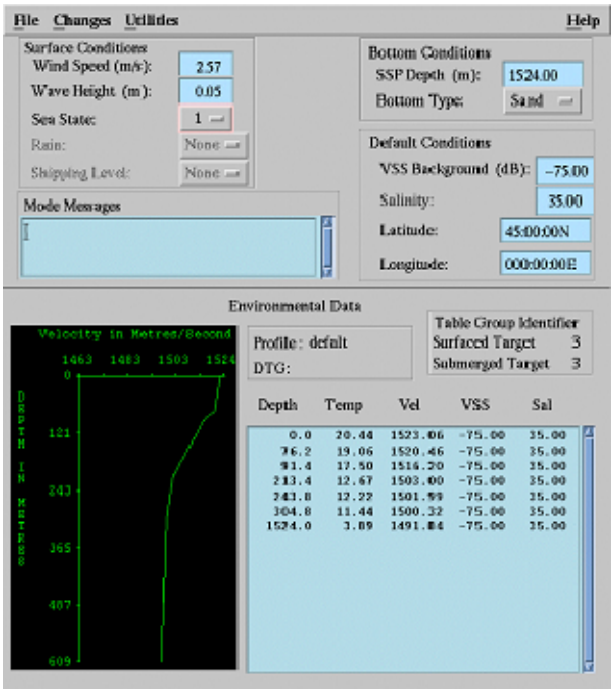

Figure 13. EDE GUI

a. WAPP EDE Surface Conditions

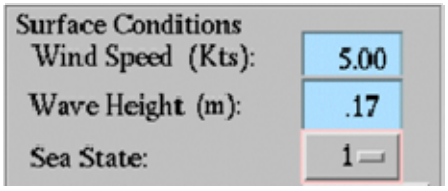

Figure 14. WAPP EDE Sea Surface input

WMO Sea State	Wind Speed (kts)	Significant Wave Height (m)
0	1.5	0
1	5	0.17
2	8.5	0.46
3	13.5	0.91
4	19	1.8
5	24.5	3.2
6	37.5	5.0
7	51.5	7.6
8	59.5	11.4
9	>64	>13.7

Table 2. WMO Convention (Sea State/Wind Speed/ Wave Height)

The sea surface condition is input directly by the operator into the EDE (Figure 14), or the wind speed and wave height is calculated using the World Metrological Organization convention (Table 2).

The sea surface condition impacts the WAPP predictions because acoustic energy suffers forward reflection loss after interacting with the surface (NUWC 2005). Additionally, the active SONAR pulse are reflected by the surface bubbles that increase with sea state; consequently reverberation increases with sea state and target detection decreases with sea state.

b. WAPP EDE Sea Bottom Conditions

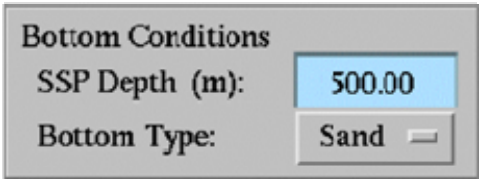

Figure 15. EDE Sea Bottom Condition

The sea bottom entry (Figure 15) consists of the SSP depth and bottom type. The bottom depth is directly extracted from the SSP. The SSP in use determines the depth. The bottom type button provides the operator the selection of the clay, mud, sand, gravel, and rock. The bottom is characterized by the upper 10 cm of the bottom for High-Frequency sonar. The Bottom Sediment Type (BST) is undergoing OAML certification. Once the BST database is OAML certified, the bottom type will automatically update in WAPP. Clay and mud bottom have the highest sound attenuation, and the rock bottom has the highest reflection.

c. WAPP EDE Water Column and Sound Speed Profile Display

Depth	Temp	Vel	VSS	Sal
.0	68.80	4996.90	-75.00	35.00
213.0	68.80	5000.40	-75.00	35.00
250.0	66.30	4988.40	-75.00	35.00
300.0	63.50	4974.40	-75.00	35.00
500.0	58.50	4949.80	-75.00	35.00
700.0	54.80	4931.10	-75.00	35.00
800.0	54.00	4927.80	-75.00	35.00
1000.0	52.60	4922.30	-75.00	35.00
1500.0	48.30	4902.50	-75.00	35.00

Figure 16. Water Column Table

WAPP generates a water column characteristics table (Figure 16) in the EDE with depth (ft or meters), temperature (degrees Celsius and Fahrenheit), volume scattering strength (dB), and salinity (ppt). WAPP uses an empirical formula in calculating the SSP given two of the three parameters (Temperature, Salinity, or SSP).

3. WAPP Acoustic Coverage Prediction

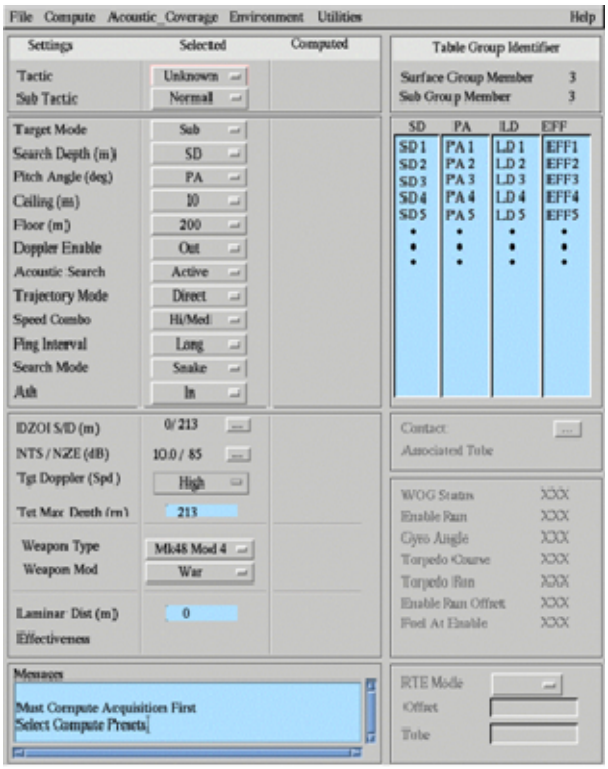

Figure 17. Acoustic Presets Module

The Acoustics Presets Module (Figure 17) is the GUI that allows the operator to set MK 48 tactical presets. The operators identifies tactics, target type (Surface or Submarine), Search Depth, Pitch Angle, search ceiling and floor, Doppler mode, ping interval, and search mode. Additionally, the operator can refine the Depth Zone of Interest (DZ), acoustic target strength (NTS), acoustic radiated noise of the target (NZE), and the anticipated target Doppler (Dead in Water, Low, High). Base on the variant of the MK 48 selected by the operator and other ballistic parameters, WAPP displays the ranked list-set calculated with the given environmental inputs, acoustic presets, target type, and ballistic parameters.

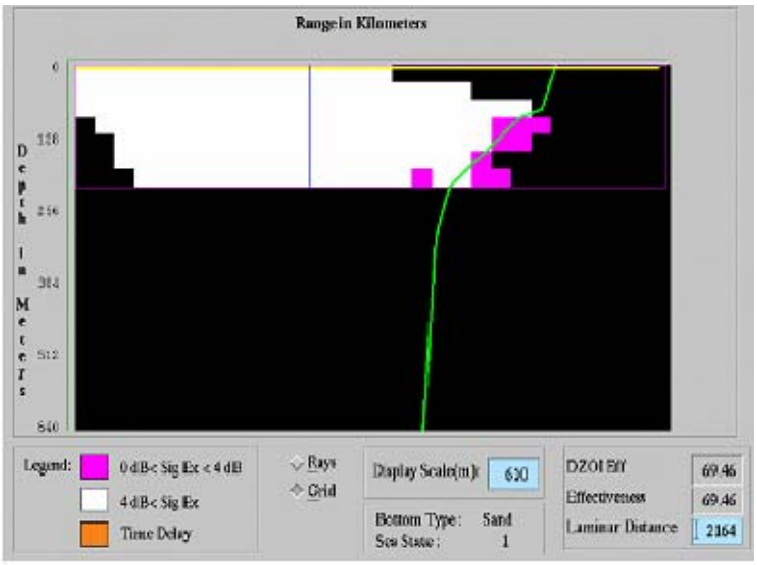

Figure 18. WAPP Acoustic Coverage Map

WAPP generates a graphical display (Figure 18) of the acoustic coverage base on the inputs in the EDE and Acoustic Preset Module. The acoustic coverage map graphically displays the ray trace, search ceiling and floor, laminar distance, and signal excess.

4. WAPP Preset Process

The WAPP preset process begins once all input parameters have been selected in the above described GUIs. The process is outlined in Figure 19 (NUWC, 2005, Mancini, 2004). First, valid search depth (SD) and search angle (SA) combinations are computed by utilizing a search angle selection algorithm to identify the optimal pitch angle for each search depth. Second, in series of time steps, the program traces a fan of rays that define the torpedo beam pattern for each resulting SD/SA combination (NUWC, 2005). The signal excess computation is mapped and gridded to the search region at each time step The signal excess map is used to depicts the area coverage (AC)of the search region with signal excess greater than 0 dB (Figure 18, white blocks) and 4 db (Figure 18, magenta blocks). The laminar distance (Figure 18, blue line), signal excess 'center of mass', is also depicted in the signal excess map. Third, WAPP then ranks the SD/SA combinations based on tactical guidance for the weapon and given tactical scenario. Finally, WAPP generates a recommendation based on the ranked list which preset combination is best for the given scenario.

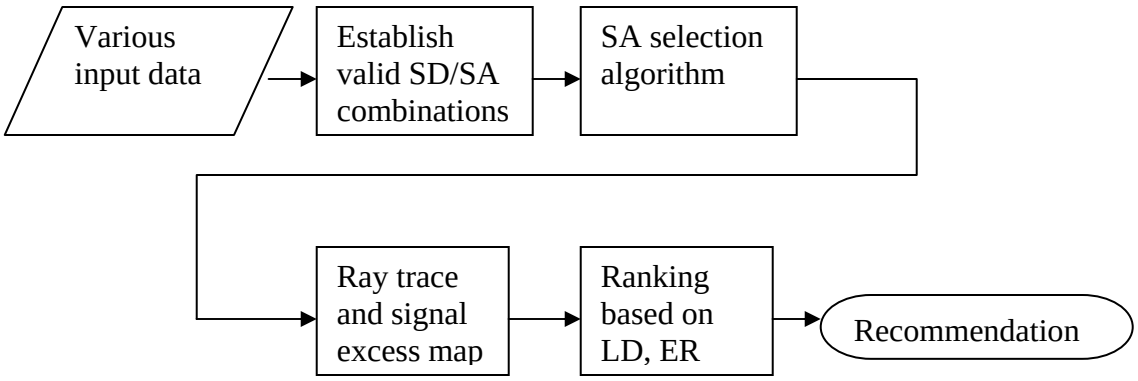

Figure 19. WAPP preset process (from Mancini, 2005)

THIS PAGE INTENTIONALLY LEFT BLANK

VI. SENSITIVITY OF WAPP TO OCEAN NOWCAST AND FORECAST SYSTEMS

A. WAPP OUTPUT

Figure 20 outlines the flow chart for the WAPP sensitivity analysis for SCSMEX MODAS and SCSMEX POM datasets. First, the SCSMEX MODAS and SCSMEX POM temperature and salinity fields were fed into WAPP. WAPP then calculates the sound speed from the respective temperature and salinity grid point pairs from the respective model. The default values in WAPP for volume scattering strength and surface and bottom roughness/reflectivity were used for each tactical scenario. Five different tactical scenarios were selected. The tactical scenarios are selected using the Acoustic Preset GUI (Figure 17). The five tactical scenario selected were high Doppler anti surface warfare (HD ASUW), low Doppler anti surface warfare (LD ASUW), low Doppler shallow anti submarine warfare (LD shallow ASW), high Doppler shallow anti submarine warfare (HD deep ASW), and low Doppler shallow anti submarine warfare (LD deep ASW). Shallow ASW is defined as maximum target depth of 213 meters, and deep ASW is define as maximum target depth of 396 meters (NUWC, 2005).

Second, WAPP outputs a ranked list-set of different SD/SA combination and acoustic coverage generated for the aforementioned tactical scenario for the respective MODAS and POM temperature and salinity fields. Third, a configuration management program which included a statistical software package was employed to compare the generated list set. Any differences in the output were attributed to differences in the input (NUWC, 2005).

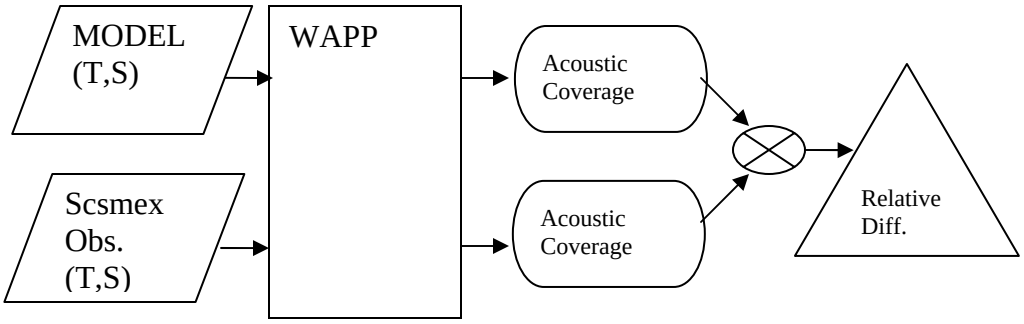

Figure 20. Flow chart of the sensitivity study of the model (POM and MODAS, respectively), temperature and salinity datasets, versus SCSMEX observational datasets, temperature and salinity datasets. The SCSMEX evaluation datasets of Models (POM and MODAS, respectively) versus Observations are ingested into WAPP to generate two sets (POM vs Obs, and MODAS vs OBS) of weapon acoustic preset (Acoustic Coverage). Computing the relative difference between the two acoustic coverages gives the sensitivity of the FORECAST and NOWCAST models (POM and MODAS, respectively).

Finally, the relative difference was calculated using a statistical package, which produced absolute values of the relative differences (RD) in area coverage (AC) for the identical SD/SA combination generated by WAPP,

$$\mathrm{RD} = \frac{\left|\mathrm{AC}_m - \mathrm{AC}_o\right|}{\mathrm{AC}_m} \tag{10}$$

and

$$\mathrm{RD} = \frac{\left|\mathrm{AC}_p - \mathrm{AC}_o\right|}{\mathrm{AC}_p} \tag{11}$$

Here, the subscripts *m* denotes MODAS, *p* denotes POM and *o* denotes observation.(Mancini, 2004)

WAPP generated SD/SA combinations that were the same and some that were different. The SD/SA combinations that were the same but had a different acoustic coverage were attributed to differences in the oceans environment (NUWC, 2005). The SD/SA combinations that were different and had different acoustic coverage were attributed to differences in torpedo target motion analysis (TMA) and ballistics.

A histogram of RD displays the number of same SD/SA combinations with area coverage relative differences in specified ranges, or bins. The probabilities of RD being greater than 0.1 and 0.15

$$\mu_1 = \text{Prob}\,(\text{RD} > 0.1), \quad \mu_2 = \text{Prob}\,(\text{RD} > 0.15),$$

are used for the determination of the sensitivity (Mancini, 2004).

Figures 21 and 22 below depict the distribution of the RD for the HD Deep ASW scenario for both POM and MODAS. The WAPP output for MODAS in the HD Deep ASW has a mean RD of 11.3, a standard deviation of 4.88, probability of RD>0.10 is 43.75 percent, and probability of RD>0.20 is 3.25 percent. The WAPP output for POM in the HD Deep ASW has a mean RD of 8.98, a standard deviation of 2.95, probability of RD>0.10 is 6 percent, and probability of RD>0.20 is 0.25 percent. Table 3 below summarizes the general statistics for all 10 tactical scenarios.

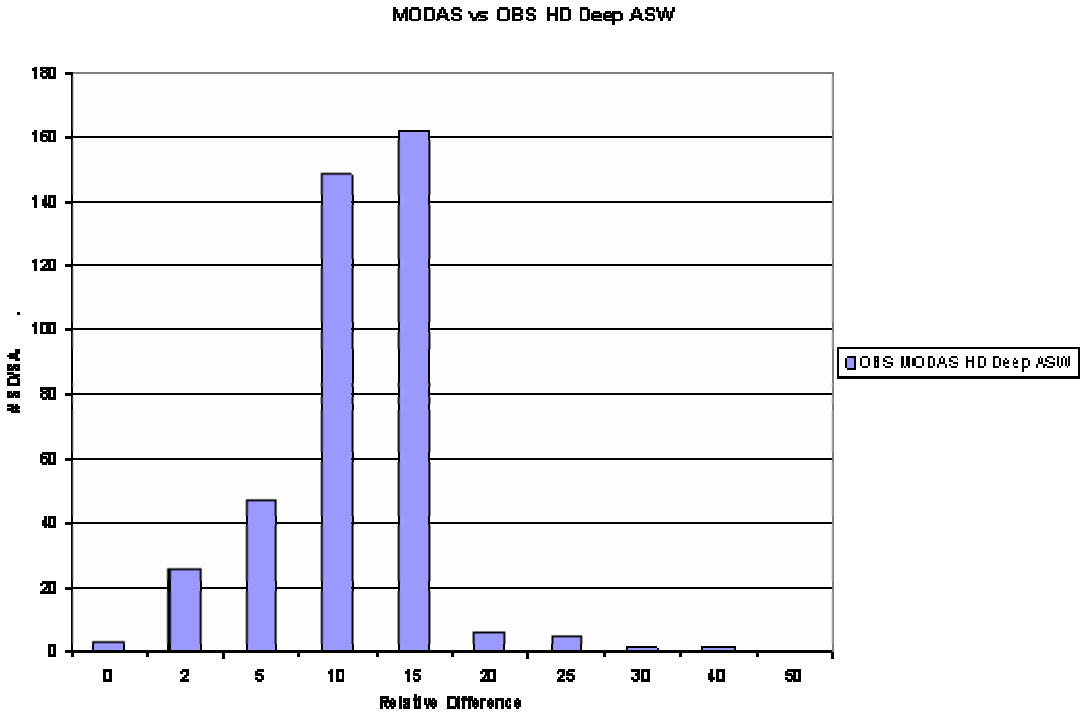

Figure 21. Wapp output for the relative difference between MODAS and SCSMEX (OBS) for HD deep ASW scenario. Mean is 11.3, standard deviation is 4.88, Prob (RD> 0.10) is 43.75%, and Prob (RD>0.15) is 3.25.

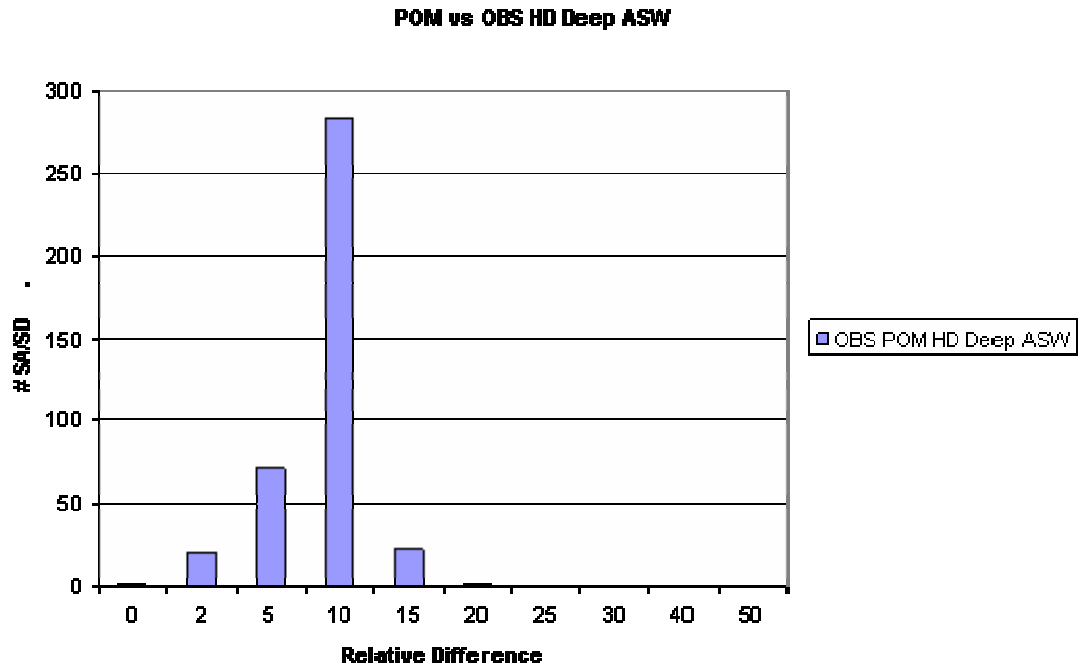

Figure 22. Wapp output for the relative difference between POM and SCSMEX (OBS) for HD deep ASW scenario. Mean is 8.98, standard deviation is 2.95, Prob (RD= 0.10) is 6%, and Prob (RD= 0.15) is 0.25%.

Figures 23 and 24 also provide a depiction of the probability curves for MODAS and POM, respectively. The probability curves for both MODAS and POM demonstrated the RD is greatest in the ASUW scenarios. The probability curves also demonstrate that probability of the RD>10 for MODAS is greater than POM. For example, the probability of the RD>10 for POM for the three ASW tactical scenarios is less than 10 percent; on the other hand, the probability of the RD>10 for MODAS for the three ASW tactical scenarios is greater than 10 percent.

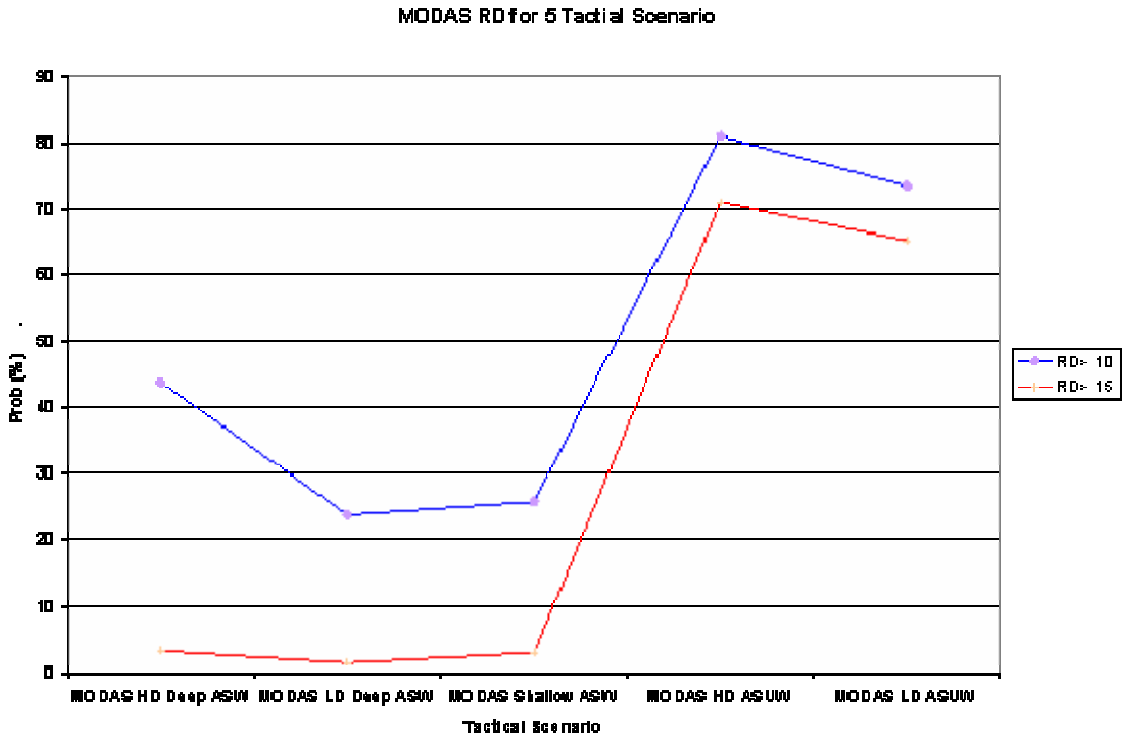

Figure 23. MODAS RD for 5 Tactical Scenarios

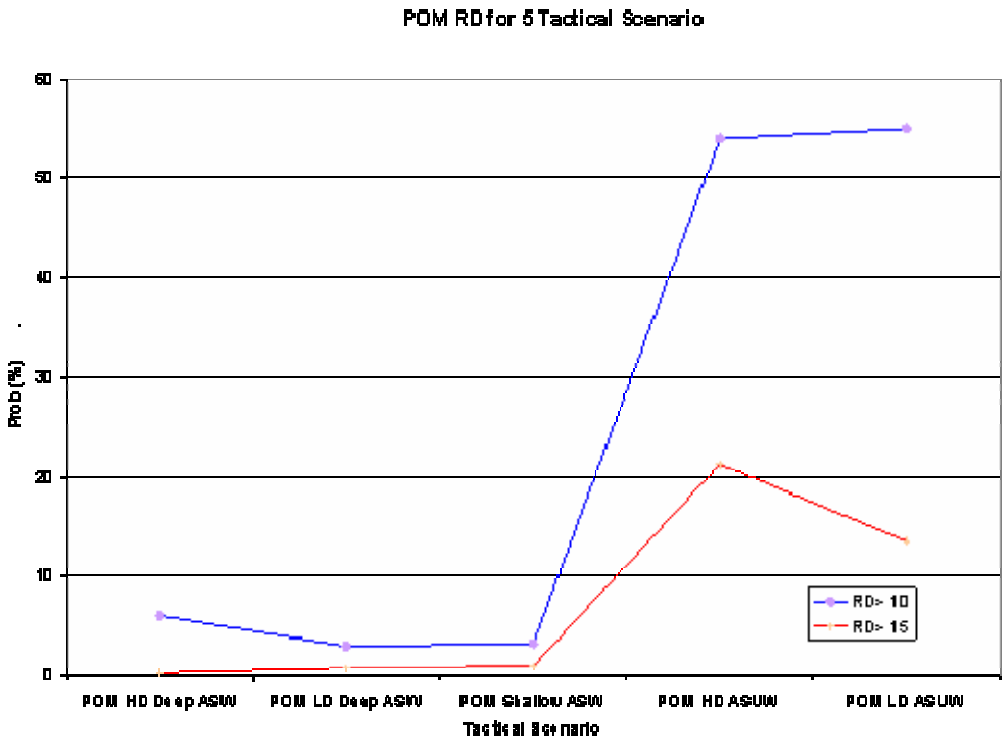

Figure 24. POM RD for 5 Tactical Scenarios

The mean RD probability curves for MODAS and POM have the same general shape (Figure 25). The mean RD for POM is less than the MODAS mean RD for all scenarios (Table 3). The difference for mean RD for the three ASW scenarios for POM is generally 2% less than the MODAS mean RD. The difference for the mean RD for the three ASUW scenarios for POM is generally 5% less than the MODAS mean RD. POM therefore adds more value to the ASW weapons system than MODAS, as summarized in Table 3.

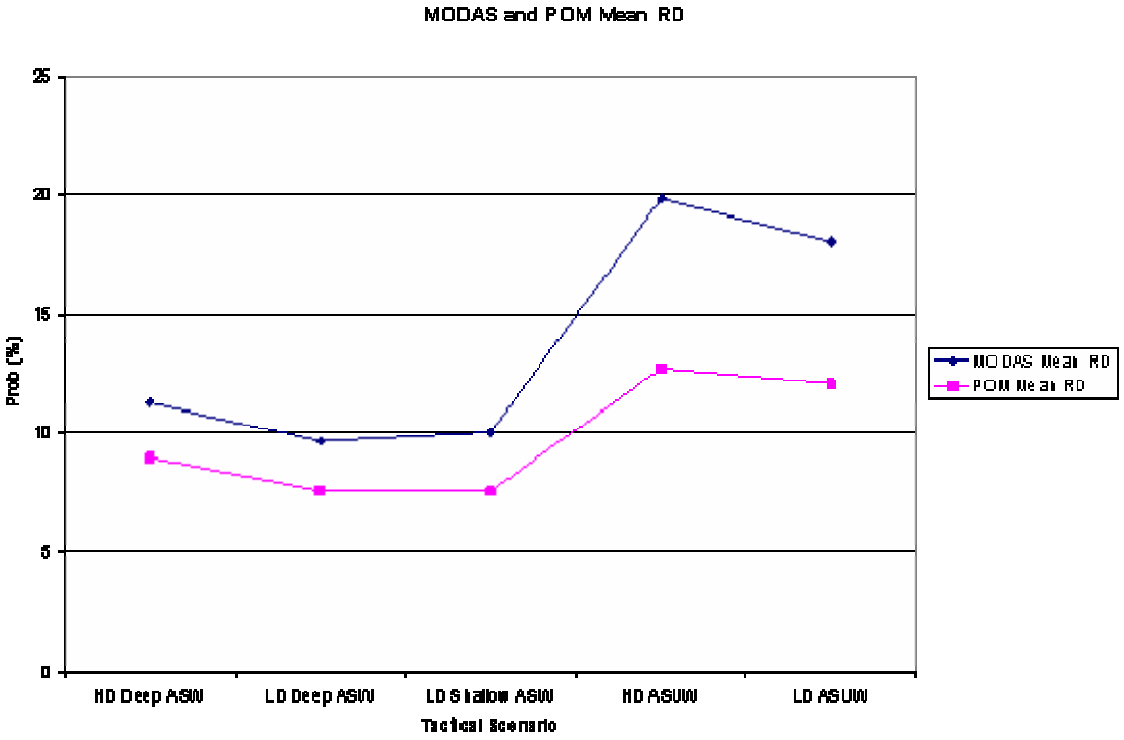

Figure 25. MODAS and POM Mean RD

Scenario	**Prob (RD>0.1) (%)**	**Prob (RD>0.15) (%)**	**Mean RD**	**Std Dev**
MODAS HD Deep ASW	43.75	3.25	11.3	4.88
POM HD Deep ASW	**6**	**0.25**	**8.98**	**2.95**
MODAS LD Deep ASW	23.75	1.5	9.66	4.41
POM LD Deep ASW	**3**	**0.75**	**7.59**	**3.56**
MODAS LD Shallow ASW	25.75	3	10.04	4.76
POM LD Shallow ASW	**3.25**	**1**	**7.58**	**3.62**
MODAS HD ASUW	81	71	19.83	7.89
POM HD ASUW	**54**	**21.21**	**12.73**	**5.79**
MODAS LD ASUW	73.5	65.25	18.04	7.76
POM LD ASUW	**55**	**13.25**	**12.08**	**5.51**

Table 3. Statistics summary of WAPP output for all tactical scenarios for MODAS and POM vs. Observations. For any given tactical scenario, POM (bold) has a smaller RD than MODAS.

THIS PAGE INTENTIONALLY LEFT BLANK

VII. SENSITIVITY OF WAPP TO SATELLITE ORBIT

Figure 26 outlines the flow chart for the WAPP sensitivity analysis for MODAS-GFO and MODAS-TPX datasets. MODAS fields initialized independently with GFO altimetry and TPX sea surface height (SSH) data were compared. The only difference between the MODAS field was the altimetry data. Once again, it is assumed that MODAS fields initialized by GFO (MODAS-GFO) will be more accurate than MODAS fields initialized by TPX (MODAS-TPX). The MODAS-GFO and MODAS-TPX fields were ingested into WAPP to examine the sensitivity of the USW weapon system. The MODAS-GFO fields were used as the benchmark to determine the error statistics for MODAS-TPX. The chief aim of this study is to identify the WAPP sensitivity to altimeter orbit. If there is a large relative difference between MODAS-GFO and MODAS-TPX fields in WAPP, WAPP is sensitive to altimeter orbit.

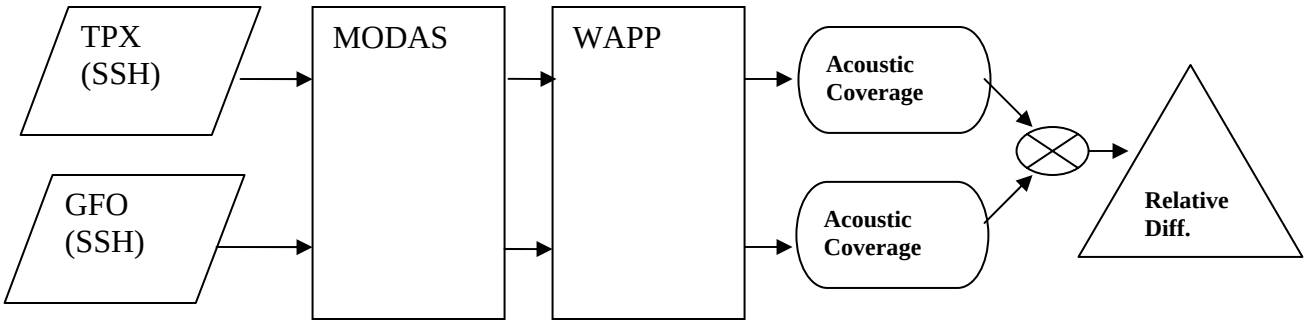

Figure 26. Flow chart of the sensitivity study of WAPP to TPX and GFO Sea Surface Height (SSH).

A. MODAS INPUT DIFFERENCE

MODAS-GFO and MODAS-TPX data are represented by ψ (temperature, salinity, sound speed (SS)). The difference in ψ between MODAS-TPX and MODAS-GFO data is:

$$\Delta_m \psi(x_{i,} y_j, z, t) = \psi_{mt}(x_{i,} y_j, z, t) - \psi_{mg}(x_{i,} y_j, z, t) \tag{12}$$

The bias, mean-square–error (MSE), and root-mean-square-error (RMSE) for MODAS,

$$BIAS(mt,mg) = \frac{1}{N}\sum_i \sum_j \Delta_m \psi(x_{i,} y_j, z, t) \tag{13}$$

$$MSE(mt,mg) = \frac{1}{N}\sum_i \sum_j [\Delta_m \psi(x_{i,} y_j, z, t)]^2 \tag{14}$$

$$RMSE(mt,mg) = \sqrt{MSE(mt,mg)} \tag{15}$$

where, N is the total number of horizontal points (Chu et al., 2004).

A total of 24 cases were analyzed. A case is comprised of an AOI (ECS or SCS), month (JAN or JUL), and day (5, 10, 15, 20, 25, or 30). Each was individually analyzed. The case for January 05, 2001 is a representative case of entire data set. The results of the remainder of the cases can be found in the appropriate appendix. The results are also summarized in table format in the conclusion section.

First, a statistical analysis was conducted on the on the MODAS-TPX and MODAS-GFO fields (SS, temperature, and salinity) before the respective MODAS fields were input into WAPP. The scatter plot (Figure27) for sound speed (SS) in the SCS on January 05, 2001 demonstrates a clustering around the $SS_{mg} = SS_{mt}$ line. The SS difference between MODAS-TPX and MODAS-GFO demonstrate a Gaussian-type distribution with a mean SS difference of -0.123 m/s and a standard deviation of 2.76 m/s. This result indicates that MODAS-GFO SS is generally faster than MODAS-TPX SS. The RMSD of SS between MODAS-TPX and MODAS-GFO increases from 1m/s at the surface to maximum of 5 m/s at 170 m and then decreases to approximately 0 m/s at 1000 m.

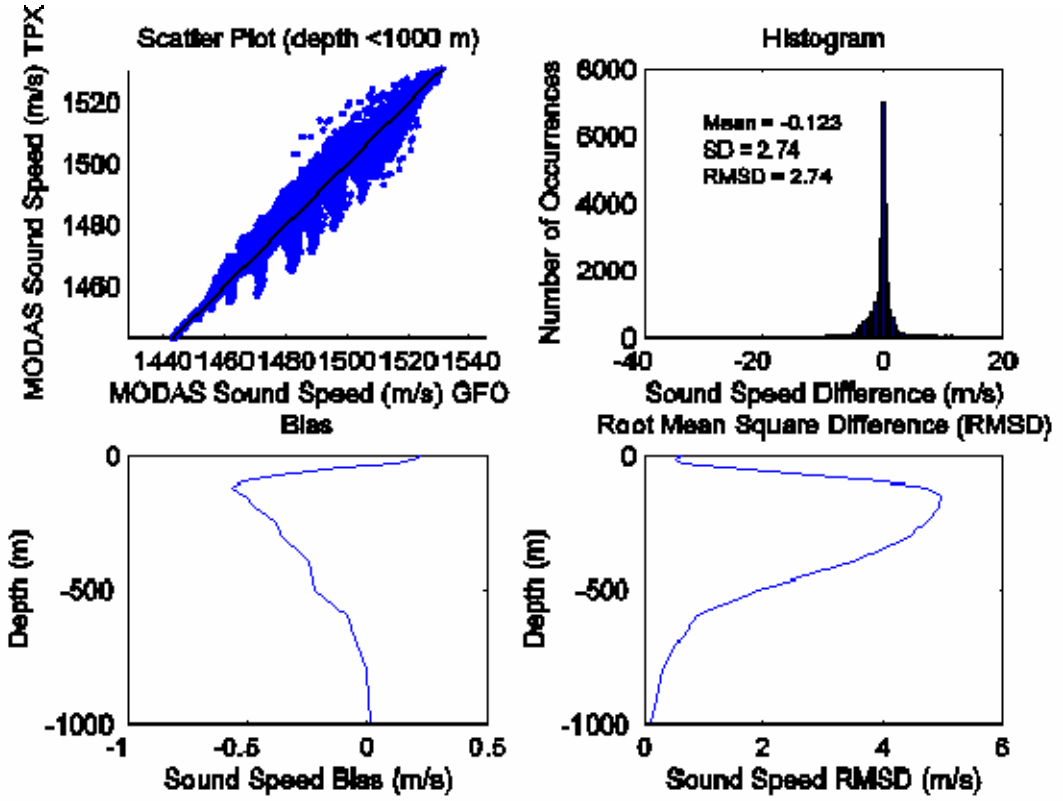

Figure 27. SCS MODAS sound speed statistics for January 05, 2001. Scatter plot MODAS-TPX vs MODA-GFO (a), Sound speed difference histogram (b), Sound speed bias (c), and sound speed RMDS (d).

The horizontal difference in SS between MODAS-TPX and MODAS-GFO is depicted in both Figures 28 and 29. Figure 28 depicts the horizontal difference at four depths (75m, 200m, 400m, and 600 m) in the SCS, and the red asterisks indicate the position of the SSPs in Figure 29. Figure 29 is a plot of the SSPs for MODAS-TPX and MODAS-GFO at the indicated position for all depths. For example, in Figures 29(d) and 29(g), MODAS-TPX SSP is faster than MODAS-GFO, and Figure 28 indicates a positive horizontal difference in SSP for the respective positions of Figures 29(d) and 29(g). The general shape of the SSP is the same for both MODAS-TPX and MODAS-GFO; however there is an offset in SSPs for MODAS-TPX and MODAS-GFO.

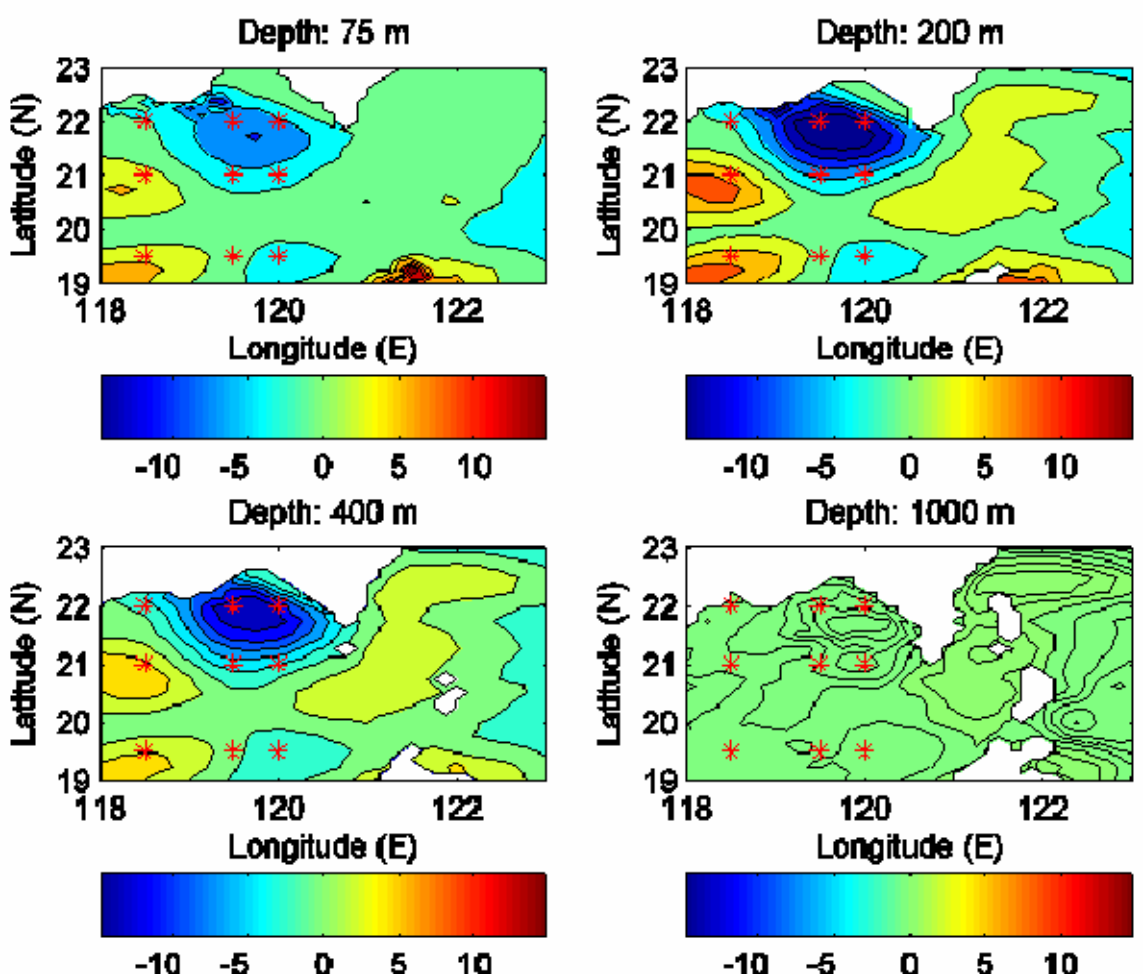

Figure 28. SCS MODAS horizontal difference in SSPs for January 05, 2001. The horizontal difference in SSP (m/s) between MODAS-GFO and MODAS-TPX is depicted at four depths (75m, 200m, 400m, and 600 m). The red asterisk indicates position of SSP in Figure 29.

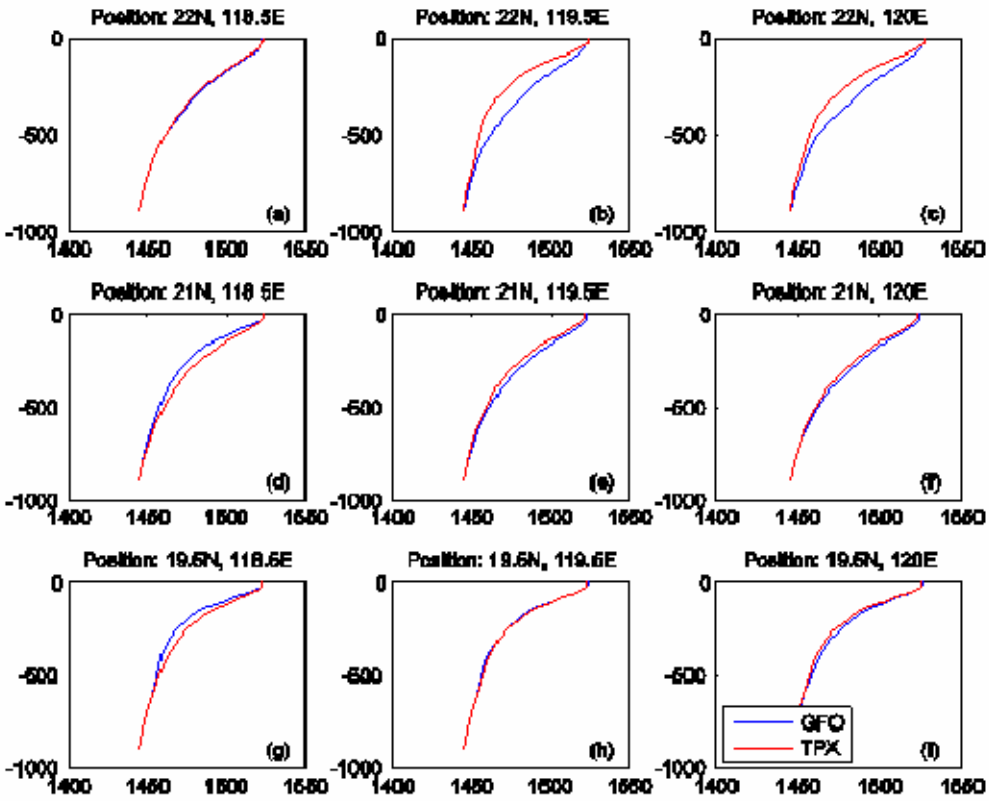

Figure 29. SCS MODAS SSPs for January 05, 2001. The MODAS-TPX SSP is red and MODAS-GFO is blue. The respective SSP is plotted in the position where there was a large positive or negative difference in SSP (red asterisks in Figure 28).

MODAS-TPX and MODAS-GFO SSPs had the largest difference in January 05, 2001 in the SCS, and the difference between MODAS-TPX and MODAS-GFO SSPs continued to decrease through out the month of January 2001. Figures 30 and 31 depict the horizontal difference is SS for January 30, 2001. Both Figures 30 and 31 show that horizontal SS difference between MODAS-TPX and MODAS-GFO is decreasing for the SCS. In fact, by inspection of the SSPs for January 05 (Figure 30) and January 30 (Figure 31), the SSPs for MODAS-TPX and MODAS-GFO are converging.

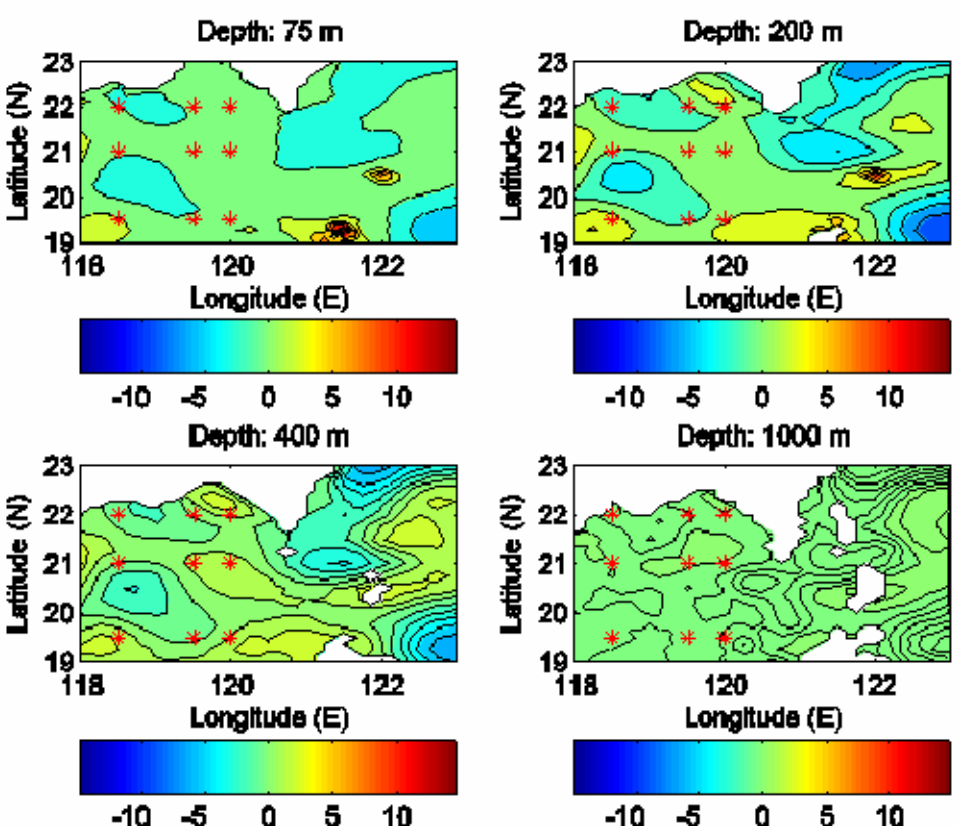

Figure 30. SCS MODAS horizontal difference in SSPs for January 30, 2001. The horizontal difference in SSP (m/s) between MODAS-GFO and MODAS-TPX is depicted at four depths (75m, 200m, 400m, and 600 m). The red asterisk indicates position of SSP in Figure 31.

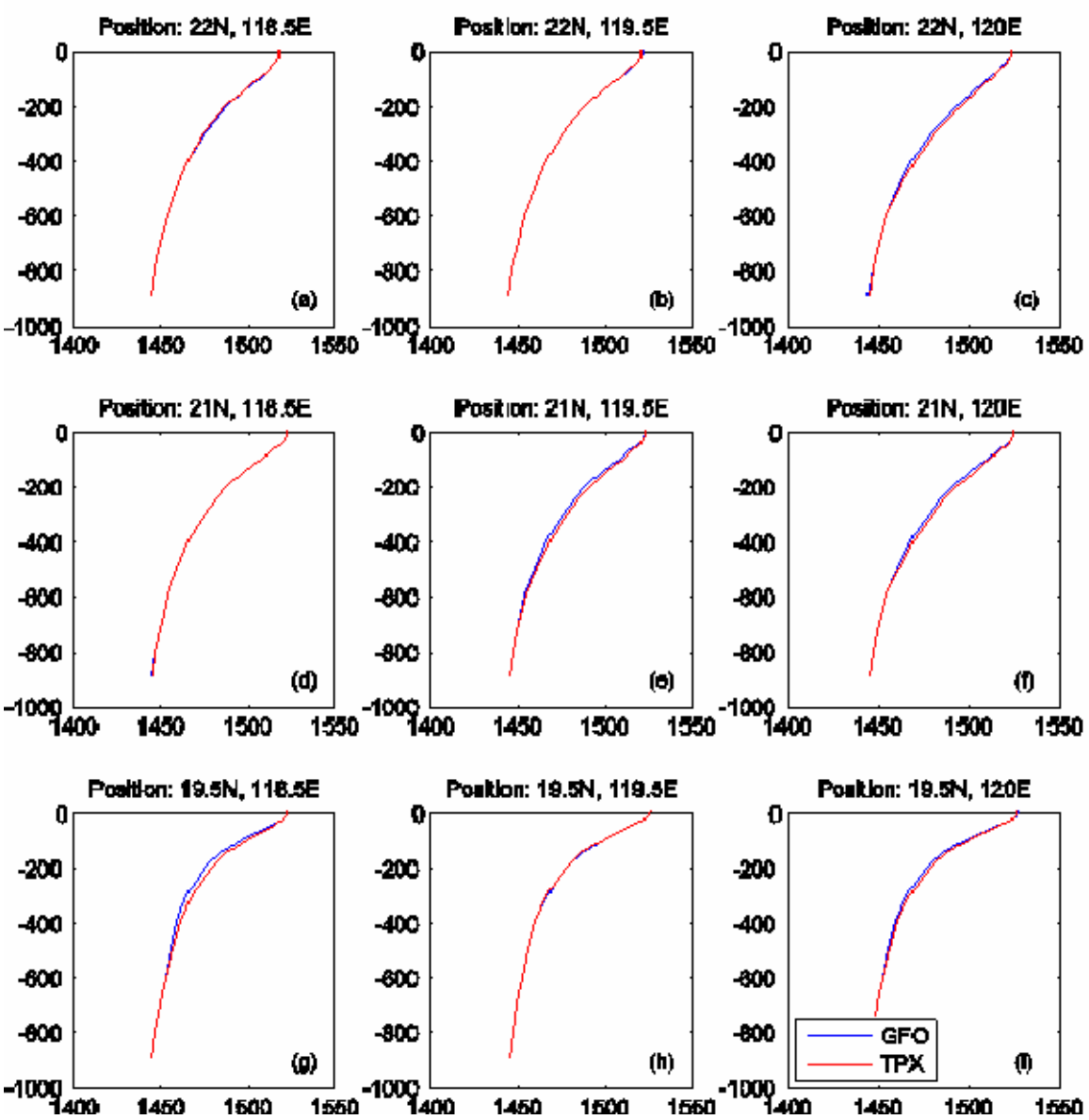

Figure 31. SCS MODAS SSPs for January 30, 2001. The MODAS-TPX SSP is red and MODAS-GFO is blue. The respective SSP is plotted in the position where there was a large positive or negative difference in SSP (red asterisks in Figure 30).

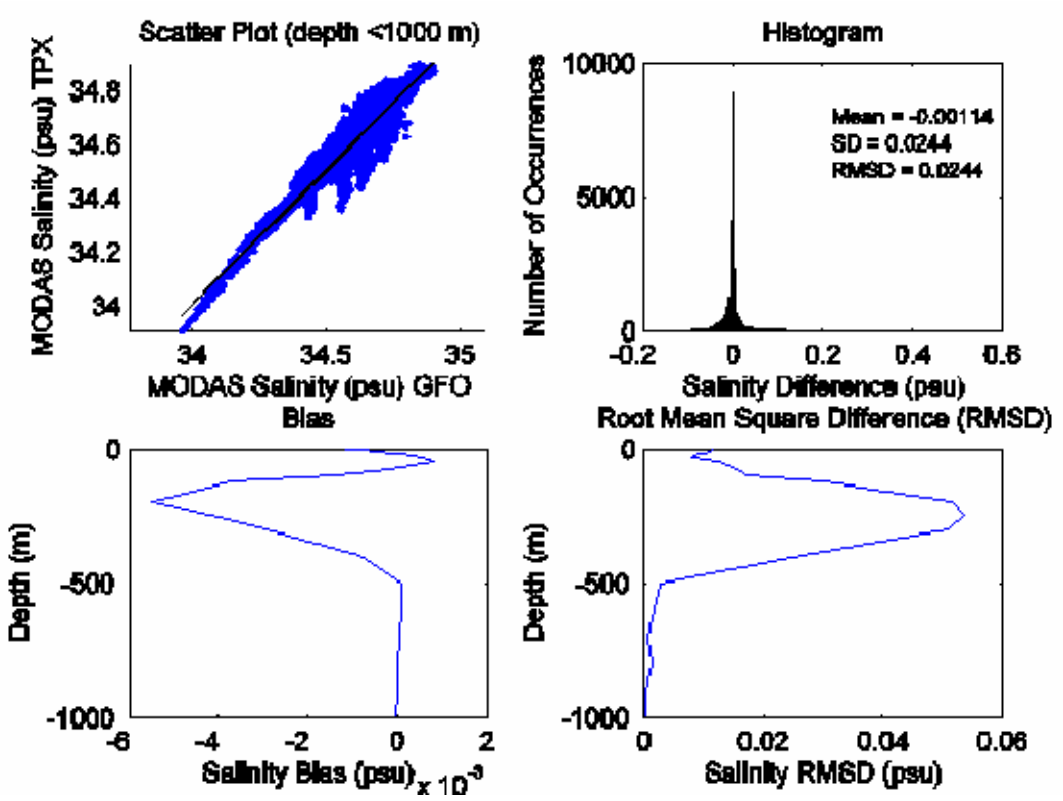

Figure 32. SCS MODAS salinity statistics for January 05, 2001. Scatter plot MODAS-TPX vs MODA-GFO (a), salinity difference histogram (b), salinity bias (c), and salinity speed RMSD (d).

The scatter plot for salinity (Figure 32) demonstrates a clustering around the $S_{mg} = S_{mt}$ line. The errors for temperature demonstrate a Gaussian-type distribution with a mean salinity difference of 0.00114 psu and a standard deviation of 0.0244 psu. This result indicates MODAS-GFO salinity is statically identical to the MODAS-TPX salinity. The RMSD of salinity between MODAS-GFO and MODAS-TPX increases from 0.02 psu at the surface to maximum of 0.06 psu at 300 m and then decreases to 0.05 psu at 1000 m.

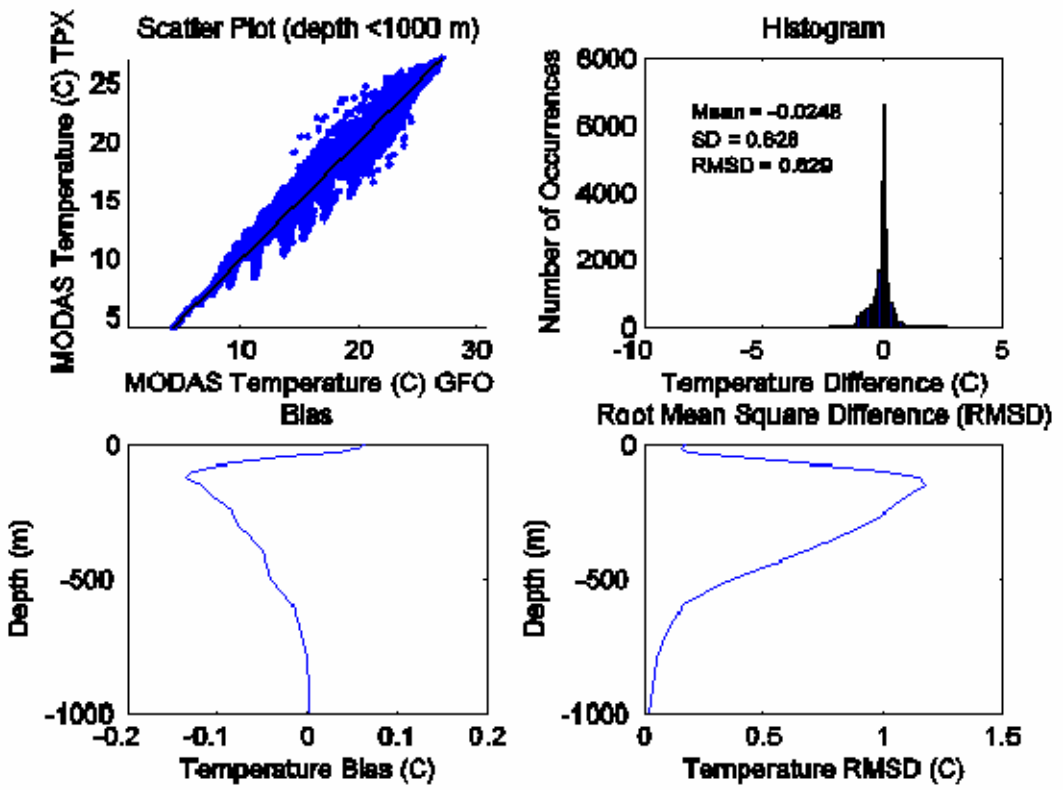

Figure 33. SCS MODAS temperature statistics for January 05, 2001. Scatter plot MODAS-TPX vs MODA-GFO (a), temperature difference histogram (b), temperature bias (c), and temperature RMDS (d).

The scatter plot for temperature (Figure 33) demonstrates a clustering around the $T_{mg} = T_{mt}$ line. The errors for temperature demonstrate a Gaussian-type distribution with a mean temperature difference of $0.0248^{\circ}C$ and a standard deviation of $0.628^{\circ}C$. This result indicates MODAS-GFO temperature is warmer MODAS-TPX temperature. The RMSD of temperature between MODAS-GFO and MODAS-TPX increases from $0.25^{\circ}C$ at the surface to maximum of $1.25^{\circ}C$ at 200 m and then decreases to $0.20^{\circ}C$ at 1000 m.

B. WAPP OUTPUT DIFFERENCE

The MODAS-GFO and MODAS-TPX temperature and salinity fields were fed into WAPP. WAPP then calculated the sound speed from the respective temperature and salinity grid point pairs from the respective MODAS fields. The default values in WAPP for volume scattering strength and surface and bottom roughness/reflectivity were used for each tactical scenario. Five different tactical scenarios were selected. The tactical scenarios are selected using the Acoustic Preset GUI (Figure17). The five tactical

scenario selected were high Doppler anti surface warfare (HD ASUW), low Doppler anti surface warfare (LD ASUW), low Doppler shallow anti submarine warfare (LD shallow ASW), high Doppler shallow anti submarine warfare (HD deep ASW), and low Doppler shallow anti submarine warfare (LD deep ASW). Shallow ASW is defined as maximum target depth of 213 meters, and deep ASW is define as maximum target depth of 396 meters (NUWC, 2005). In other words, each of the 24 cases has 5 tactic scenarios (120 tactic scenarios were analyzed), and each tactic scenario was comprised of over 14,000 MODAS-TPX and MODAS-GFO grid point pairs.

Second, WAPP outputs a ranked list-set of different SD/SA combination and acoustic coverage generated for the aforementioned tactical scenario for the respective MODAS-GFO and MODAS-TPX grid point pairs. The same configuration management program used to evaluate POM and MODAS was employed to generate the list set.

Finally, the relative difference was calculated using a statistical package, which produced absolute values of the relative differences (RD) in area coverage (AC) for the identical SD/SA combination generated by WAPP,

$$\mathrm{RD} = \frac{\left|\mathrm{AC}_{mg} - \mathrm{AC}_{mt}\right|}{\mathrm{AC}_{mg}}.$$

Here, the subscripts *mg* denotes MODAS-GFO and *mt* denotes MODAS-TPX.

WAPP generated SD/SA combinations that were the same and some that were different. The SD/SA combinations that were the same but had a different acoustic coverage were attributed to differences in the ocean's environment (NUWC, 2005). The SD/SA combinations that were different and had different acoustic coverage were attributed to differences in torpedo target motion analysis (TMA) and ballistics. So, any differences in the output were attributed to differences in the input because all other parameters were constant (NUWC, 2005).

Initially, it was assumed that a RD in acoustic coverage of 20% will significantly change the outcome of a tactical engagement. Figure 34 depicts two cases where there is a 20 % difference of acoustic coverage in the torpedo acoustic cone (NUWC, 2005). The two cases depicted in Figure 34 are a screen capture of torpedo engagement simulation in

MATLAB conduct by the Naval Undersea Warfare Command (NUWC, Newport). Each dot is a probable contact and is red until the acoustic cone of the torpedo passes over the dot. The dot turns yellow when the torpedo has a detection opportunity. The torpedo then enters into its detection, acquisition, and verification phases. If a dot remains in the acoustic cone long enough to complete the detection, acquisition, and verification phases, the torpedo will likely enter homing, a green dot.

In the first case (Figure 34a), 94.2% of tracks enter the acoustic cone and 46.7% enter homing with an overall coverage score of 47.7 %. In the second case (Figure 34b), when the acoustic coverage was reduce by 20%, 89.6% of tracks enter the acoustic cone and only 16.3% enter homing with an overall coverage score of 33.8%. In other words, a relative difference greater than 20% leads to an engagement that is 1/3 as likely to lead to mission success. So, a relative difference of 20% is large enough to change an engagement. A speculative regression curve that is bound by the by first and second case infers that a RD of between 10 and 15 percent would yield an overall coverage score between 47.7% and 33.8%.

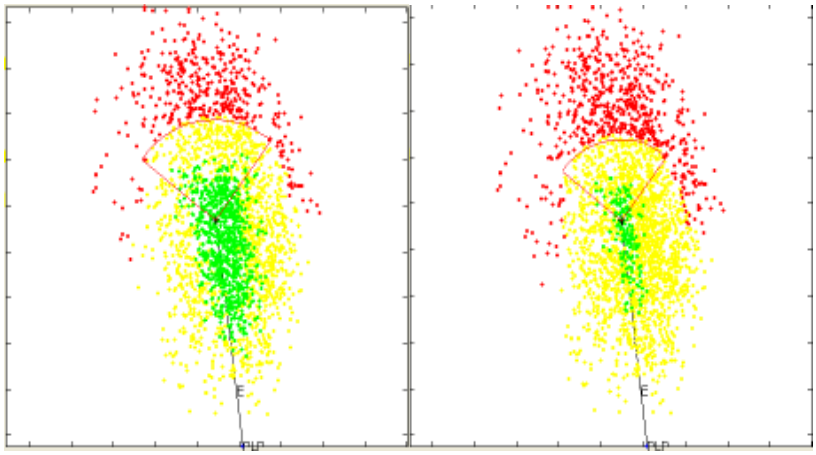

Figure 34. Horizontal acoustic coverage map. The two case depicted a typical acoustic cone for a torpedo (a) and an acoustic cone reduced by 20% (b). A red indicates a probable contact. A red dot turns yellow when the torpedo has a detection opportunity. If a dot remains in the acoustic cone long enough to complete the detection, acquisition, and verification phases, the torpedo will likely enter homing, a green dot.

Data analysis proved that most the cases studied herein had a low probability that the RD is greater than 20%. A histogram of RD displays the number of same SD/SA combinations with area coverage relative differences in specified ranges, or bins, and the probabilities of RD being greater than 0.1 and 0.15

$$\mu_1 = \text{Prob}\,(\text{RD} > 0.10), \quad \mu_2 = \text{Prob}\,(\text{RD} > 0.15),$$

are then used for the determination of the sensitivity.

1. WAPP Results

The results for the 24 cases analyzed have the same general trend. Similar to the results from Mancini, 2004, the ASUW scenarios had larger relative differences than the ASW scenarios. Mancini found the probability values (RD) decrease with increasing tactic depth band. In all scenarios, the probability values decreased with increasing tactic band; Figure 35 depicts that all three ASW scenarios have lower probability values than the ASUW scenarios for January 05, 2001.

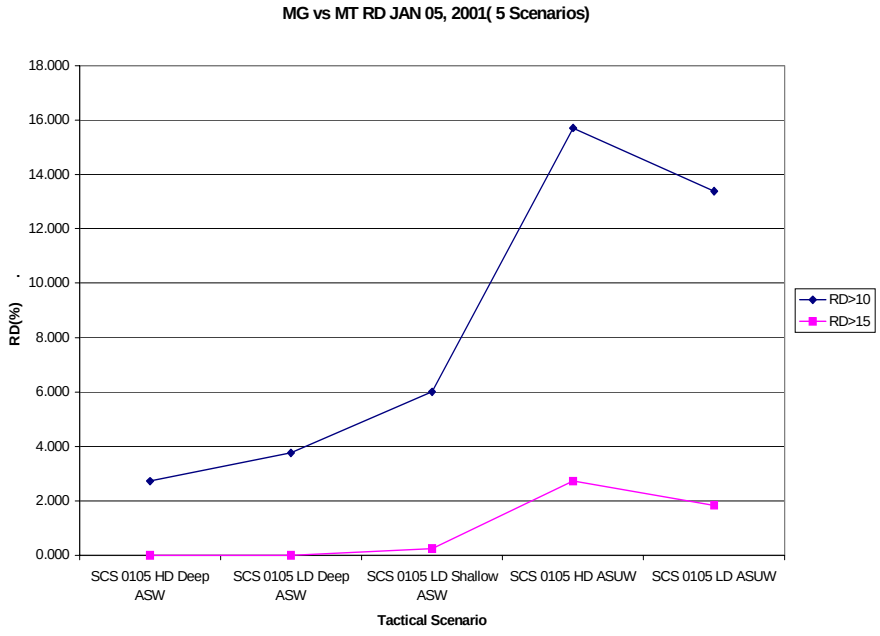

Figure 35. Probability curve SCS January 05,2001

The histogram of the HD ASW scenario (Figure 36), lowest probability value, on January 05, 2001 had a mean RD of 4.60 with a standard deviation of 2.58, or the mean

value of the relative difference between the two acoustic coverages generated by MODAS-TPX and MODAS-GFO in the HD ASW scenario is 4.60%. The histogram HD ASUW (Figure 37), highest probability value, for January 05, 2001 has mean RD of 6.60 with a standard deviation of 4.88

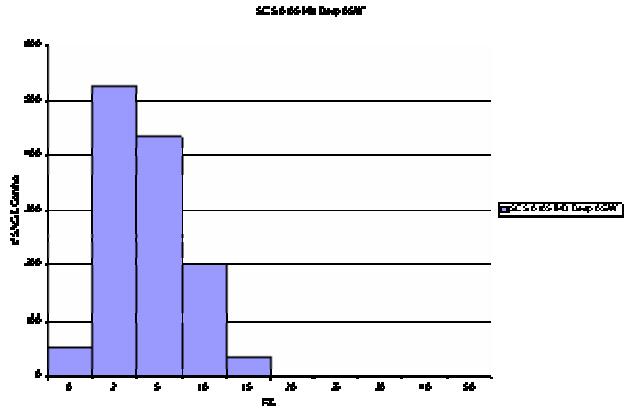

Figure 36. Wapp output for the relative difference between MODAS-TPX and MODAS-GFO for the HD deep ASW scenario. Mean is 4.60, standard deviation is 2.58.

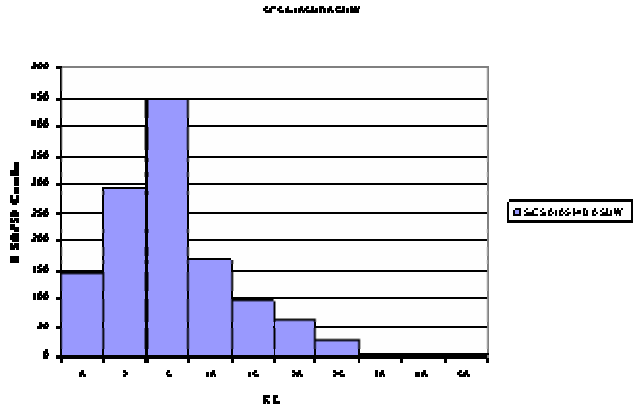

Figure 37. Wapp output for the relative difference between MODAS-TPX and MODAS-GFO for the HD ASUW scenario. Mean is 6.60, standard deviation is 4.88.

The mean RD for all five tactical scenarios for January 2001 in the SCS (Figure 38) and the ECS (Figure 39) are decreasing as function of time. The mean RD for all cases in both the ECS and SCS are less than 6.60 %

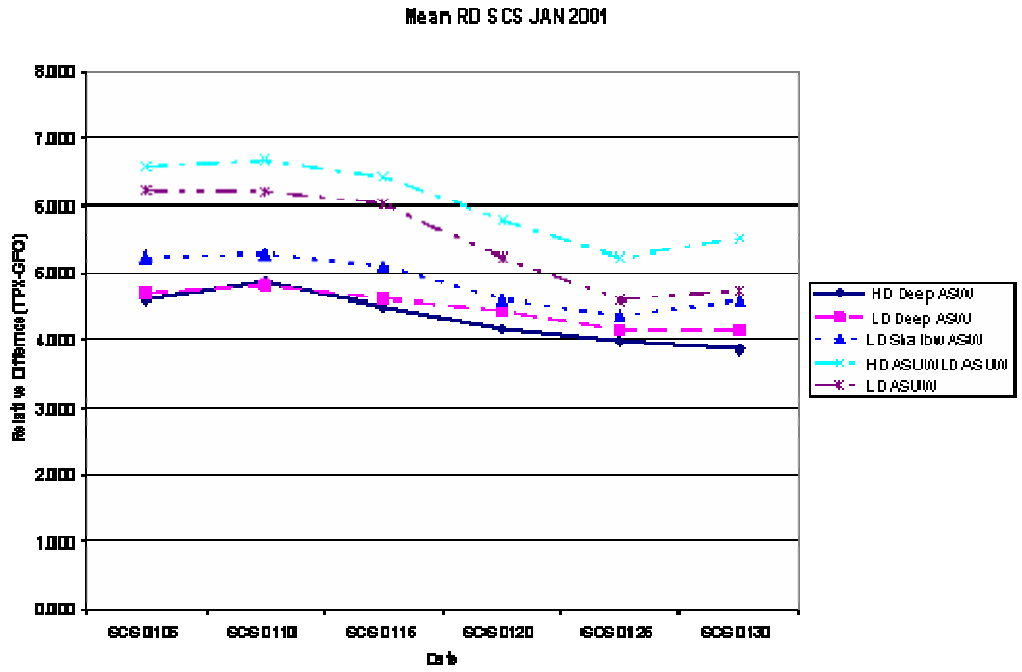

Figure 38. Mean RD in the SCS January 2001

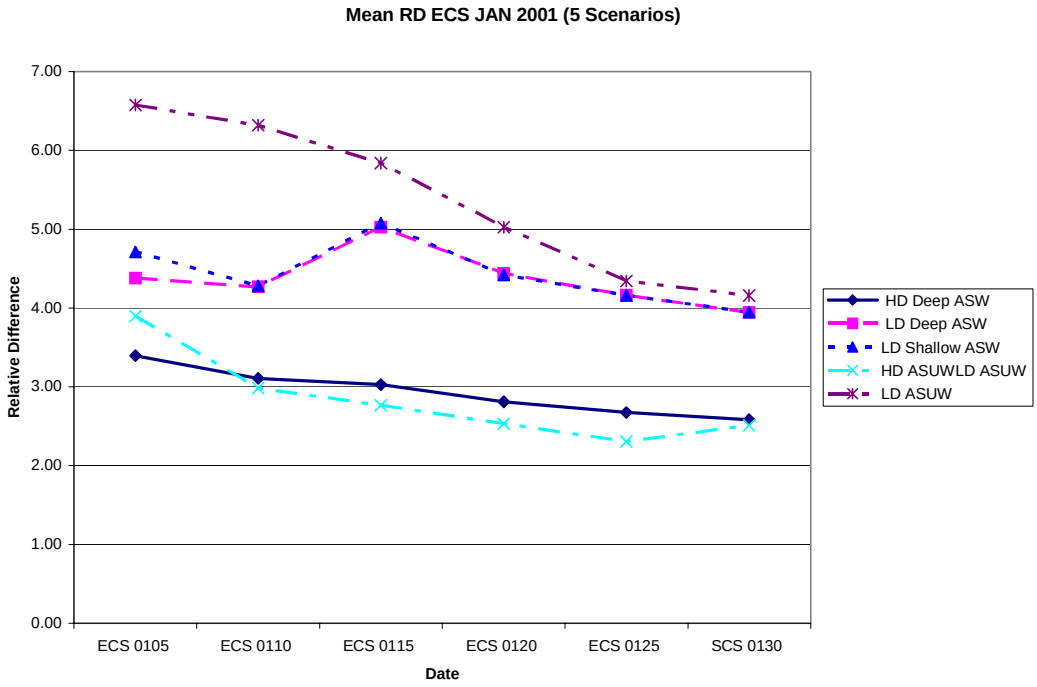

Figure 39. Mean RD in the ECS January 2001

VIII. CONCLUSION

The chief aim of this study was to determine the sensitivity of an USW system to altimeter orbit. Two area of interest with high mesoscale variability were analyzed. A key assumption of this study is that GFO has better spatial resolution than TPX; therefore, it was assumed that MODAS fields initialized with GFO sea surface heights are more accurate than MODAS fields initialized with TPX sea surface heights. A second assumption is that greatest relative difference in acoustic coverage in WAPP will be in areas of high mesoscale variability.

Both MODAS and POM were evaluated with observational data from SCSMEX. The availability of the SCSMEX evaluation of MODAS and POM provided an opportunity to test of the sensitivity of WAPP to the respective models. POM outperformed MODAS in all five tactical scenarios (Table 3). POM had smaller relative differences in acoustic coverage than MODAS. The results make sense since POM is a physics based model that uses the primitive equation to forecast the sub-surface structure of the ocean; on the other hand, MODAS is a dynamic climatology which is a statistically based model. The purpose of evaluating the sensitivity of both MODAS and POM in WAPP was to compare the relative difference between the respective model and 'ground truth' (SCSMEX observational data). The sensitivity analysis of MODAS and POM also confirmed that probability values decrease with increasing tactic depth, in agreement with Mancini, 2004.

Tables 4 and 5 are a summary of the sensitivities of the all the tactic scenarios in January for both the ECS and SCS. In the 60 tactic scenarios in Tables 4 and 5, the mean RD for all tactic scenarios is less than 6.68 (SCS 0110 HD ASUW). Furthermore, the probability that the RD is greater that 15 is less than 4.01% (SCS 0110 HD ASUW) for all 60 tactic scenarios in January, and the probability that the RD is greater that 10 is less than 17.01% for all 60 tactic scenarios in January.

	Prob(RD>10)	Prob(RD>15)	Mean RD	SD
SCS 0105 HD Deep ASW	2.72	0.00	4.60	2.59
SCS 0110 HD Deep ASW	3.04	0.08	4.87	2.73
SCS 0115 HD Deep ASW	2.08	0.08	4.50	2.60
SCS 0120 HD Deep ASW	0.56	0.00	4.16	2.25
SCS 0125 HD Deep ASW	0.80	0.00	3.97	2.31
SCS 0130 HD Deep ASW	0.32	0.00	3.86	2.10

	Prob(RD>10)	Prob(RD>15)	Mean RD	SD
SCS 0105 LD Deep ASW	3.77	0.00	4.69	2.75
SCS 0110 LD Deep ASW	3.69	0.08	4.81	2.87
SCS 0115 LD Deep ASW	2.72	0.08	4.61	2.66
SCS 0120 LD Deep ASW	1.28	0.08	4.44	2.46
SCS 0125 LD Deep ASW	1.04	0.08	4.15	2.36
SCS 0130 LD Deep ASW	0.88	0.00	4.14	2.29

	Prob(RD>10)	Prob(RD>15)	Mean RD	SD
SCS 0105 LD Shallow ASW	6.01	0.24	5.23	3.30
SCS 0110 LD Shallow ASW	5.85	0.32	5.28	3.21
SCS 0115 LD Shallow ASW	3.77	0.32	5.11	3.05
SCS 0120 LD Shallow ASW	2.16	0.16	4.60	2.71
SCS 0125 LD Shallow ASW	2.88	0.24	4.37	2.81
SCS 0130 LD Shallow ASW	3.37	0.24	4.59	2.87

	Prob(RD>10)	Prob(RD>15)	Mean RD	SD
SCS 0105 HD ASUW	15.71	2.72	6.60	4.88
SCS 0110 HD ASUW	15.63	**4.01**	**6.68**	5.19
SCS 0115 HD ASUW	13.86	2.32	6.44	4.82
SCS 0120 HD ASUW	10.74	0.80	5.79	4.14
SCS 0125 HD ASUW	6.97	0.40	5.22	3.60
SCS 0130 HD ASUW	7.77	0.48	5.51	3.52

	Prob(RD>10)	Prob(RD>15)	Mean RD	SD
SCS 0105 LD ASUW	13.38	1.84	6.23	4.58
SCS 0110 LD ASUW	13.06	0.96	6.22	4.18
SCS 0115 LD ASUW	11.22	1.20	6.02	4.21
SCS 0120 LD ASUW	7.45	0.80	5.23	3.67
SCS 0125 LD ASUW	5.21	0.72	4.59	3.47
SCS 0130 LD ASUW	4.49	0.80	4.73	3.47

Table 4. WAPP output differences between GFO and TPX for the SCS January 2001

	Prob(RD>10)	Prob(RD>15)	Mean RD	SD
ECS 0105 HD Deep ASW	0.94	0.00	3.40	2.75
ECS 0110 HD Deep ASW	0.80	0.00	3.11	2.55
ECS 0115 HD Deep ASW	0.37	0.00	3.03	2.24
ECS 0120 HD Deep ASW	0.09	0.00	2.81	1.99
ECS 0125 HD Deep ASW	0.14	0.00	2.68	2.00
ECS 0130 HD Deep ASW	0.09	0.00	2.59	1.98

	Prob(RD>10)	Prob(RD>15)	Mean RD	SD
ECS 0105 LD Deep ASW	5.29	0.89	4.38	4.45
ECS 0110 LD Deep ASW	5.90	0.89	4.27	4.58
ECS 0115 LD Deep ASW	9.08	2.15	5.03	6.30
ECS 0120 LD Deep ASW	6.18	2.76	4.44	6.22
ECS 0125 LD Deep ASW	5.52	2.29	4.16	6.03
ECS 0130 LD Deep ASW	4.92	2.43	3.94	5.79

	Prob(RD>10)	Prob(RD>15)	Mean RD	SD
ECS 0105 LD Shallow ASW	5.81	0.84	4.71	4.68
ECS 0110 LD Shallow ASW	6.51	0.94	4.28	4.78
ECS 0115 LD Shallow ASW	9.97	2.15	5.08	6.47
ECS 0120 LD Shallow ASW	6.98	2.81	4.42	6.39
ECS 0125 LD Shallow ASW	6.23	2.29	4.16	6.18
ECS 0130 LD Shallow ASW	5.52	2.43	3.95	5.91

	Prob(RD>10)	Prob(RD>15)	Mean RD	SD
ECS 0105 HD ASUW	5.76	1.08	3.90	4.60
ECS 0110 HD ASUW	5.24	0.89	2.99	4.59
ECS 0115 HD ASUW	4.12	0.80	2.76	4.29
ECS 0120 HD ASUW	3.28	0.05	2.53	3.76
ECS 0125 HD ASUW	2.39	0.14	2.31	3.49
ECS 0130 HD ASUW	3.32	0.19	2.51	3.87

	Prob(RD>10)	Prob(RD>15)	Mean RD	SD
ECS 0105 LD ASUW	**17.51**	3.60	6.57	7.72
ECS 0110 LD ASUW	15.03	3.89	6.32	7.84
ECS 0115 LD ASUW	13.90	3.89	5.84	7.18
ECS 0120 LD ASUW	10.96	3.09	5.03	6.64
ECS 0125 LD ASUW	8.47	1.69	4.35	5.79
ECS 0130 LD ASUW	7.82	1.22	4.16	5.46

Table 5. WAPP output differences between GFO and TPX for the ECS in January 2001

In conclusion, there is small probability(less than 18 %) that the RD is greater 10 between MODAS-TPX and MODAS-GFO for all scenarios. It appears that the USW weapon system is not overly sensitive to altimeter orbit. That is not to say, that altimeter orbit is not important. Jaing et al., 1996, showed that spatially dense altimeter sampling is preferred over temporal frequency sampling to resolve mesoscale features. The resolving of mesoscale features in essential to the warfighter at the strategic level. At strategic level, the warfighter is concerned with placement of assets, where to conduct operations, where the enemy submarine is hiding and so on. The US Navy's USW weapons is technological advance, so it appears that, in the case of different altimeter orbits, the USW weapon system is adequately robust to overcome the difference in between the two altimeters.

APPENDIX A. MODAS AND POM TACTICAL SCENARIO HISTOGRAMS

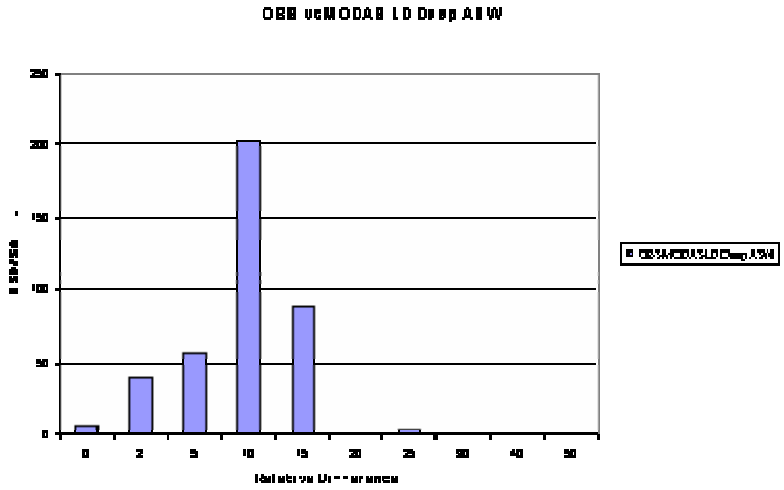

Figure 40. Wapp output for the relative difference between POM and SCSMEX (OBS) for HD deep ASW scenario. Mean is 8.98, standard deviation is 2.95, Prob (RD= 0.10) is 6%, and Prob (RD= 0.15) is 0.25%.

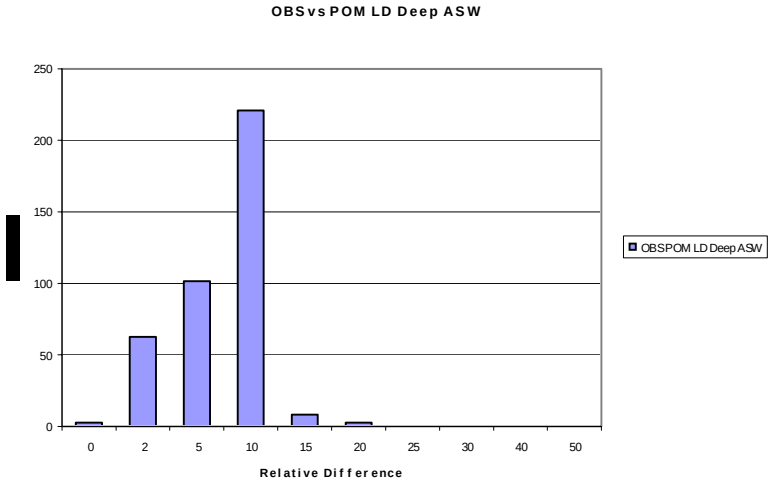

Figure 41. Wapp output for the relative difference between POM and SCSMEX (OBS) for HD deep ASW scenario. Mean is 8.98, standard deviation is 2.95, Prob (RD= 0.10) is 6%, and Prob (RD= 0.15) is 0.25%.

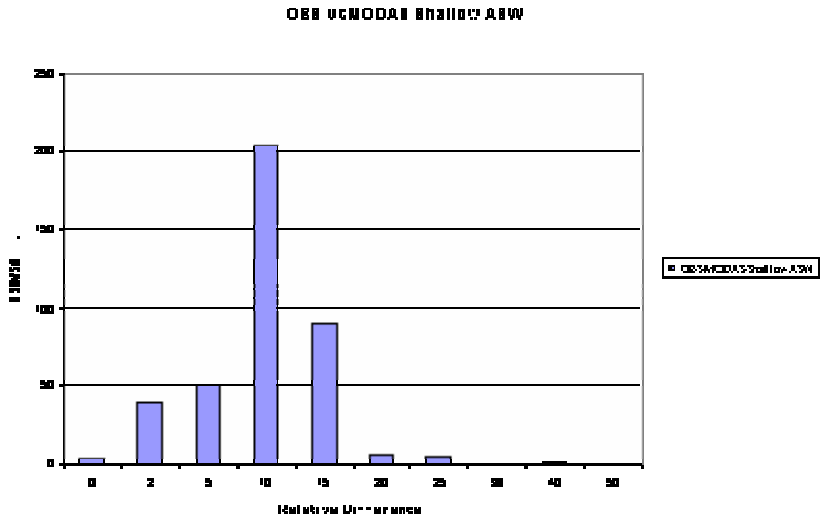

Figure 42. Wapp output for the relative difference between POM and SCSMEX (OBS) for HD deep ASW scenario. Mean is 8.98, standard deviation is 2.95, Prob (RD= 0.10) is 6%, and Prob (RD= 0.15) is 0.25%.

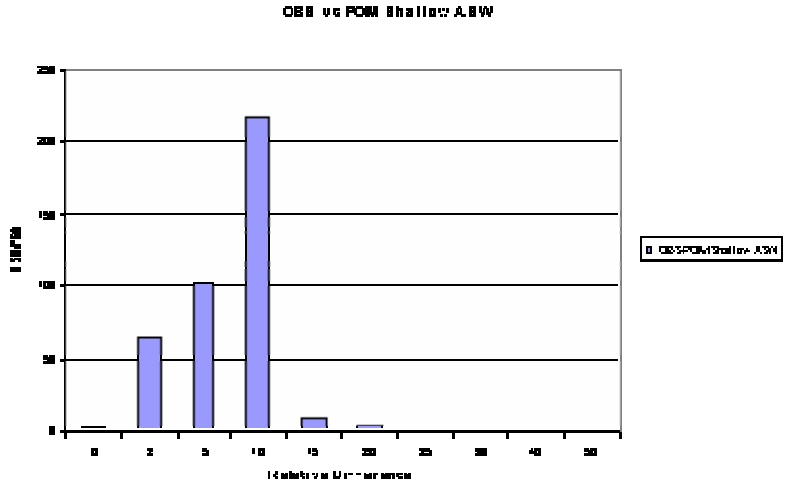

Figure 43. Wapp output for the relative difference between POM and SCSMEX (OBS) for HD deep ASW scenario. Mean is 8.98, standard deviation is 2.95, Prob (RD= 0.10) is 6%, and Prob (RD= 0.15) is 0.25%.

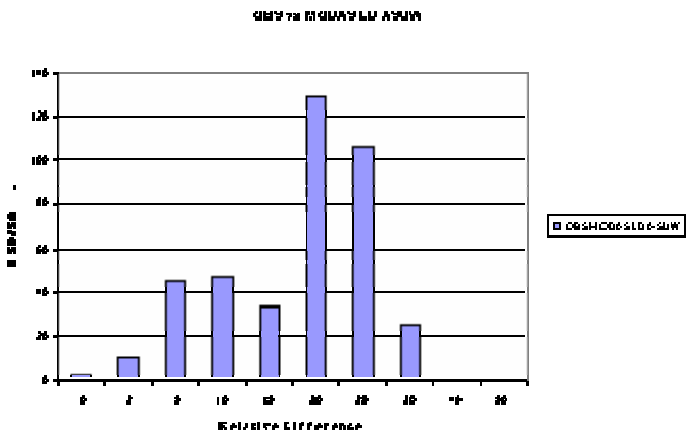

Figure 44. Wapp output for the relative difference between POM and SCSMEX (OBS) for HD deep ASW scenario. Mean is 8.98, standard deviation is 2.95, Prob (RD= 0.10) is 6%, and Prob (RD= 0.15) is 0.25%.

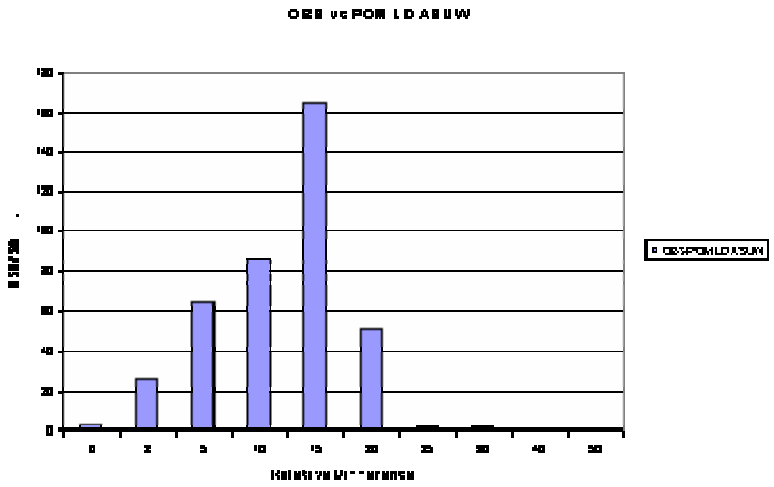

Figure 45. Wapp output for the relative difference between POM and SCSMEX (OBS) for HD deep ASW scenario. Mean is 8.98, standard deviation is 2.95, Prob (RD= 0.10) is 6%, and Prob (RD= 0.15) is 0.25%.

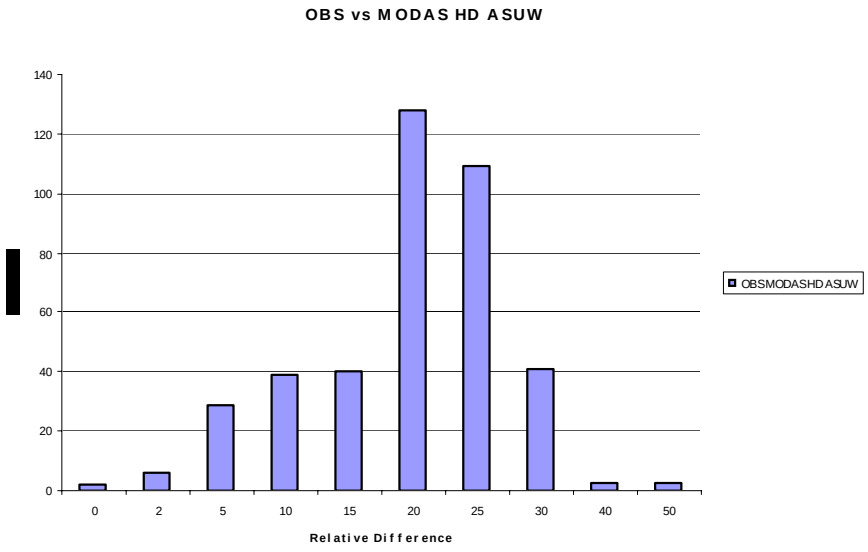

Figure 46. Wapp output for the relative difference between POM and SCSMEX (OBS) for HD deep ASW scenario. Mean is 8.98, standard deviation is 2.95, Prob (RD= 0.10) is 6%, and Prob (RD= 0.15) is 0.25%.

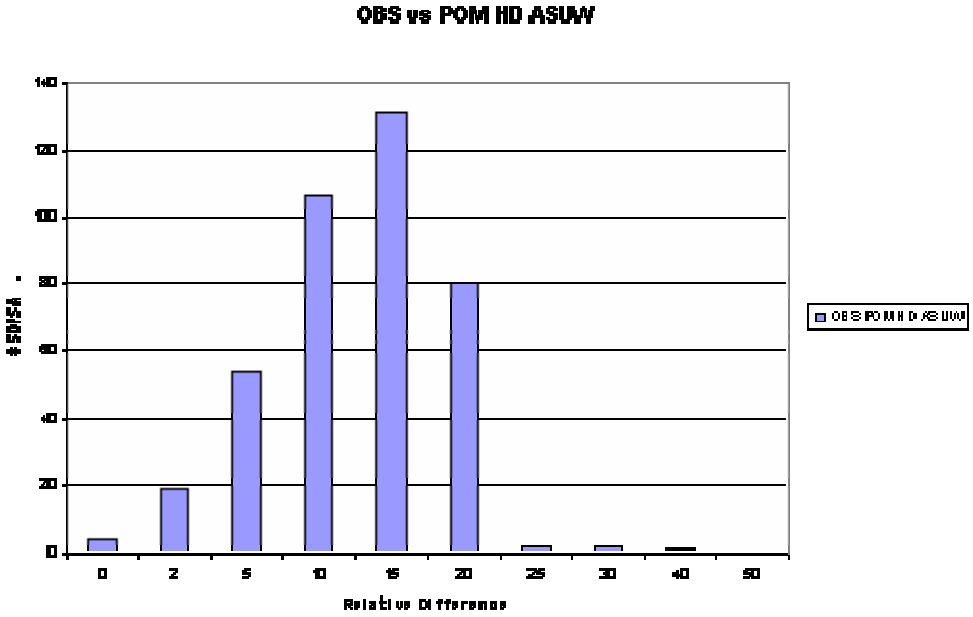

Figure 47. Wapp output for the relative difference between POM and SCSMEX (OBS) for HD deep ASW scenario. Mean is 8.98, standard deviation is 2.95, Prob (RD= 0.10) is 6%, and Prob (RD= 0.15) is 0.25%.

APPENDIX B. MODAS HORIZONTAL SSP DIFFERENCE

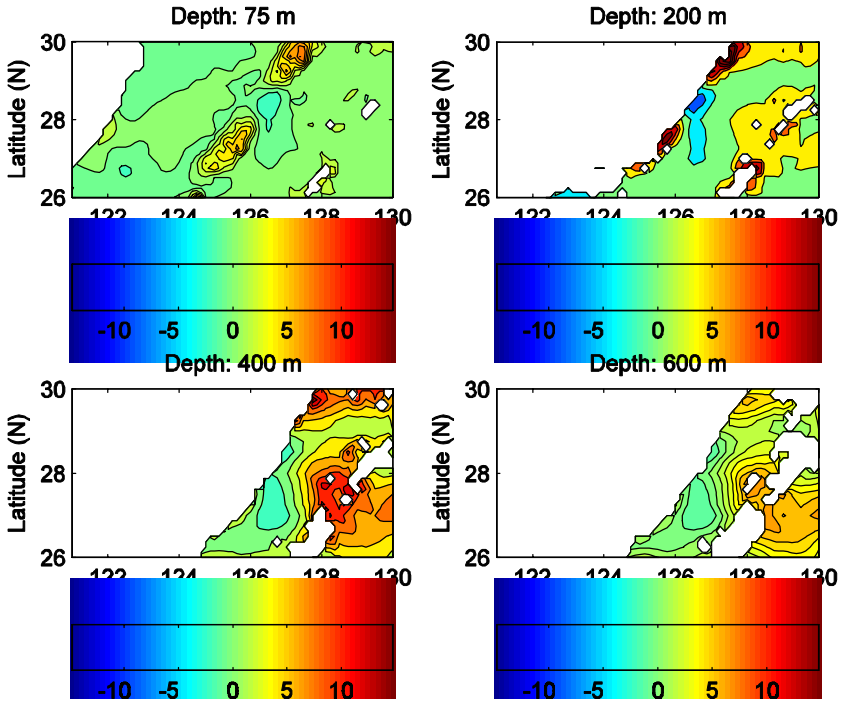

Figure 48. ECS MODAS horizontal difference in SSPs for January 10, 2001.

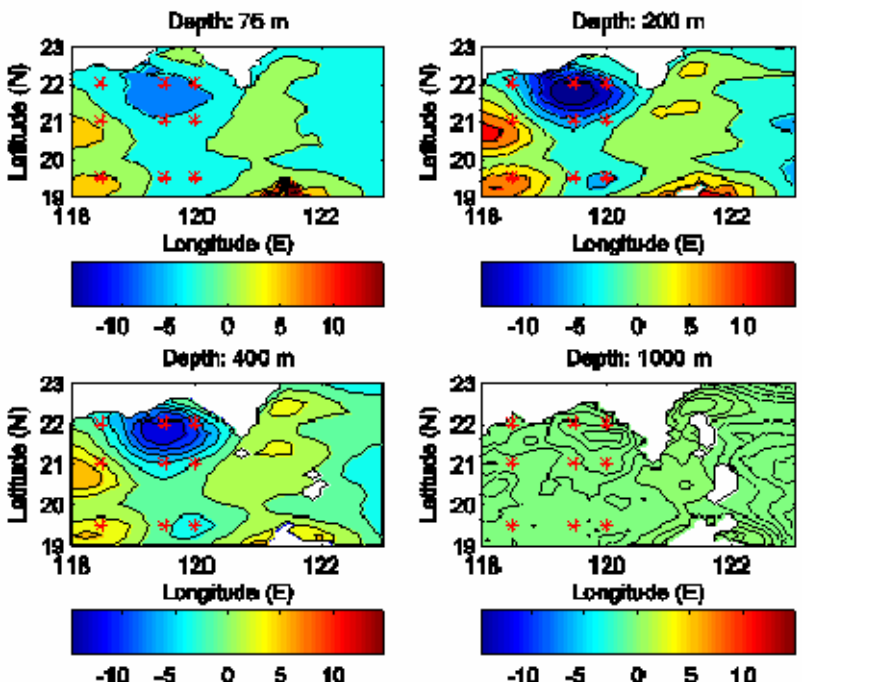

Figure 49. SCS MODAS horizontal difference in SSPs for January 10, 2001.

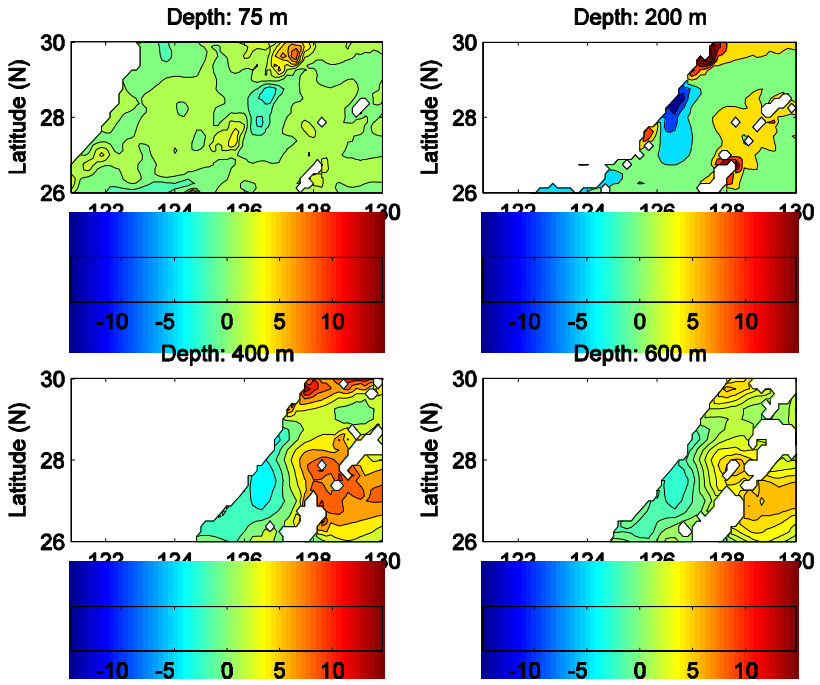

Figure 50. ECS MODAS horizontal difference in SSPs for January 15, 2001.

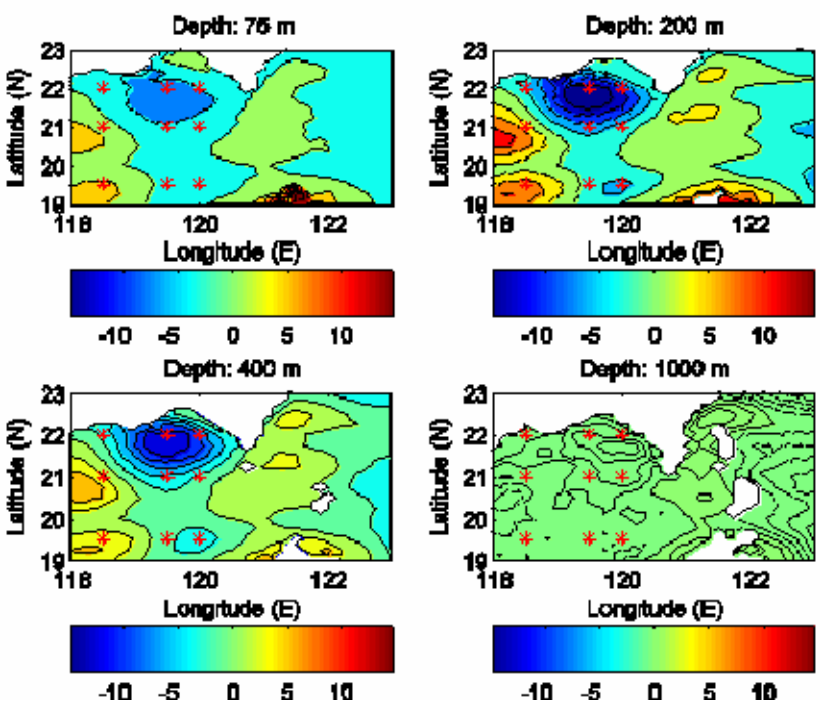

Figure 51. SCS MODAS horizontal difference in SSPs for January 15, 2001.

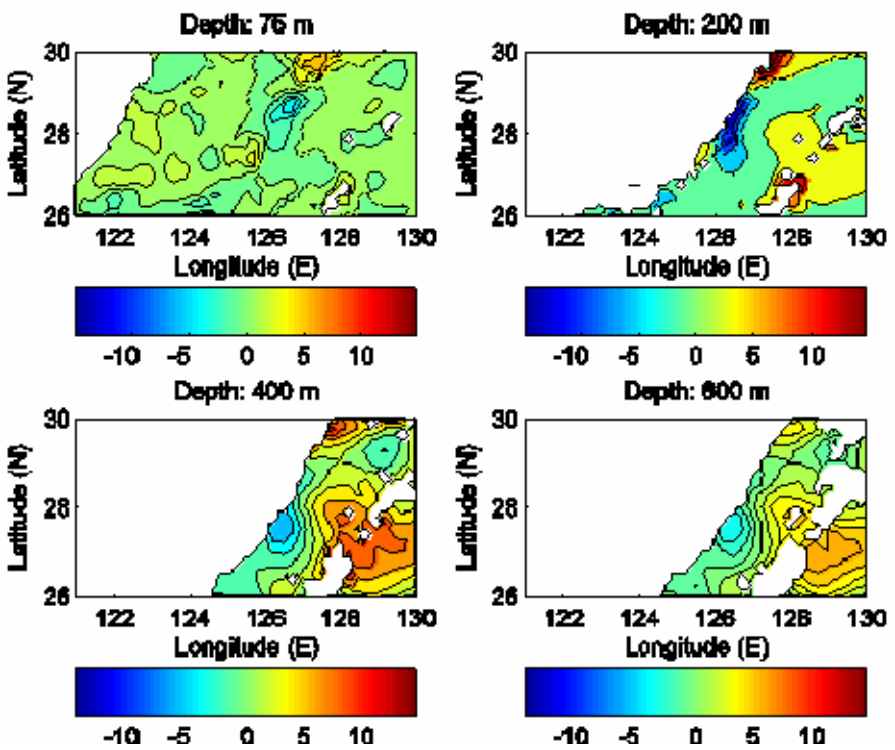

Figure 52. ECS MODAS horizontal difference in SSPs for January 20, 2001.

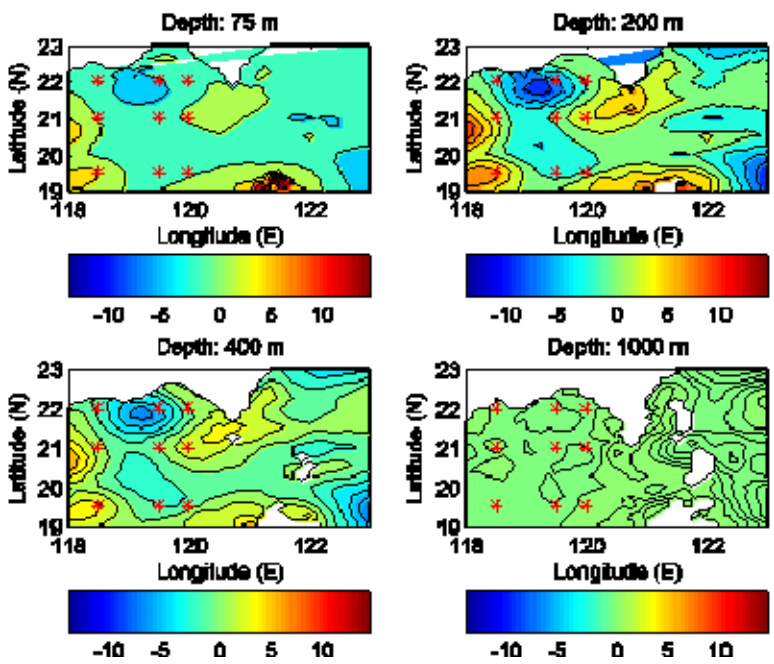

Figure 53. SCS MODAS horizontal difference in SSPs for January 20, 2001.

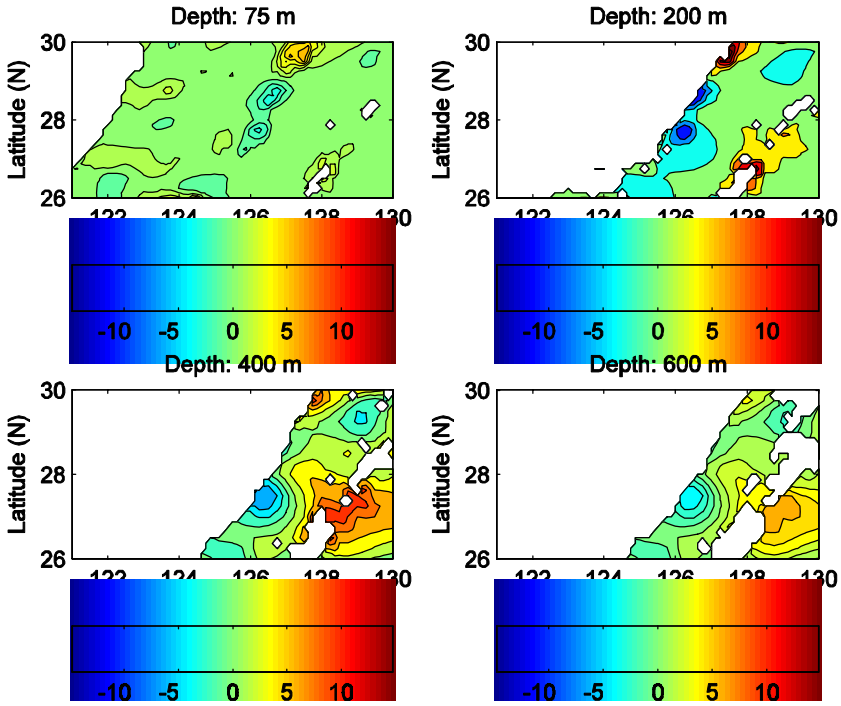

Figure 54. ECS MODAS horizontal difference in SSPs for January 25, 2001.

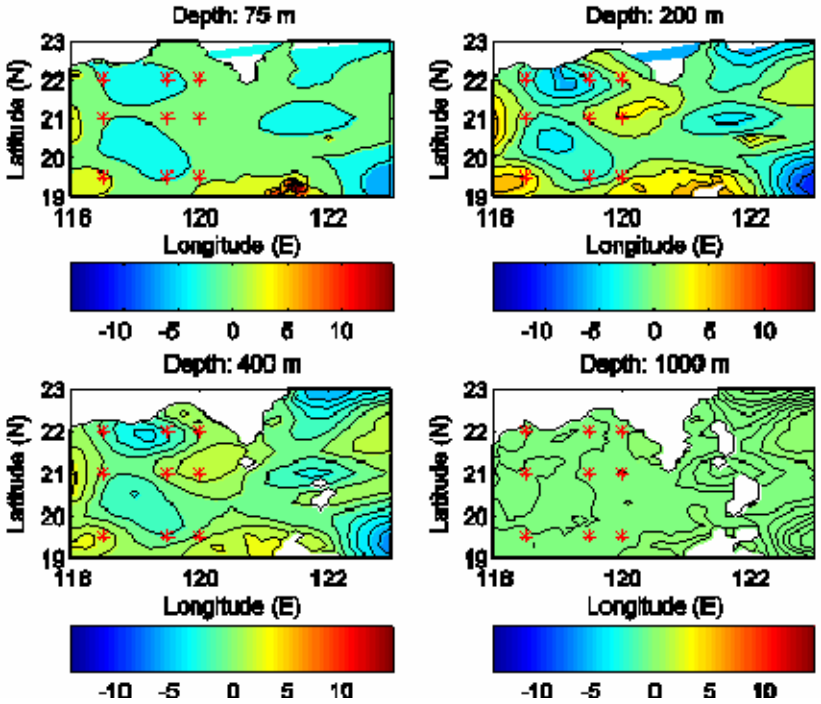

Figure 55. SCS MODAS horizontal difference in SSPs for January 25, 2001.

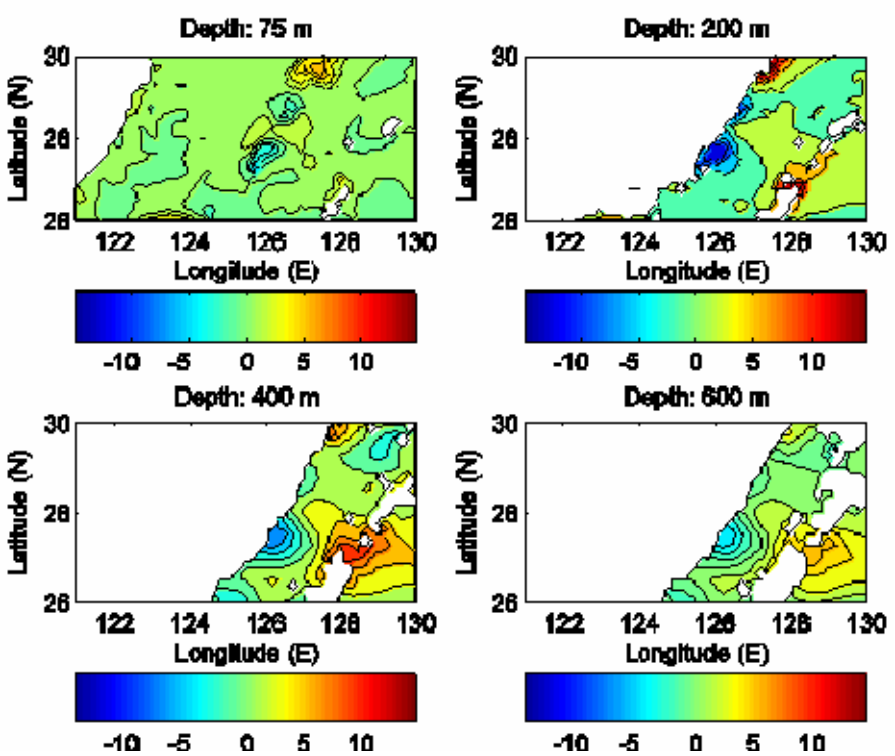

Figure 56. ECS MODAS horizontal difference in SSPs for January 30, 2001.

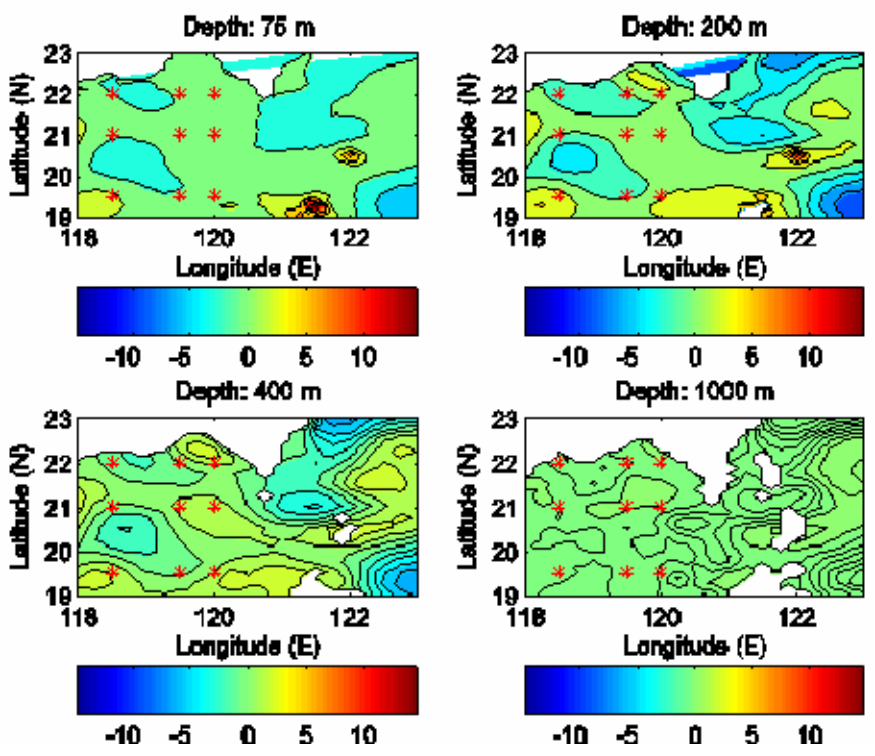

Figure 57. SCS MODAS horizontal difference in SSPs for January 30, 2001.

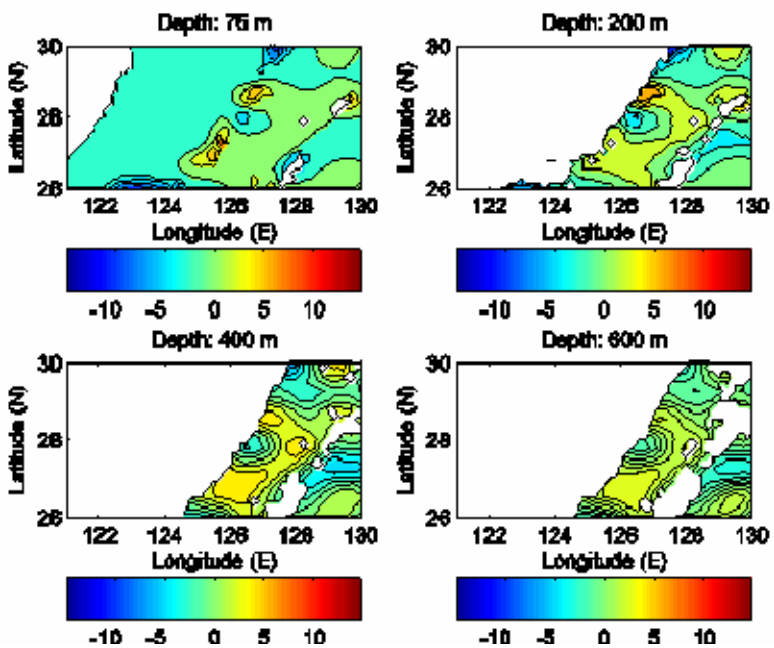

Figure 58. ECS MODAS horizontal difference in SSPs for July 05, 2001.

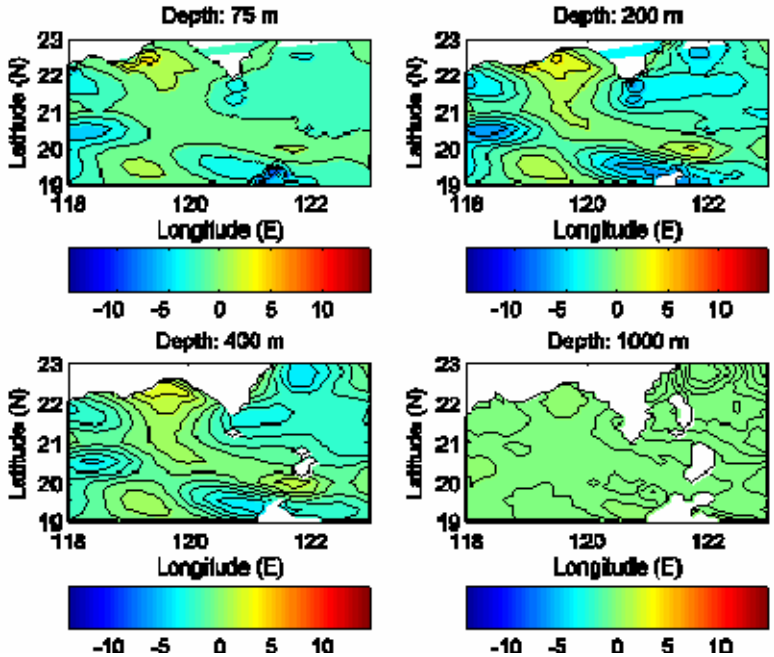

Figure 59. SCS MODAS horizontal difference in SSPs for July 05, 2001.

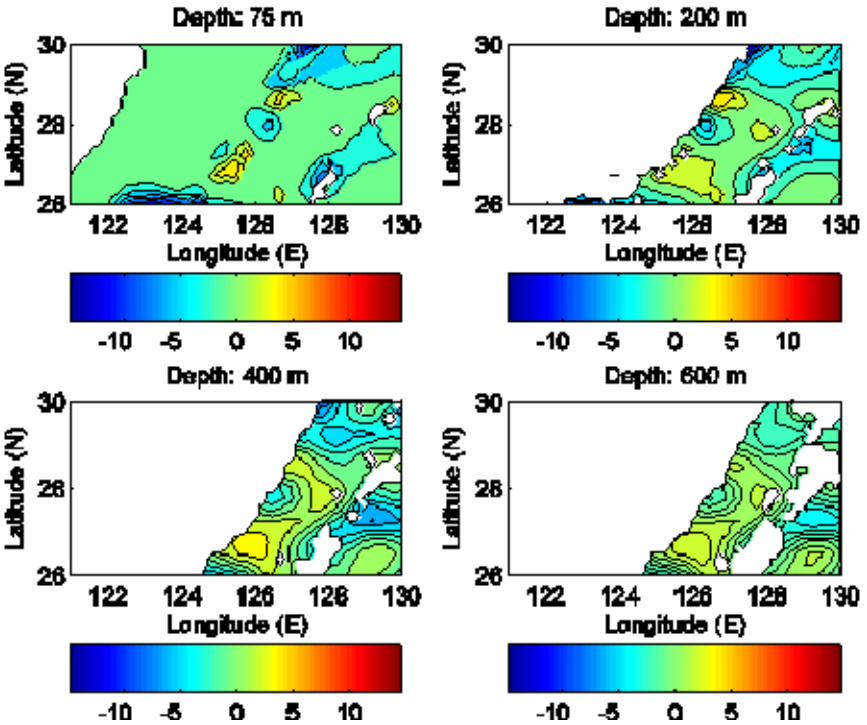

Figure 60. ECS MODAS horizontal difference in SSPs for July 10, 2001.

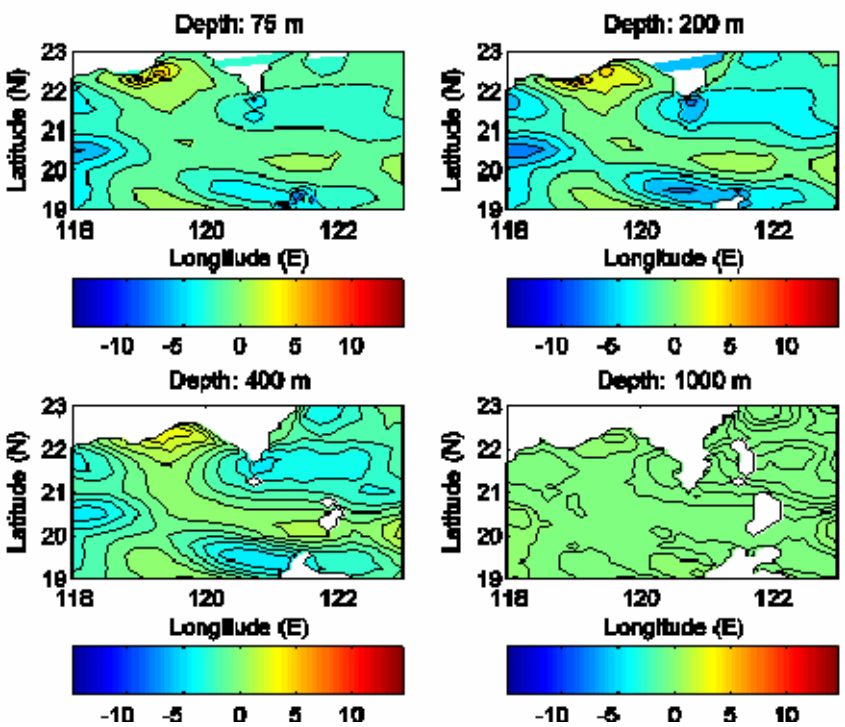

Figure 61. SCS MODAS horizontal difference in SSPs for July 10, 2001.

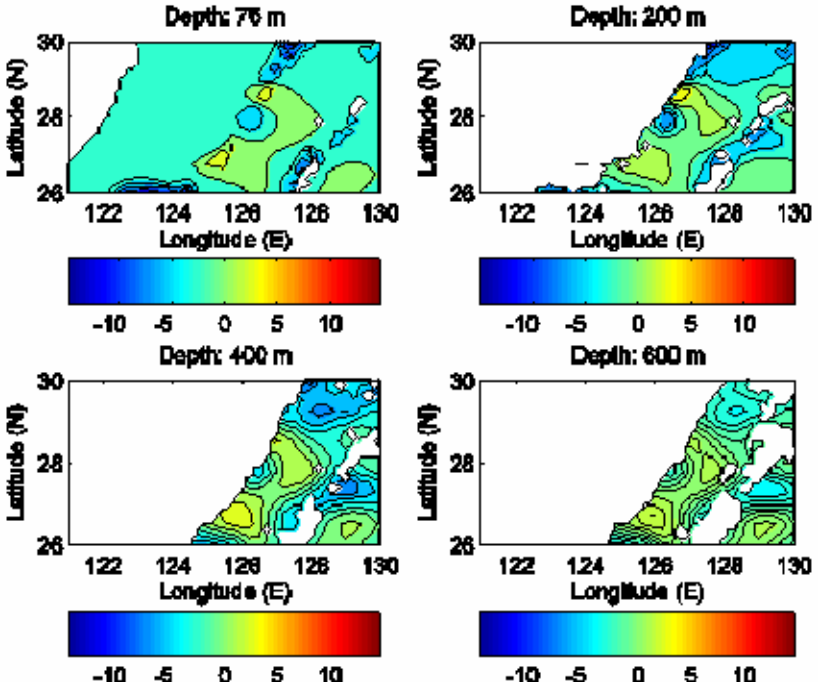

Figure 62. ECS MODAS horizontal difference in SSPs for July 15, 2001.

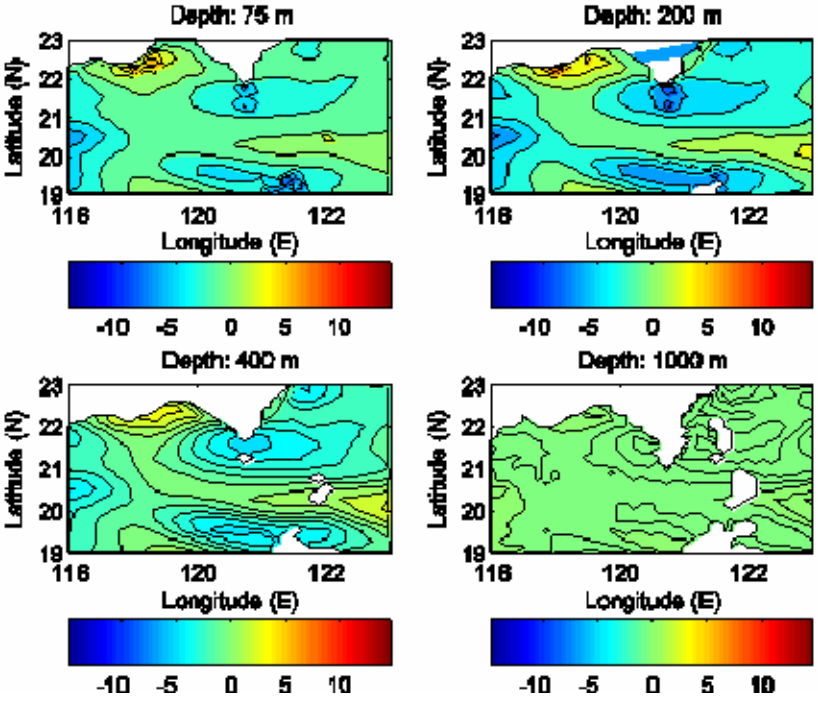

Figure 63. SCS MODAS horizontal difference in SSPs for July 15, 2001.

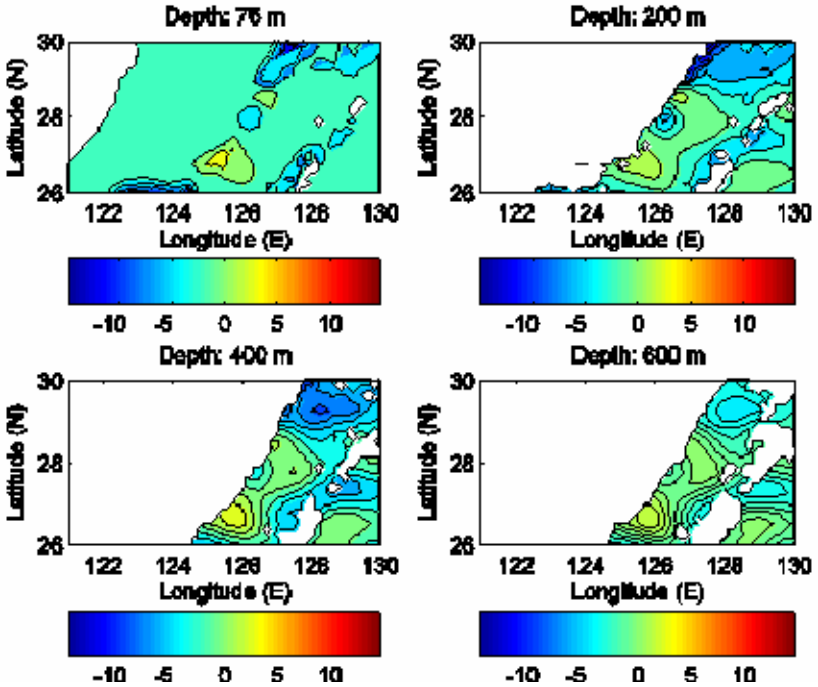

Figure 64. ECS MODAS horizontal difference in SSPs for July 20, 2001.

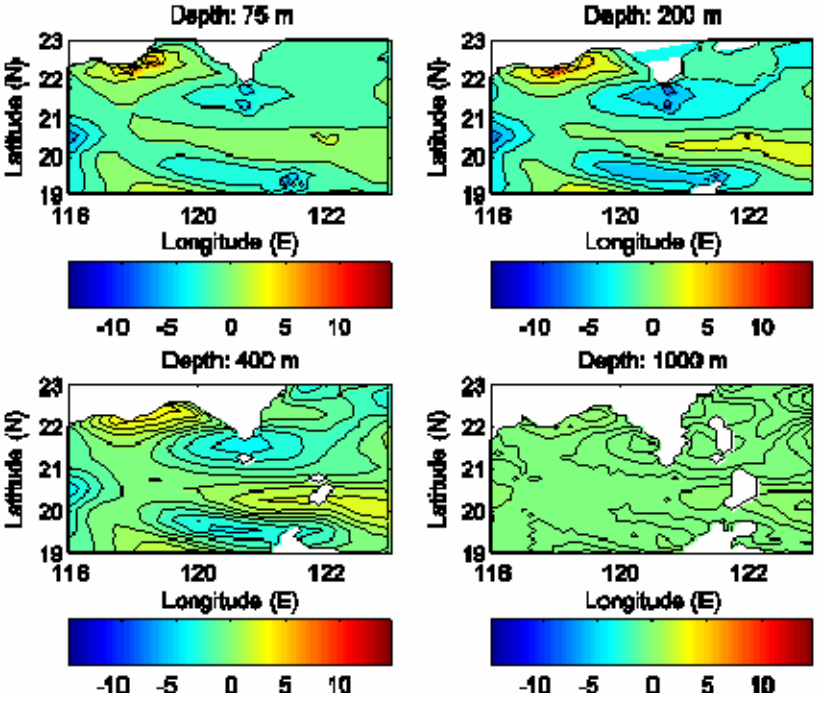

Figure 65. SCS MODAS horizontal difference in SSPs for July 20, 2001.

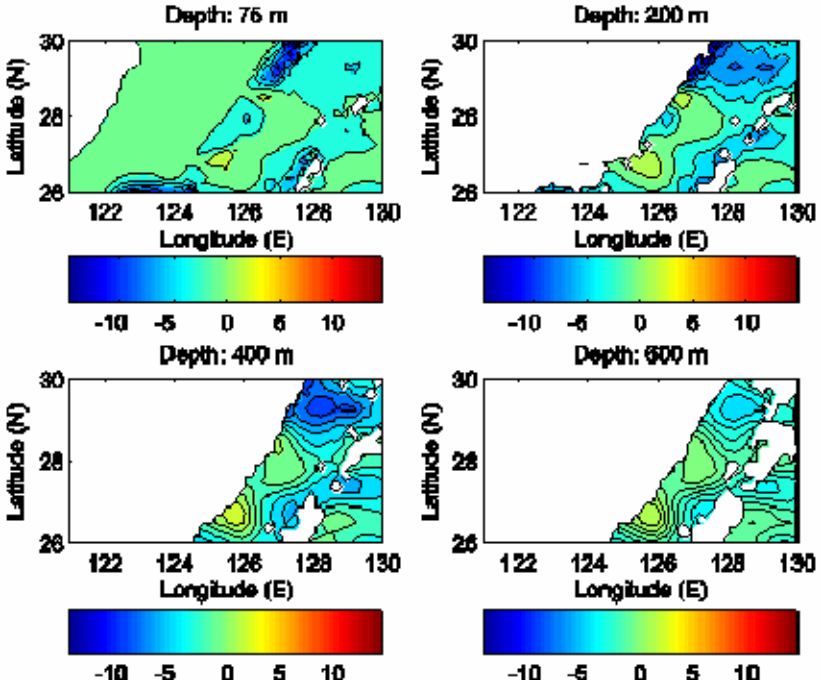

Figure 66. ECS MODAS horizontal difference in SSPs for July 25, 2001.

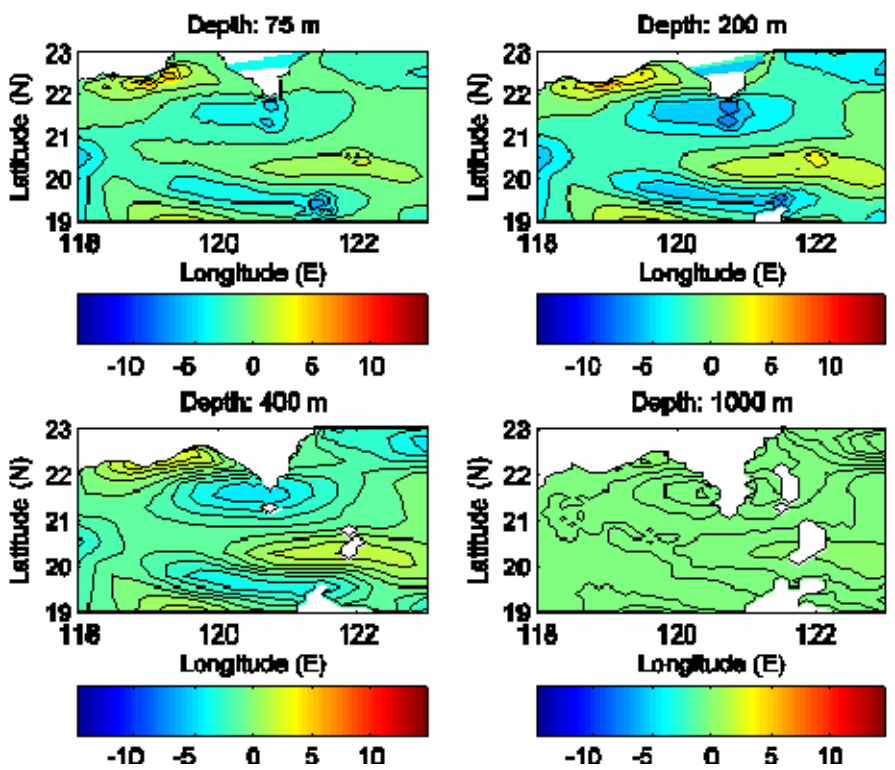

Figure 67. SCS MODAS horizontal difference in SSPs for July 25, 2001.

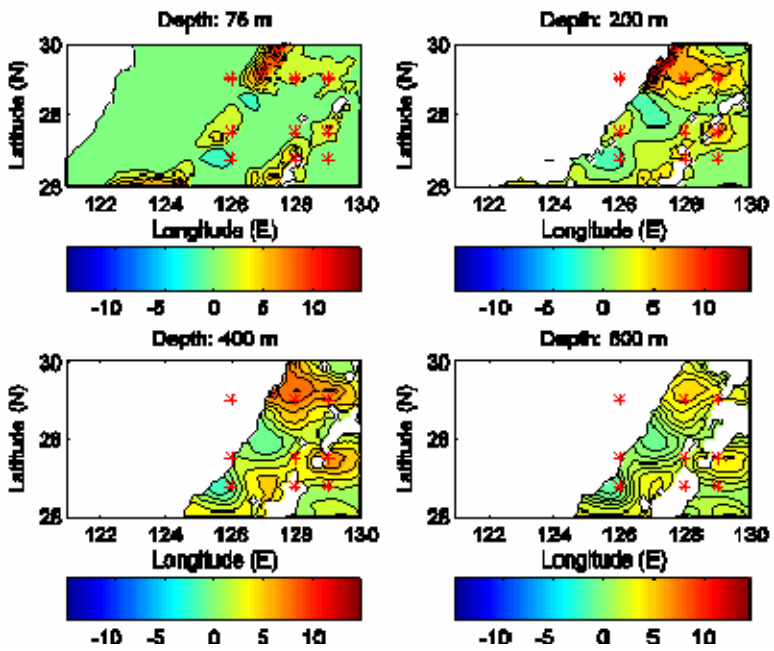

Figure 68. ECS MODAS horizontal difference in SSPs for July 30, 2001.

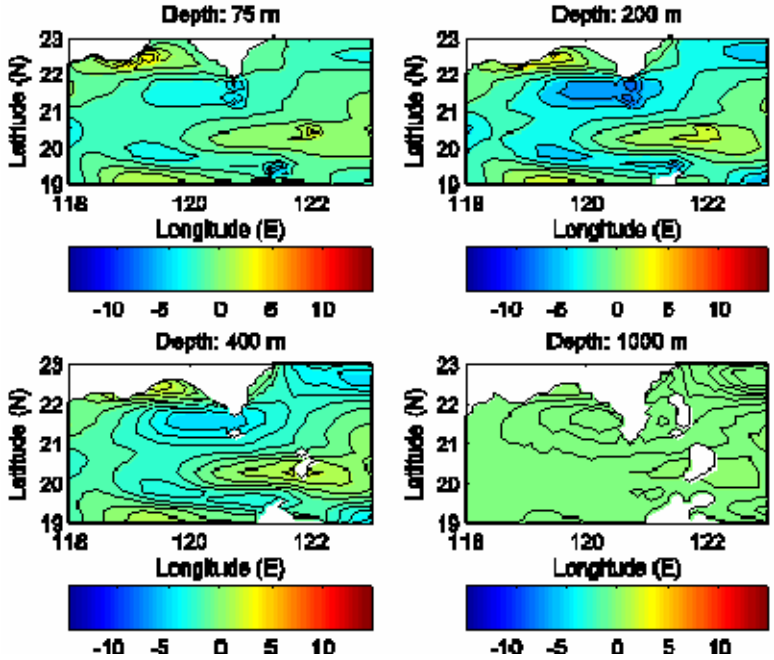

Figure 69. SCS MODAS horizontal difference in SSPs for July 30, 2001.

THIS PAGE INTENTIONALLY LEFT BLANK

APPENDIX C. MODAS SSP

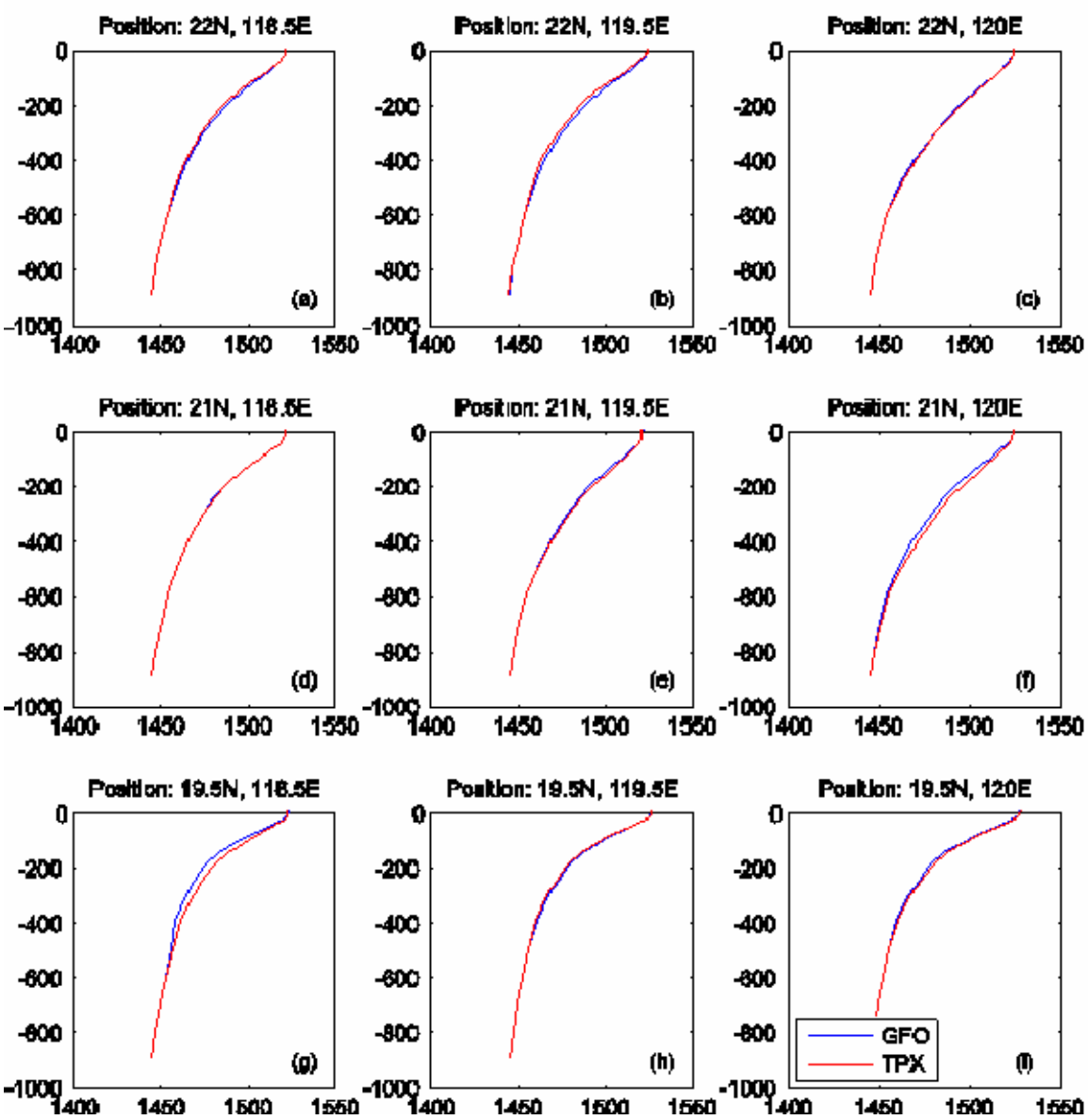

Figure 70. SCS MODAS SSP January 10, 2001

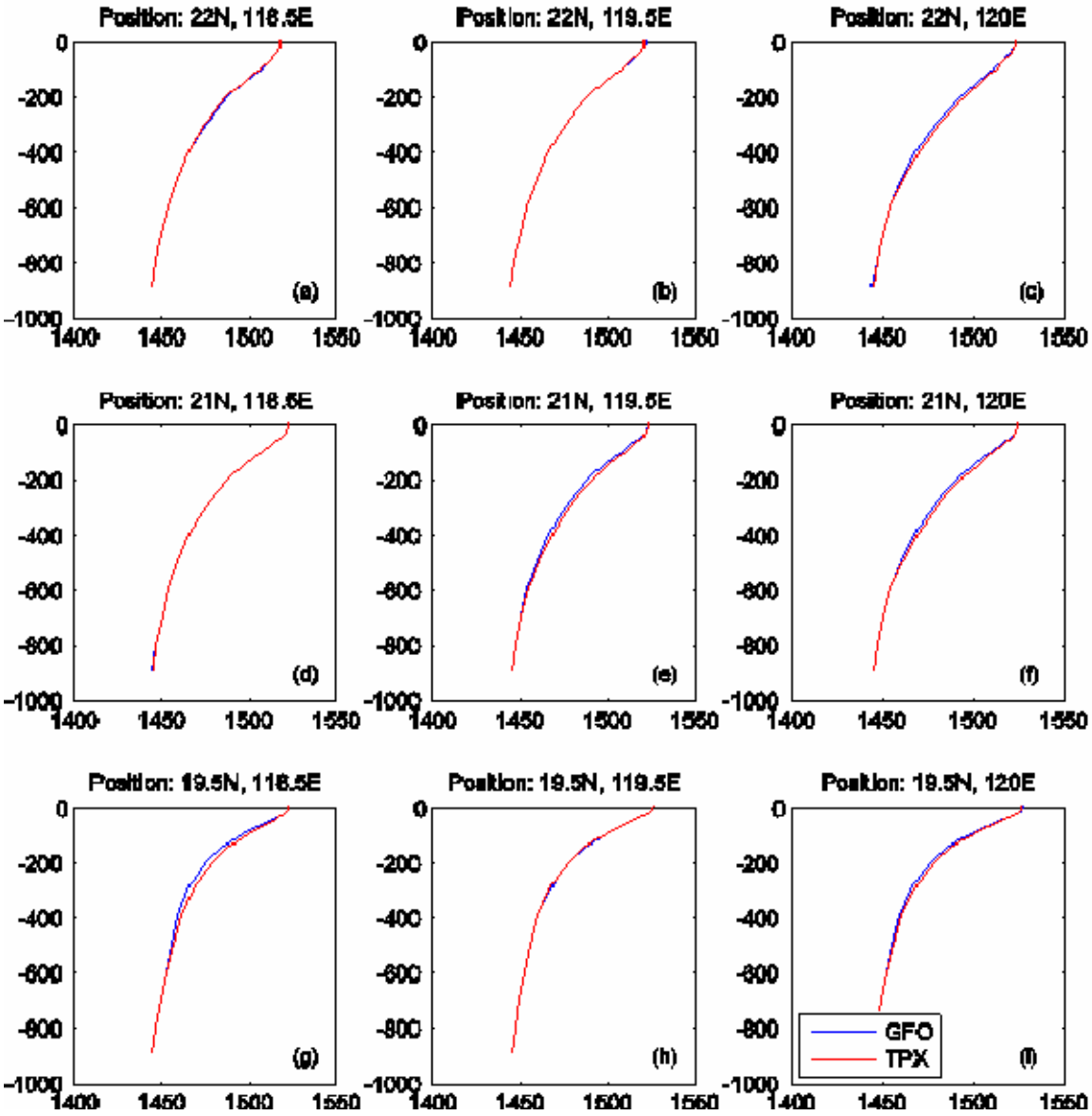

Figure 71. SCS MODAS SSP January 15, 2001

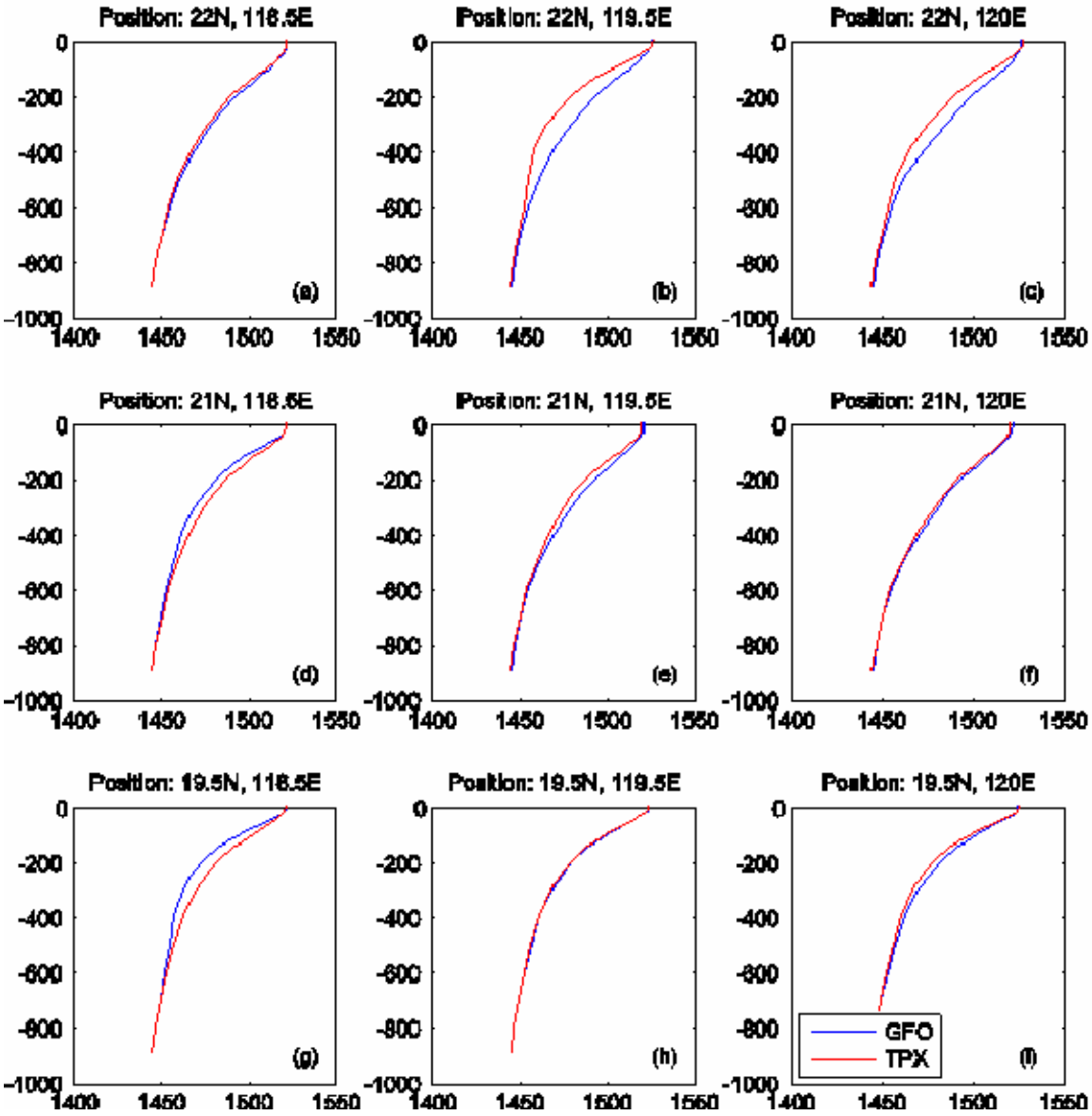

Figure 72. SCS MODAS SSP January 20, 2001

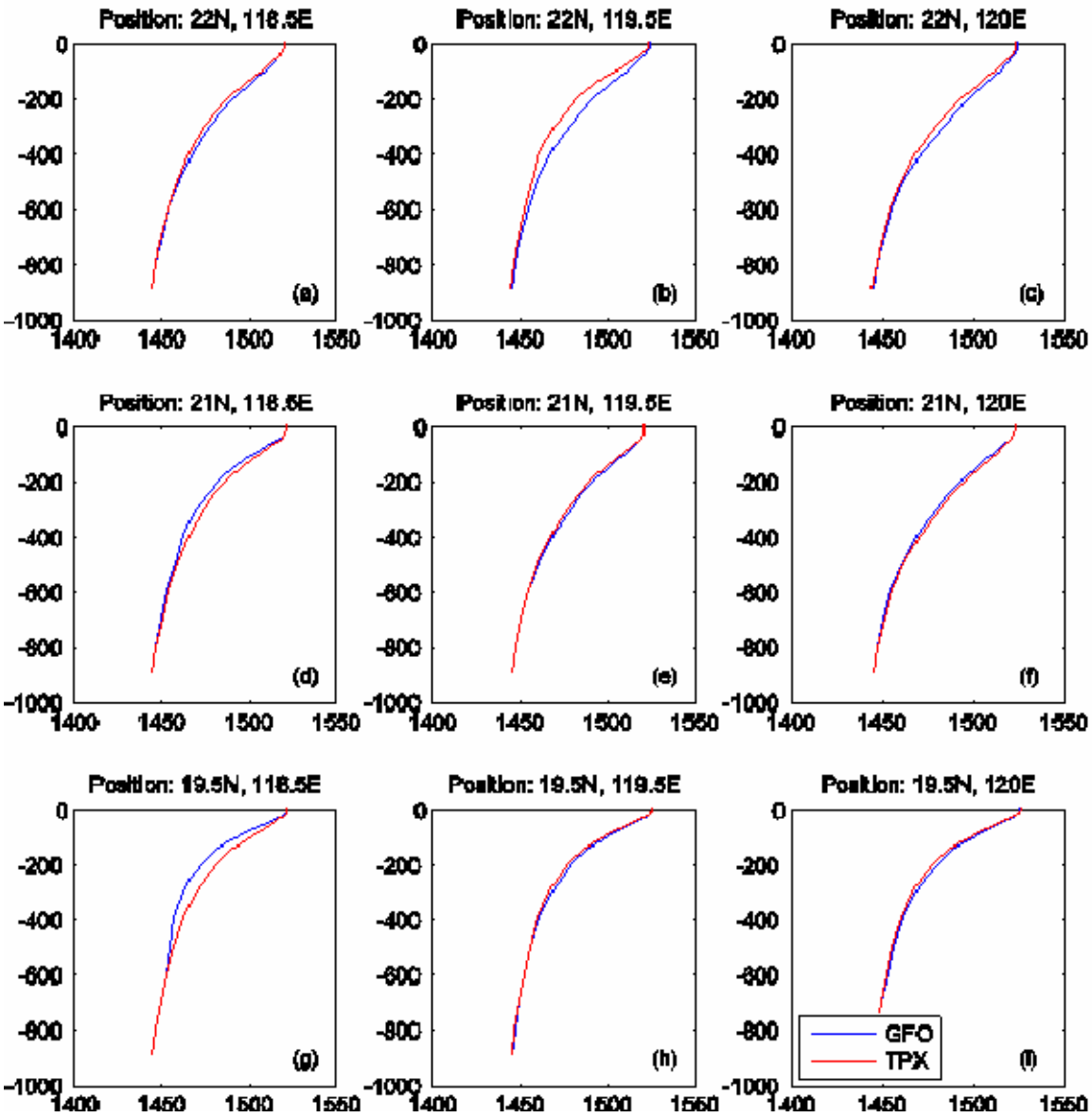

Figure 73. SCS MODAS SSP January 25, 2001

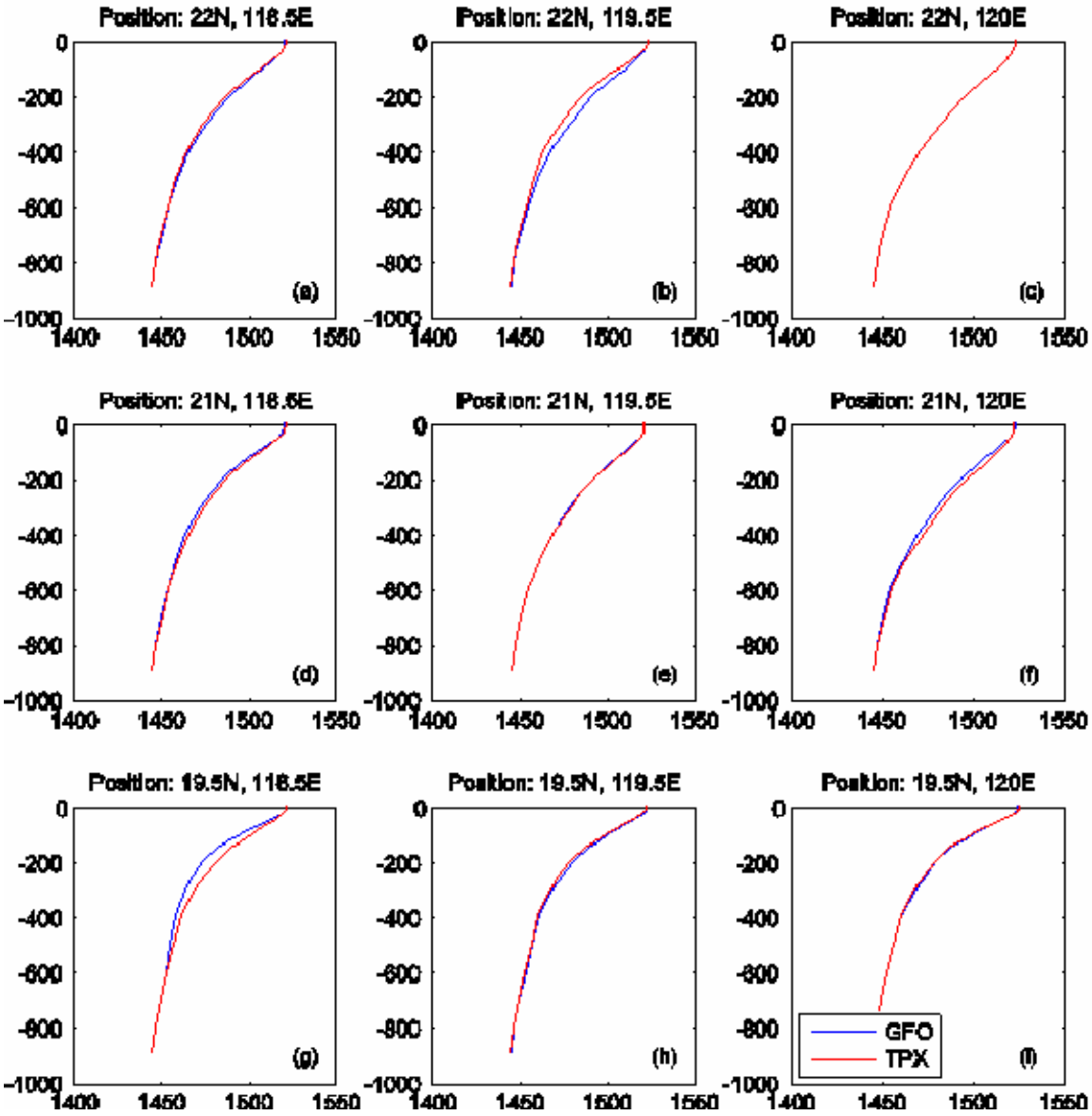

Figure 74. SCS MODAS SSP January 30, 2001

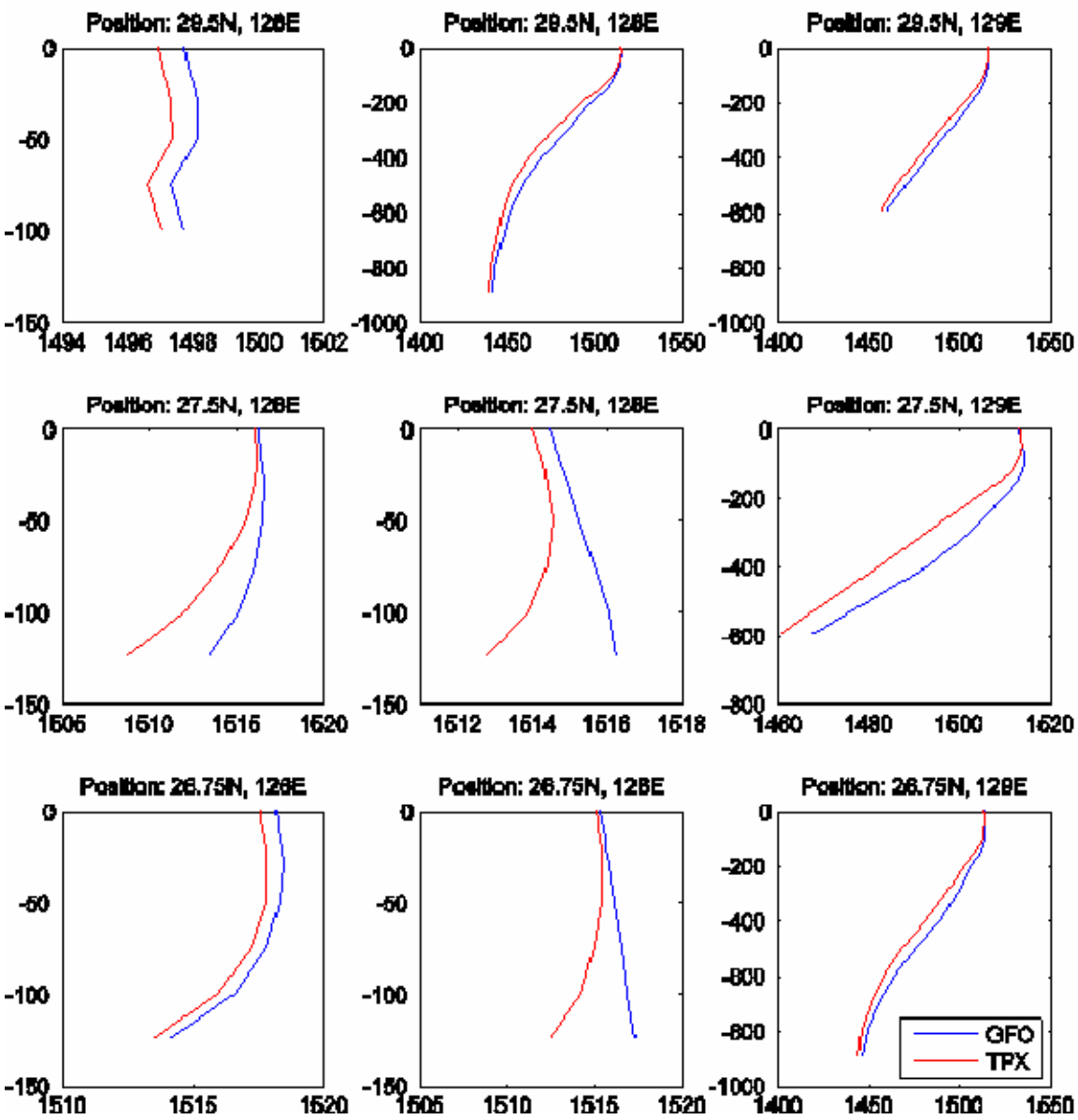

Figure 75. ECS MODAS SSP January 10, 2001

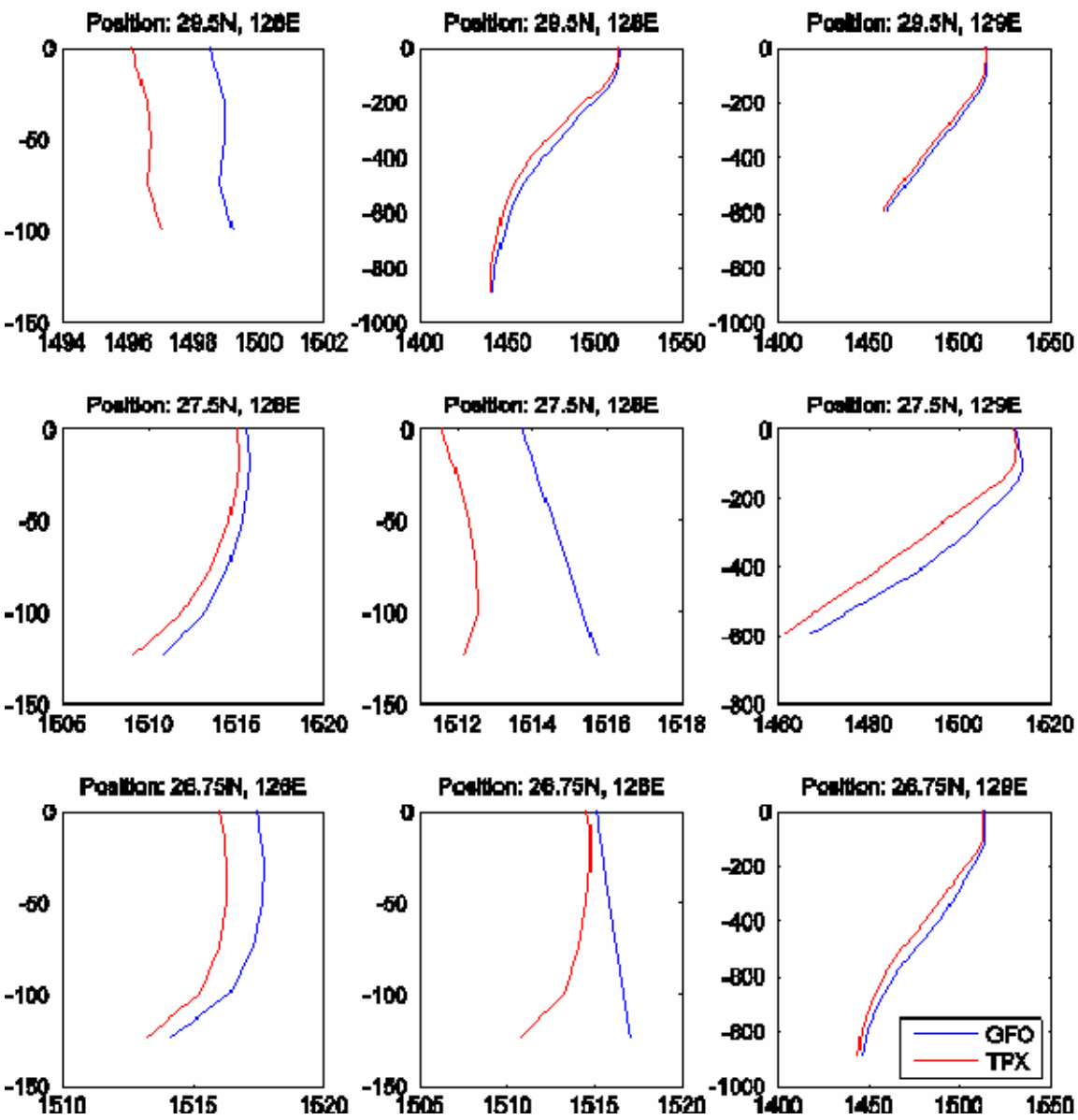

Figure 76. ECS MODAS SSP January 15, 2001

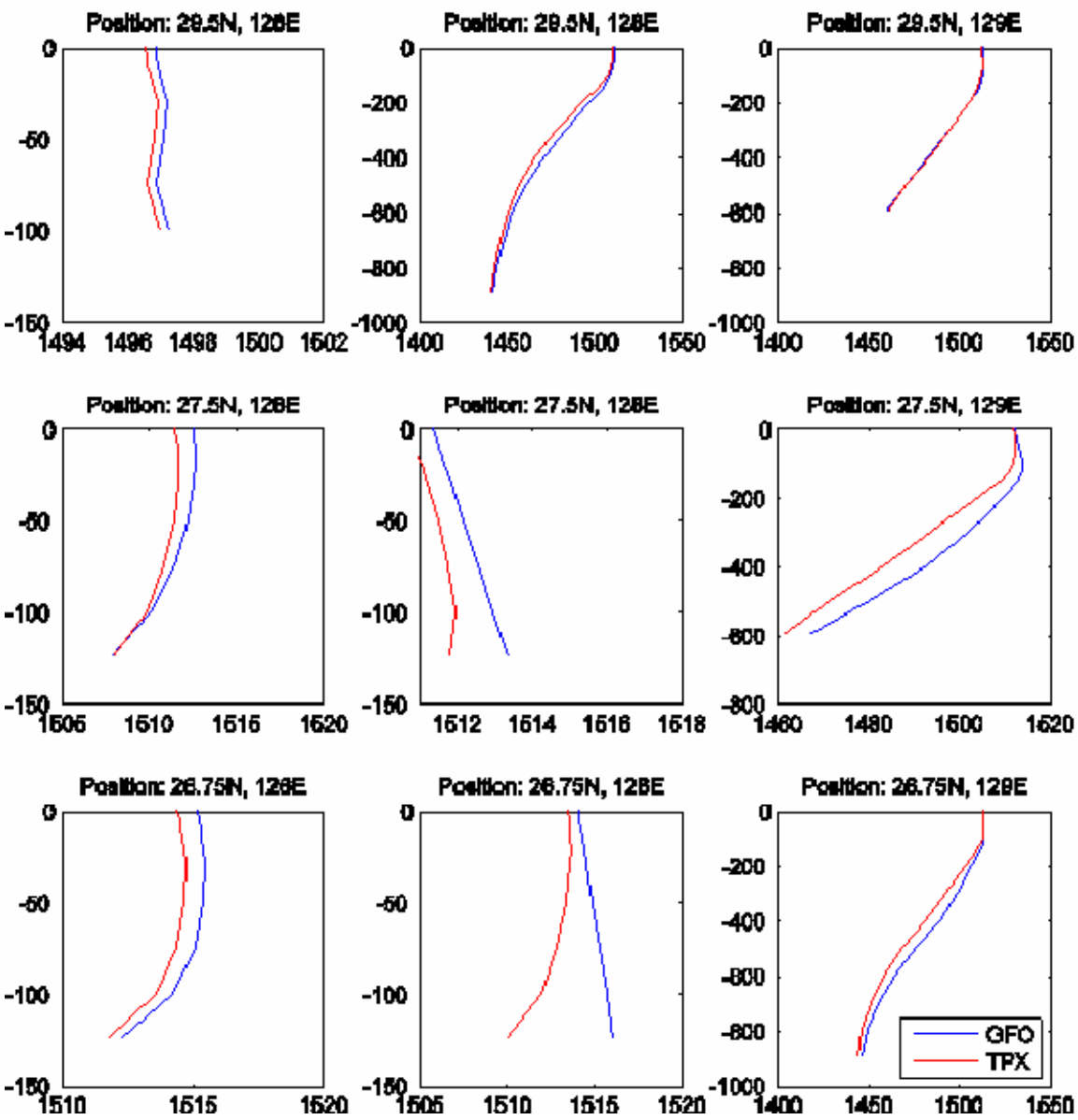

Figure 77. ECS MODAS SSP January 20, 2001

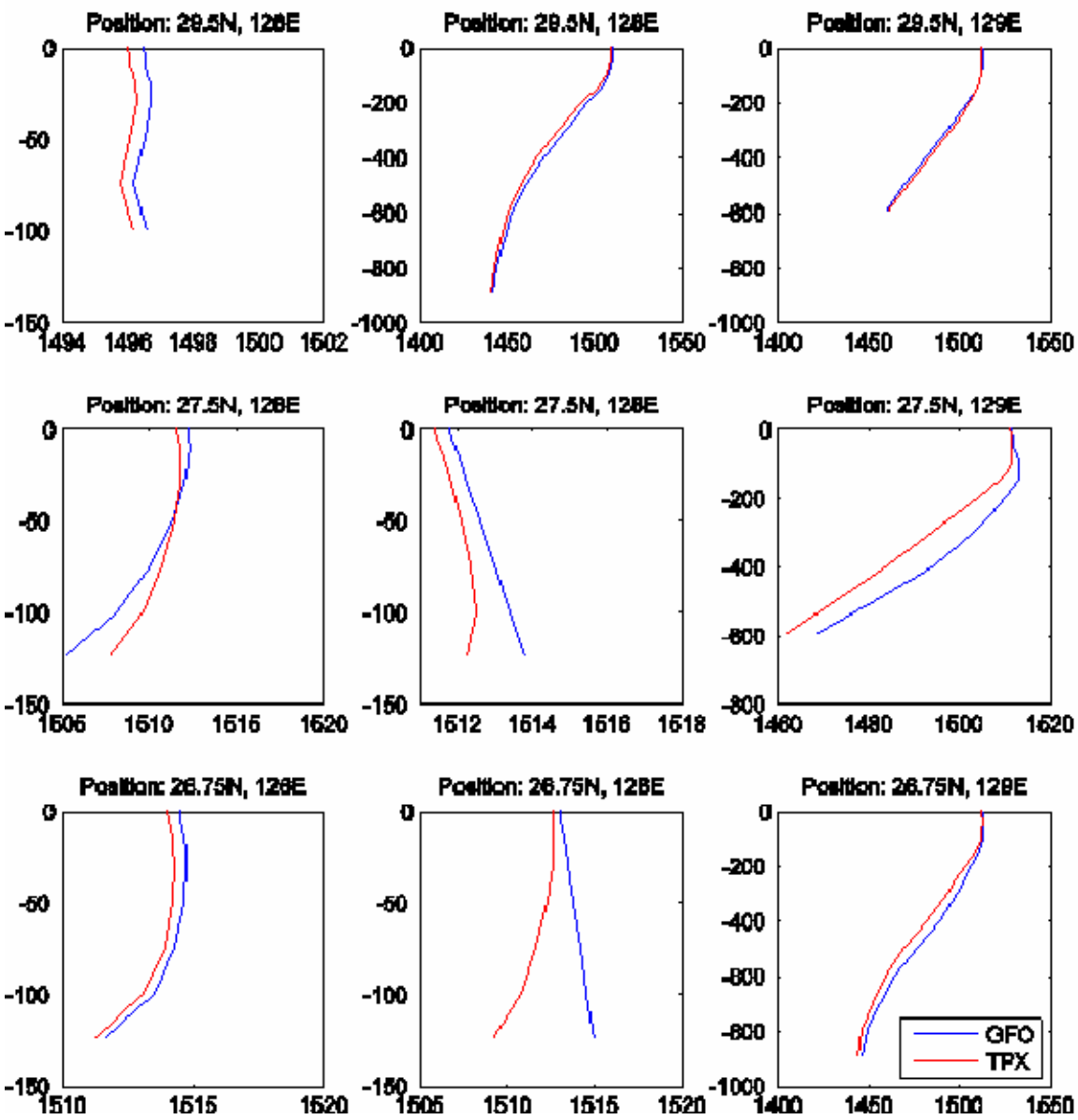

Figure 78. ECS MODAS SSP January 25, 2001

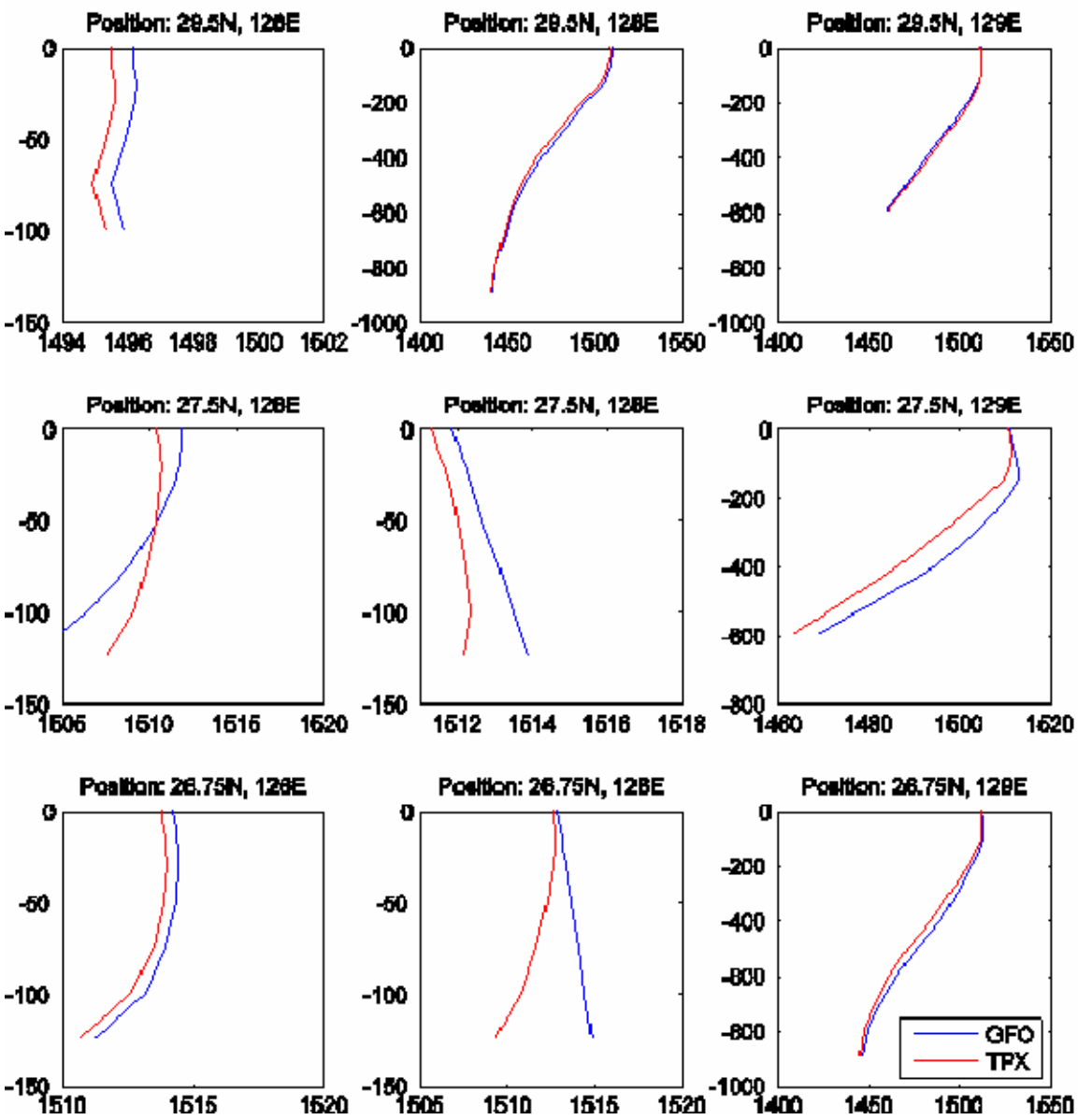

Figure 79. ECS MODAS SSP January 30, 2001

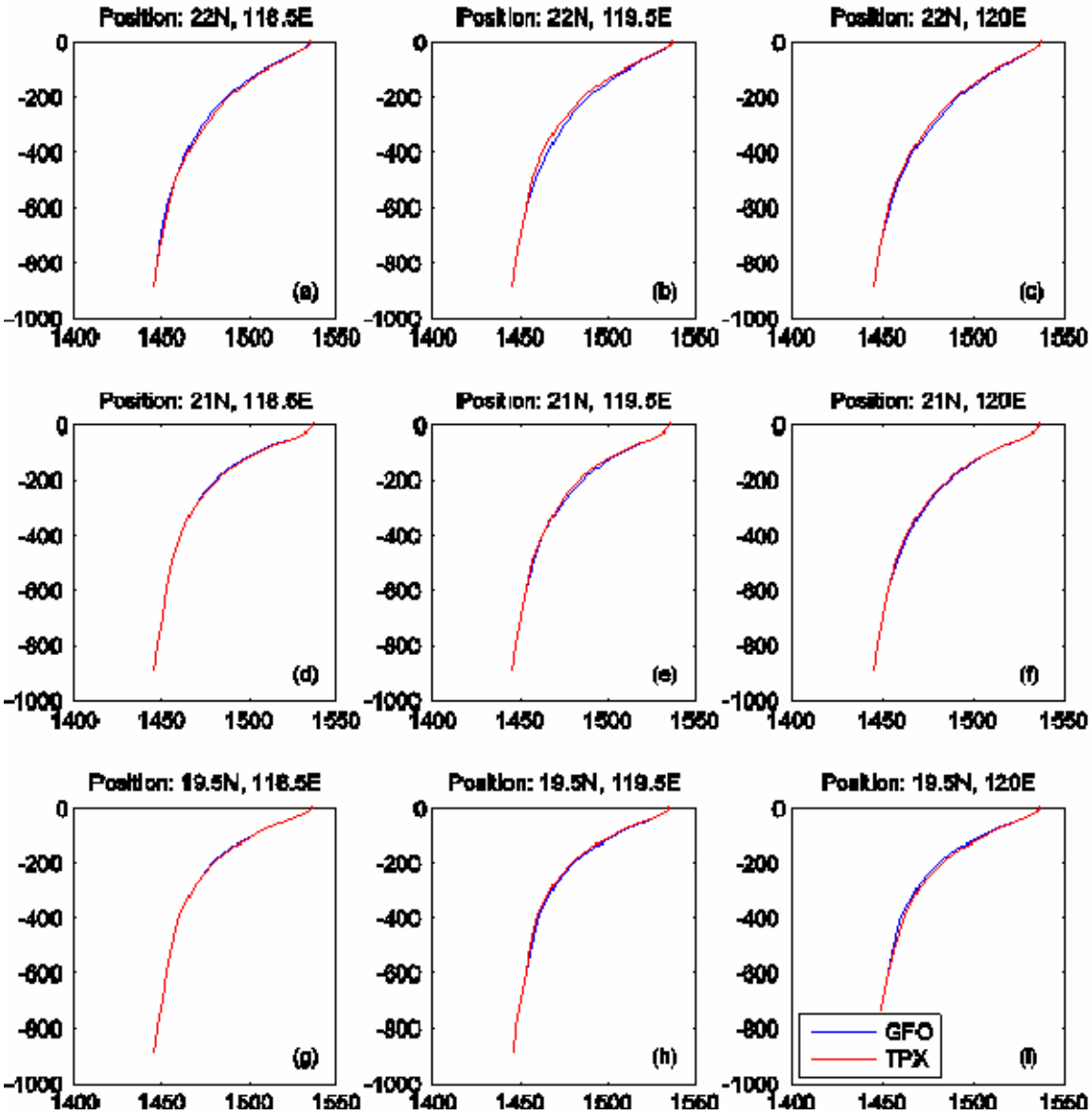

Figure 80. SCS MODAS SSP July 05, 2001

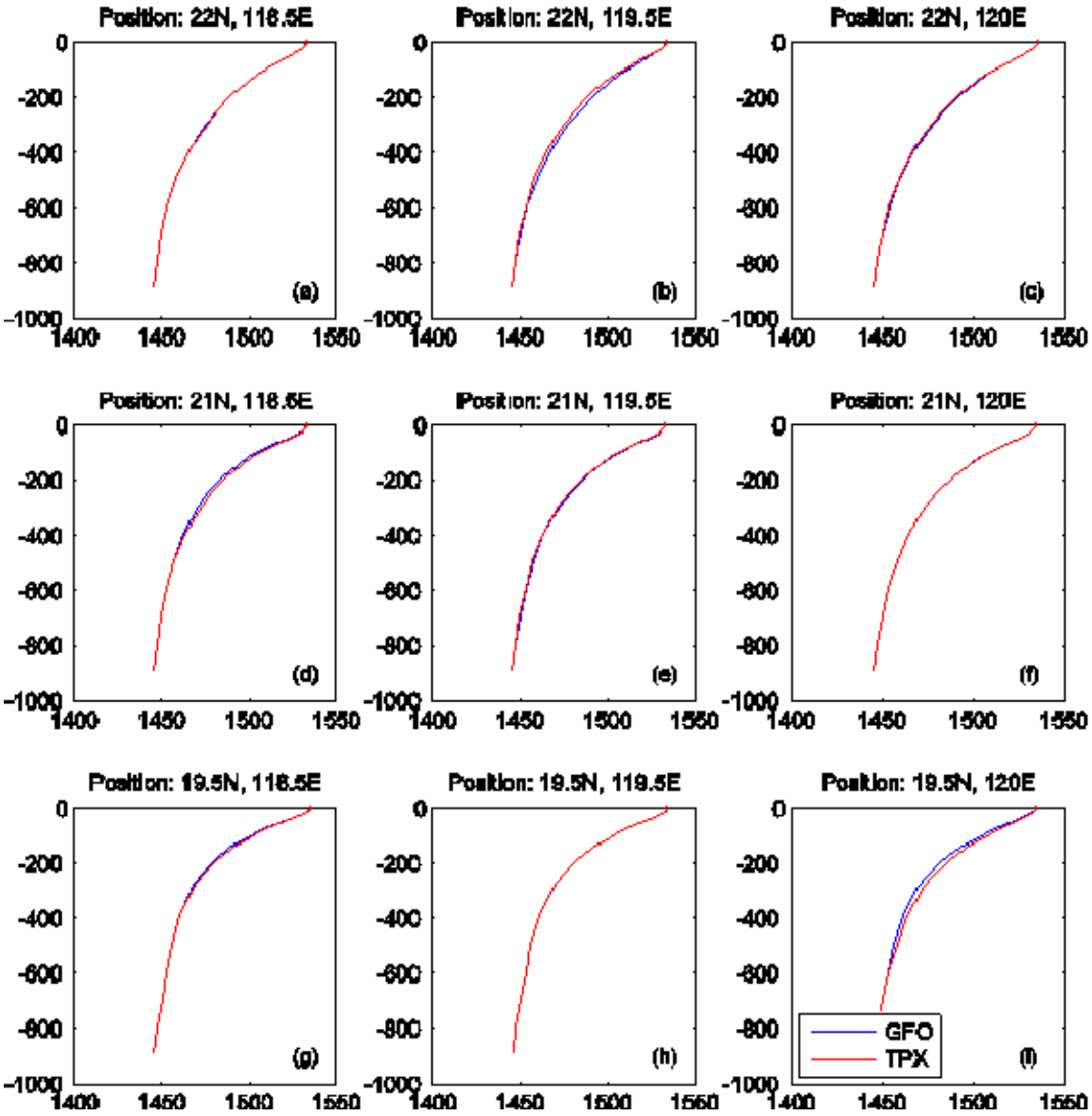

Figure 81. SCS MODAS SSP July 10, 2001

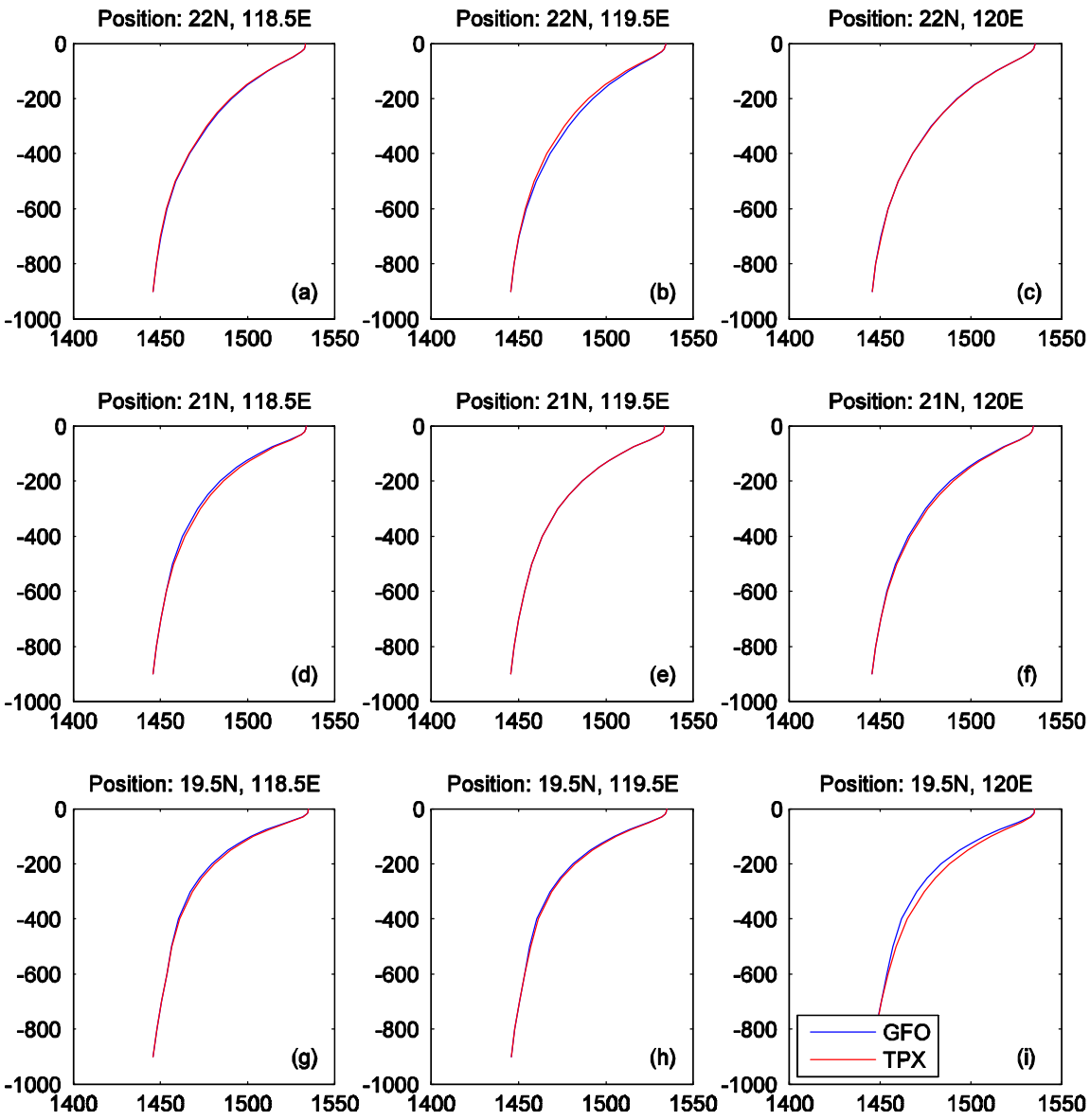

Figure 82. SCS MODAS SSP July 15, 2001

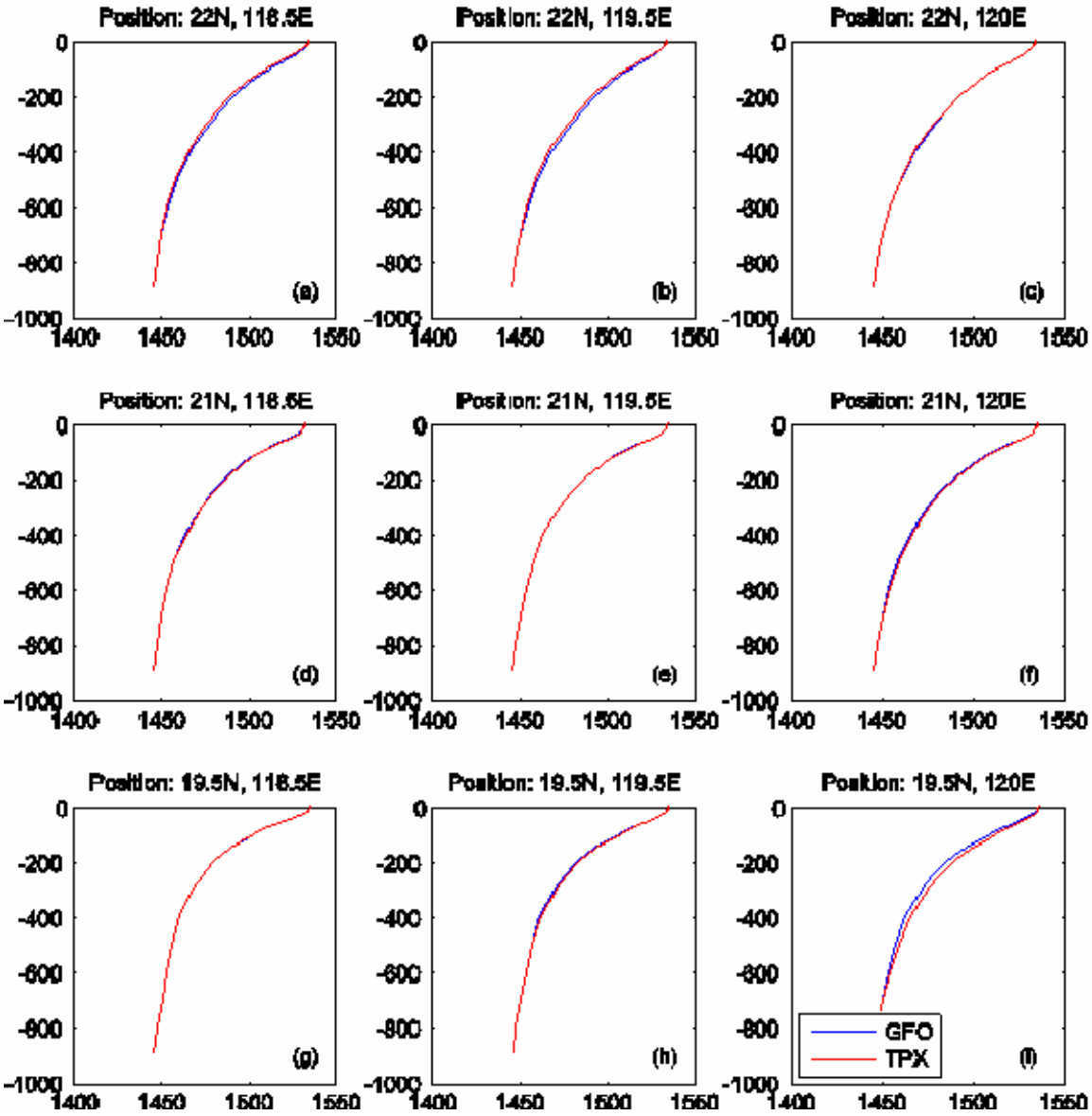

Figure 83. SCS MODAS SSP July 20, 2001

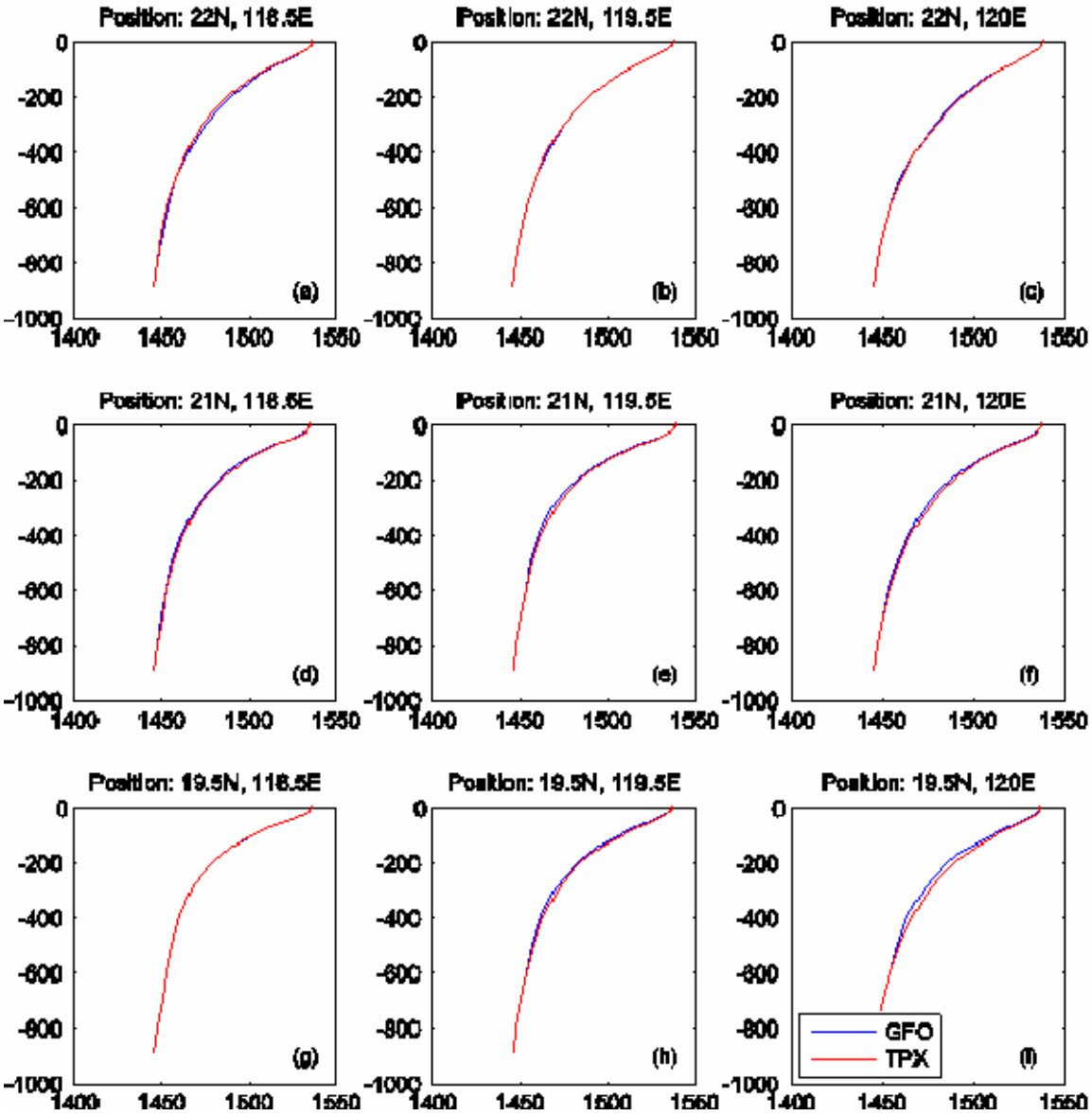

Figure 84. SCS MODAS SSP July 25, 2001

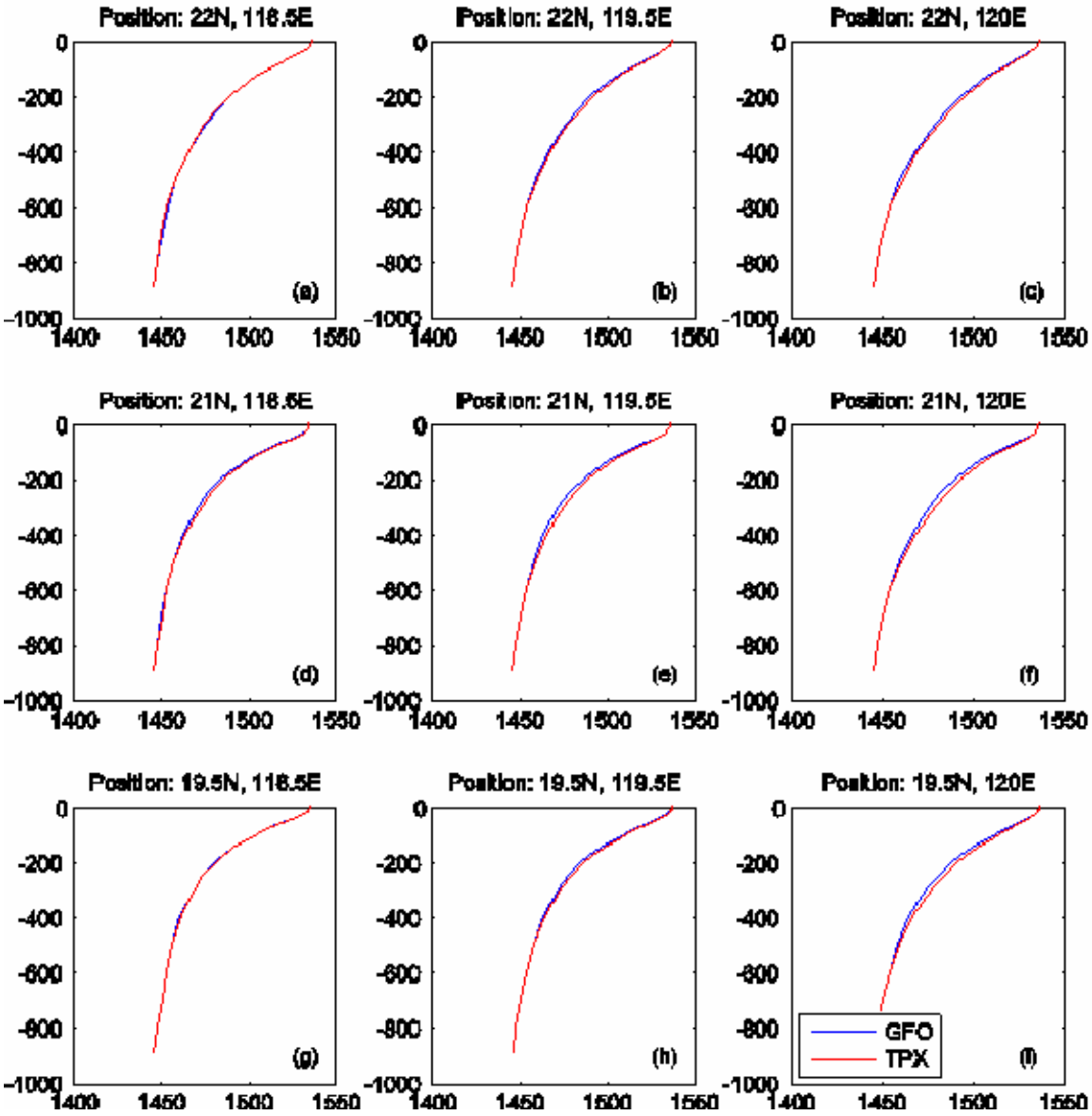

Figure 85. SCS MODAS SSP July 30, 2001

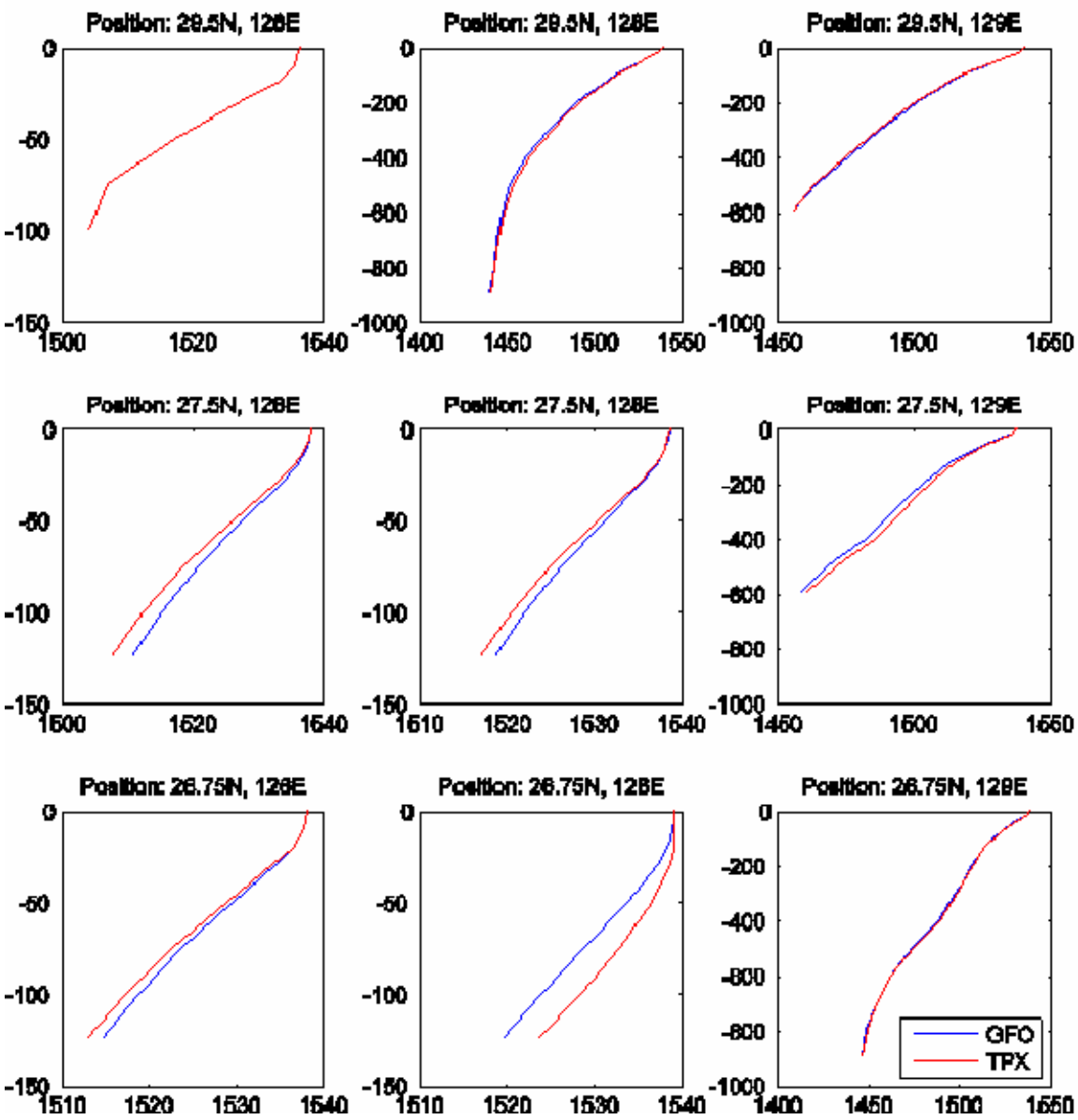

Figure 86. ECS MODAS SSP July 05, 2001

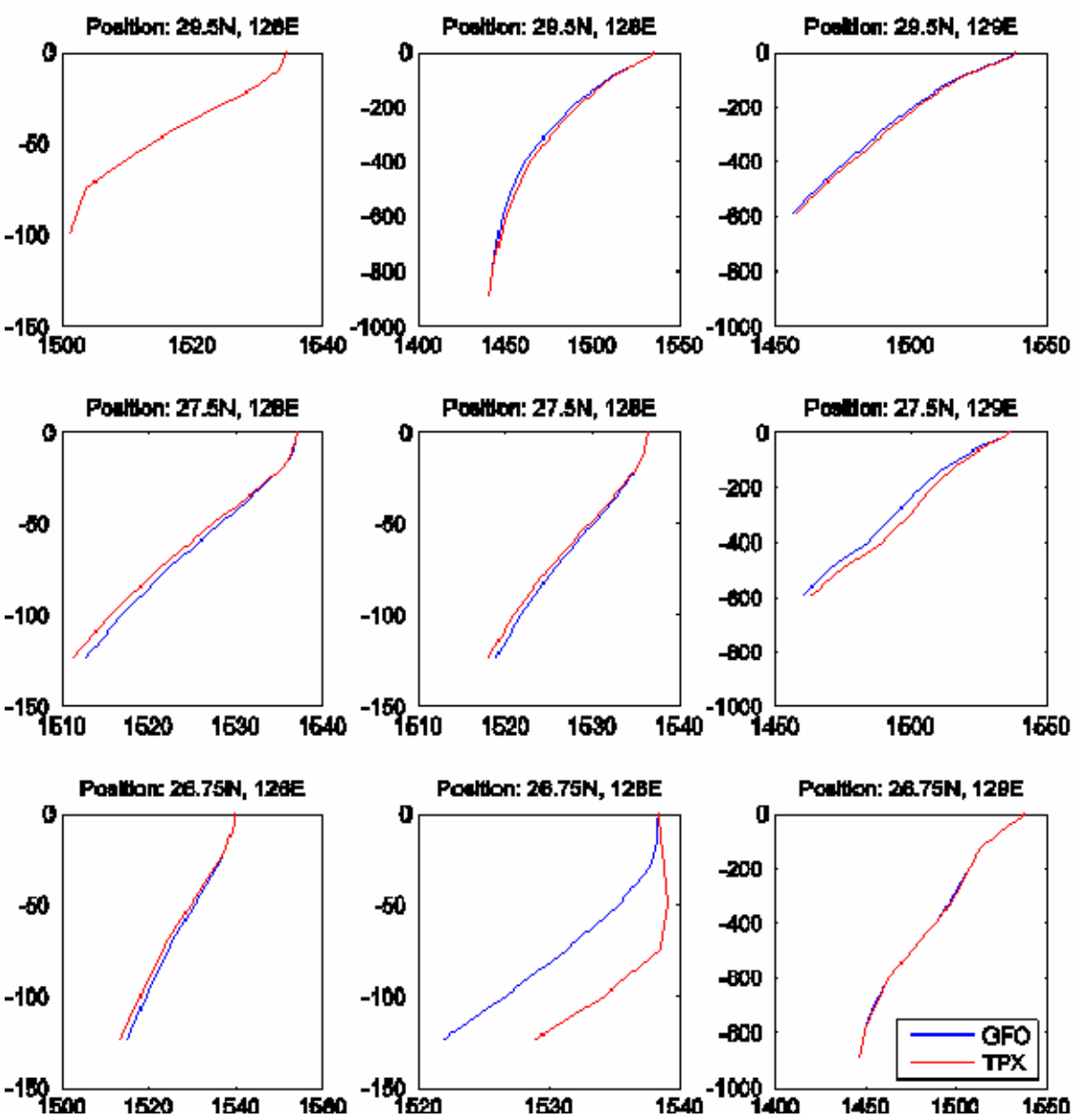

Figure 87. ECS MODAS SSP July 10, 2001

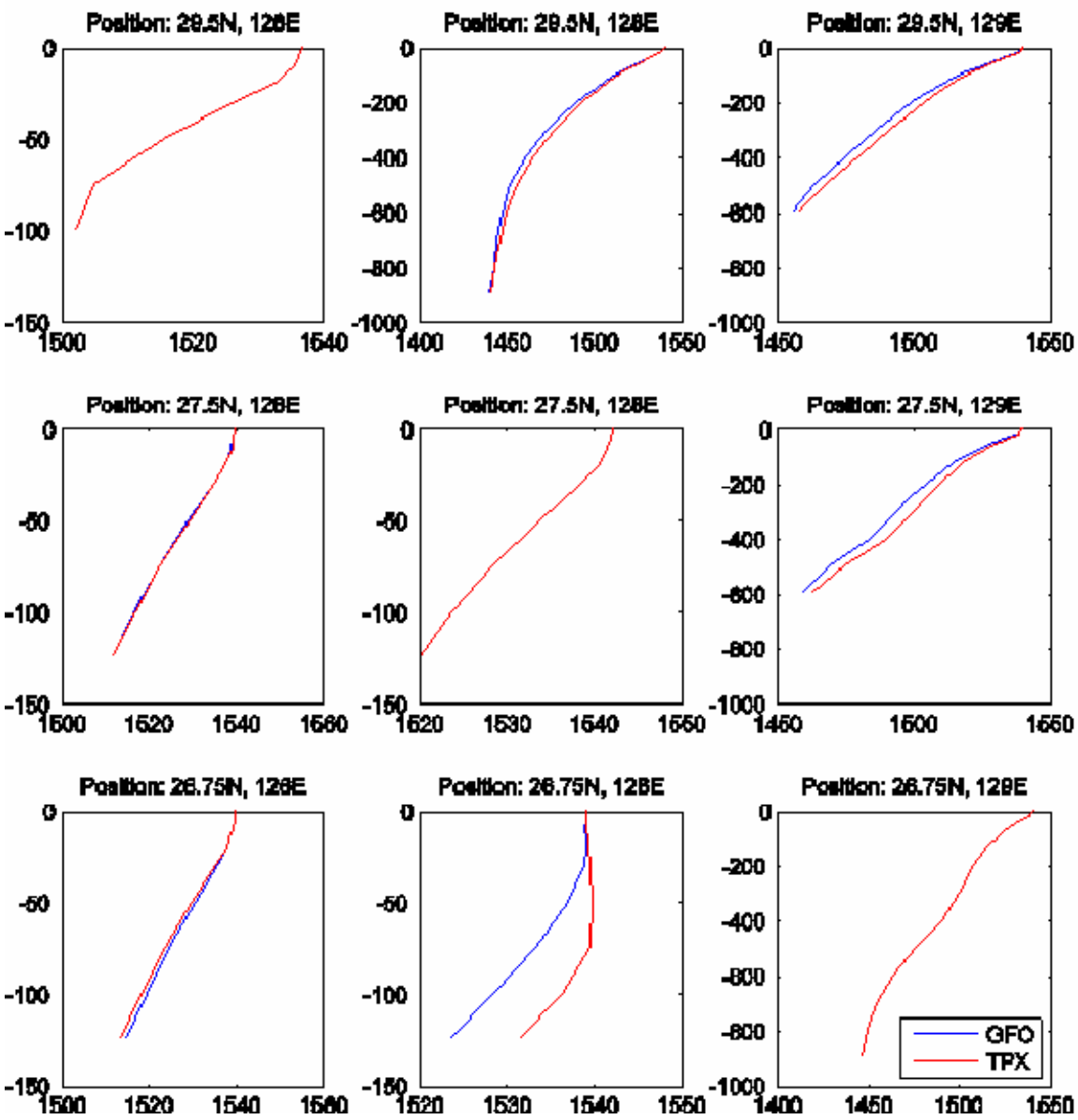

Figure 88. ECS MODAS SSP July 15, 2001

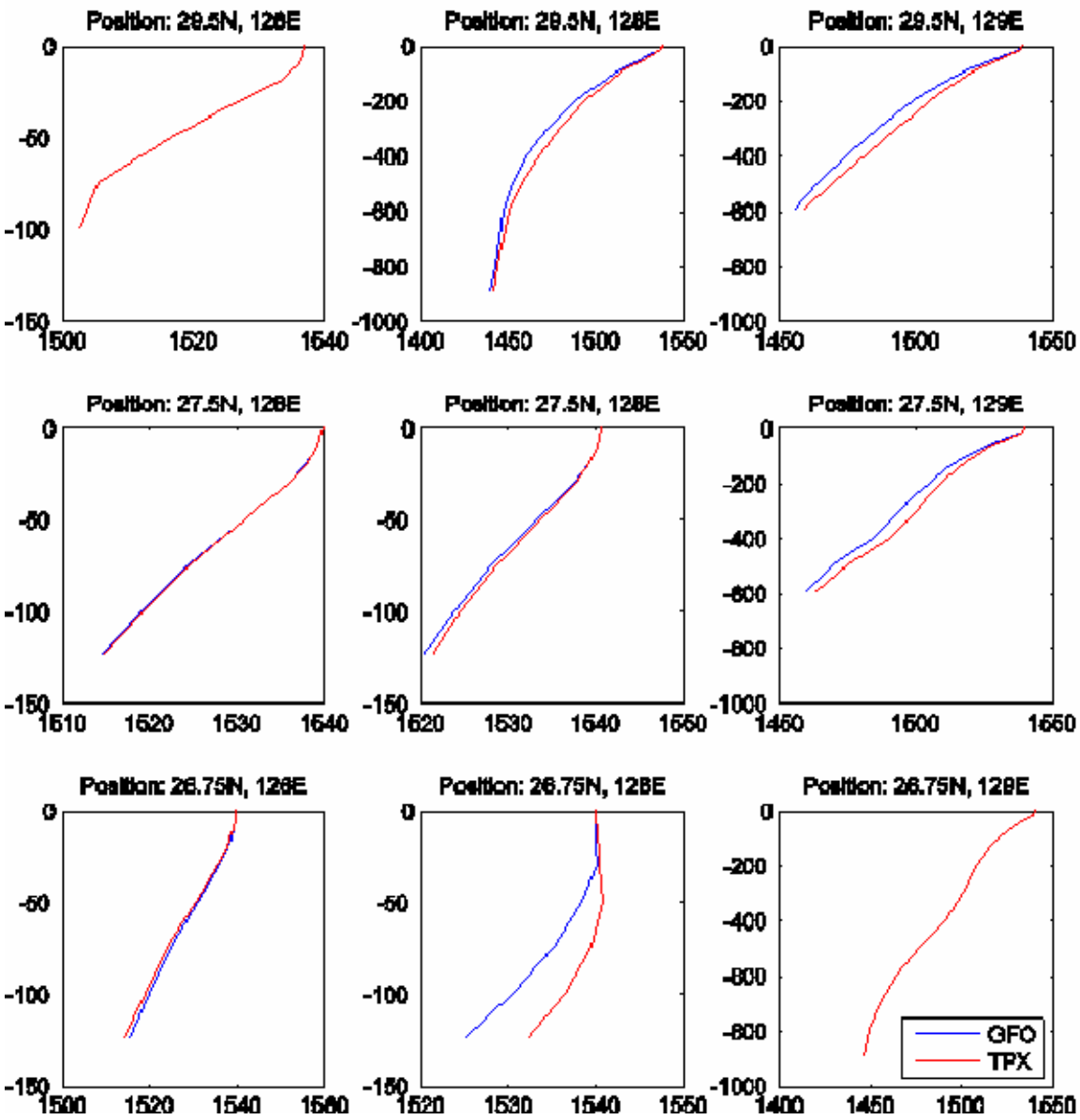

Figure 89. ECS MODAS SSP July 20, 2001

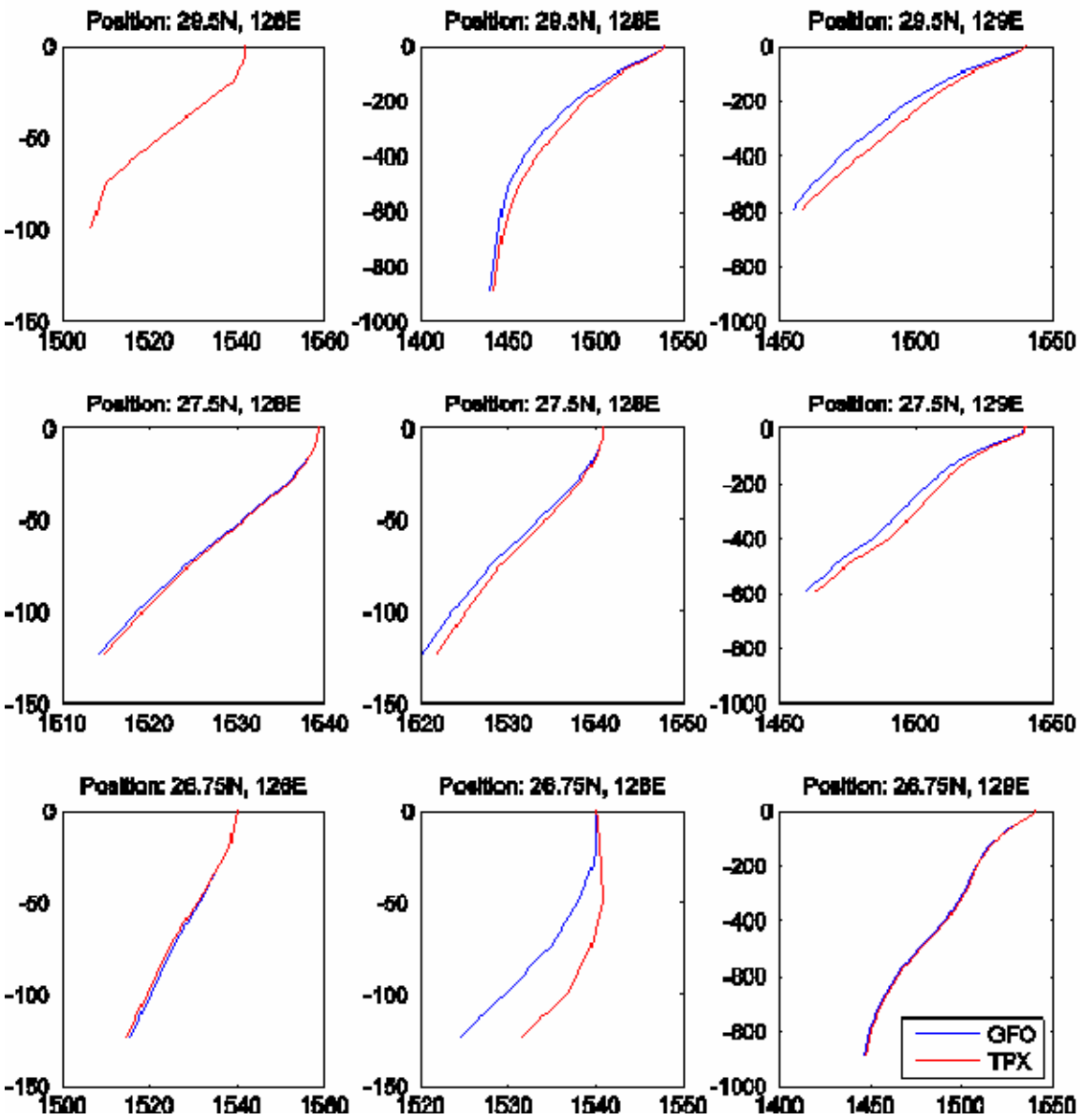

Figure 90. ECS MODAS SSP July 25, 2001

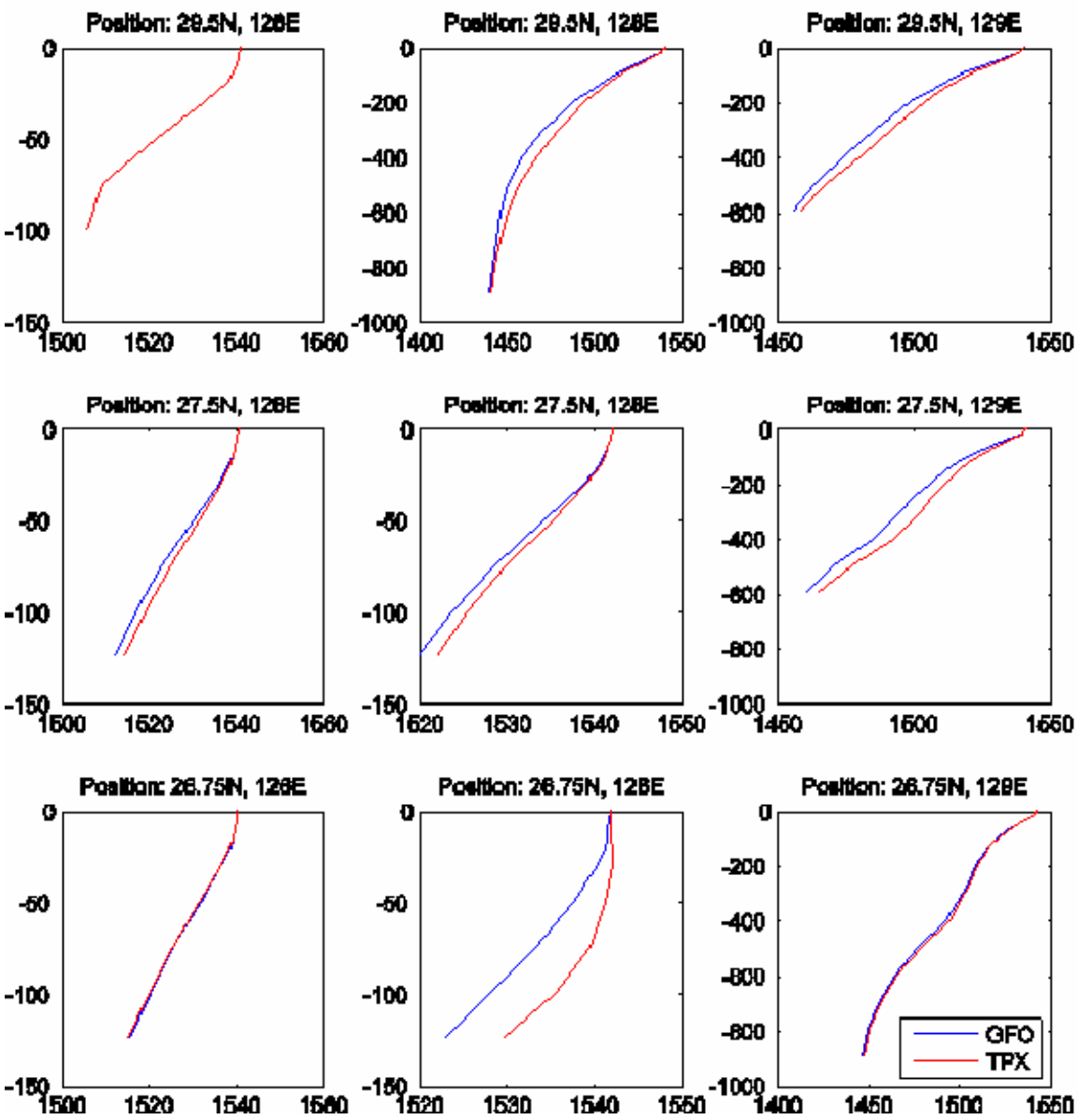

Figure 91. ECS MODAS SSP July 30, 2001

APPENDIX D. MODAS INPUT STATISTICS

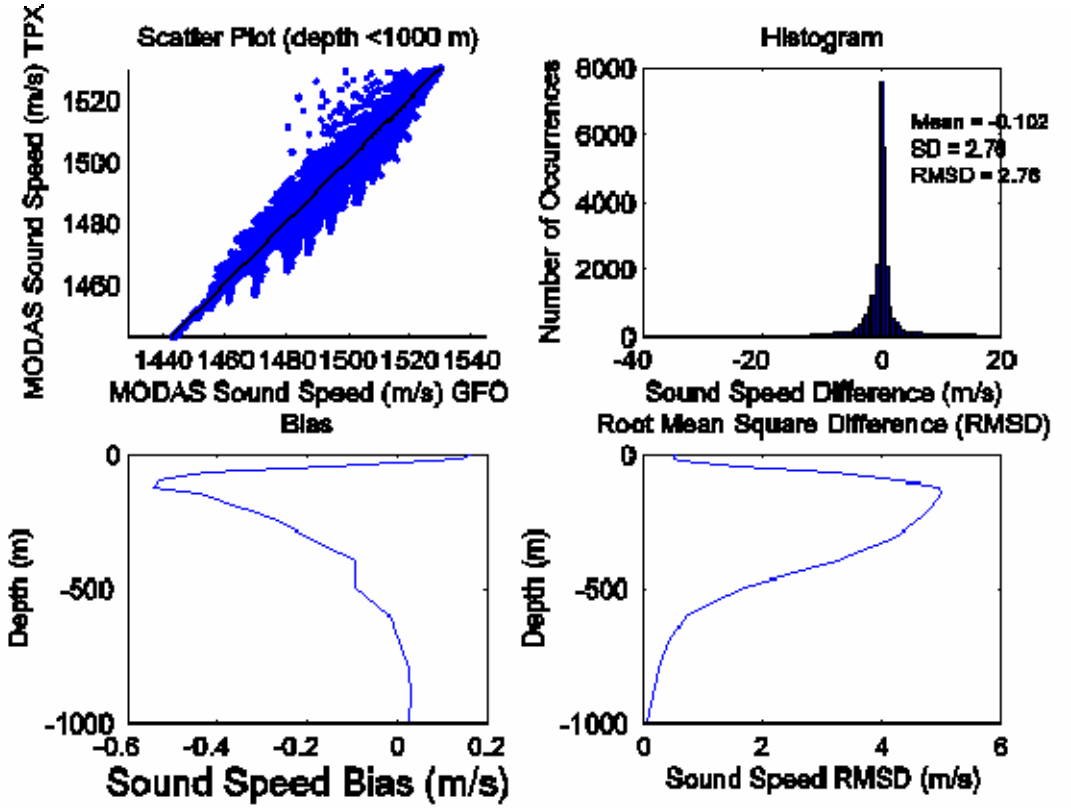

Figure 92. SCS MODAS sound speed January 10, 2001

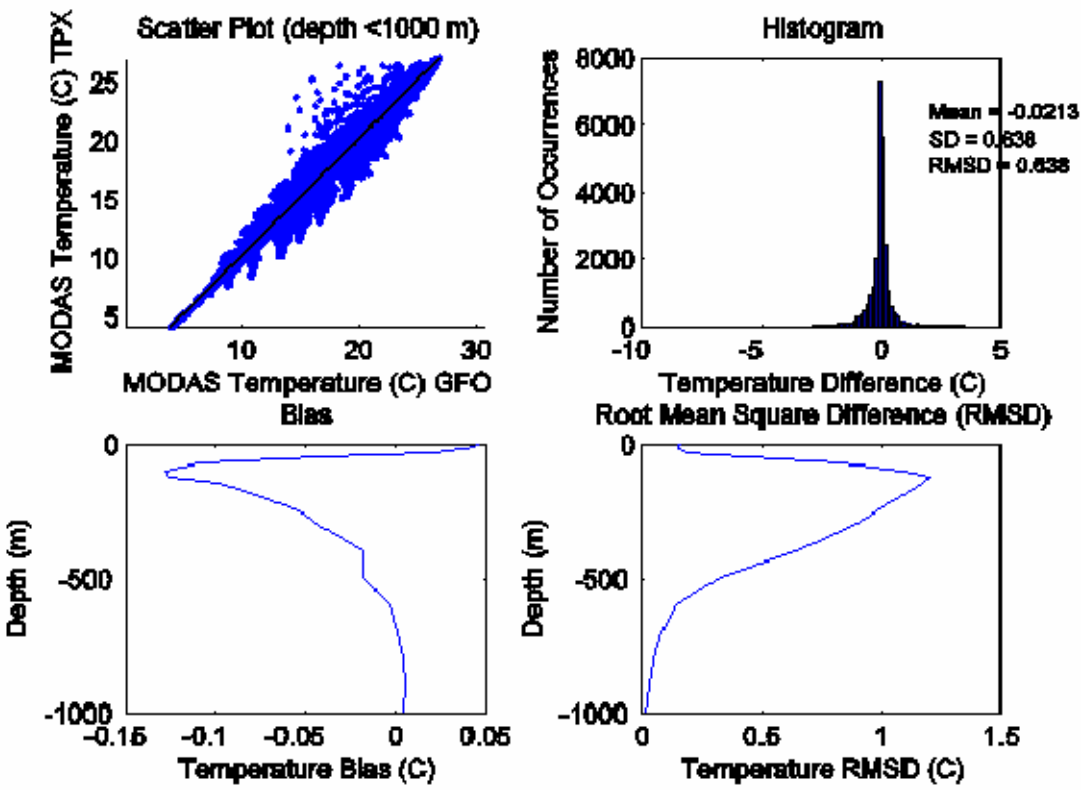

Figure 93. SCS MODAS temperature January 10, 2001

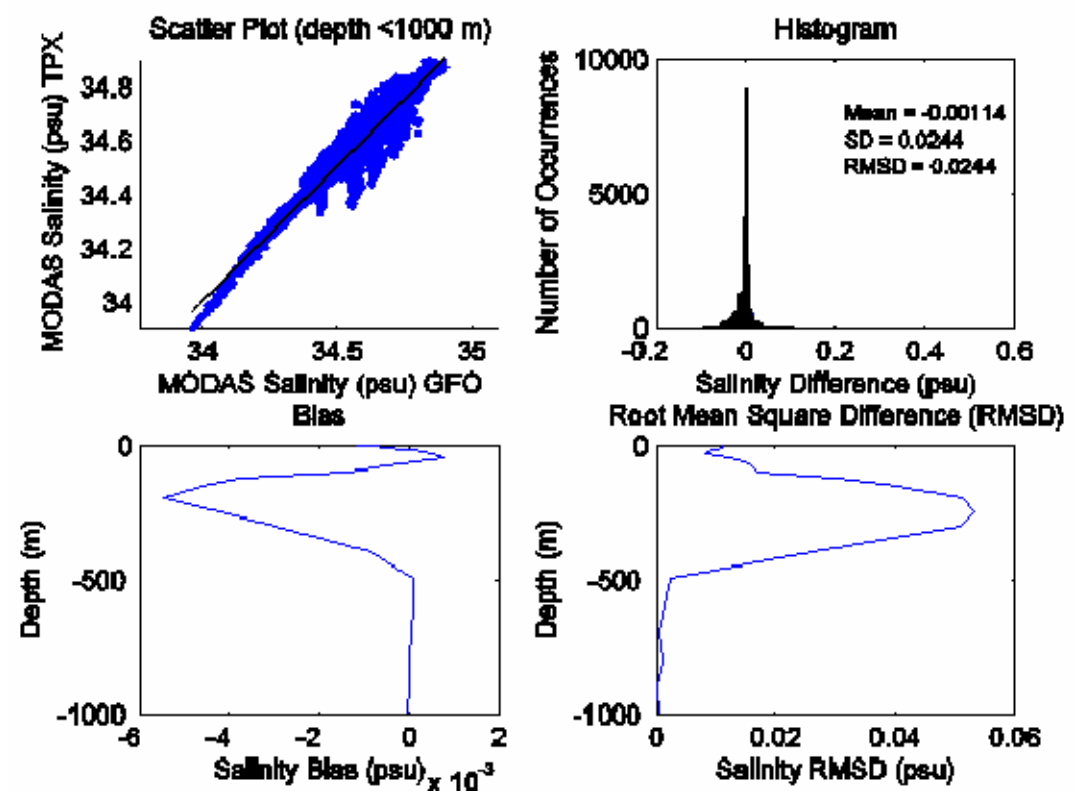

Figure 94. SCS MODAS salinity January 10, 2001

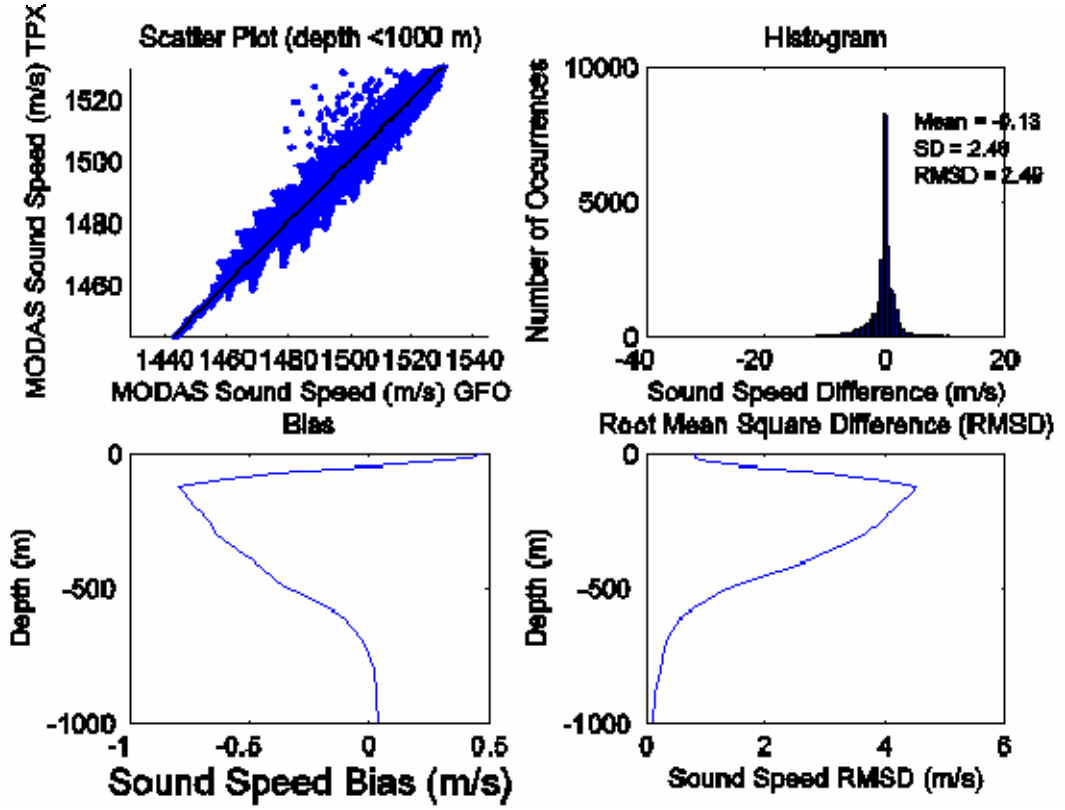

Figure 95. SCS MODAS sound speed January 15, 2001

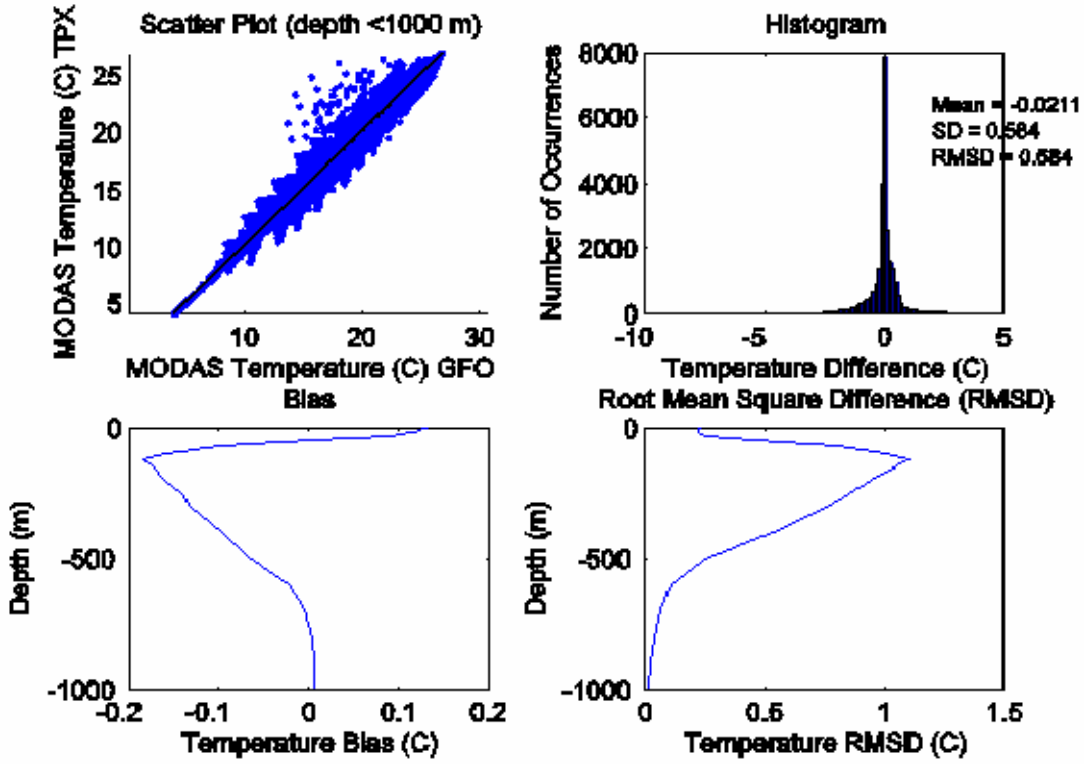

Figure 96. SCS MODAS temperature January 15, 2001

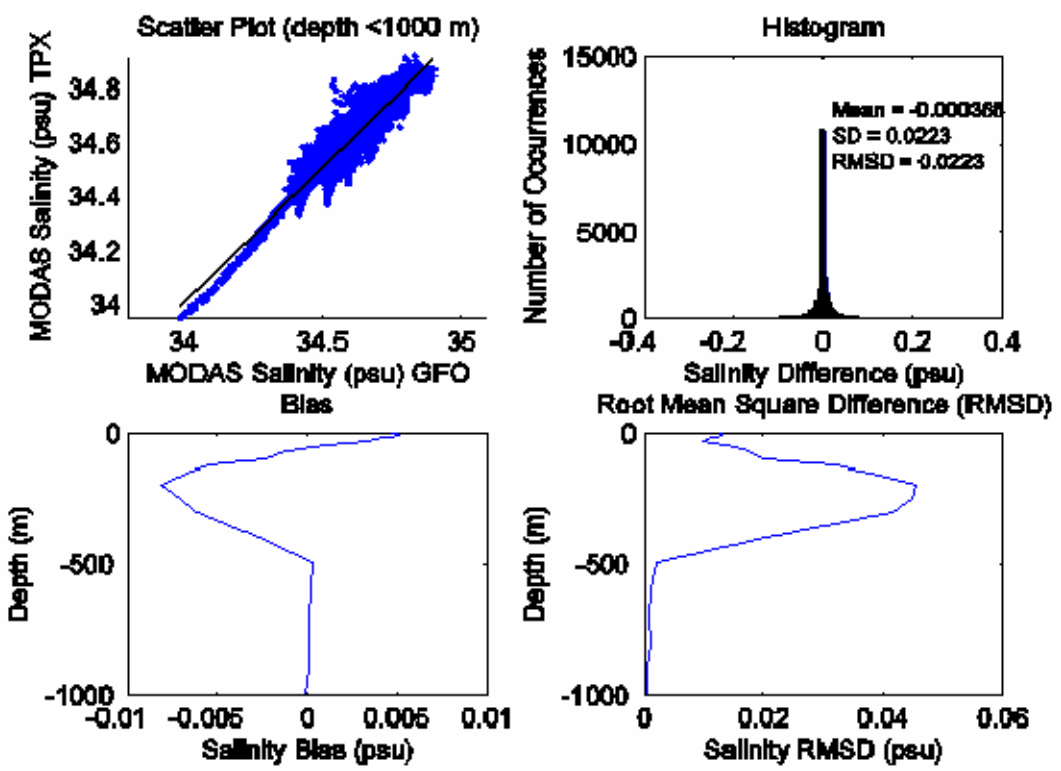

Figure 97. SCS MODAS salinity January 15, 2001

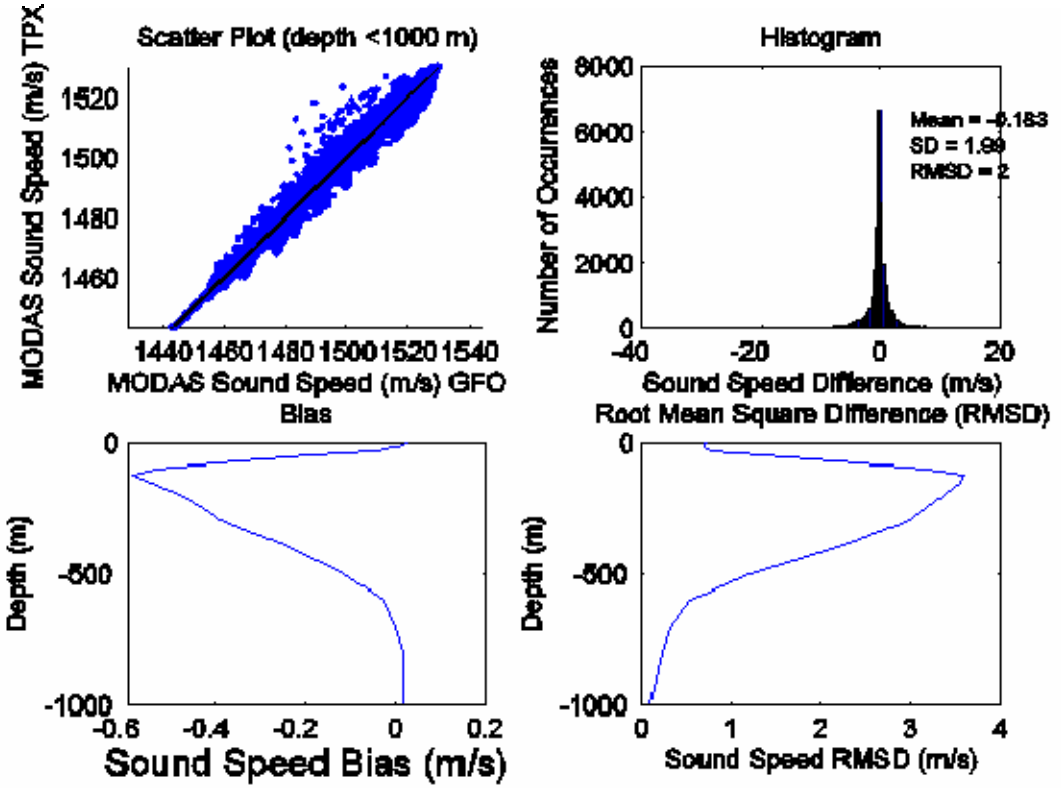

Figure 98. SCS MODAS sound speed January 20, 2001

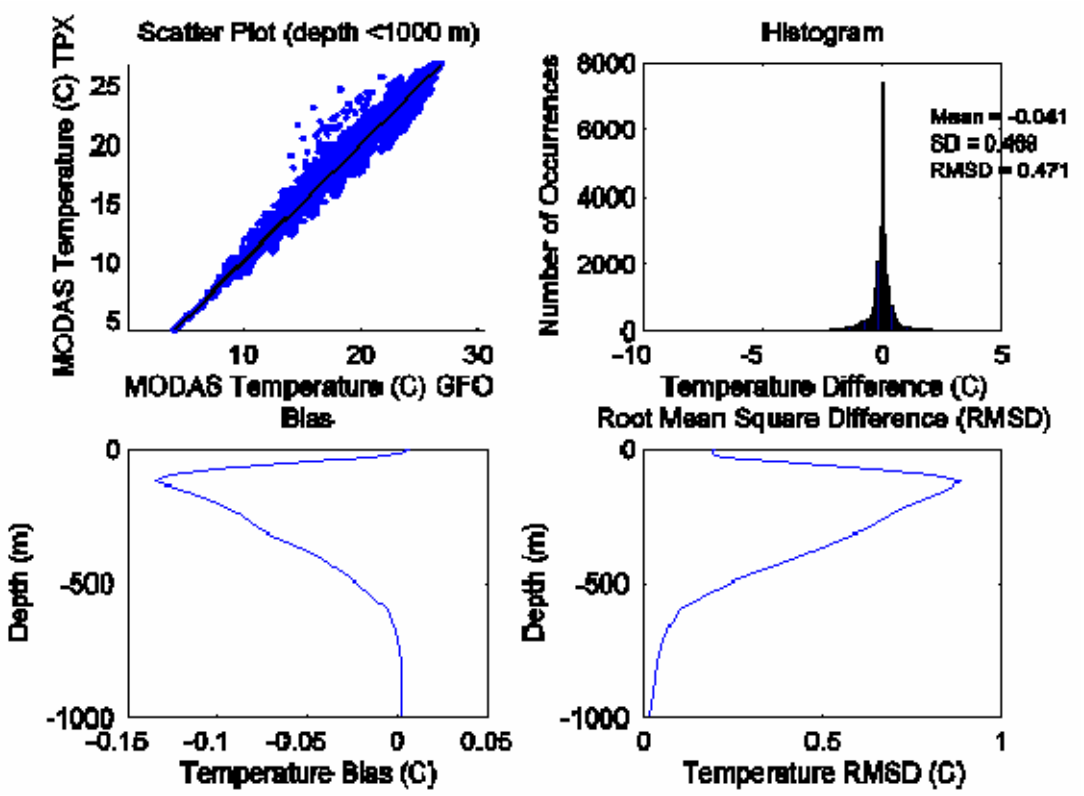

Figure 99. SCS MODAS temperature January 20, 2001

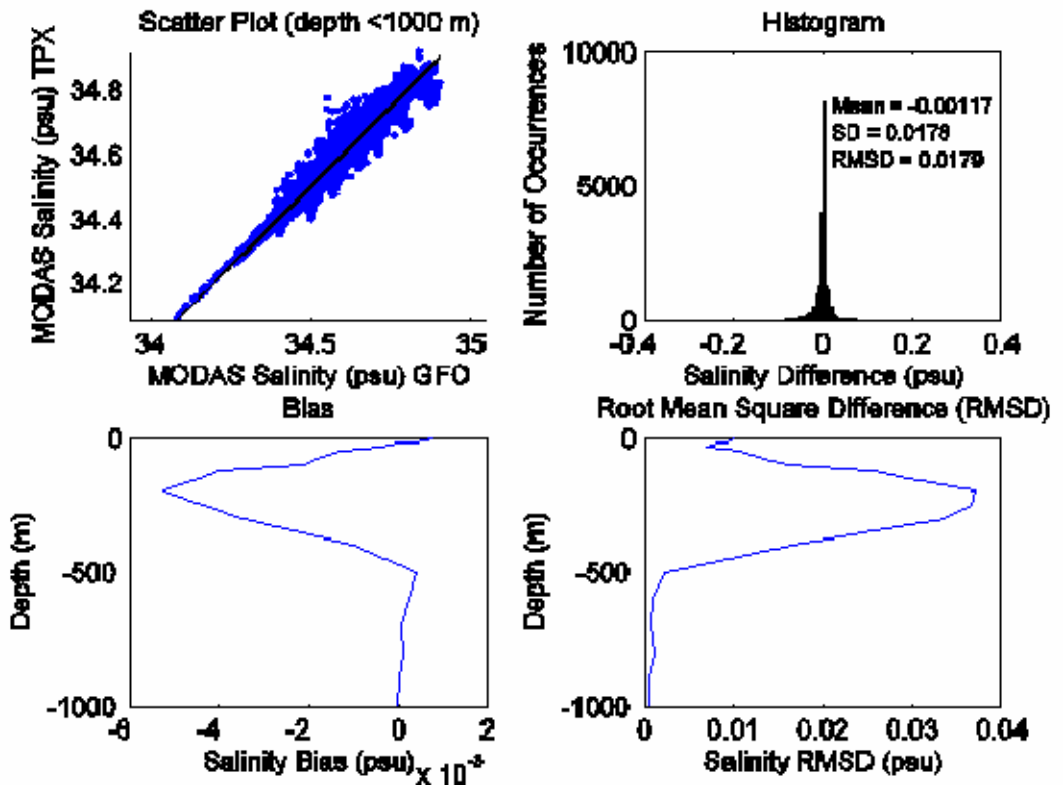

Figure 100. SCS MODAS salinity January 20, 2001

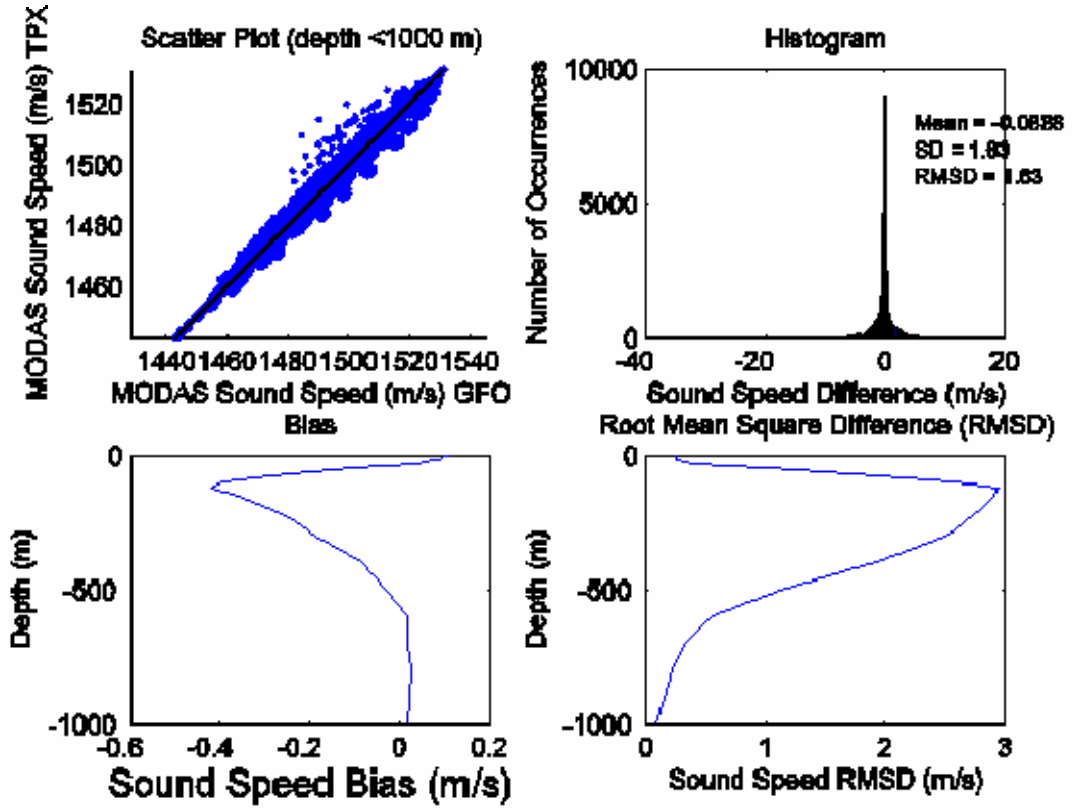

Figure 101. SCS MODAS sound speed January 25, 2001

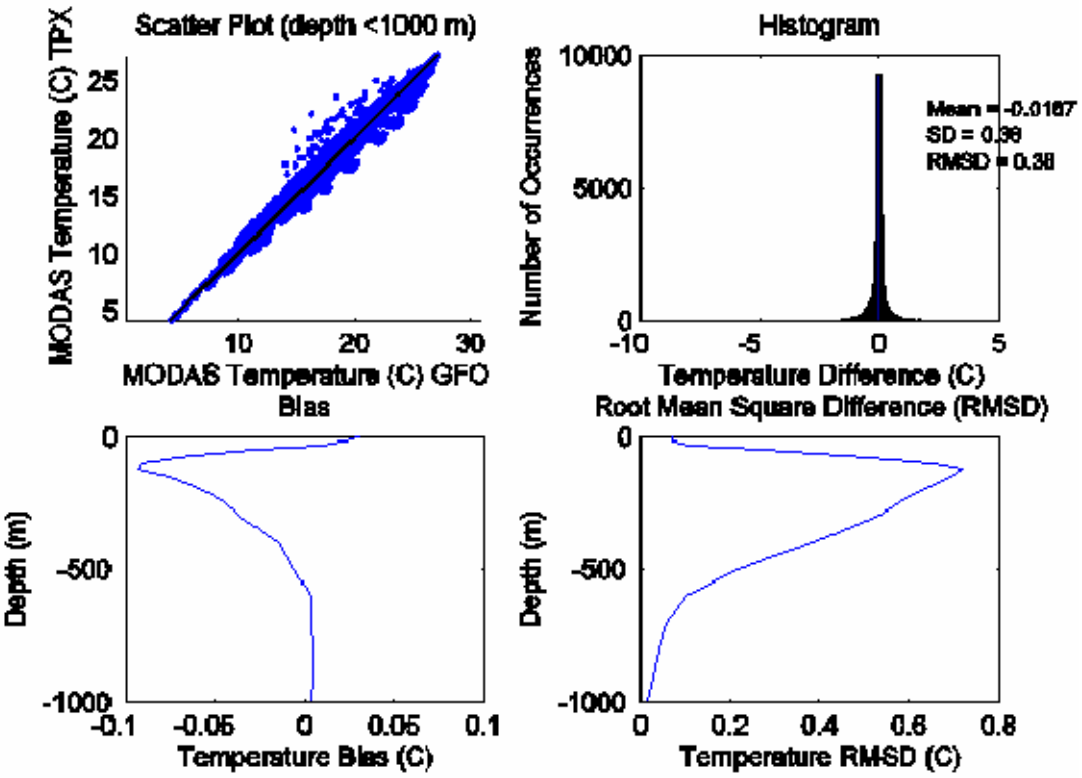

Figure 102. SCS MODAS temperature January 25, 2001

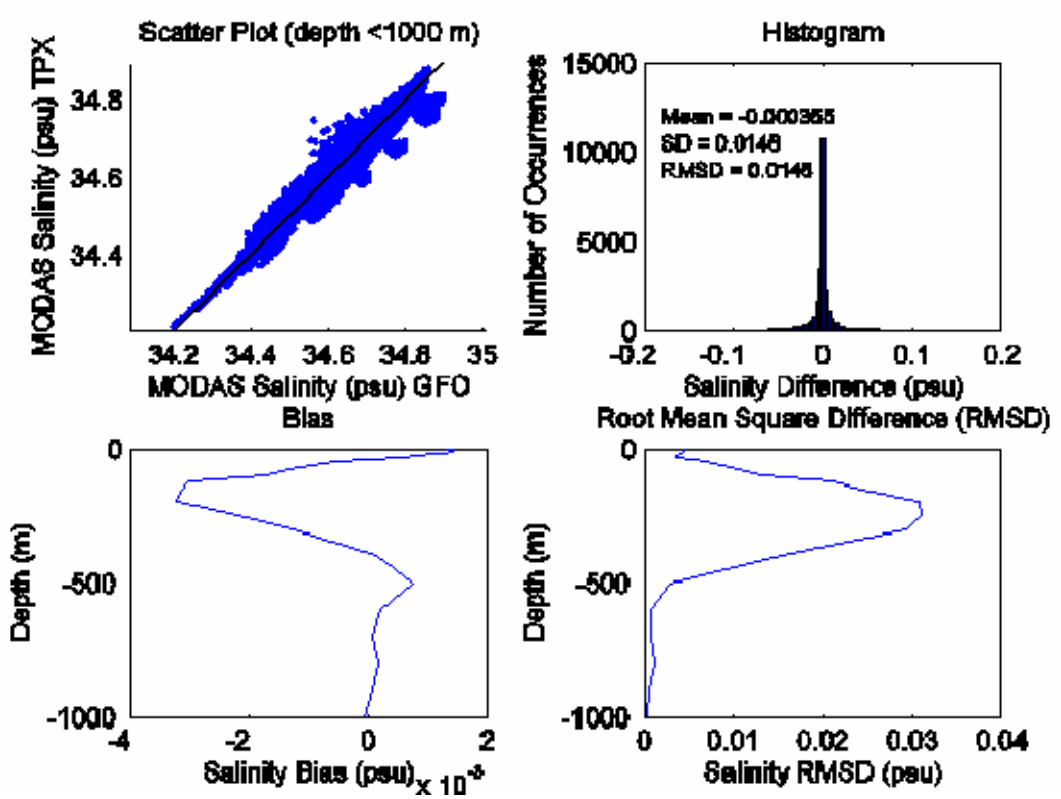

Figure 103. SCS MODAS salinity January 25, 2001

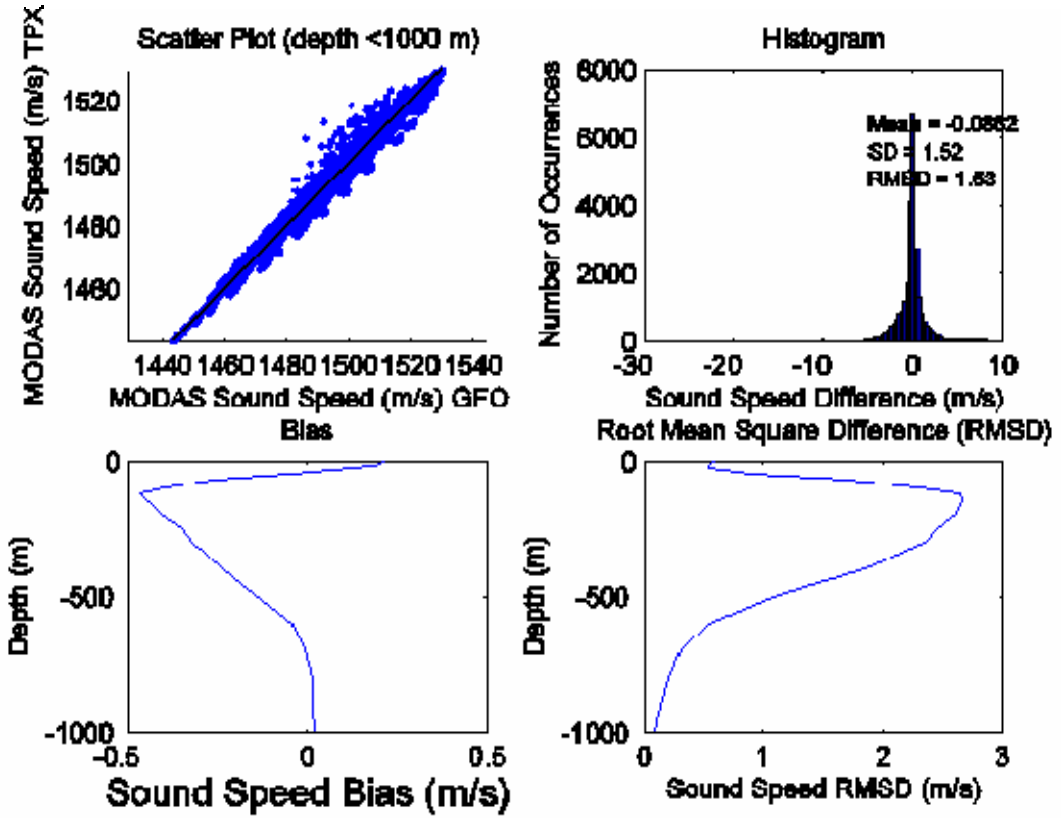

Figure 104. SCS MODAS sound speed January 30, 2001

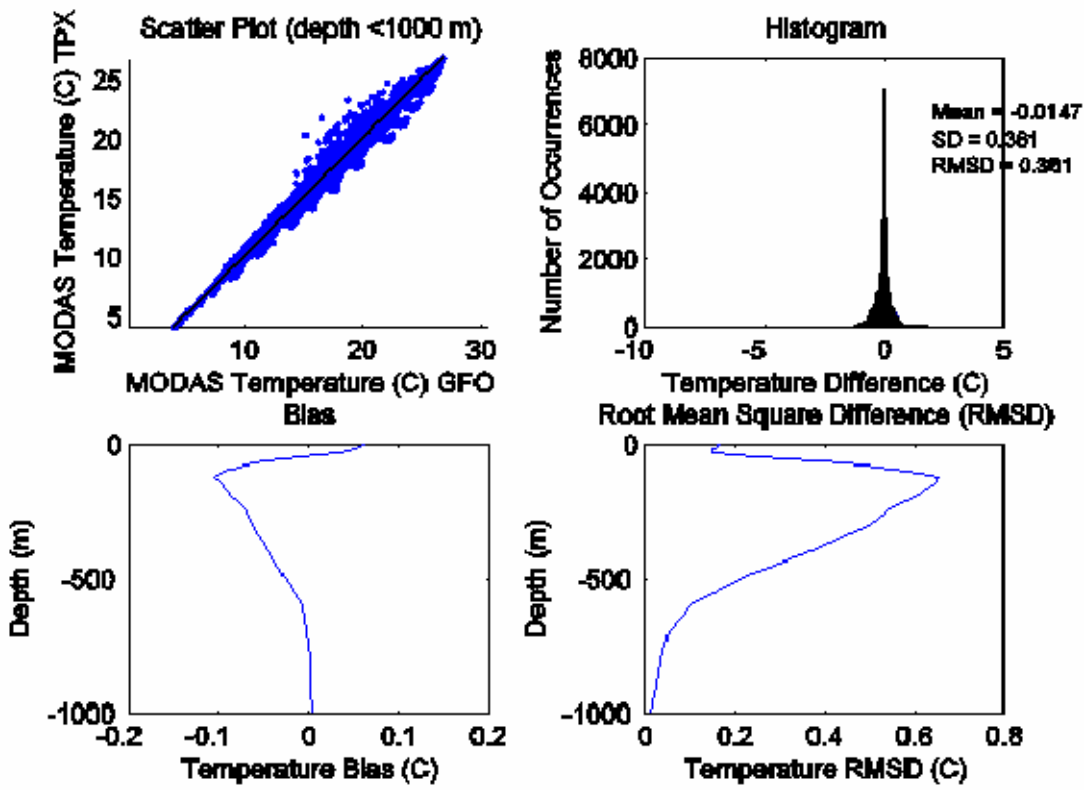

Figure 105. SCS MODAS temperature January 30, 2001

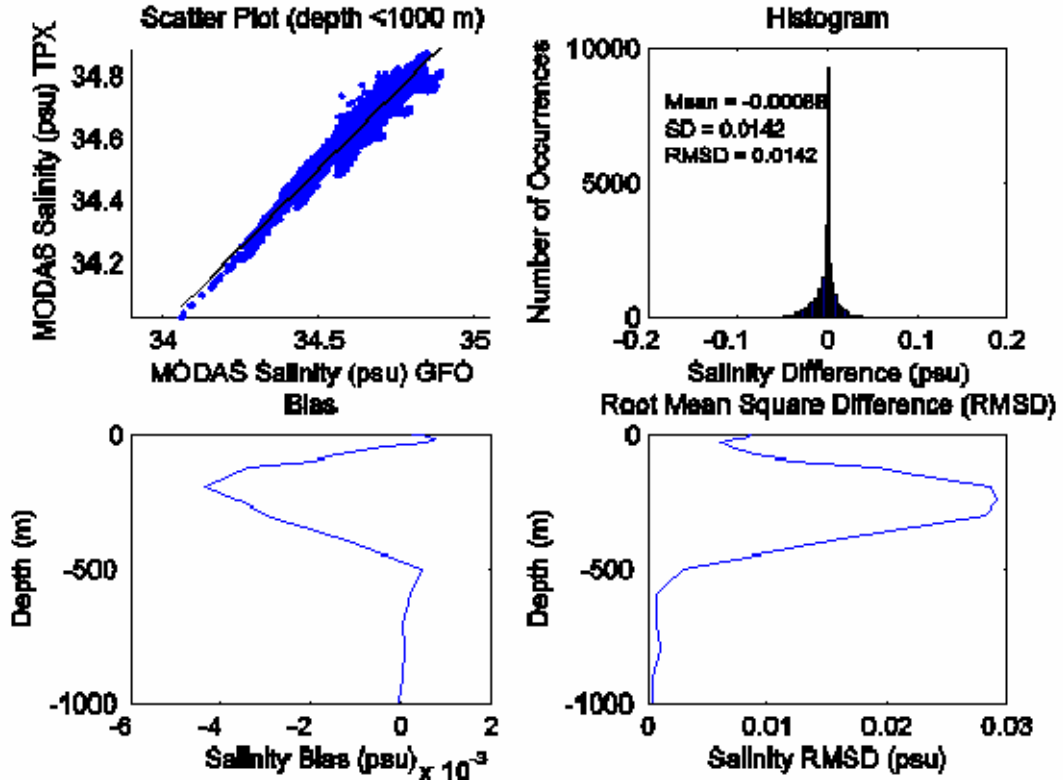

Figure 106. SCS MODAS salinity January 30, 2001

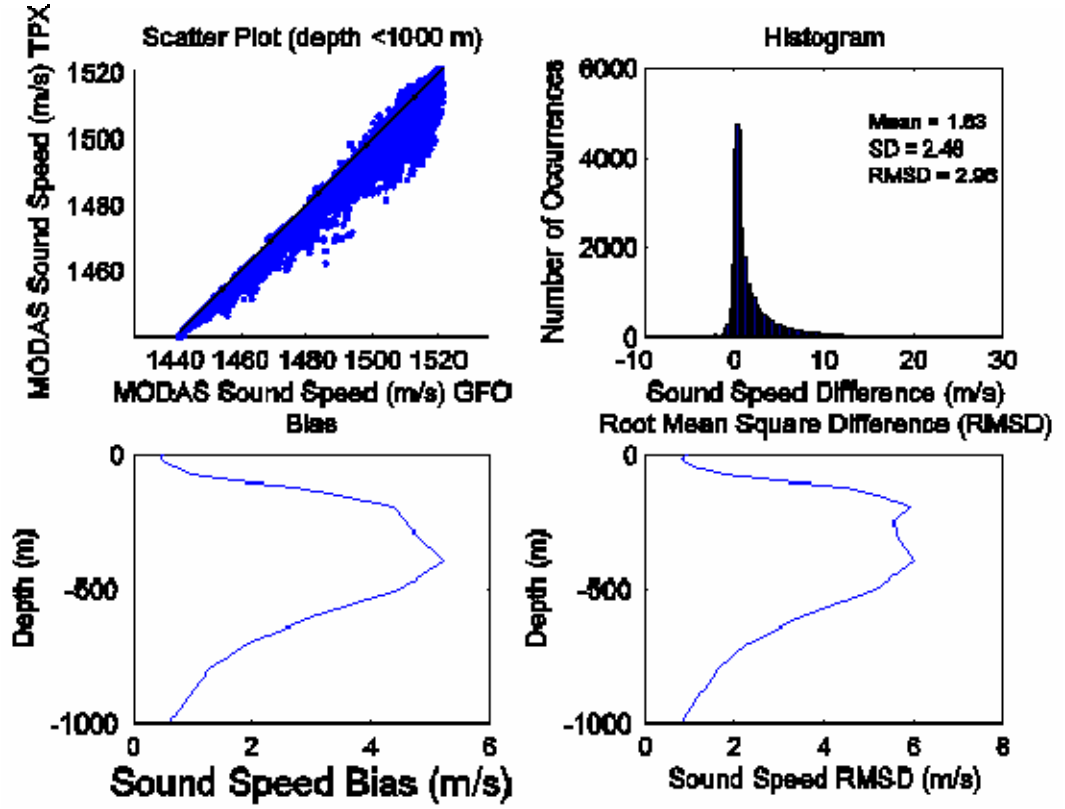

Figure 107. ECS MODAS sound speed January 05, 2001

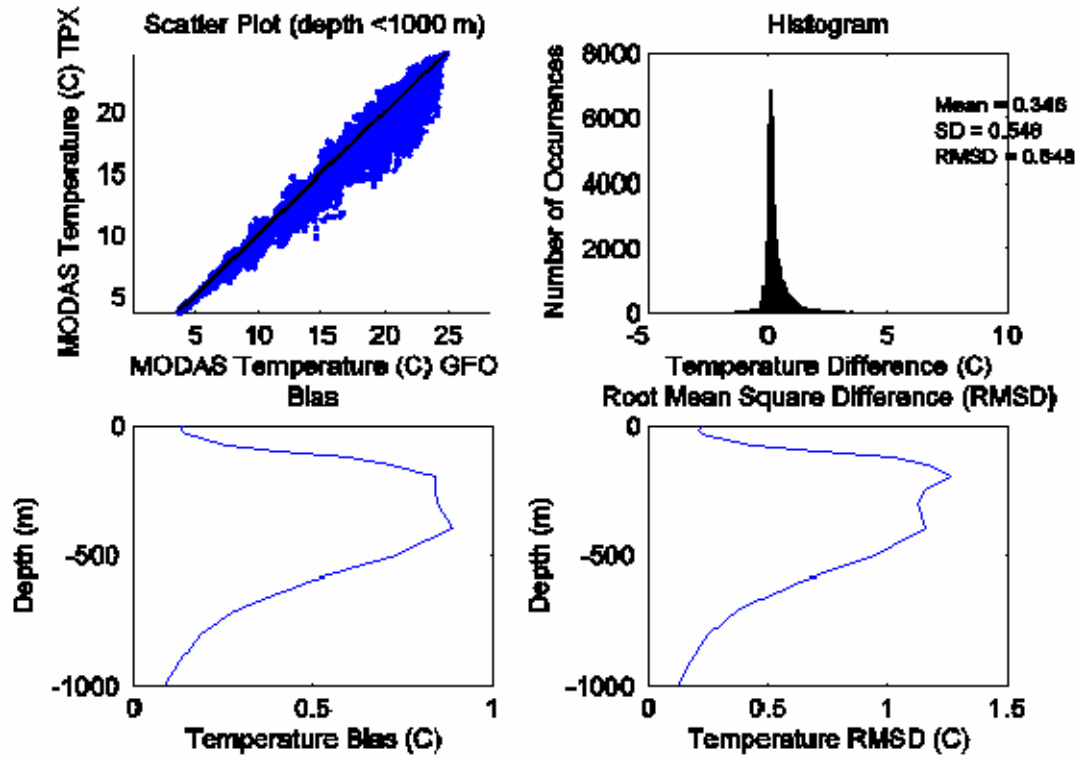

Figure 108. ECS MODAS temperature January 05, 2001

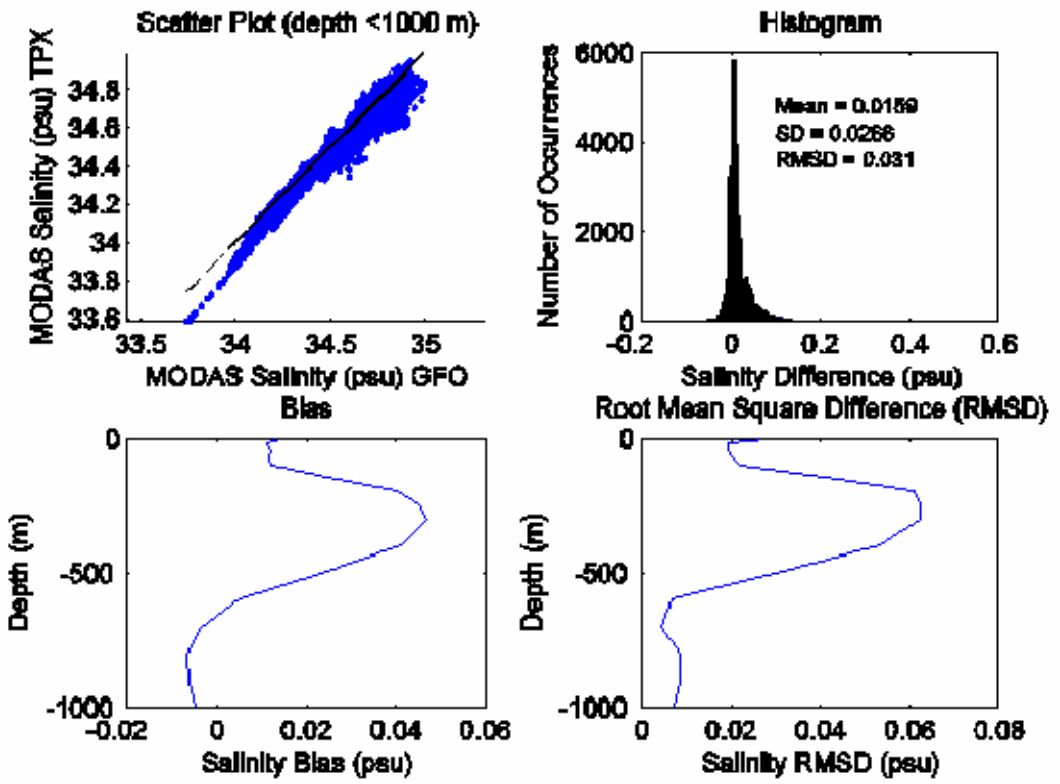

Figure 109. ECS MODAS salinity January 05, 2001

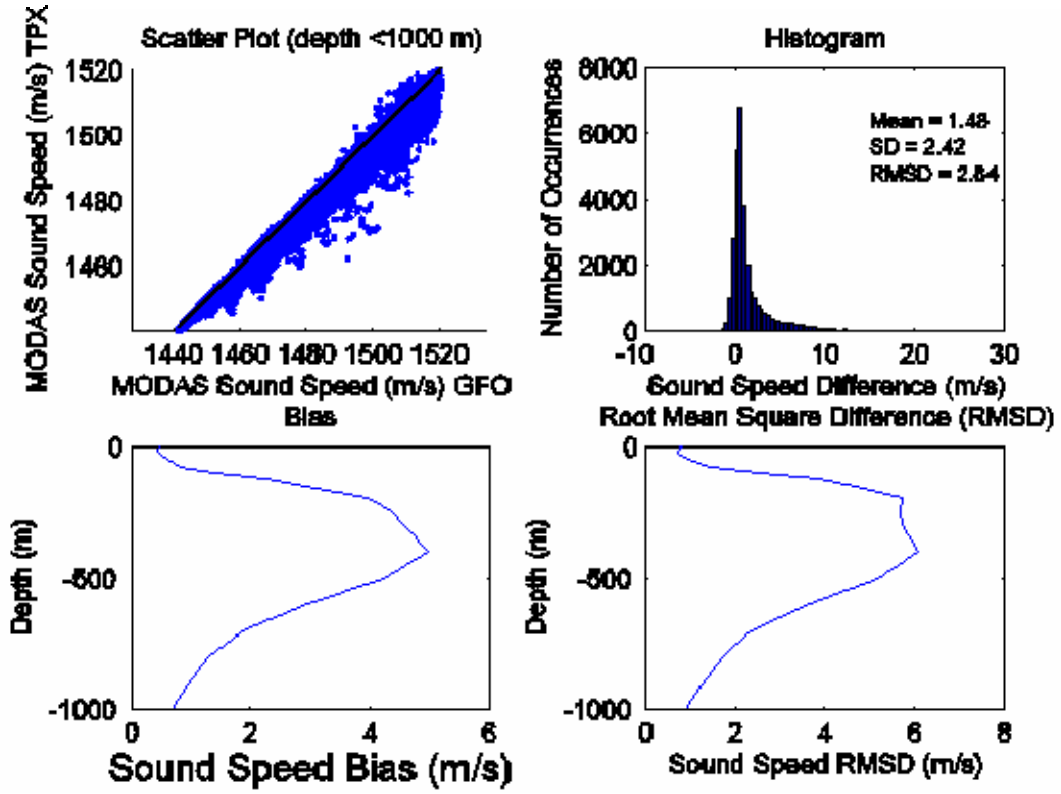

Figure 110. ECS MODAS sound speed January 10, 2001

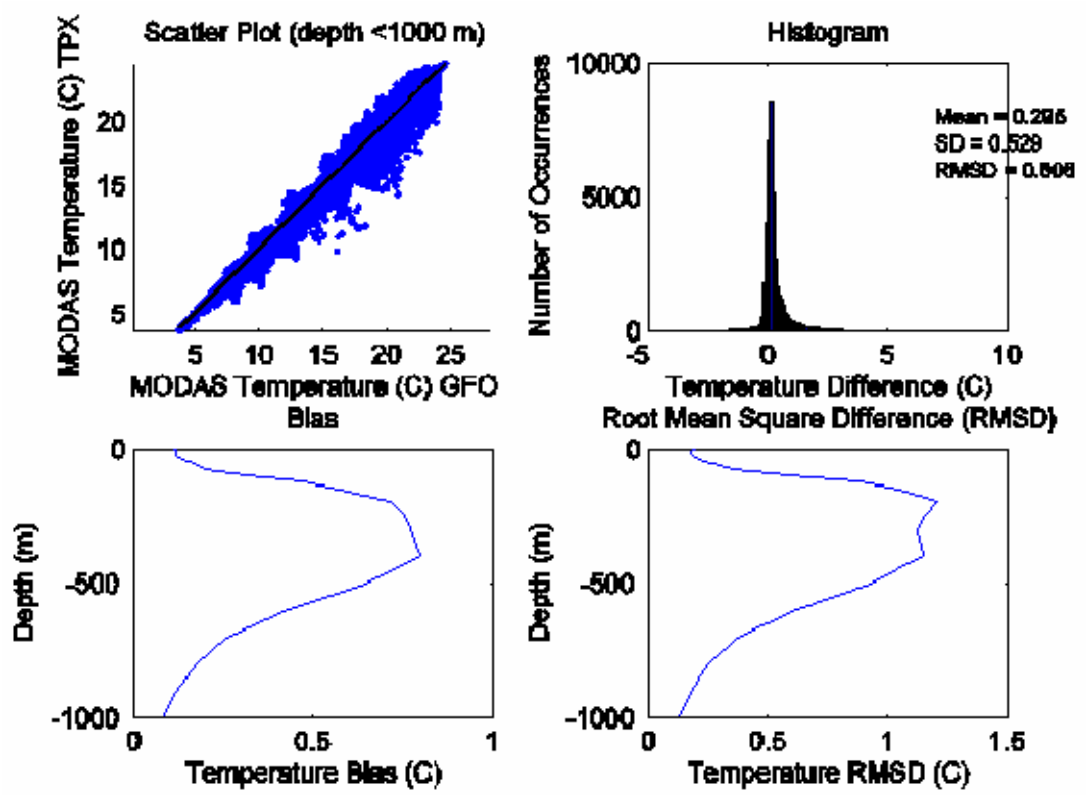

Figure 111. ECS MODAS temperature January 10, 2001

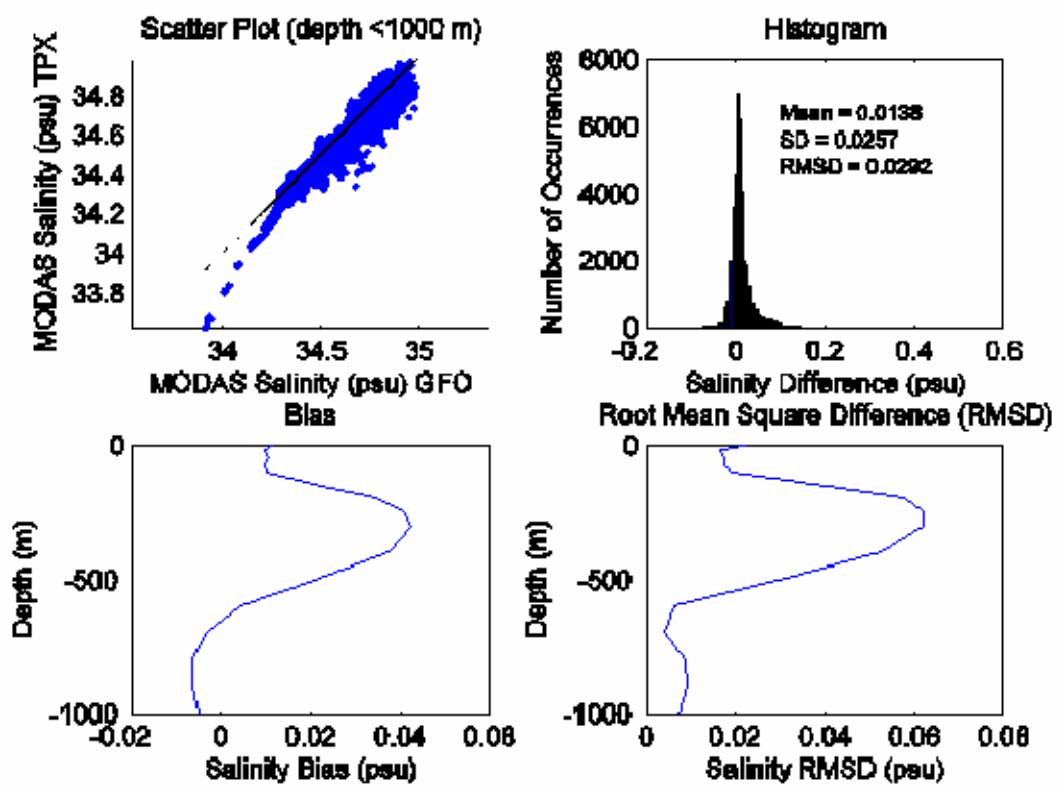

Figure 112. ECS MODAS salinity January 10, 2001

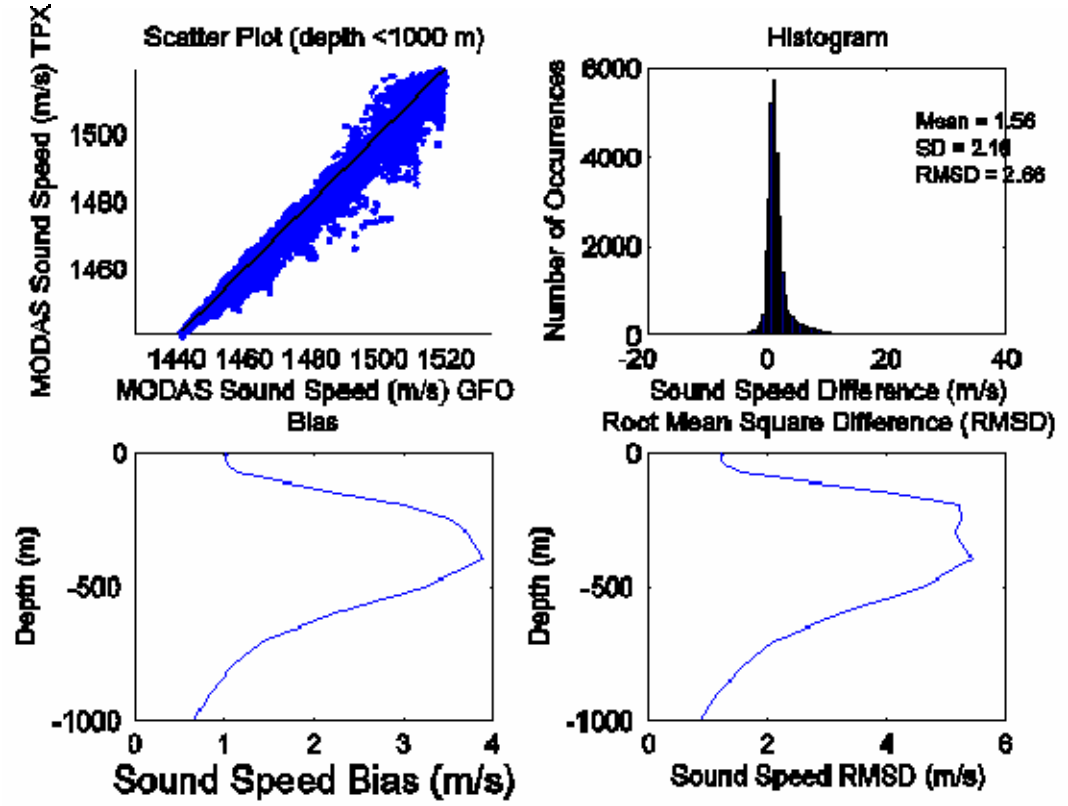

Figure 113. ECS MODAS sound speed January 15, 2001

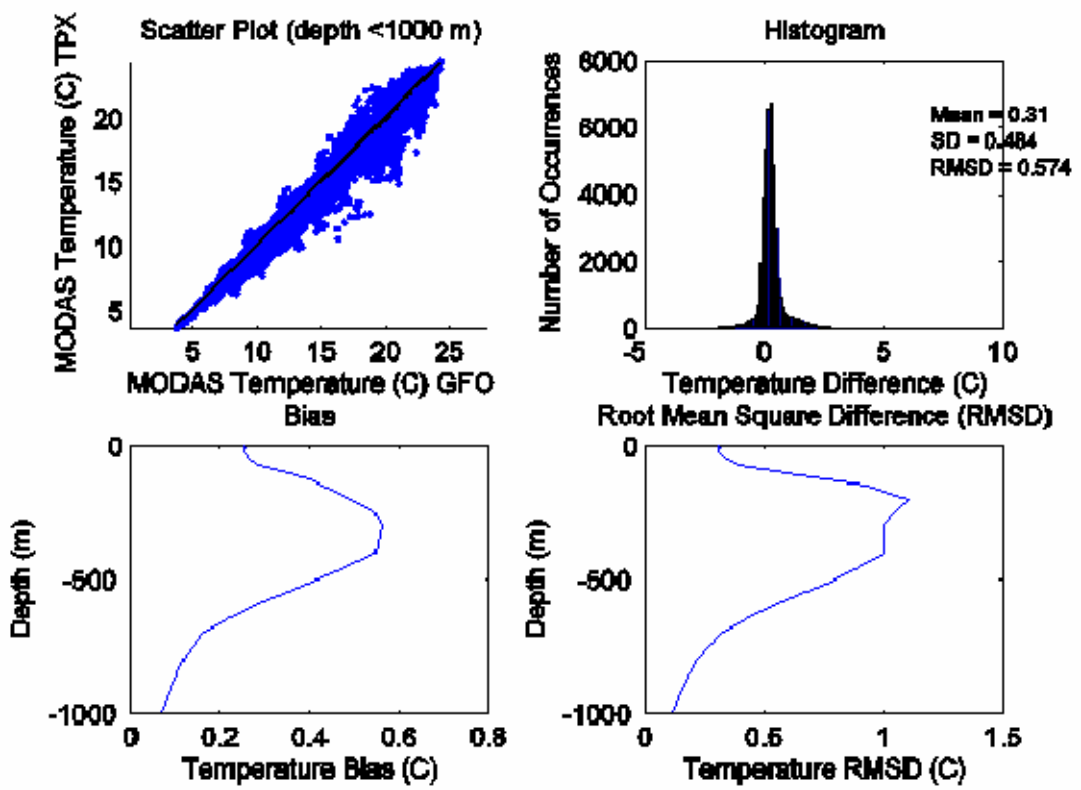

Figure 114. ECS MODAS temperature January 15, 2001

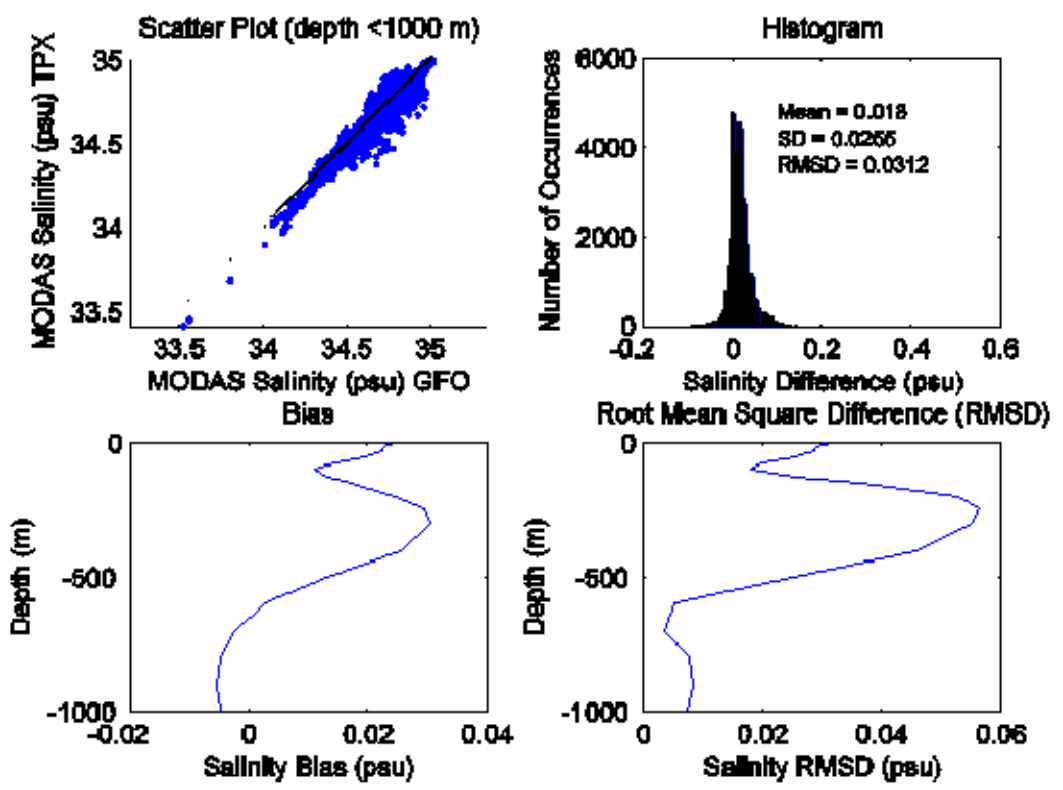

Figure 115. ECS MODAS salinity January 15, 2001

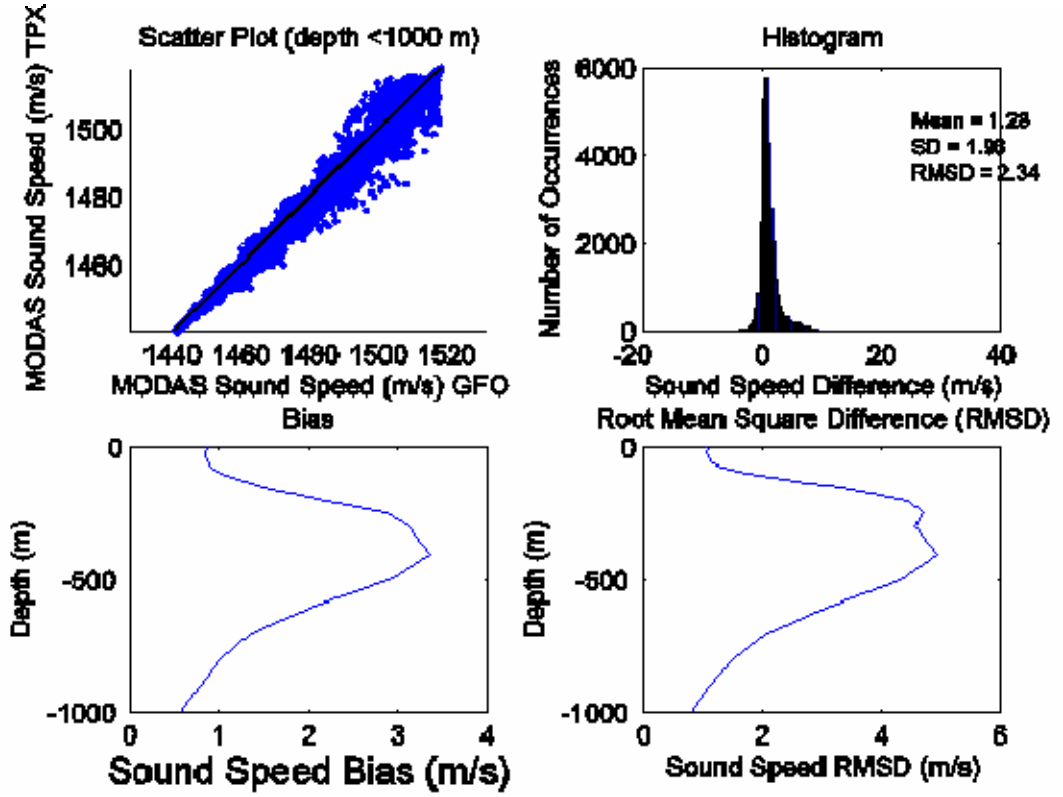

Figure 116. ECS MODAS sound speed January 20, 2001

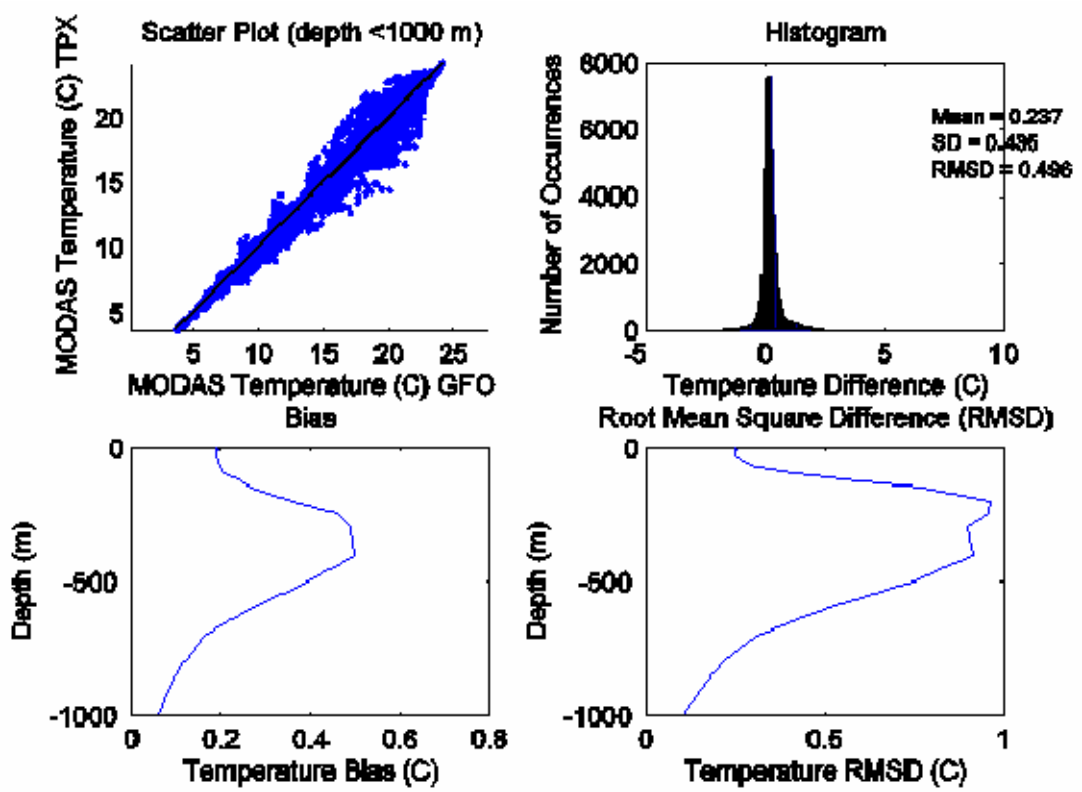

Figure 117. ECS MODAS temperature January 20, 2001

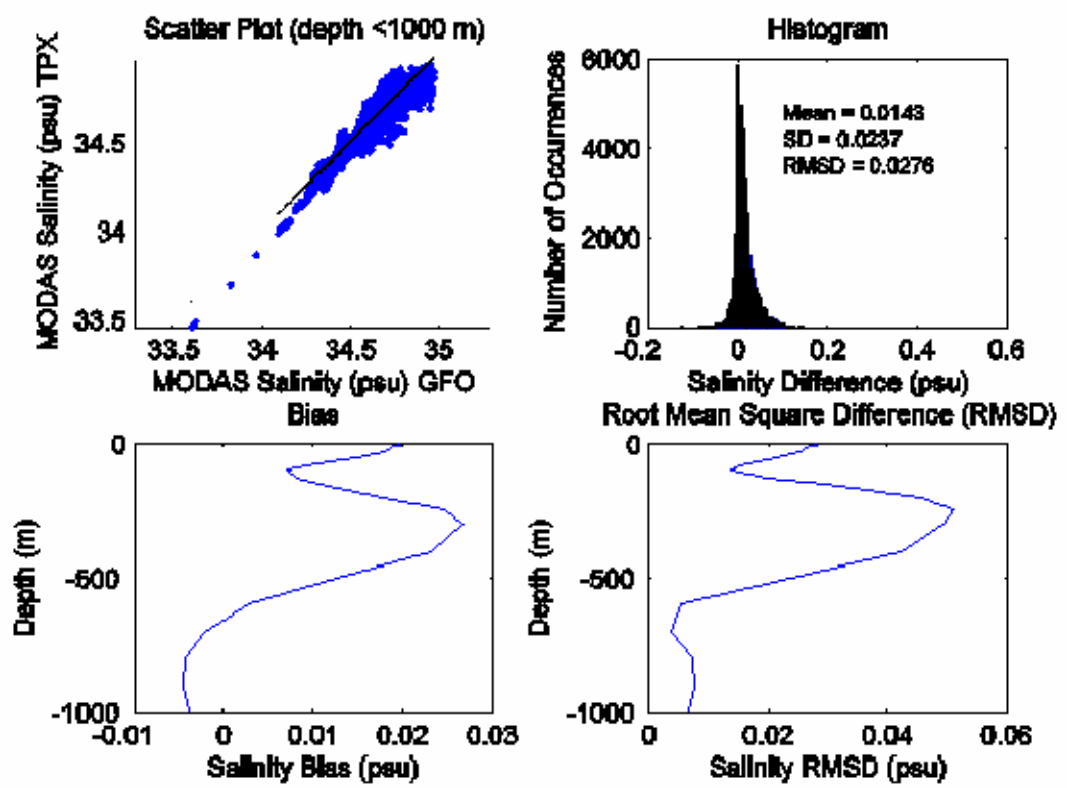

Figure 118. ECS MODAS salinity January 20, 2001

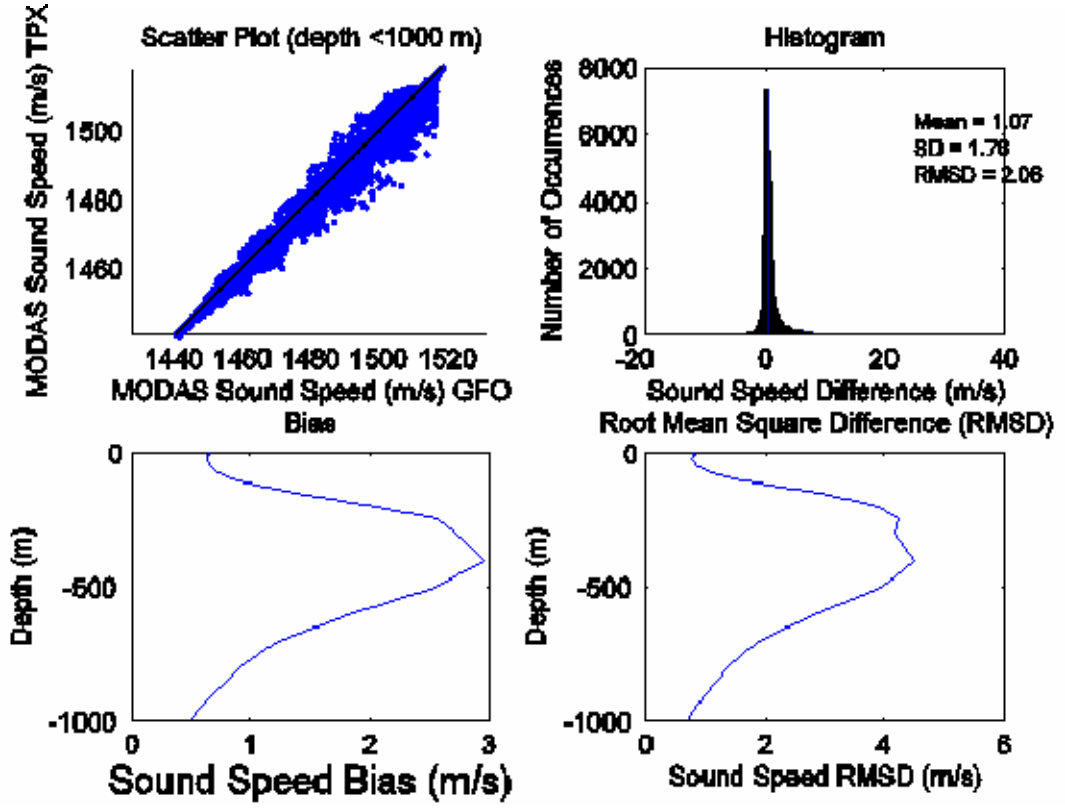

Figure 119. ECS MODAS sound speed January 25, 2001

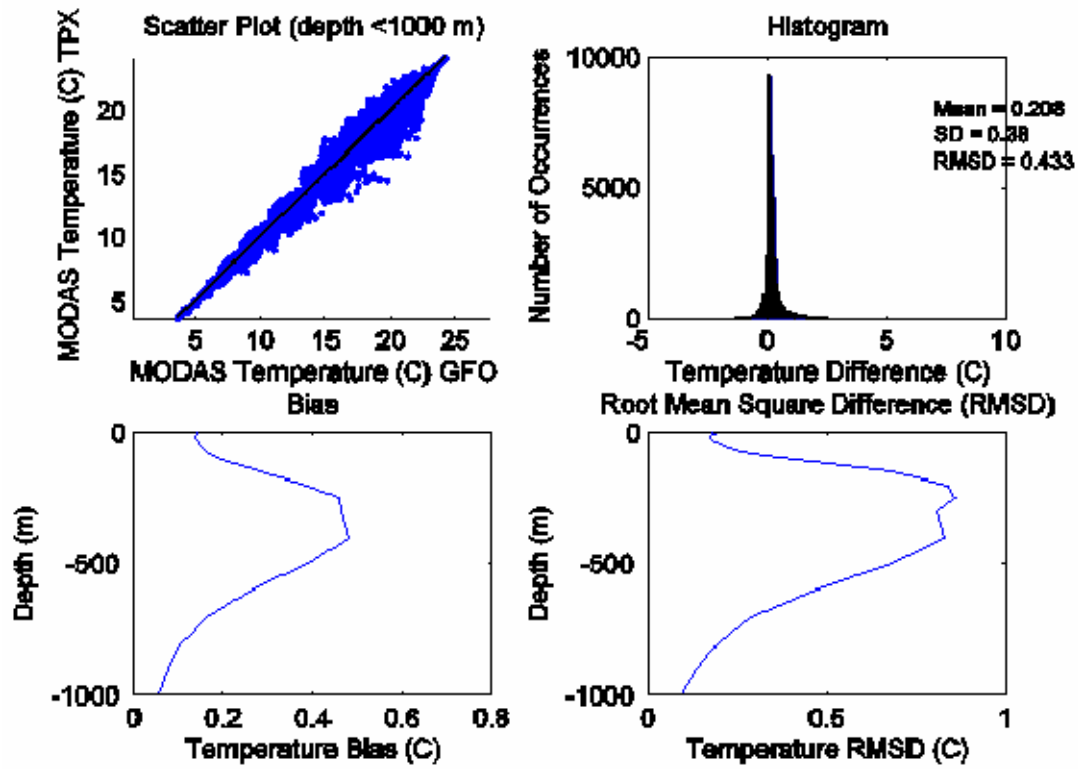

Figure 120. ECS MODAS temperature January 25, 2001

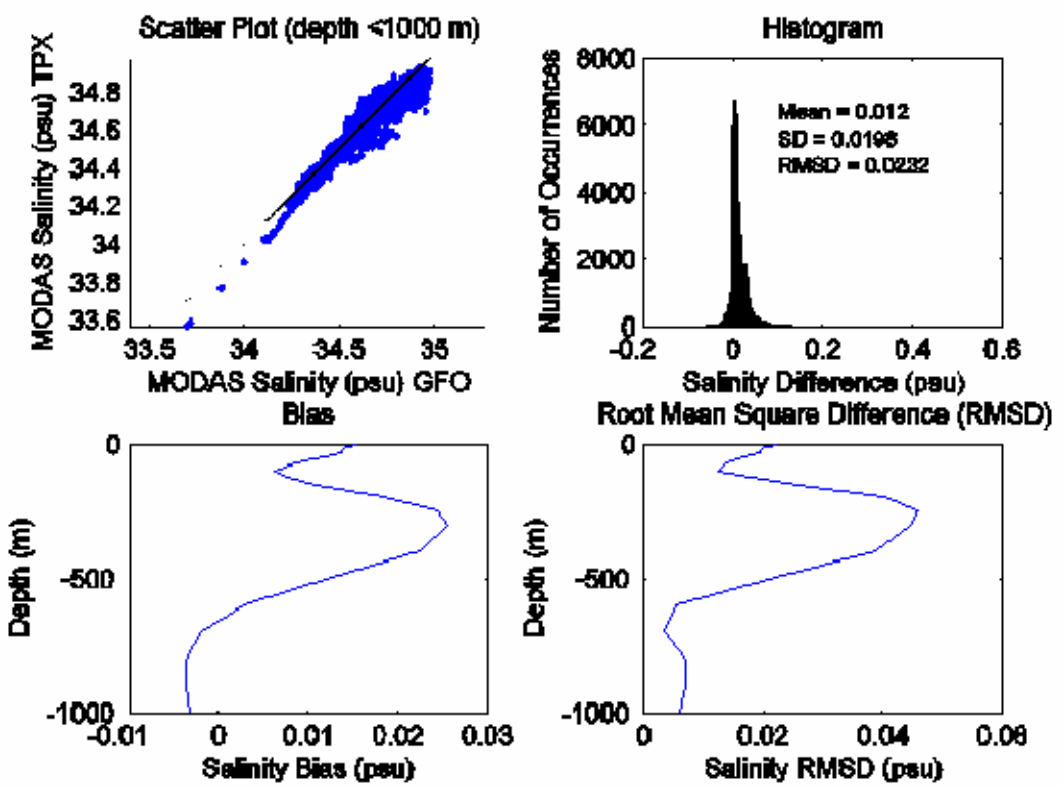

Figure 121. ECS MODAS salinity January 25, 2001

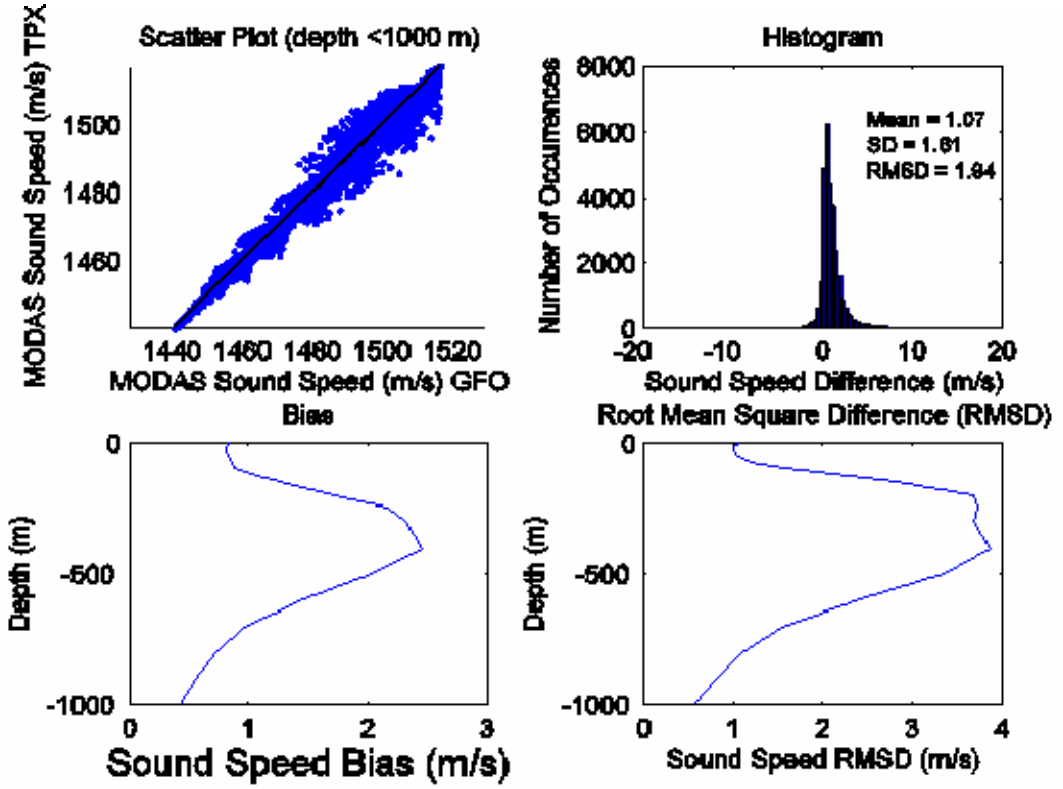

Figure 122. ECS MODAS sound speed January 30, 2001

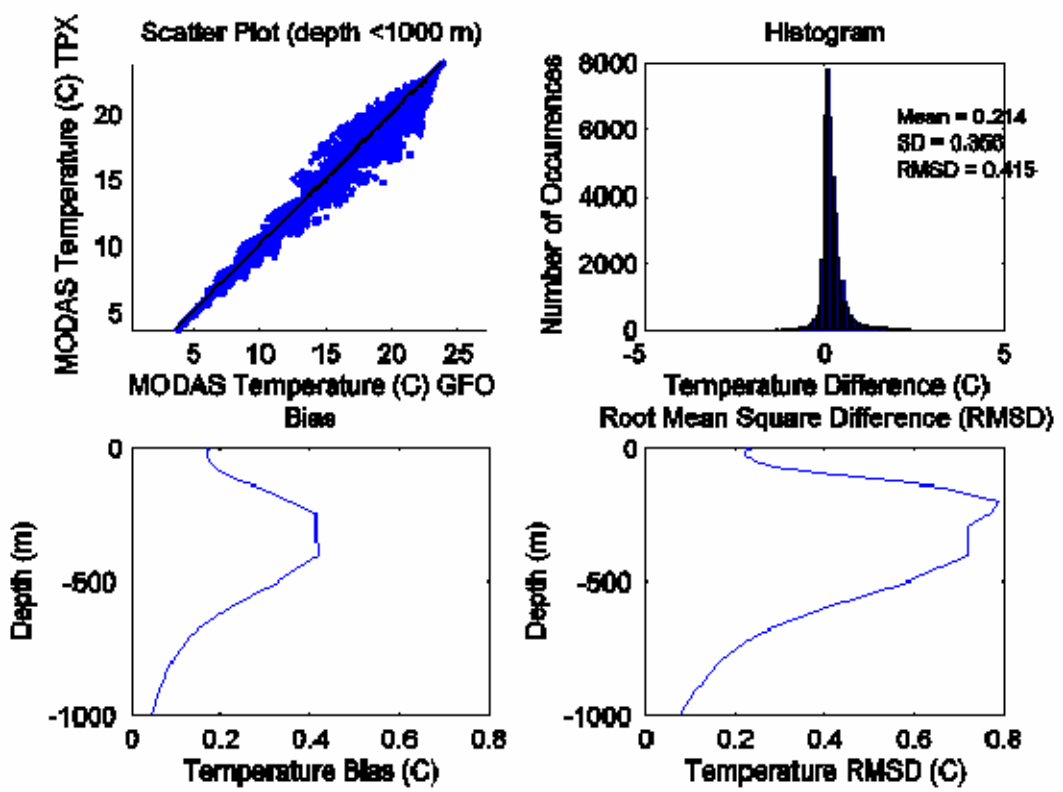

Figure 123. ECS MODAS temperature January 30, 2001

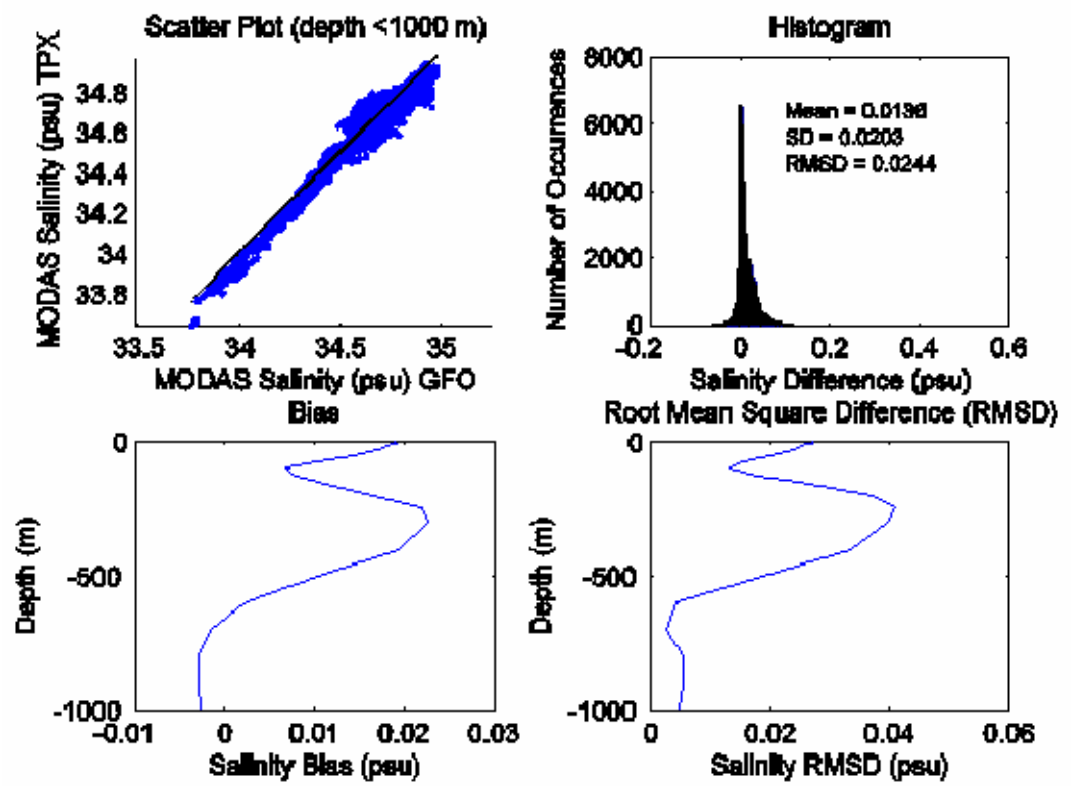

Figure 124. ECS MODAS salinity January 30, 2001

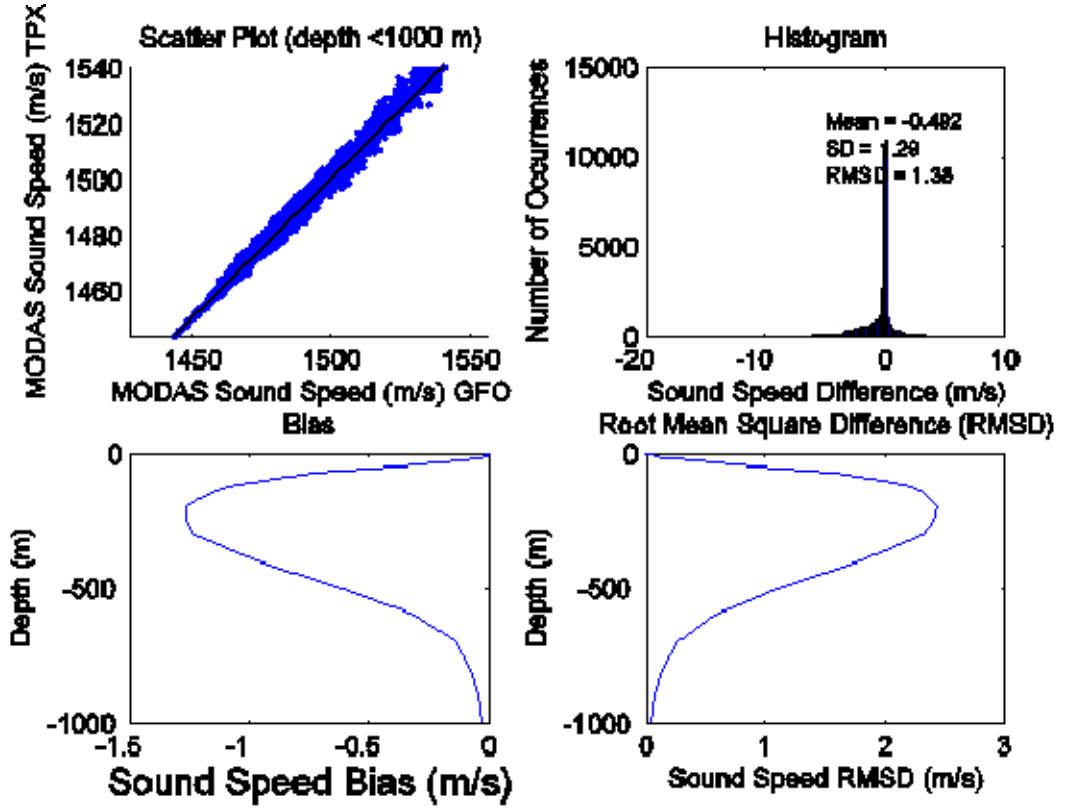

Figure 125. SCS MODAS sound speed July 05, 2001

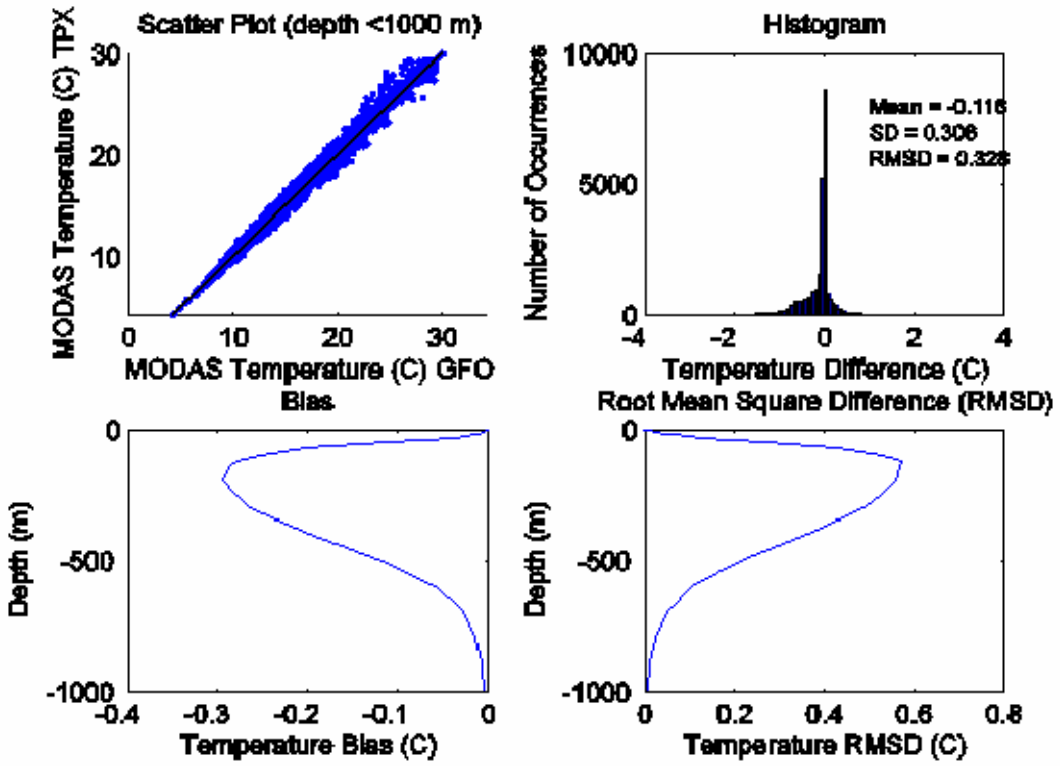

Figure 126. SCS MODAS temperature July 05, 2001

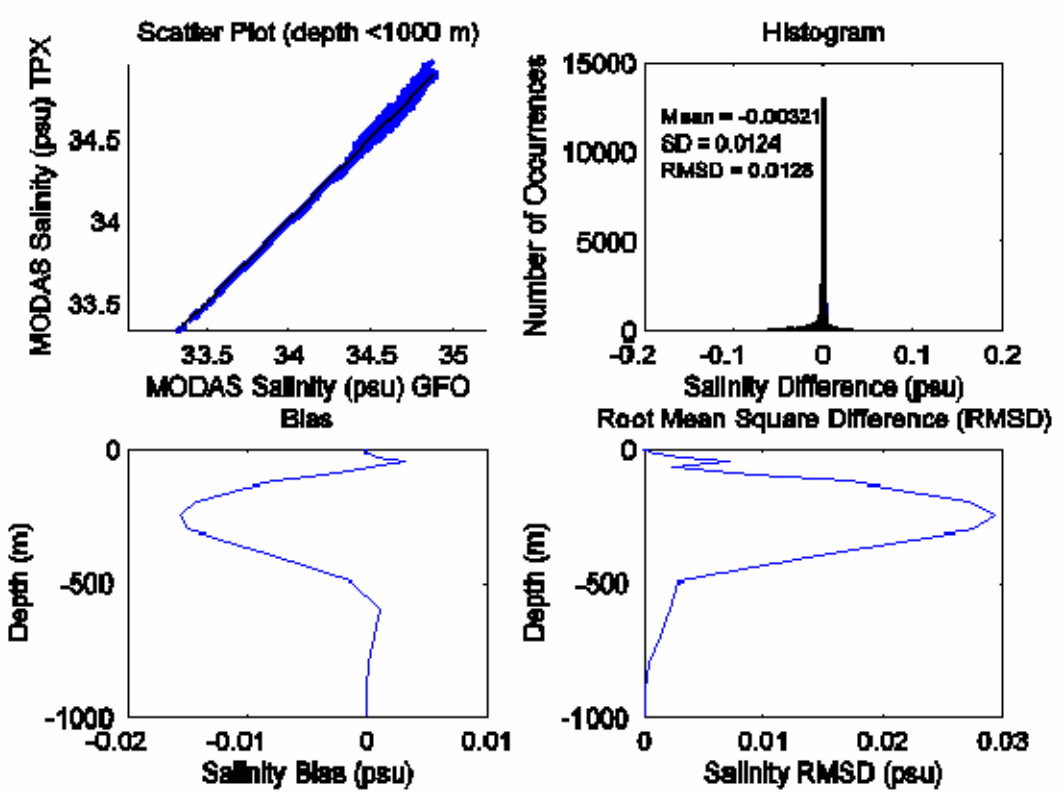

Figure 127. SCS MODAS salinity July 05, 2001

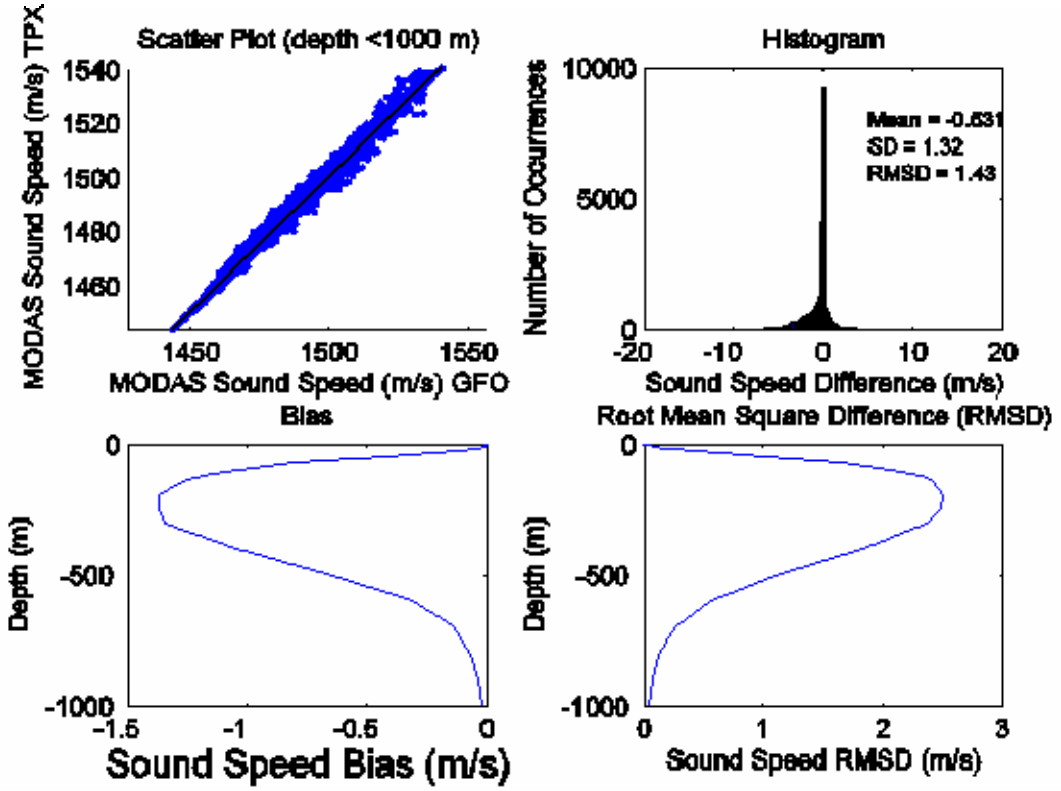

Figure 128. SCS MODAS sound speed July 10, 2001

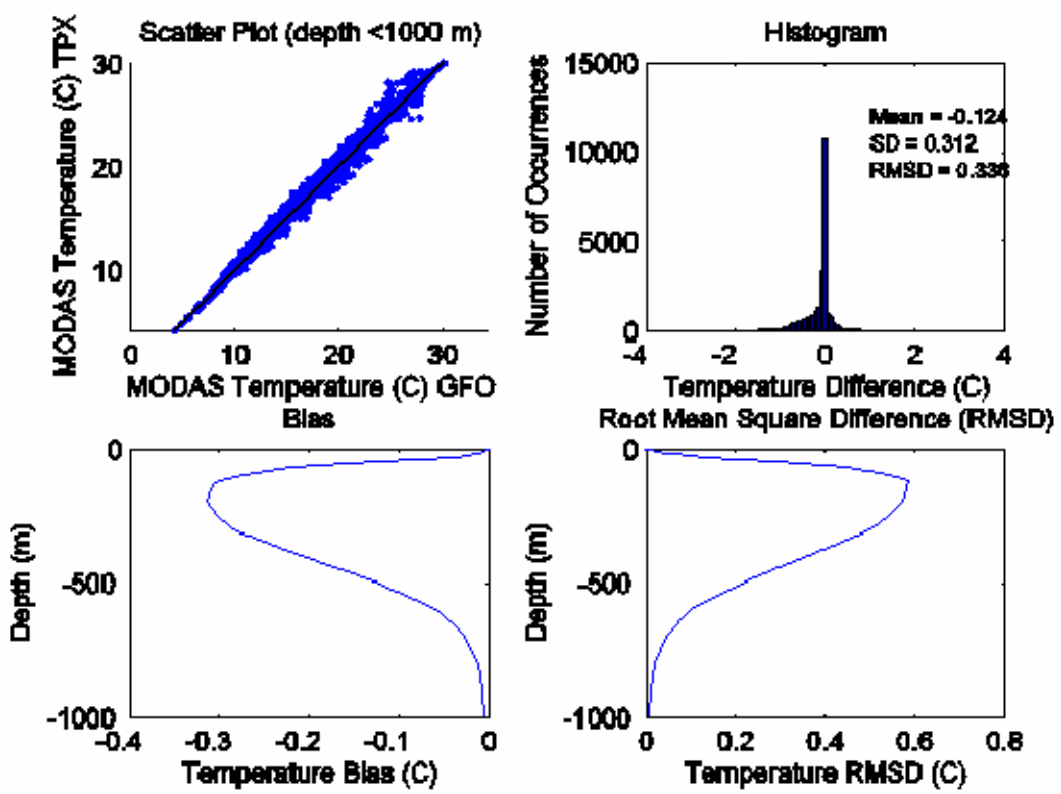

Figure 129. SCS MODAS temperature July 10, 2001

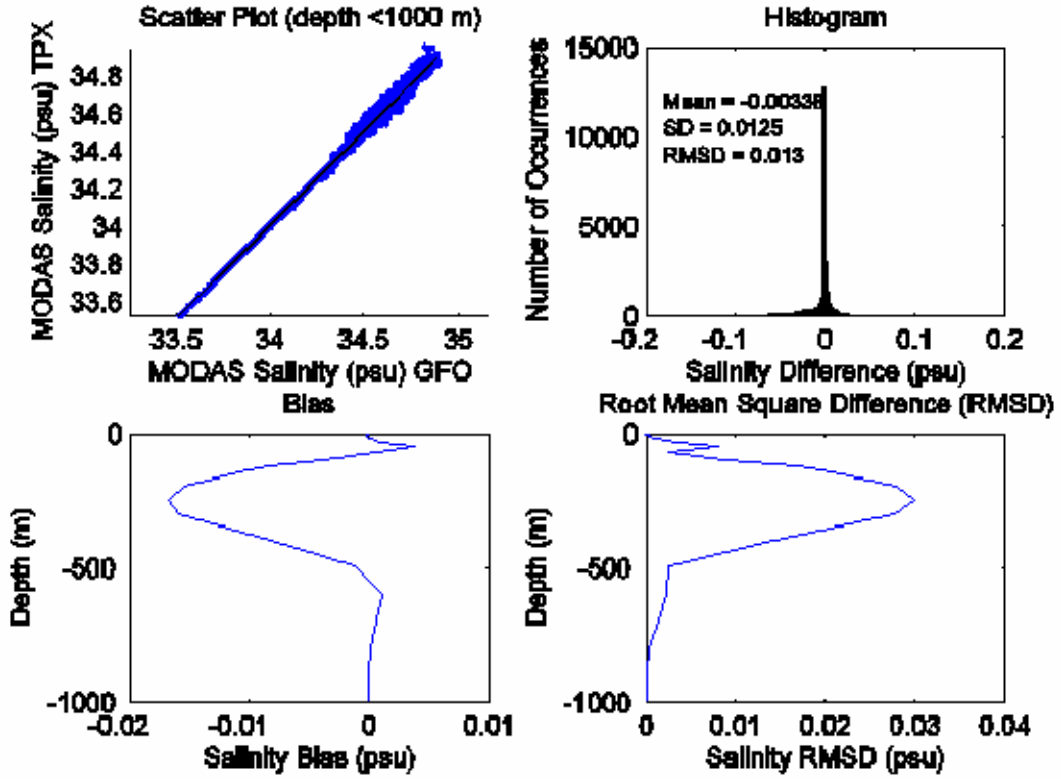

Figure 130. SCS MODAS salinity July 10, 2001

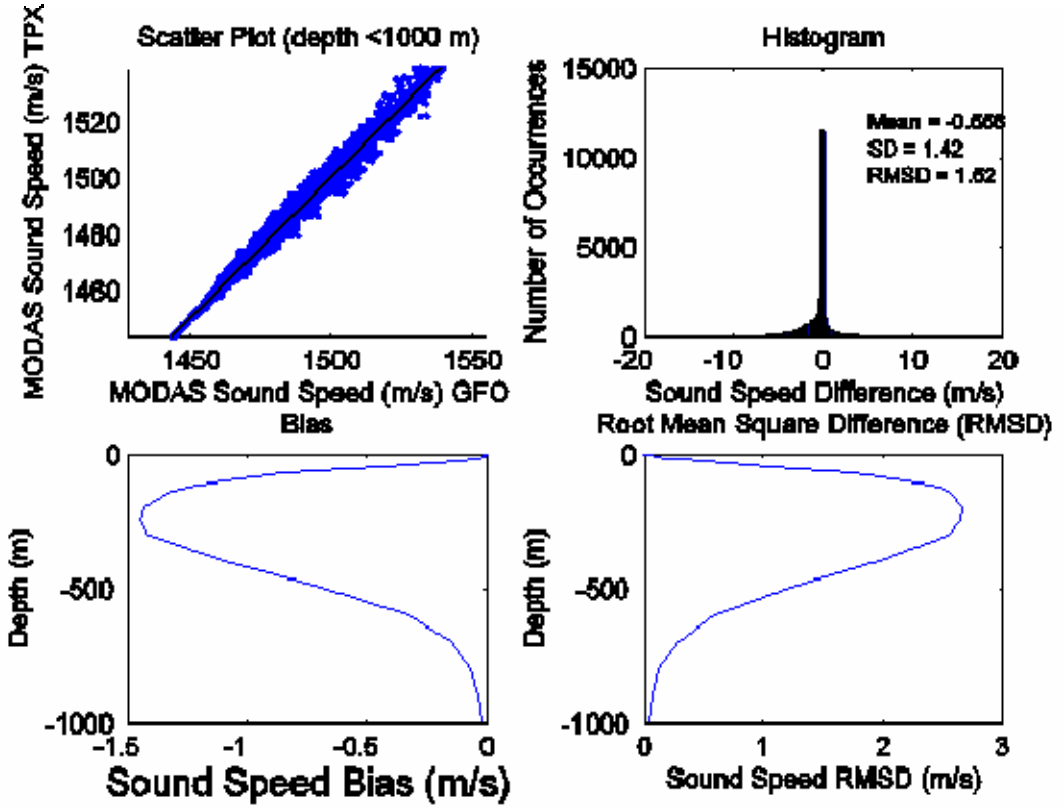

Figure 131. SCS MODAS sound speed July 15, 2001

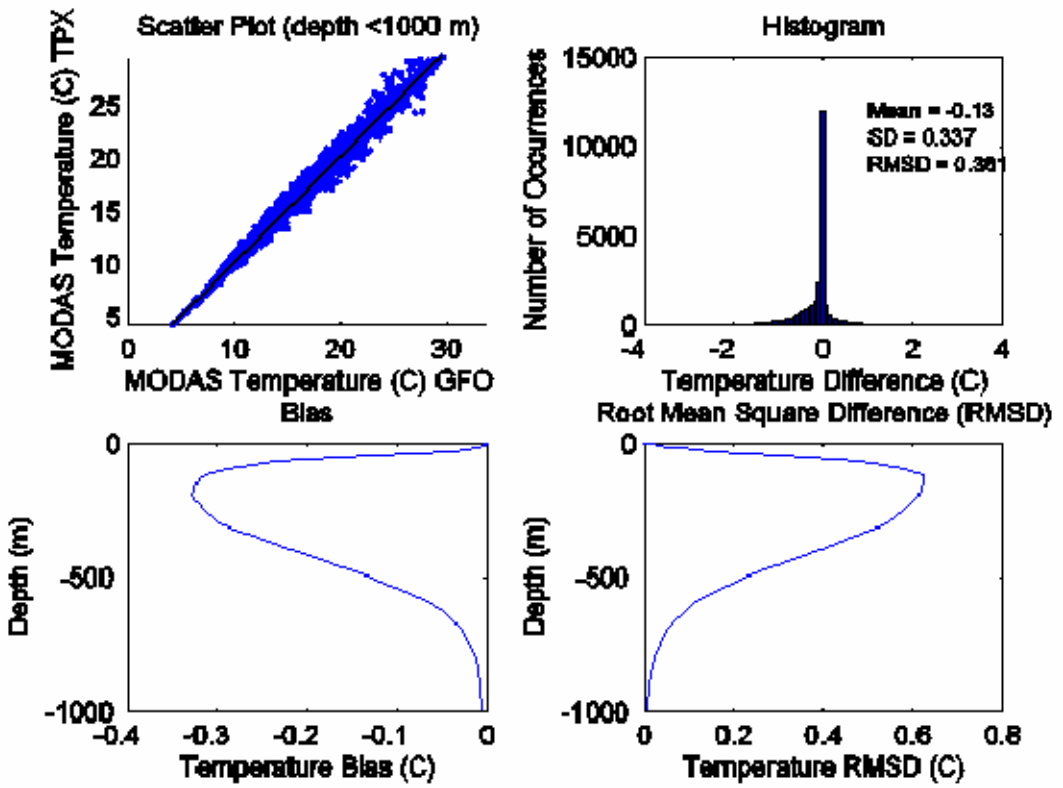

Figure 132. SCS MODAS temperature July 15, 2001

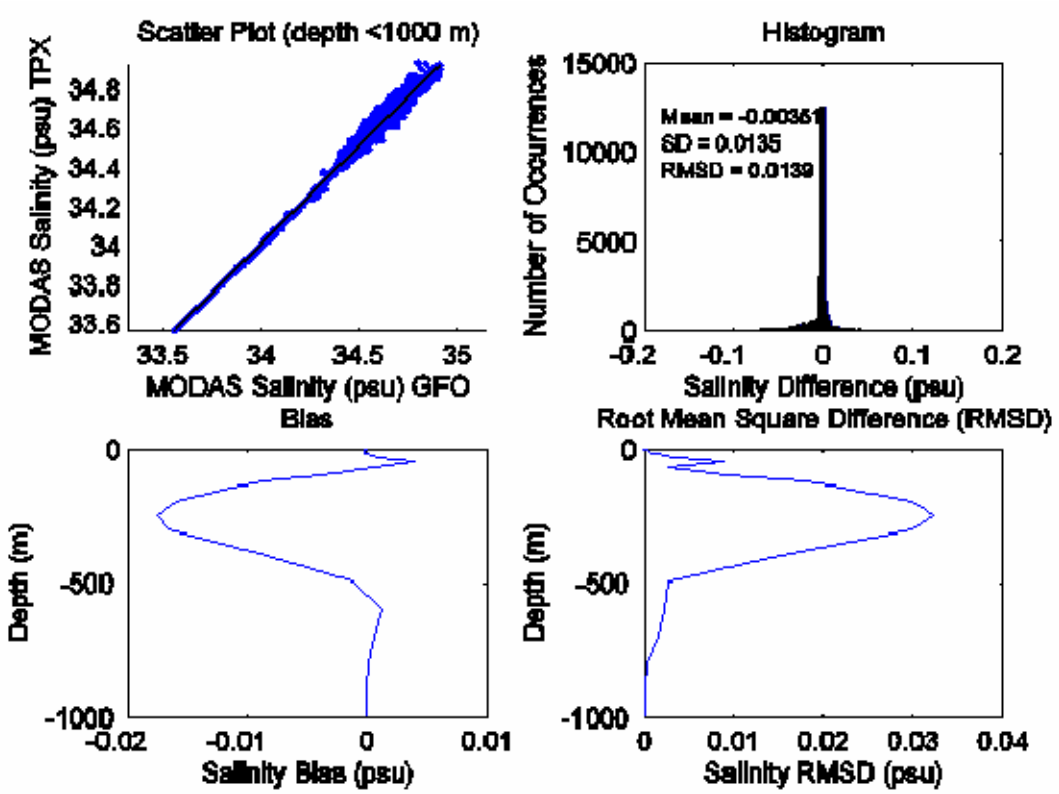

Figure 133. SCS MODAS salinity July 15, 2001

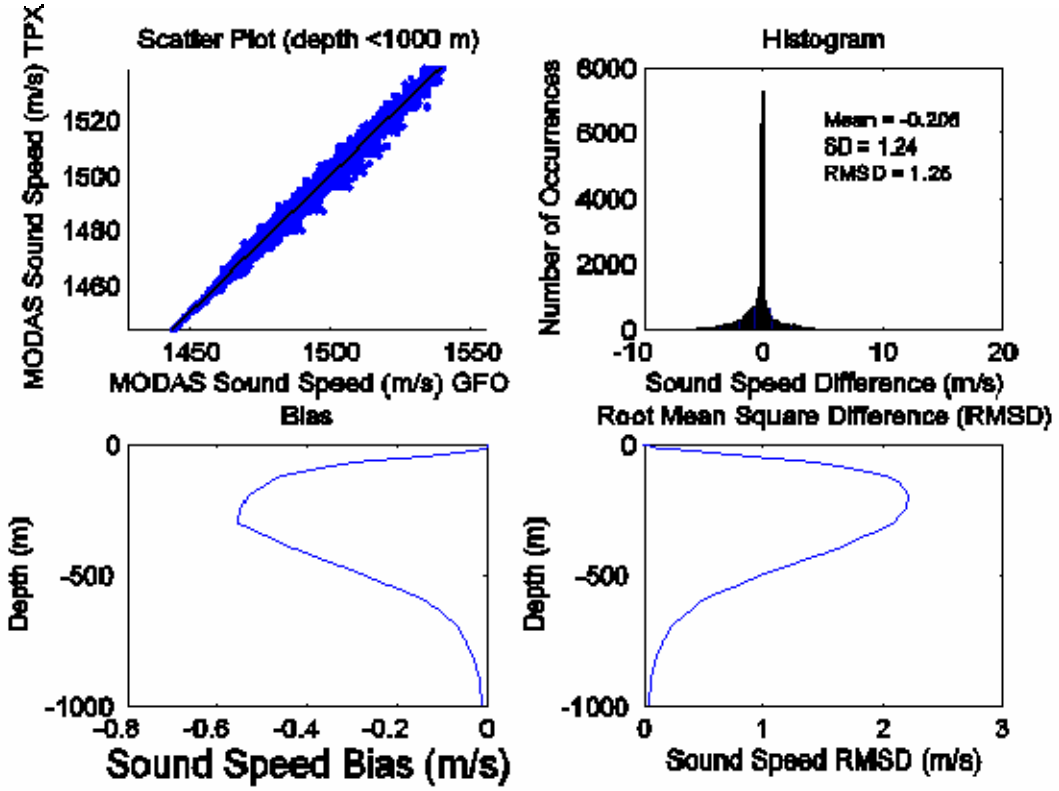

Figure 134. SCS MODAS sound speed July 20, 2001

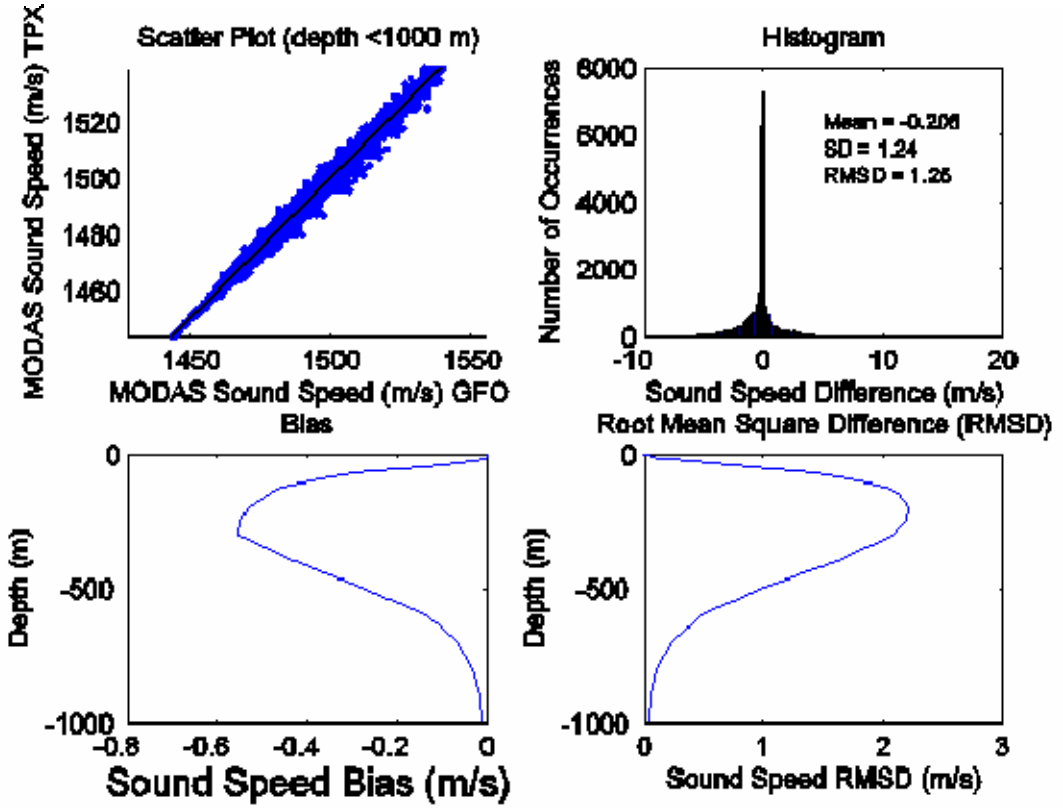

Figure 135. SCS MODAS temperature July 20, 2001

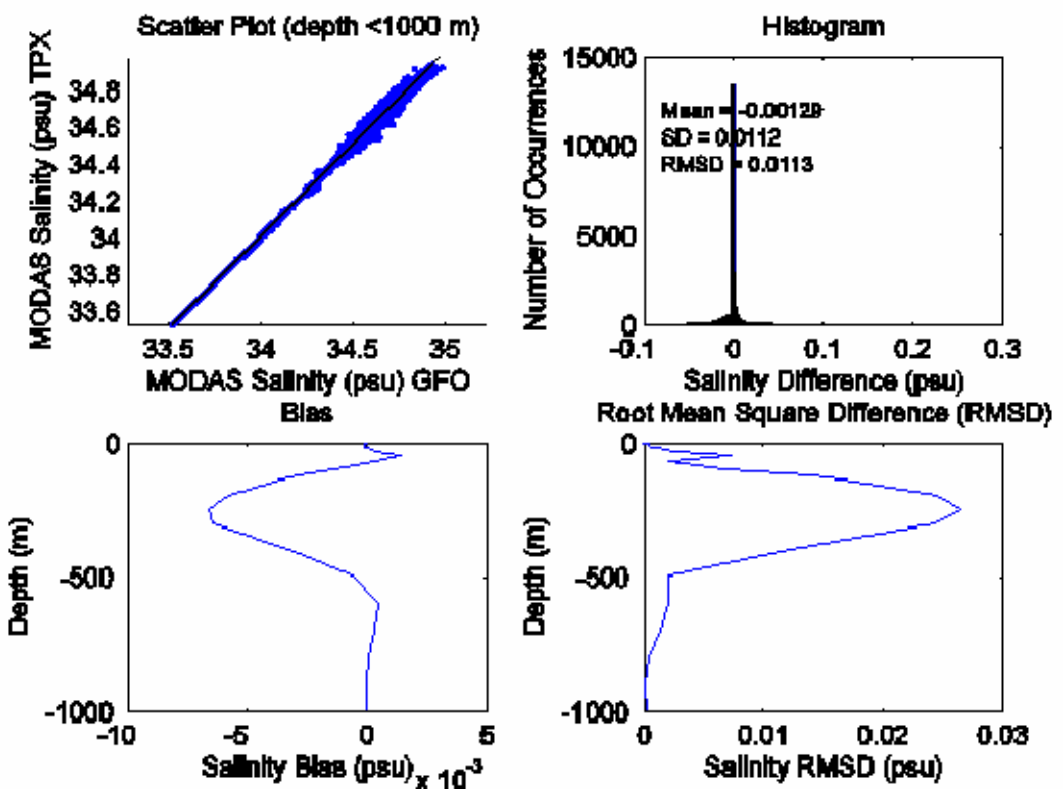

Figure 136. SCS MODAS salinity July 20, 2001

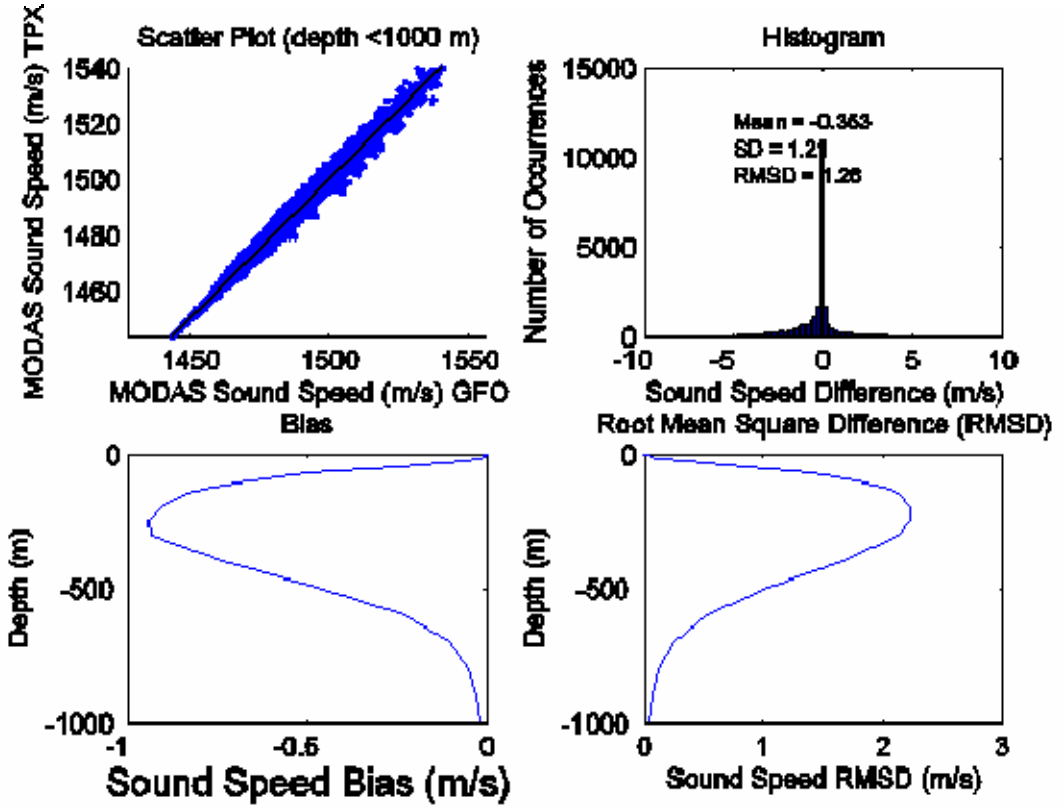

Figure 137. SCS MODAS sound speed July 25, 2001

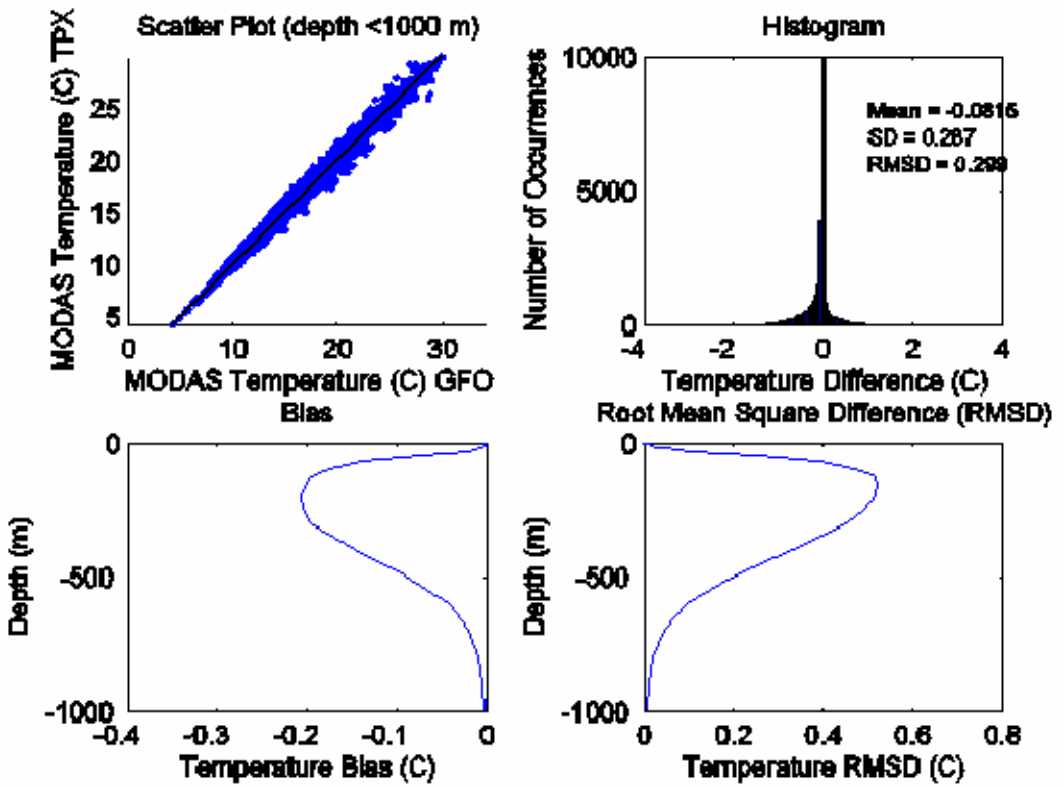

Figure 138. SCS MODAS temperature July 25, 2001

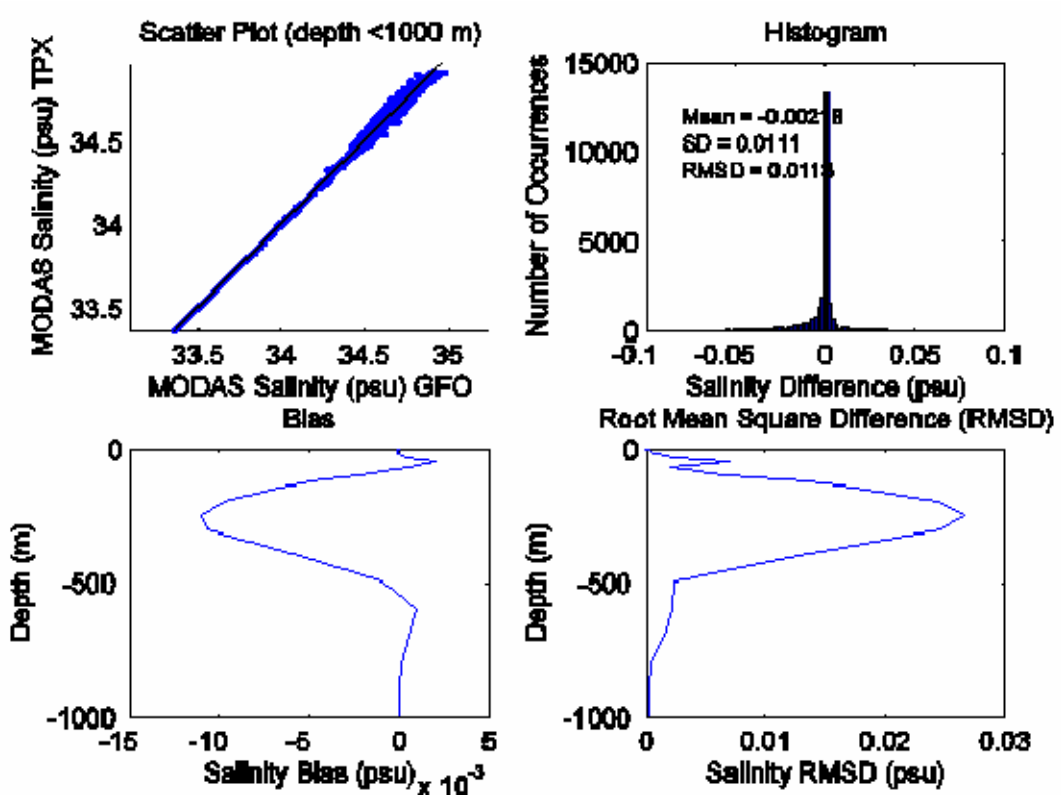

Figure 139. SCS MODAS salinity July 25, 2001

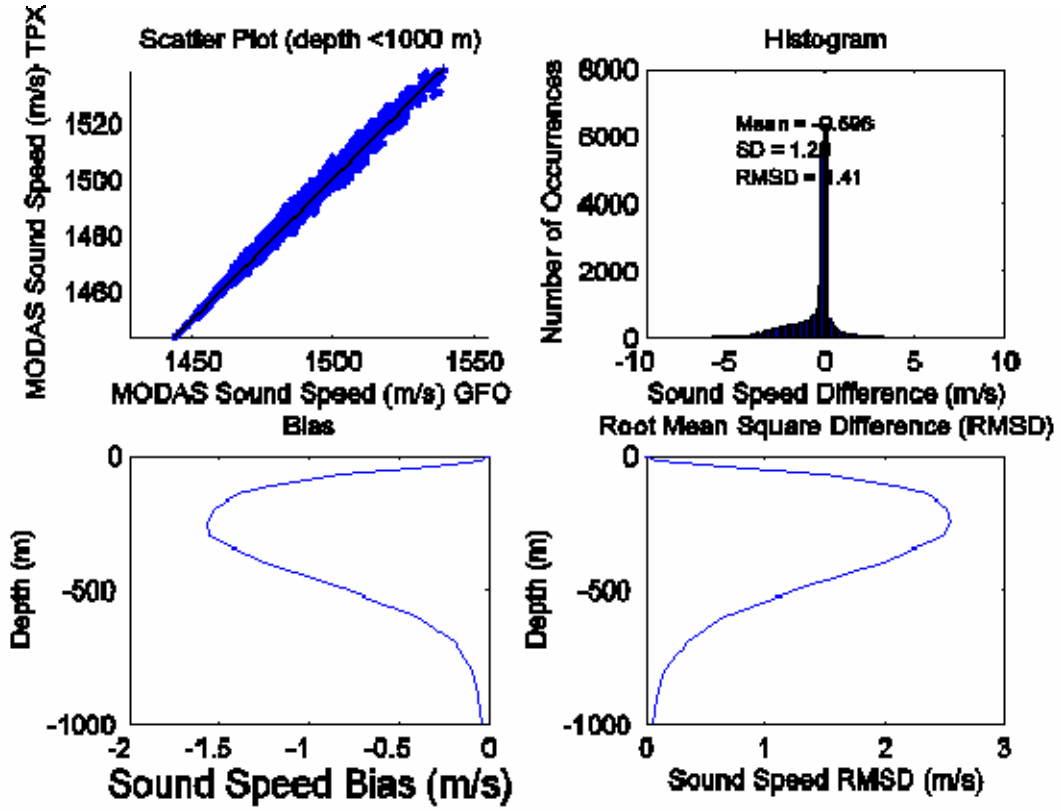

Figure 140. SCS MODAS sound speed July 30, 2001

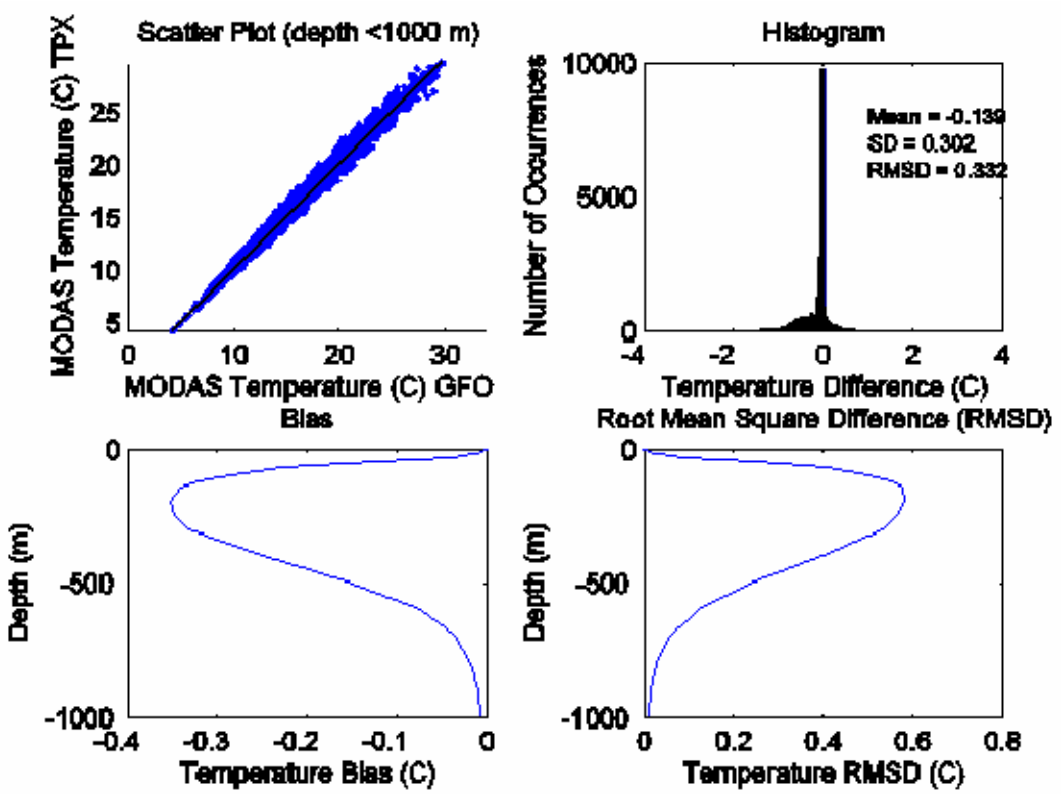

Figure 141. SCS MODAS temperature July 30, 2001

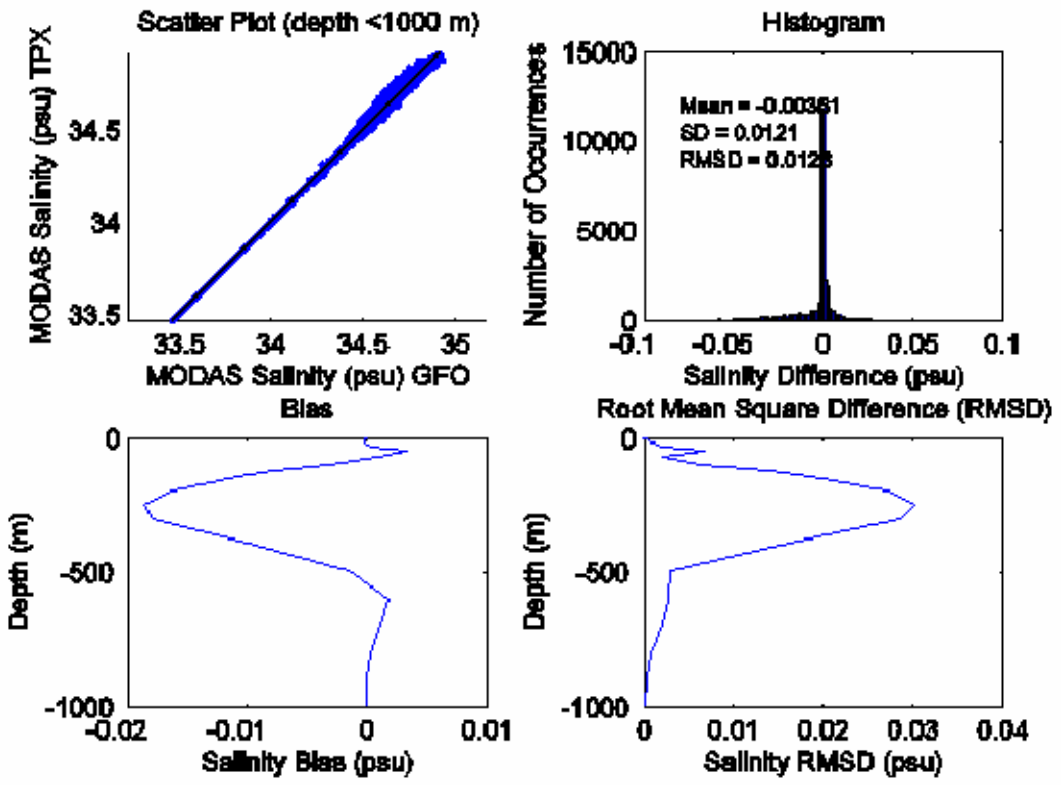

Figure 142. SCS MODAS salinity July 30, 2001

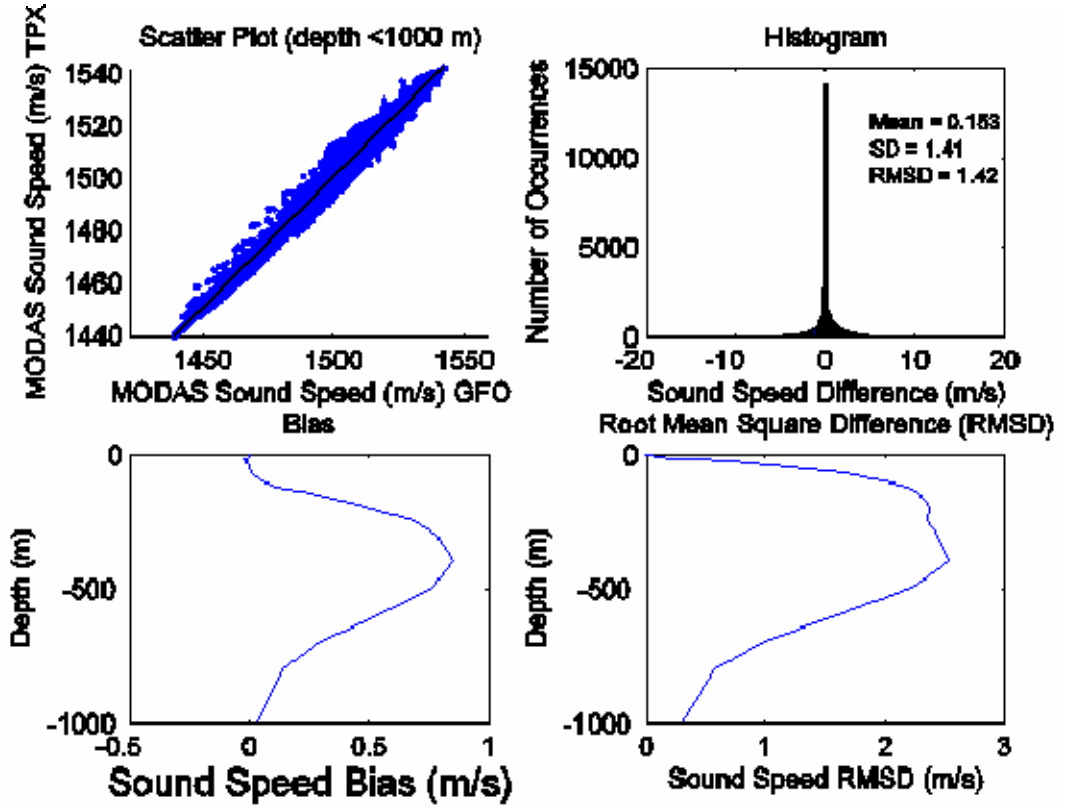

Figure 143. ECS MODAS sound speed July 05, 2001

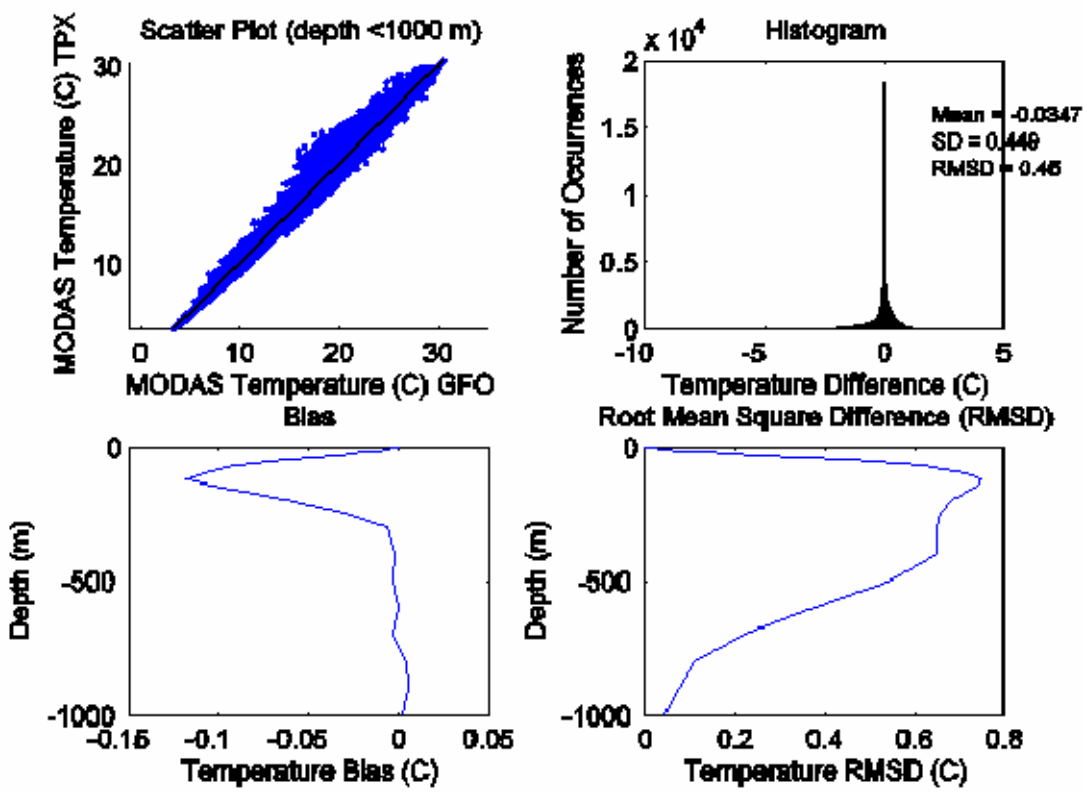

Figure 144. ECS MODAS temperature July 05, 2001

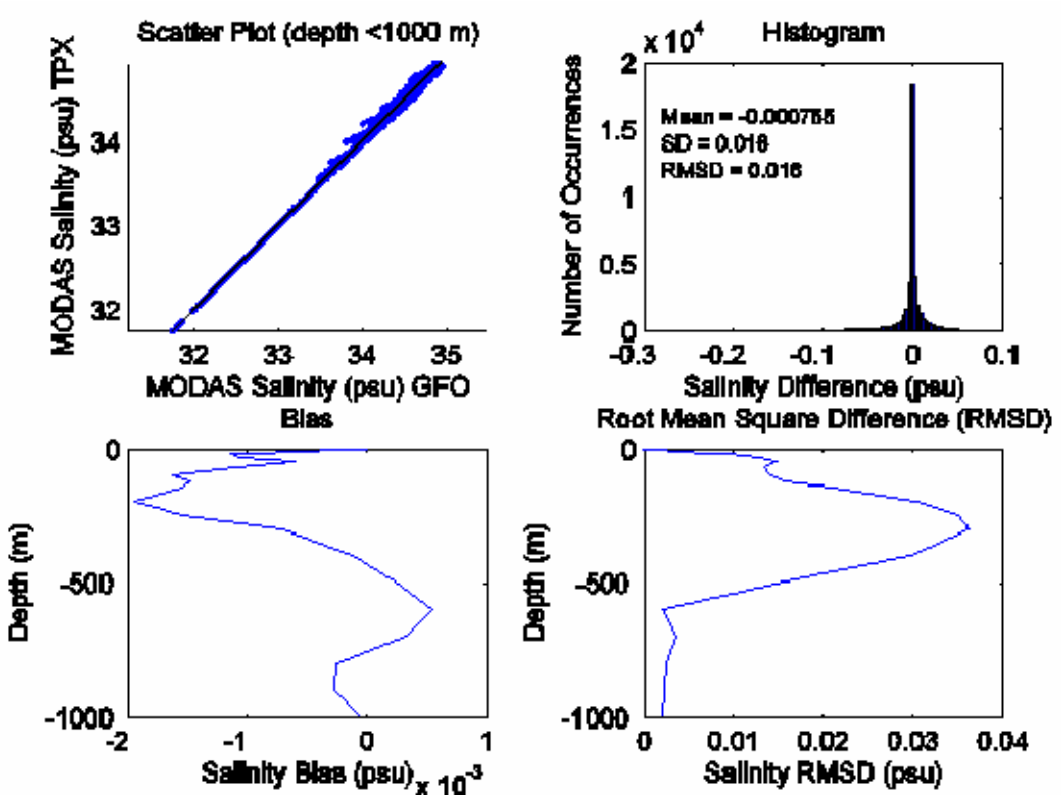

Figure 145. ECS MODAS salinity July 05, 2001

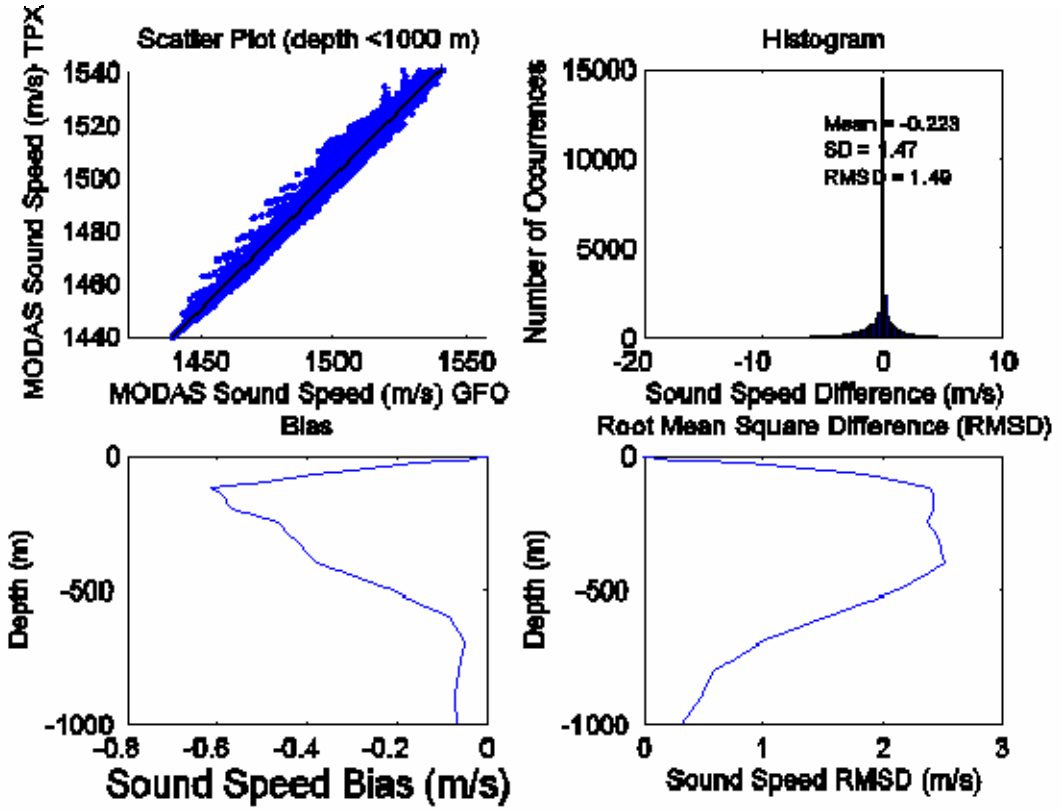

Figure 146. ECS MODAS sound speed July 10, 2001

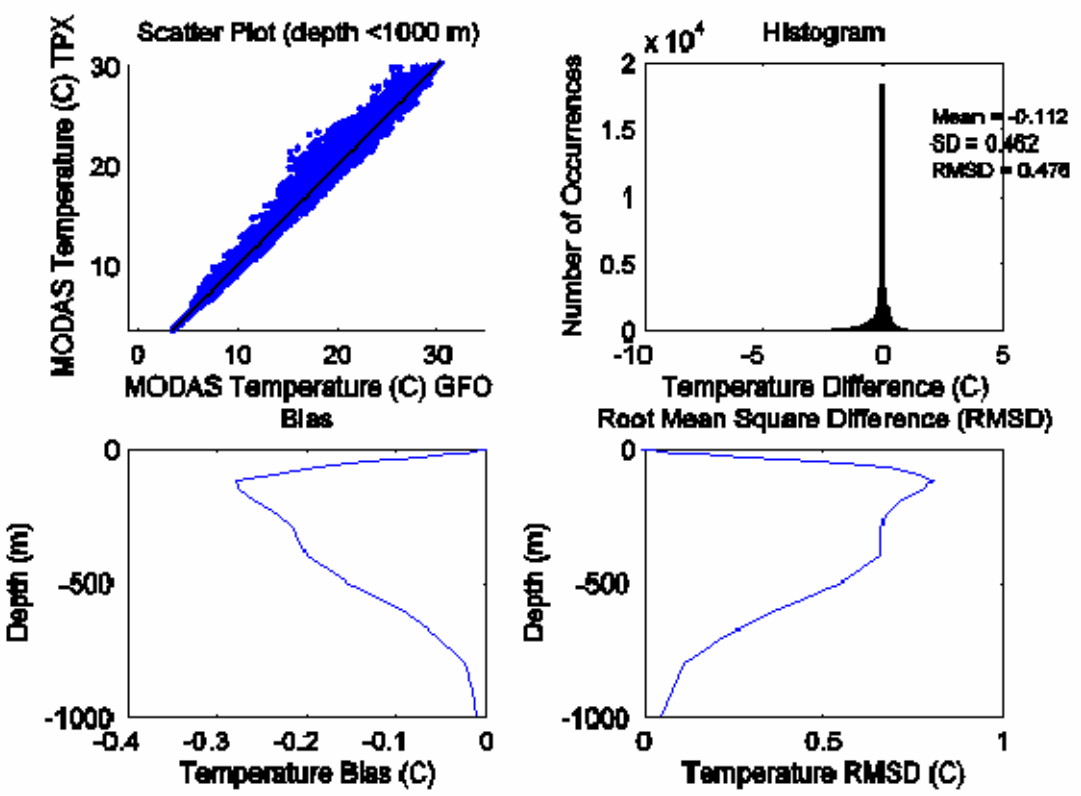

Figure 147. ECS MODAS temperature July 10, 2001

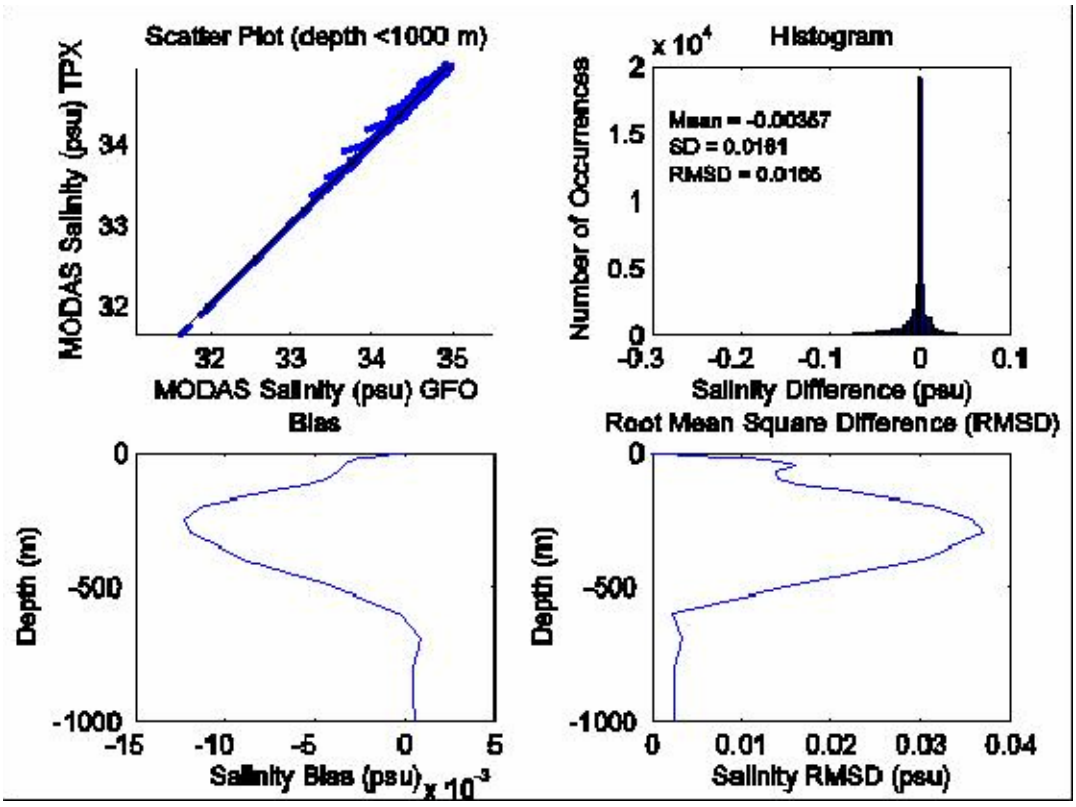

Figure 148. ECS MODAS salinity July 10, 2001

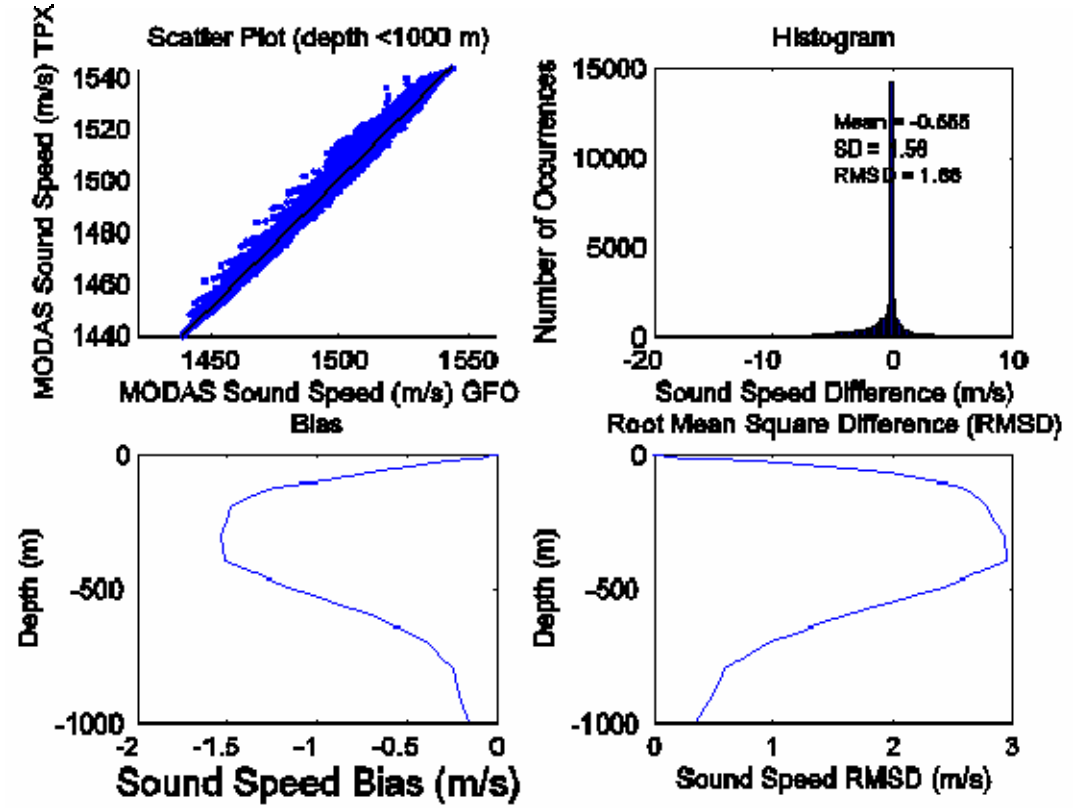

Figure 149. ECS MODAS sound speed July 15, 2001

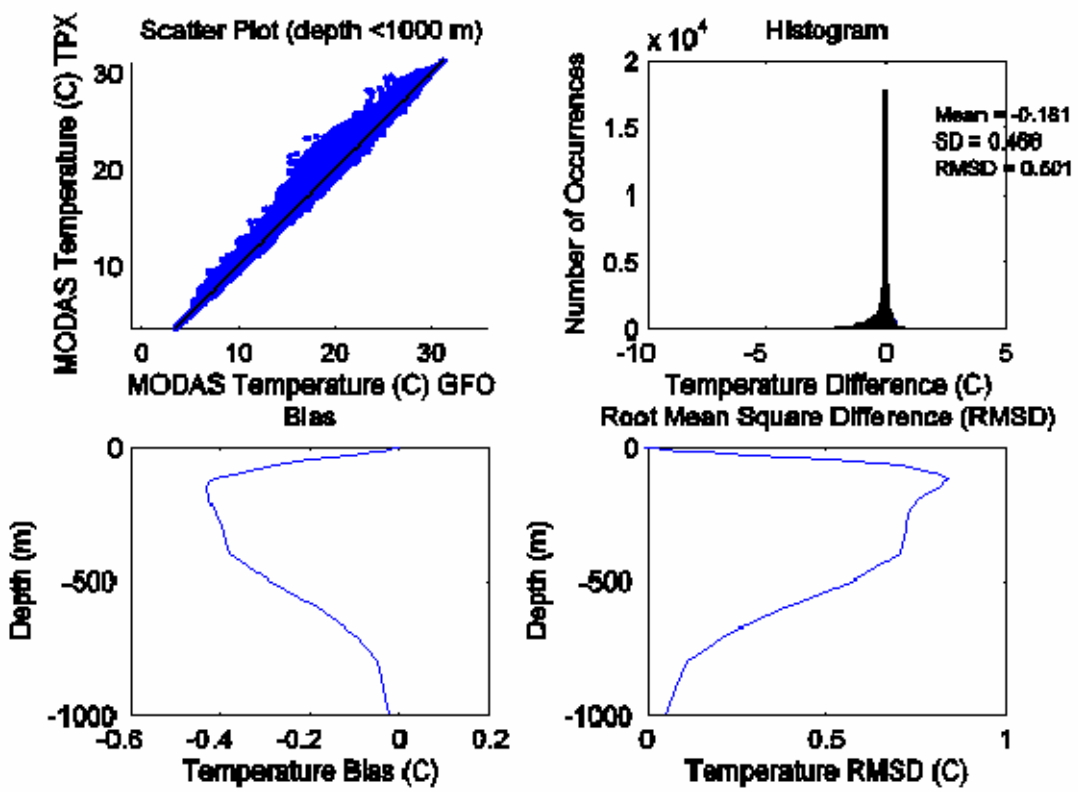

Figure 150. ECS MODAS temperature July 15, 2001

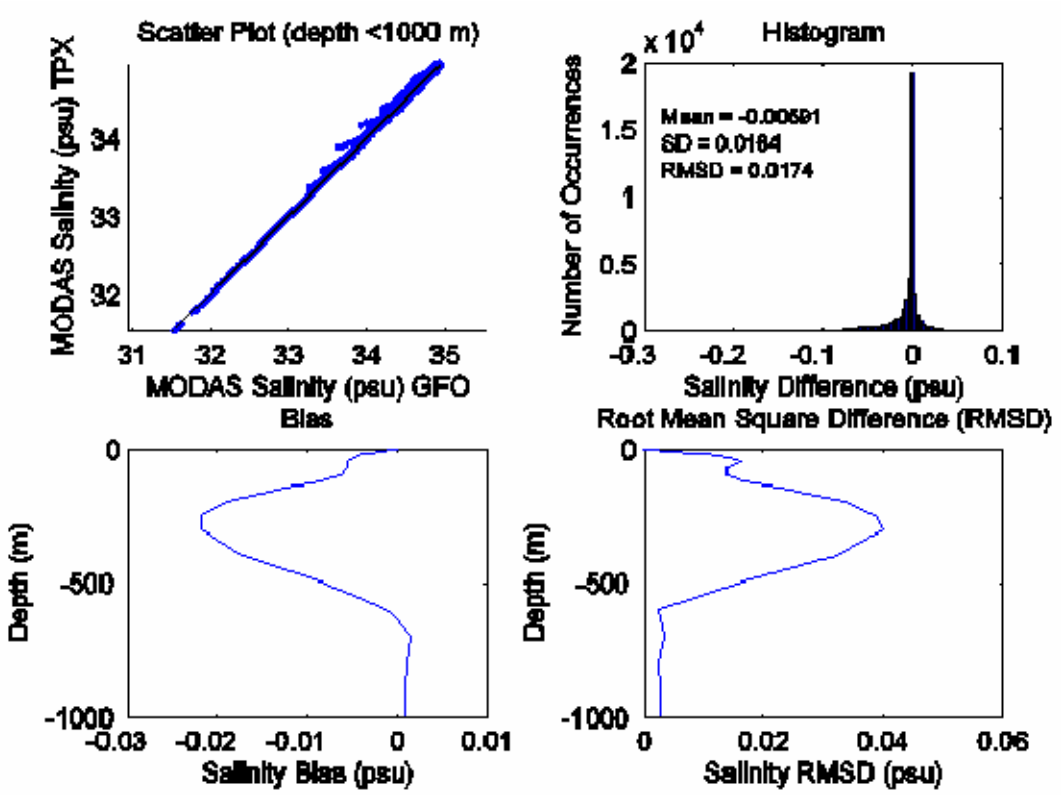

Figure 151. ECS MODAS salinity July 15, 2001

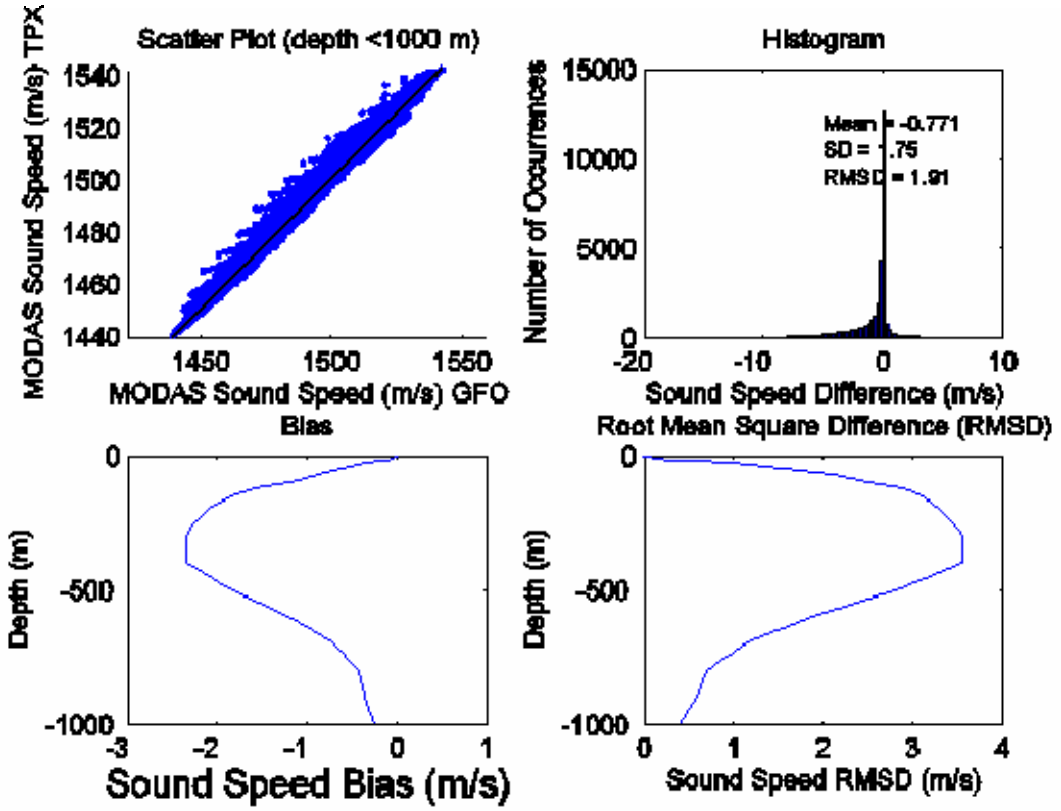

Figure 152. ECS MODAS sound speed July 20, 2001

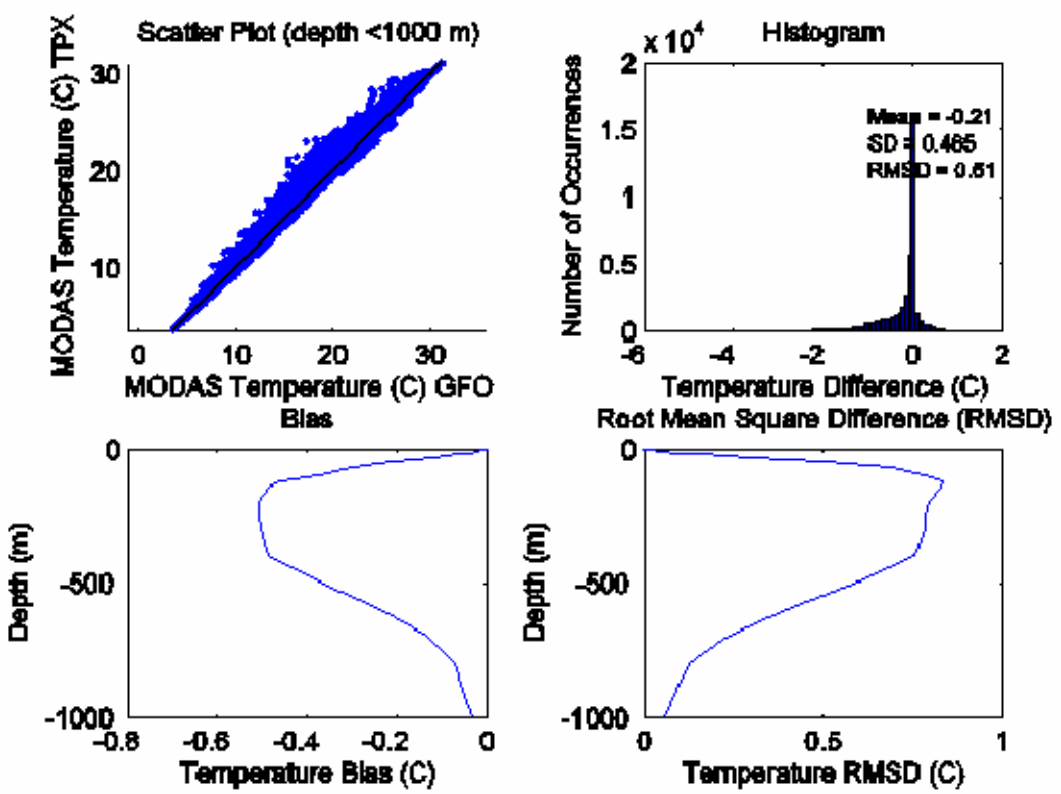

Figure 153. ECS MODAS temperature July 20, 2001

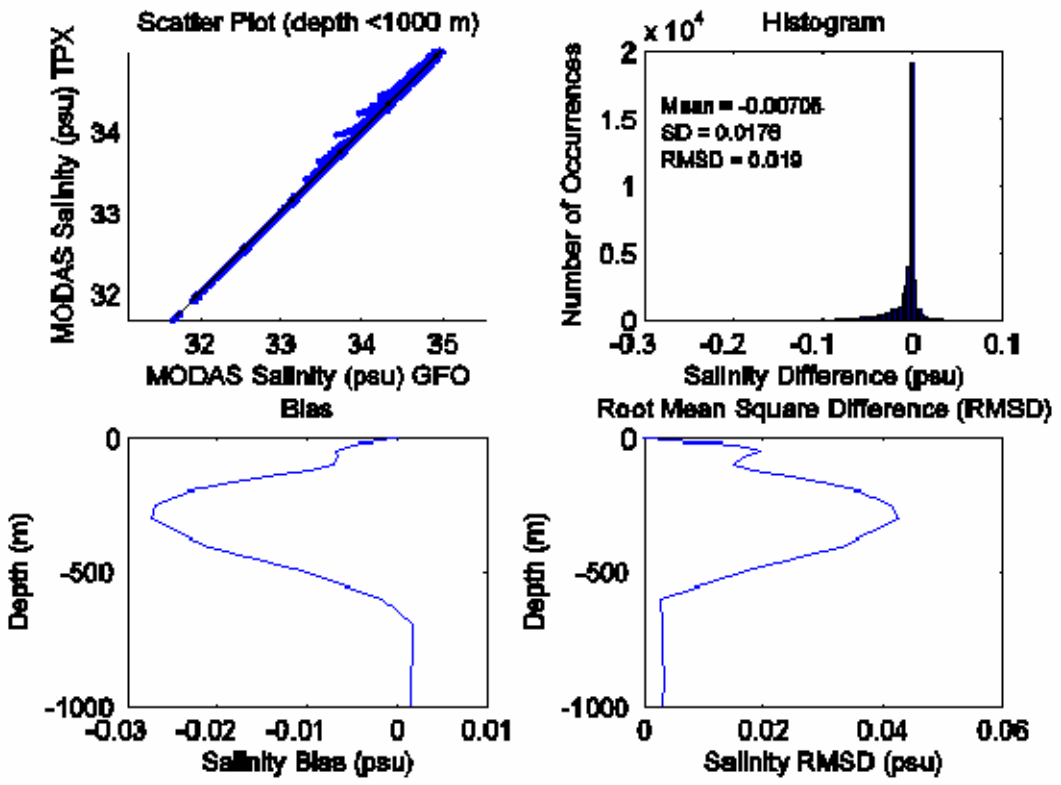

Figure 154. ECS MODAS salinity July 20, 2001

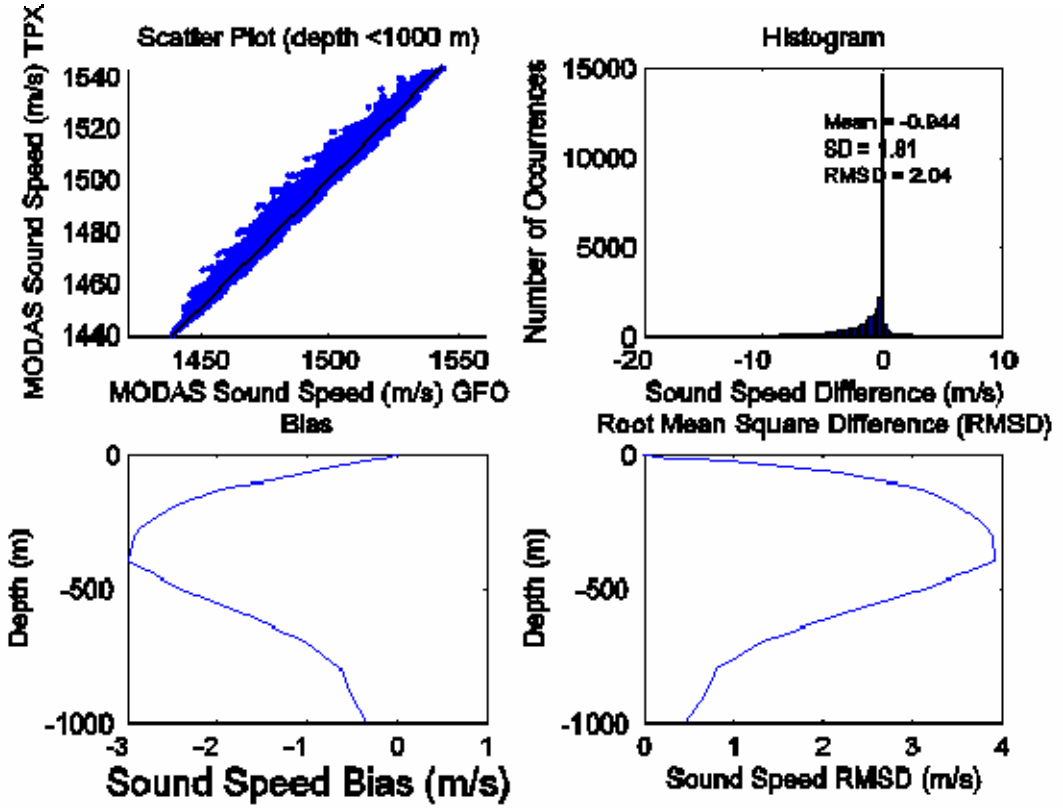

Figure 155. ECS MODAS sound speed July 25, 2001

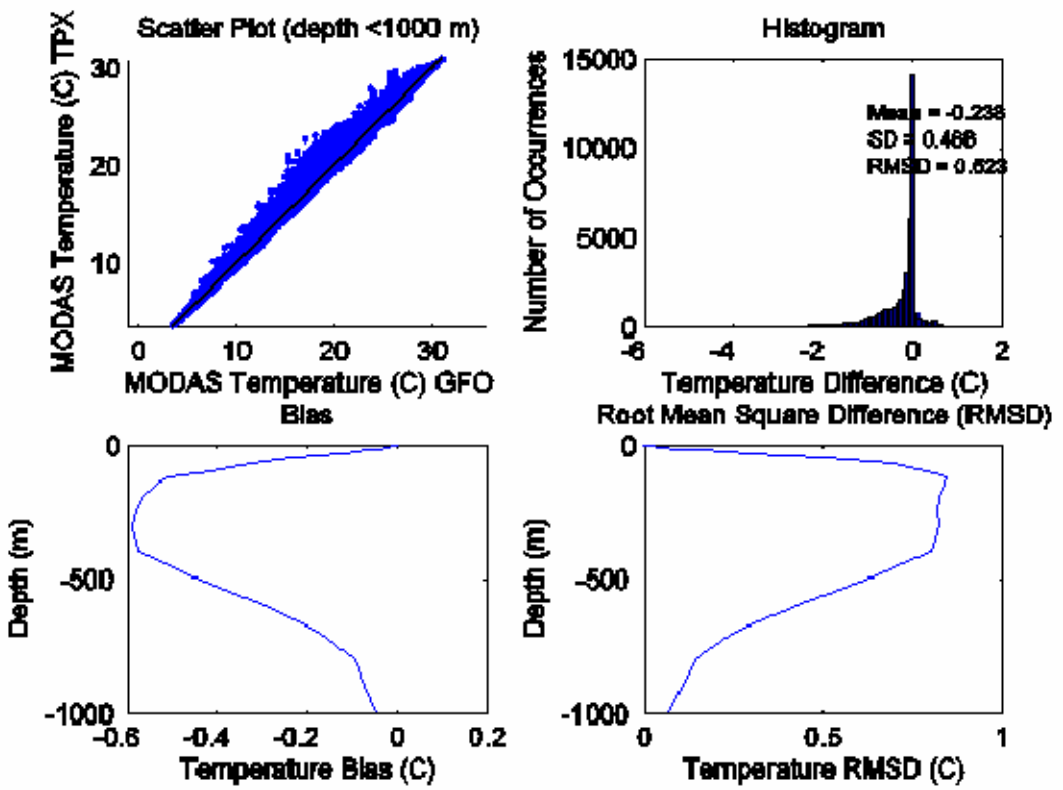

Figure 156. ECS MODAS temperature July 25, 2001

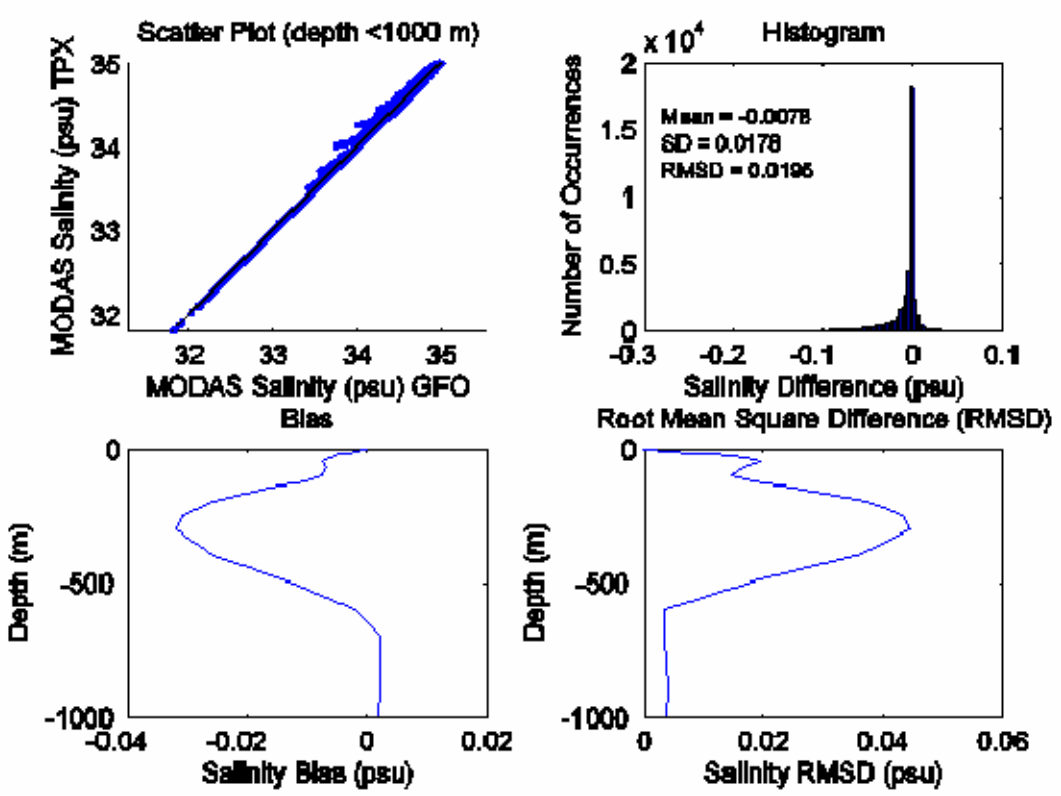

Figure 157. ECS MODAS salinity July 25, 2001

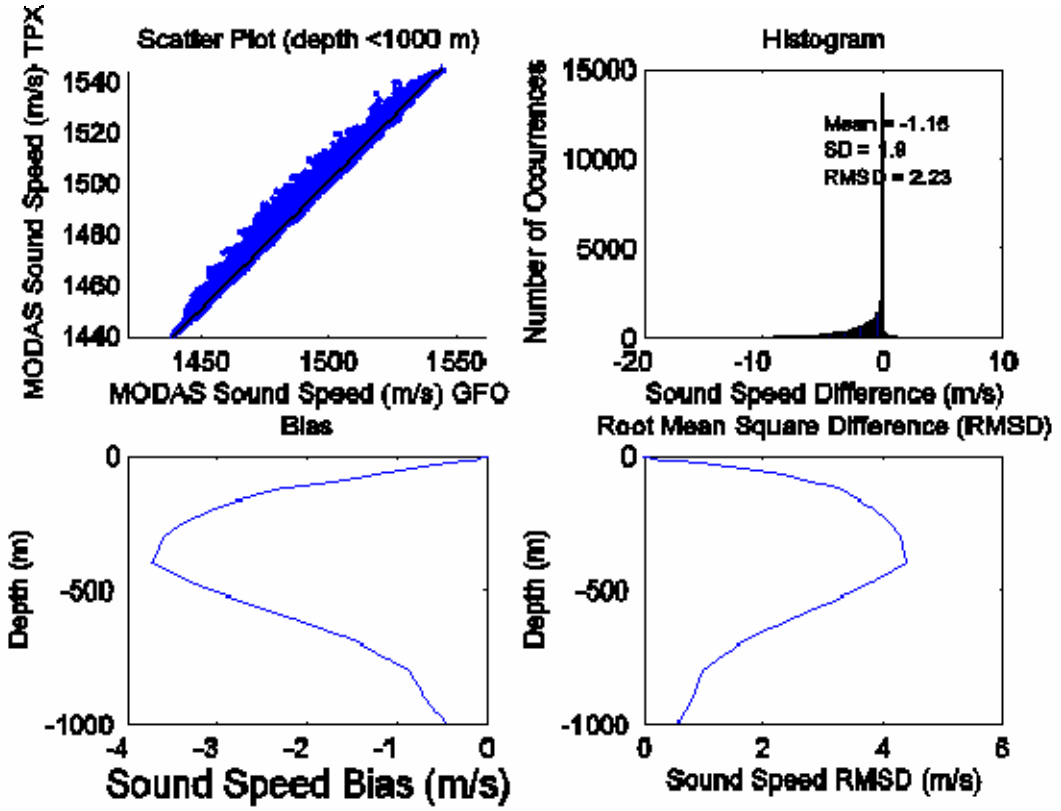

Figure 158. ECS MODAS sound speed July 30, 2001

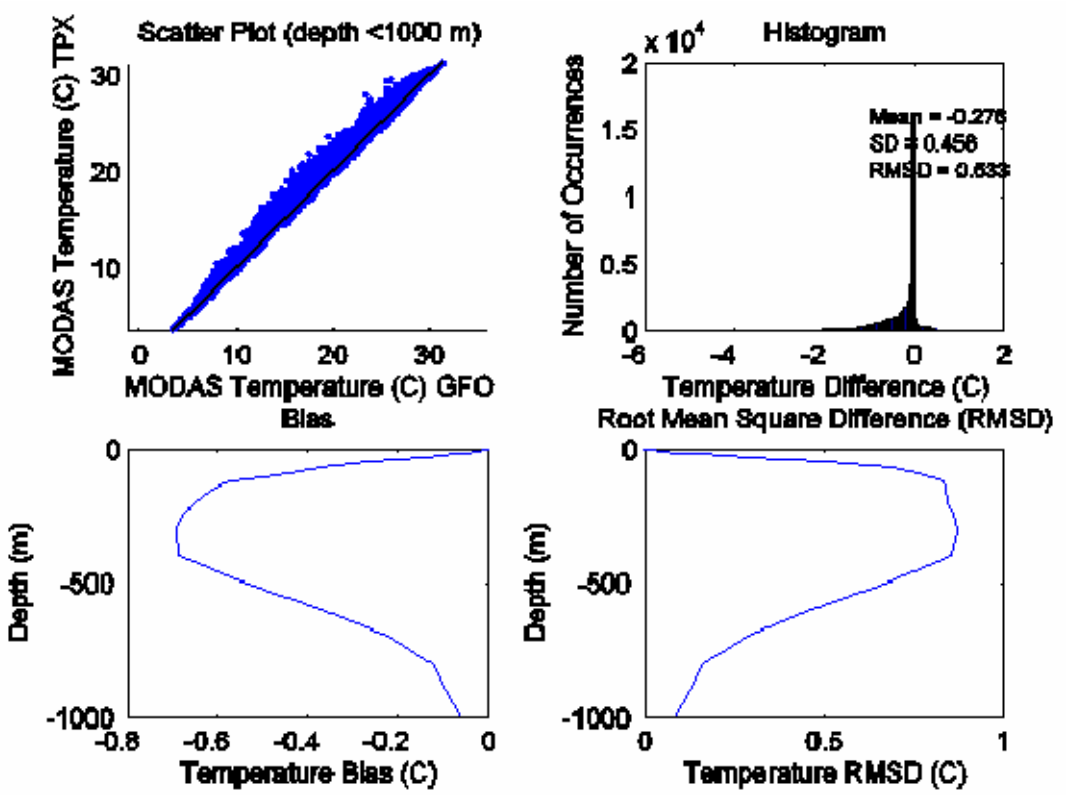

Figure 159. ECS MODAS temperature July 30, 2001

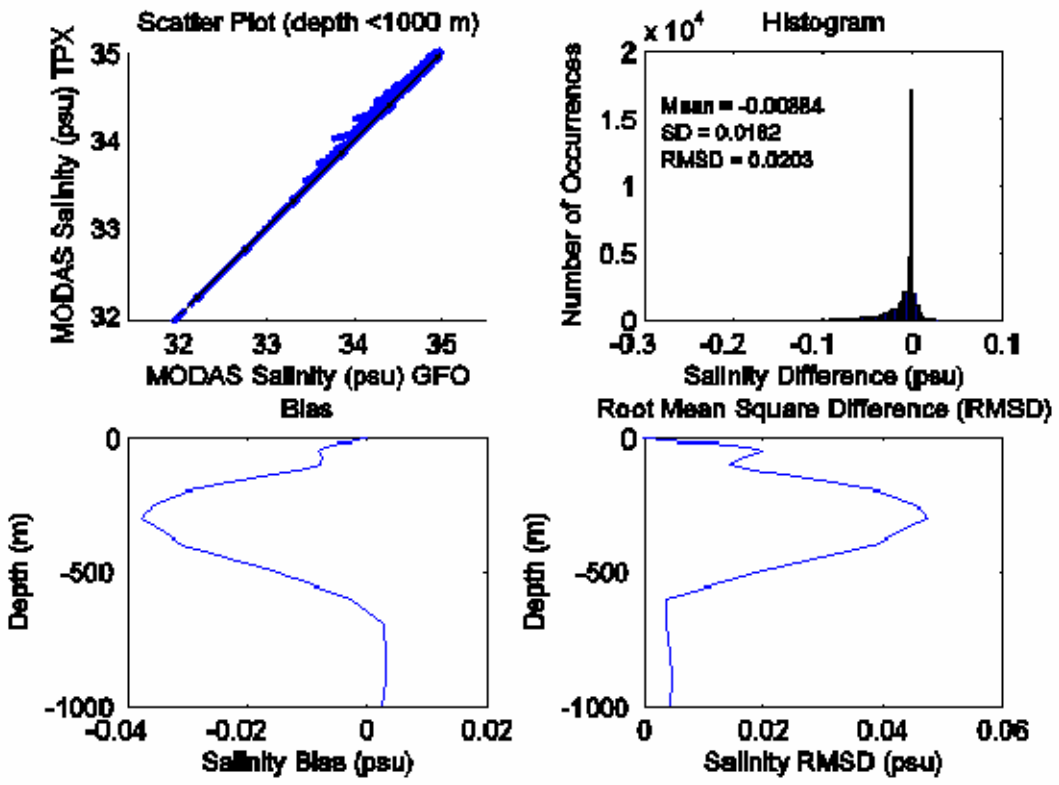

Figure 160. ECS MODAS salinity July 30, 2001

THIS PAGE INTENTIONALLY LEFT BLANK

APPENDIX E. JULY WAPP OUT SENSITIVITY SUMMARY

	RD>10	RD>15	Mean	SD
SCS 0705 HD Deep ASW	0.962	0.080	3.964	3.055
SCS 0710 HD Deep ASW	1.282	0.000	4.130	3.172
SCS 0715 HD Deep ASW	1.362	0.000	3.929	3.185
SCS 0720 HD Deep ASW	0.721	0.000	3.753	2.939
SCS 0725 HD Deep ASW	0.642	0.000	3.748	2.903
SCS 0730 HD Deep ASW	1.122	0.000	3.928	2.922
	RD>10	**RD>15**	**Mean**	**SD**
SCS 0705 LD Deep ASW	1.202	0.000	4.143	3.151
SCS 0710 LD Deep ASW	1.282	0.000	4.226	3.226
SCS 0715 LD Deep ASW	1.442	0.000	4.187	3.349
SCS 0720 LD Deep ASW	1.282	0.000	3.993	3.264
SCS 0725 LD Deep ASW	0.802	0.000	3.957	3.039
SCS 0730 LD Deep ASW	1.683	0.000	4.100	3.106
	RD>10	**RD>15**	**Mean**	**SD**
SCS 0705 LD Shallow ASW	6.571	0.321	4.896	4.440
SCS 0710 LD Shallow ASW	6.891	0.160	4.979	4.475
SCS 0715 LD Shallow ASW	4.728	0.240	4.674	4.162
SCS 0720 LD Shallow ASW	4.247	0.401	4.348	4.066
SCS 0725 LD Shallow ASW	6.576	0.241	4.855	4.394
SCS 0730 LD Shallow ASW	3.606	0.000	4.599	3.840
	RD>10	**RD>15**	**Mean**	**SD**
SCS 0705 HD ASUW	12.500	1.522	5.640	5.776
SCS 0710 HD ASUW	22.676	2.724	7.458	7.418
SCS 0715 HD ASUW	27.083	3.205	7.831	7.647
SCS 0720 HD ASUW	17.628	2.163	5.900	6.898
SCS 0725 HD ASUW	7.298	0.080	4.141	4.310
SCS 0730- HD ASUW	8.333	0.881	4.789	4.816
	RD>10	**RD>15**	**Mean**	**SD**
SCS 0705 LD ASUW	8.013	1.923	4.951	5.855
SCS 0710 LD ASUW	9.535	1.683	5.550	6.042
SCS 0715 LD ASUW	12.580	2.644	6.034	6.719
SCS 0720 LD ASUW	9.054	2.083	5.049	5.848
SCS 0725 LD ASUW	5.373	1.203	4.367	4.866
SCS 0730 LD ASUW	6.490	1.282	4.773	5.036

Table 6. WAPP sensitivity summary for the SCS July 2001

	RD>10	RD>15	Mean	SD
ECS 0705 HD Deep ASW	0.609	0.000	2.432	3.131
ECS 0710 HD Deep ASW	0.702	0.000	2.320	3.030
ECS 0715 HD Deep ASW	0.890	0.000	2.450	3.156
ECS 0720 HD Deep ASW	0.890	0.000	2.495	3.166
ECS 0725 HD Deep ASW	1.358	0.000	2.566	3.388
ECS 0730 HD Deep ASW	1.592	0.000	2.756	3.580
	RD>10	**RD>15**	**Mean**	**SD**
ECS 0705 LD Deep ASW	0.702	0.047	2.565	3.242
ECS 0710 LD Deep ASW	0.655	0.094	2.428	3.205
ECS 0715 LD Deep ASW	1.264	0.094	2.707	3.501
ECS 0720 LD Deep ASW	1.124	0.140	2.673	3.508
ECS 0725 LD Deep ASW	1.358	0.047	2.735	3.502
ECS 0730 LD Deep ASW	1.217	0.000	2.869	3.572
	RD>10	**RD>15**	**Mean**	**SD**
ECS 0705 LD Shallow ASW	2.809	0.562	3.136	4.316
ECS 0710 LD Shallow ASW	1.919	0.187	2.909	3.888
ECS 0715 LD Shallow ASW	2.622	0.234	3.088	4.071
ECS 0720 LD Shallow ASW	3.277	0.281	3.258	4.320
ECS 0725 LD Shallow ASW	3.324	0.375	3.374	4.362
	RD>10	**RD>15**	**Mean**	**SD**
ECS 0705 HD ASUW	11.096	2.856	4.407	6.680
ECS 0710 HD ASUW	10.908	3.792	4.427	7.353
ECS 0715 HD ASUW	12.079	3.652	4.585	7.281
ECS 0720 HD ASUW	12.406	3.277	4.685	7.362
ECS 0725 HD ASUW	15.403	4.120	5.264	7.745
ECS 0730 HD ASUW	16.854	4.728	5.719	8.061
	RD>10	**RD>15**	**Mean**	**SD**
ECS 0705 LD ASUW	11.470	7.163	5.241	9.402
ECS 0710 LD ASUW	13.062	7.116	5.178	9.530
ECS 0715 LD ASUW	12.266	7.116	5.232	9.362
ECS 0720 LD ASUW	13.764	6.039	5.226	8.955
ECS 0725 LD ASUW	15.543	7.350	5.798	9.715
ECS 0730 LD ASUW	16.339	7.678	6.157	9.933

Table 7. WAPP sensitivity summary for the ECS July 2001

LIST OF REFERENCES

Applied Physics Laboratory University of Washington (APL-UW). *APL-UW High-Frequency Ocean Environmental Acoustic Models Handbook (TR 9407).* Seattle, Washington: APL-UW, 1994.

Chu, P. C., S. H. Lu, Y. C. Chen and C. Fan. "Evaluation of the Princeton Ocean Using South China Sea Monsoon Experiment (SCSMEX) Data." *J. Atmos. Oceanic Technol.*, 2001.

Chu, P. C., W. Guihua and C. Fan. "Evaluation of the U. S. Navy's Modular Ocean Data Assimilation System (MODAS) Using South China Sea Monsoon Experiment (SCSMEX) Data." *Journal of Oceanography*, 2004.

Fox, D. N., W. J. Teague, C. N. Barron, M. R. Carnes and C. M. Lee. "The Modular Ocean Data Assimilation System (MODAS)." *Journal of Atmospheric and Oceanic Technology* 19 (February 2002): 240-252.

Fox, D. N., C. N. Barron, M. R. Carnes, M. Booda, G. Peggion, and J. Gurley. "The Modular Ocean Data Assimilation System." *Oceanography* 15 (No. 1 2002a): 22-28.

Fox, Dan N. MODAS Homepage: http://www7320.nrlssc.navy.mil/modas/ Accessed 25 December 2005.

Jacobs, G. A., M. R. Carnes, D. N. Fox, H. E. Hurlburt, R. C. Rhodes, W. J. Teague, J. P. Blaha, R. Crout and O. M. Smedstad, Naval Research Laboratory Report NRL/MR/7320-96-7722, Warfighting Contributions of the Geosat Follow-On Altimeter, 1996.

Jacobs, G. A., C. N. Barron, M. R. Carnes, D. N. Fox, H. E. Hurlburt, P. Pistek, R. C. Rhodes and W. J. Teague, Naval Research Laboratory Report NRL/FR/7320-99-9696, Navy Altimeter Requirements, 1999.

Jiag, S. and M. Ghil, "Tracking Nonlinear Solutions with Simulated Altimetric Data in a Shallow-Water Model." *J. Phys. Oceanogr:* Vol. 27, No. 1, pp. 72-95, 1996.

Liang, W. -D., T. Y. Tang, Y. J. Yang, M. T. Ko and W.-S. Chuang, "Upper-ocean currents around Taiwan." *Deep-Sea Research II 50 (2003):*1085-1105.

Mancini, S., "Sensitivity of satellite altimetry data assimilation on a naval anti-submarine weapon system" Master's Thesis, Naval Postgraduate School, Monterey, California, 2004 p. 77.

Mellor, G. L., 1998 "Users Guide for a Three-Dimensional, Primitive Equation Numerical Ocean Model". Available on the Princeton Ocean Model web site.

Murphy, A. H., 1988, “Skill score based on the mean square error and their relationships to the correlation coefficient. *Mon Wea. Rev.*, 116, 2416-2424.

Naval Undersea Warfare Center (NUWC). WAPP overview, PowerPoint view graphs, 2005.

INITIAL DISTRIBUTION LIST

1. Defense Technical Information Center
   Ft. Belvoir, VA

2. Dudley Knox Library
   Naval Postgraduate School
   Monterey, CA

3. Dr. Charlie Barron
   Naval Research Laboratory
   Stennis Space Center, MS

4. CDR Eric Gottshall
   ONR-Global
   London, UK

5. Dr. Daniel Fox
   Naval Research Laboratory
   Stennis Space Center, MS

6. PMW 180
   SPAWAR
   San Diego, CA

7. Mr. Steve Haeger
   Naval Oceanographic Office
   Stennis Space Center, MS

8. CDR Van Gurley
   Naval Oceanographic Office
   Stennis Space Center, MS

9. RDML Timothy McGee
   Commander, Naval Meteorology and Oceanography Command
   Stennis Space Center, MS

10. Mr. Bruce Northridge
    Commander, Naval Meteorology and Oceanography Command
    Stennis Space Center, MS

11. VADM Roger Bacon
    Naval Postgraduate School
    Monterey, CA

12. Oceanography Chair
Naval Postgraduate School
Monterey, CA

13. Mr. David Cwalina
Naval Undersea Warfare Center
Newport, RI

14. Mr. Roberts Rhodes
Naval Research Laboratory
Stennis Space Center, MS

15. Dr. Greg Jacobs
Naval Research Laboratory
Stennis Space Center, MS

16. METOC
Fleet Anti-Submarine Warfare Command
San Diego, CA

17. Oceanographer of the Navy
CNO-N7C
Washington D.C.

18. Dr. Peter Chu
Naval Postgraduate School
Monterey, CA

19. CDR Rebecca Stone
Naval Postgraduate School
Monterey, CA

20. CDR Ben Reeder
Naval Postgraduate School
Monterey, CA

21. CDR Denise Kruse
Naval Postgraduate School
Monterey, CA

22. LT Guillermo Amezaga
Naval Postgraduate School
Monterey, CA